AD-A062 612 RENSSELAER POLYTECHNIC INST TROY NY LAB FOR VISCOELA--ETC F/G 11/8
MEASUREMENT OF PROPERTIES AND RESPONSE FUNCTIONS OF LIQUID LUBR--ETC(U)
JUN 78 M H BIRNBOIM F33615-76-C-5101

UNCLASSIFIED AFML-TR-78-69 NL

1 OF 3
ADA
062612

AFML-TR-78-69

LEVEL II

2 B.S.

A037 183

MEASUREMENT OF PROPERTIES AND RESPONSE FUNCTIONS OF LIQUID LUBRICANTS RELATED TO TRANSIENT VISCOELASTIC REGIMES

410987

LABORATORY FOR VISCOELASTICITY
RENSSELAER POLYTECHNIC INSTITUTE
TROY, NEW YORK 12181

JUNE 1978

TECHNICAL REPORT AFML-TR-78-69
Final Report – April 1976 - September 1977

Approved for public release; distribution unlimited.

AIR FORCE MATERIALS LABORATORY
AIR FORCE WRIGHT AERONAUTICAL LABORATORIES
AIR FORCE SYSTEMS COMMAND
WRIGHT-PATTERSON AIR FORCE BASE, OHIO 45433

NOTICE

When Government drawings, specifications, or other data are used for any purpose other than in connection with a definitely related Government procurement operation, the United States Government thereby incurs no responsibility nor any obligation whatsoever; and the fact that the Government may have formulated, furnished, or in any way supplied the said drawings, specifications, or other data, is not to be regarded by implication or otherwise as in any manner licensing the holder or any other person or corporation, or conveying any rights or permission to manufacture, use, or sell any patented invention that may in any way be related thereto.

This report has been reviewed by the Information Office (OI) and is releaseable to the National Technical Information Service (NTIS). At NTIS, it will be available to the general public, including foreign nations.

This technical report has been reviewed and is approved for publication.

Frederick C. Brooks
Project Monitor

R.J. Benzing, Chief
Lubricants and Tribology
Branch

FOR THE DIRECTOR

J.M. KELBLE, CHIEF
Nonmetallic Materials Division

Copies of this report should not be returned unless return is required by security considerations, contractual obligations, or notice on a specific document.

AIR FORCE/56780/12 December 1978 — 150

Unclassified

SECURITY CLASSIFICATION OF THIS PAGE (When Data Entered)

REPORT DOCUMENTATION PAGE	READ INSTRUCTIONS BEFORE COMPLETING FORM
1. REPORT NUMBER: AFML-TR-78-69	2. GOVT ACCESSION NO.
3. RECIPIENT'S CATALOG NUMBER	
4. TITLE (and Subtitle): MEASUREMENT OF PROPERTIES AND RESPONSE FUNCTIONS OF LIQUID LUBRICANTS RELATED TO TRANSIENT VISCOELASTIC REGIMES. AD A037183	5. TYPE OF REPORT & PERIOD COVERED: 4/1/76 to 9/30/77
	6. PERFORMING ORG. REPORT NUMBER
7. AUTHOR(s): Meyer H. Birnboim	8. CONTRACT OR GRANT NUMBER(s): F33615-76-C-5101
9. PERFORMING ORGANIZATION NAME AND ADDRESS: Rensselaer Polytechnic Institute, ~~Department of Mechanical Engineering~~ Lab. for Viscoelastics, Troy, New York 12181	10. PROGRAM ELEMENT, PROJECT, TASK AREA & WORK UNIT NUMBERS: 2303-Q5-02
11. CONTROLLING OFFICE NAME AND ADDRESS: Air Force Materials Laboratory (MBT), Air Force Systems Command, Wright-Patterson AFB, Ohio 45433	12. REPORT DATE: June 1978 (279 p.)
	13. NUMBER OF PAGES
14. MONITORING AGENCY NAME & ADDRESS (if different from Controlling Office)	15. SECURITY CLASS. (of this report): Unclassified
	15a. DECLASSIFICATION/DOWNGRADING SCHEDULE

16. DISTRIBUTION STATEMENT (of this Report)

Approved for public release; distribution unlimited.

17. DISTRIBUTION STATEMENT (of the abstract entered in Block 20, if different from Report)

Final rept. 1 Apr 76 – 30 Sep 77,

18. SUPPLEMENTARY NOTES

19. KEY WORDS (Continue on reverse side if necessary and identify by block number)

Lubrication
High Pressure
Viscoelastic
Light Scattering
Ultrasonic
Liquid/Glass

20. ABSTRACT (Continue on reverse side if necessary and identify by block number)

This report is concerned with measurements of the viscoelastic response functions over a wide range of frequency and pressure that are required for the mechanical characterization of lubricating oils. Both rheo-optical (light scattering) and mechanical (ultrasonic) methods are required to obtain the viscoelastic data. Several developmental aspects of the implementation of these techniques as well as some of the results are discussed herein. The emphasis of this report is on (1) development of techniques required to obtain

CONT'

DD FORM 1 JAN 73 1473 EDITION OF 1 NOV 65 IS OBSOLETE S/N 0102-LF-014-6601

Unclassified

SECURITY CLASSIFICATION OF THIS PAGE (When Data Entered)

Cont'

light scattering from lubricants in the high pressure diamond anvil cell. These low frequency data analyses based on scattering from nonmagnetic and from magnetic spheres suspended in the liquid, and Brillouin line width measurements to yield both elastic modulus and loss of the liquids in the range circa 10^8 - 10^9 Hz, (2) preliminary results on steady-state viscosity of the test fluids at atmospheric pressure, (3) new experimental results on the role of additives in determining the viscoelastic response of lubricants.

10 to the 8th power — 10 to the 9th power

FOREWORD

This report was prepared by Rensselaer Polytechnic Institute, Troy, New York under USAF Contract No. F33615-76-C-5101. The contract was initiated under Project No. 2303, Task No. Q5. The work was administered under the direction of the Air Force Materials Laboratory, with Mr. Frederick C. Brooks (AFML/MBT) acting as project engineer.

This report covers work conducted by the authors from 1 April 1976 to 30 September 1977. This report was submitted by the author in April 1978.

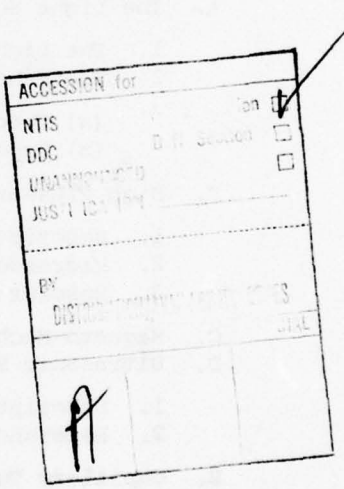

TABLE OF CONTENTS

LIST OF ILLUSTRATIONS

LIST OF SYMBOLS

μ^* - Complex shear modulus (= G^*) (dynes/cm^2)

μ' - Shear storage modulus (= G') (dynes/cm^2)

μ'' - Shear loss modulus (= G'') (dynes/cm^2)

λ - Lamé's constant (dynes/cm^2)

b - One-half thickness of delay line (cm)

SS(0) - Meitzler mode (or principal shear mode)

ρ - Density (gm/cm^3)

φ - Scalar potential

$\underset{\sim}{W}$ - Vector potential

V_D - Dilatational wave velocity (cm/sec)

V_S - Transverse wave velocity (cm/sec)

$\underset{\sim}{u}$ - Displacement vector (cm)

t - Time (sec)

ω - Angular frequency (radians/cm)

m - Complex propagation vector in z-direction

n - Complex propagation vector in x-direction

σ - Stress (σ_{xy} = shear stress) (dynes/cm^2)

I - Integer number

Z^* - Mechanical impedance (dynes $\cdot$ sec/cm^3)

R - Mechanical resistance (dynes $\cdot$ sec/cm^3)

X - Mechanical reactance (dynes $\cdot$ sec/cm^3)

A - Attenuation constant (neper/cm)

B - Propagation constant (radians/cm)

ΔA - The difference of attenuation with and without liquid (neper/cm)

ΔB - The difference of phase shift with and without liquid (neper/cm)

$|G|$ - Magnitude of complex shear modulus (dynes/cm^2)

$\eta^*(\omega)$ - Dynamic viscosity (dynes • sec/cm^2 or poise)

$\eta'(\omega)$ - Real part of dynamic viscosity (poise)

$\eta''(\omega)$ - Imaginary part of dynamic viscosity (poise)

$\overline{K}$ - Propagation constant (radians/cm)

A,C,D,E,F,H - Various constants

K' - Bulk storage modulus

K'' - Bulk loss modulus

$\eta'_v(\omega)$ - Volume viscosity junction

τ - Relaxation time

$B'(\omega)$ - Bulk storage compliance

$B''(\omega)$ - Bulk loss compliance

f - Doolittle fractional free volume

SECTION I

INTRODUCTION AND BACKGROUND

A. FLUID PROPERTIES AND THE EHD LUBRICATION PROBLEM

In the elastohydrodynamic (EHD) lubrication problem the fluid undergoes a complicated stress/deformation history: the stresses are transient, and have both isotropic (pressure) and shear components. (See, for example, reviews by Dowson and Higginson [1] and Tallian [2].) The resultant compressional and shearing deformations must depend on the viscoelastic properties of the fluid, but in a rather complicated, and unknown way. One coule pose the question: Given a particular stress history, what are the physical properties of the fluid which must be known in order to determine the resulting deformation history (or vice versa)?

Figure 1 illustrates the approach taken by Trachman [3]. The pressure distribution (peak pressure p_o) and geometry in the Hertzian contact zone (of width b) is indicated in this figure; the fluid undergoes a time varying pressure history as it flows through this contact region. By assuming a simple viscoelastic model for the liquid, and a specific pressure dependent viscosity function, the "effective" or "time dependent" viscosity for the liquid in the contact zone is calculated and shown in Figure 1b. By comparison, one sees that the "effective viscosity", hence shear traction, is much less than by assuming an equilibrium fluid with no relaxational part to the viscosity. Thus while one expects to enhance the viscosity, the transient contribution is less than the steady-state value, therefore partially compensates. For such calculations however, a more complete knowledge of the shear and volume relaxational behavior of the liquids as well as appropriate time-pressure equivalence principles are required. One would expect that two liquids of different chemical character, although of the same atmospheric pressure steady-state viscosity, would exhibit a dramatically different response in the contact zone. Thus, for practical as well as theoretical importance, a fuller understanding of the viscoelastic response is required.

B. VISCOELASTIC PROPERTIES IN THERMODYNAMIC EQUILIBRIUM-PHENOMENOLOGICAL AND MOLECULAR DESCRIPTION

1. Behavior of the Linear Viscoelastic Parameters $\eta(\omega)$, $G'(\omega)$, $K'(\omega)$, $K''(\omega)$, $M'(\omega)$, $M''(\omega)$, τ_s, τ_v

In order to phenomenologically fully describe the mechanical response of a liquid in thermodynamic equilibrium at a pressure and temperature P,T we need the shear viscosity function $\eta_s(\omega)$, the shear modulus function $G'(\omega)$, the volume viscosity function $\eta_v(\omega)$ [or equivalent $K''(\omega)$ since $\omega\eta_v = K''(\omega)$], the bulk modulus function $K'(\omega)$. It is sometimes convenient to approximate these functions by their limiting values, and refer to a shear relaxation time τ_s and volume relaxation time $\tau_v(\tau = 1/\omega)$ at which a transition occurs between limiting values.

To develop a physical feeling for the useful parameters in describing material properties, it is convenient to collectively examine Figures 3 through 6. In Figure 3 (see Plazek [4]) the specific volume (reciprocal density) of the material is shown to vary with temperature; we shall allude to analogous variation with pressure. We ignore the possibility of crystallization. If we are in the "liquid" regime of this curve, and decrease the temperature slightly, then one expects the volume to decrease to its new equilibrium value "instantaneously"; certainly faster than our "time scale of measurement" τ, for which we will assume τ = 1 second. Thus one could say that the structural relaxation time τ_v, is $\ll \tau$. The same would be true for an increment in pressure. By contrast, in the "glassy" regime of this curve, in response to a decrement in temperature (or increase in pressure) the volume would change very slowly. Thus the structural relaxation time τ_v, the time for the sample to reach a new equilibrium volume is $\gg \tau$; indeed τ_v could be years. Hence notice that the glass temperature is not unique but depends on whether $\tau_v \gg \tau$ or $\tau_v \ll \tau$, namely depends on our choice for the time scale of the measurement.

Consider the example of pressure dependence of the bulk dynamic compliance, B ($B = 1/K$, where K is the bulk modulus), the curve of Marvin [5], Figure 5b, in which the measurement time scale is taken as $\tau \sim 1/1000$ sec: at P = - 2000 bars (or at high temperatures), then $\tau_v \ll \tau$ and we obtain the liquid-like compliance B_o; whereas at ± 2000 bars, $\tau_v \gg \tau$ and then we obtain the glass-like compliance B_∞. In these examples, the τ of the measurement is kept fixed and τ_v is changed by pressure or temperature! Alternatively, if the P and T are held

constant as in Figure 5a and only τ is changed, then one measures a liquid-like compliance B_c at $\tau \gg \tau_v$, and glass-like B_g for $\tau \ll \tau_v$. This figure illustrates that τ_v can be determined at each fixed T and P if τ is variable over a wide time (frequency) range. We now conclude that even the "liquid-like" regime of Figure 3 can behave "glass-like" if τ is short enough.

Hence the viscoelastic properties of the lubricant $B_e(P)$, $B_g(P)$ and $\tau_v(P)$ must be determined as a function of pressure. And more!

Turning next to the viscoelastic response of a lubricant to (dynamic) shear deformation, Figures 4a and b indicate additional parameters required to describe the fluid. There are two characteristic relaxation times* τ_c and τ_g if the lubricant contains polymers, through molecular models these are associated with conformational change of the polymers τ_c, and orientational changes of the solvent molecules τ_s. Thus, for $\tau \gg \tau_c > \tau_g$ (or $\omega \ll \omega_c < \omega_g$), the lubricant behaves liquid-like with a shear viscosity η_o and "zero' shear modulus; for $\tau_c > \tau > \tau_g$, the viscosity drops to a new level of η_∞ and the shear modulus G' increases to rubber-like values; while for $\tau < \tau_g$ the viscosity drops further and G' reaches a glass-like value.

Hence the shear viscoelastic properties of the lubricant $\eta_o(P)$, $\eta_\infty(P)$, $G_\infty(P)$, τ_c and τ_g must also be determined as a function of pressure.

As an aside, it should be mentioned that a polymeric fluid being sheared will also generate normal stresses which tend to push the contact surfaces apart. The magnitude of these normal stresses are related to η_o and τ_c.

2. The Free-Volume Picture: Concepts of Time-Temperature Superposition

One unifying model of liquids which has had a large degree of success in tying together tempersture and pressure-dependent properties has been the free volume model of Doolittle [6]. The idea is that the actual volume occupied by the molecules is less than the actual sample volume v, so that the difference is the free volume v_f. The larger the fractional free volume $f \equiv v_f/v$, the easier it is for molecules to slide past each other or to rearrange conformations.

---

* In every case, by "characteristic relaxation time" we mean the mean value of the relaxation time distribution function.

Thus Doolittle postulated that the temperature and pressure dependence of f would be linear:

$$f = f_o + \alpha_f (T - T_o) + \beta_f (P - P_o) \tag{1}$$

and, further: that at two different temperatures T and T_o, each characteristic relaxation time would change in the same ratio as the zero shear viscosity, then a temperature shift factor is defined:

$$a_T \equiv \frac{\tau_{c/T}}{\tau_{c/T_o}} = \frac{\eta_{o/T}}{\eta_{o/T_o}} \tag{2}$$

from which he obtains

$$\ell n\, a_T = B\left(\frac{1}{f} - \frac{1}{f_o}\right) \tag{3}$$

This equation was extended by Ferry [7] to the WLF equation

$$\ell n\, a_T = \frac{-C_1 (T - T_o)}{C_2 + T - T_o} \tag{4}$$

which, in combination with Eq. (2) has formed a time-temperature superposition principle that has been successful when applied to conformational relaxation times. The inference of such an equation is that the character of the relaxation mechanism does not change with temperature (pressure), but only the magnitude and characteristic time scale will change. This is not true for all relaxation mechanisms. The utility of a time-temperature superposition principle is that predictions can be extrapolated to time (or temperature) ranges other than those measured.

3. The Free-Volume Picture: Concepts of Time-Pressure Superposition

Time-pressure superposition is far less developed for large pressure ranges. Ferry [7] has extended the concepts above to obtain:

$$\log a_P = \frac{(B/2.303\, f_o)(P - P_o)}{f_o/\beta_f - (P - P_o)} \tag{5}$$

The free-volume model would say that only the final volume is important regardless of the temperature or pressure history route. This idea needs further testing. Other approaches have been developed by Cohen [8] and by Gibbs [9].

C. VISCOELASTIC RESPONSE TO THE TRANSIENT (NONEQUILIBRIUM) EHD SITUATION

This subject of the relation of equilibrium properties to transient response has not thus far been studied extensively, and therefore is part of our experimental goals. One useful view taken by Harrison [10] and by Trachman [3] utilizes free volume concepts discussed above. The central argument can be viewed as if volume is the unifying concept, then pressure (and temperature) history may be put aside, and the response may be determined by integration over volume history, with the assumption of equilibrium properties at each segment of the history.

D. EXPERIMENTAL TECHNIQUES

1. Mechanical Spectroscopy: Steady State, Low Frequency, Ultrasonic

The mechanical relaxation spectra of interest for lubricating liquids can reach from steady state (D.C.) to 10^{10} Hz. The part of the spectrum of interest will of course change for each pressure (and temperature). As indicated earlier the functions which must be known are the shear viscosity and modulus, and the bulk viscosity and modulus. While a variety of mechanical techniques extending from 1 Hz to 10^{8} Hz have been used in this laboratory (Figure 2) for liquids at atmospheric pressure, not all of them are directly applicable to high pressure techniques. Some exceptions are applications of similar methods to high pressure problems by Barlow [11], Marvin [5] and by Lamb [12].

The primary approach taken in our studies, is to construct a practical high pressure cell optimized so that the widest frequency range of measurements can be made in the same cell - both under equilibrium and transient pressures. Because of the limit of small sample volume, we emphasize the techniques which utilize light scattering, and those which couple mechanical viscoelastic techniques with light scattering - rheo-optic techniques.

2. Light Scattering - Twelve Years of Progress

With the advent of lasers, fast photomultipliers, highest quality Fabry-Perot interferometers, high speed (computerized) autocorrelators - material property information - extracted by light scattering has developed very far indeed these past twelve years. Here we will only list a few techniques relevant to lubrication, a few developed in out laboratory for the past eight years, many developed elsewhere (see Fleury [13], Cummins [14]).

The general features of the light scattering experiment is found in Figure 8. Light from a laser is focussed into a narrow beam (circa 0.1 mm) at the liquid sample, and the light scattered at any set scattering angle θ is collected by a photomultiplier. The "liquid" scattering cell may be one of the new high pressure cells of Figures 9 or 11, or our older high pressure cell [15] of Appendix A. The scanning photometer [16] paper provides a more detailed description. Optical detection can be direct as shown in Figure 8 for autocorrelation and cross-correlation function analysis of scattered intensity; or a Fabry-Perot Interferometer (FP) may be inserted between liquid and photomultiplier (PM) for Brillouin peak and Rayleigh Wing analysis; filters for fluorescence studies and analyzers for depolarized scattering are also introduced between liquid and PM.

(i) Rayleigh line. Figure 7 shows a light scattering spectrum from Benzene at $\theta = 90^{\circ}$ taken by Cummins [17] using a FP. The central line is called the Rayleigh line because the center frequency is the same as that of the laser. However, whereas the laser line width is a few Hz, this Rayleigh line is $\sim 10^{8}$ Hz and is due to nonpropagating entropy fluctuations, i.e., changes in local ordering of the molecules or rotational ordering of the molecules (when measured in HV). Notice VV refers to the polarized component of the light, HV to the depolarized component. Speed of molecular motion is related to line width.

(ii) Brillouin lines VV polarization. The lines on either side of the central line in Figure 7 are due to pressure fluctuations inherent in all materials [18,19]; this becomes equivalent to an ultrasonically generated pressure disturbance which of course propagates as a wave. Such waves are spontoneously present at all frequencies (and wavelengths), so that one selects the acoustic wavelength by setting θ, the scattering angle, and measures the frequency shift with respect to the central line to obtain the velocity. Together with the density of the fluid, this yields the longitudinal modulus M, where $M = K + \frac{4}{3} G$, see for example Dill [20] or McSkimin [21]. A more detailed discussion of the nuances in extracting K and G, as required for lubricant properties and of structural relaxation [22] is omitted here. The width of these Brillouin peaks yields the wave attenuation, or dynamic viscosity η_M.

(iii) Brillouin lines HV polarization. If the frequency and pressure are such that the material behaves glass-like, and can sustain a shear stress, then a transverse velocity and attenuation corresponding to G_∞ and η_∞ can also be determined.

(iv) Quasi-elastic scattering. When polystyrene spheres of size $< \lambda$ are added in minute concentration to the liquid, they become the primary light scattering source, and their relative motions give rise to time varying interference of the light reaching the PM (no FP). The resulting photocount fluctuations are analyzed by the computer/autocorrelator as seen in Ref. 16 and Appendix A. The autocorrelation function yields diffusion coefficient of the spheres, hence one obtains the viscosity (low frequency limit) η_o of the liquid.

(v) Quasi-elastic scattering. A new technique under development is to replace the polystyrene spheres used above with colloidal magnets and force mechanical oscillation at medium frequencies (1 Hz to 10 KHz) by an external magnetic field. The motion is analyzed by a cross-correlation technique related to the one used above.

E. OBJECTIVES OF THIS RESEARCH PROGRAM

In elastohydrodynamic (EHD) lubrication the liquid lubricant is subjected to a complex transient stress history in which the isotropic pressure components may reach beyond 200,000 psi in durations of the order of 1 millisecond. One may ask: How do the viscoelastic characteristics of a fluid influence the stress built up in this lubrication situation: Therefore our long term objectives are:

(i) To measure the rheological properties of a variety of liquid lubricants over the full frequency range of viscoelastic response from 1 Hz to 10^{10} Hz; over a pressure range to 300,000 psi; and over a temperature range from -100°C to $+300^{\circ}$C. Knowledge of the viscoelastic response is important both under equilibrium and transient pressure and temperature histories, as well as in uniform and non-uniform pressure/temperature fields.

(ii) Phenomenological theories are to be explored which can relate the above equilibrium state viscoelastic measurements to the stress/strain response of a liquid under transient elastohydrodynamic lubrication conditions. In other words, the studies should lead to time-temperature

and time-pressure superposition principles applicable under transient and nonuniform conditions.

(iii) Molecular theories are to be examined which relate molecular structure to the measured macroscopic response, thereby establishing possible relations between lubricant properties and molecular structure.

(iv) Experimental procedures in this laboratory are based primarily on rheo-optic techniques, that is, application of stresses by external mechanical or by spontaneous means, and measurement of response by optical (laser light scattering) means.

(v) Selection of materials: After consultation with Mr. F.C. Brooks and Dr. J.F. Dill it was established that the fluid PR-143 AC would be most suitable for initial studies, and Emery 2958 and Stauffer 704 would be appropriate follow-on candidate fluids. In this discussion it was established that the most meaningful progress could be made if coordination between laboratories was established on the basis that each measured some identical fluids. Of course, an understanding of the relationship between chemical structure and mechanical properties of lubricants remains a continuing objective.

SECTION II

EXPERIMENTAL PROGRESS AND RESULTS

A. THE LIGHT SCATTERING SPECTROMETER

Our light scattering spectrometer is in the process of being upgraded to add the capability of:

1) Brillouin line width measurements for polarized and depolarized components.

2) Scattering from magnetic spheres in linear motion in the liquid.

3) Scattering from magnetic spheres in oscillatory motion in the liquid.

These are additional to the capability hitherto available of:

1) Rayleigh (quasi-elastic) scattering.

2) Scattering from suspended polystyrene spheres in Brownian motion.

In addition, for measurement of pressure, we must add the capability to measure:

1) Fluorescence spectral shift from ruby crystals.

1. The Light Scattering Photometer

The restrictions imposed by a small volume high pressure cell (see discussion of cell), together with the requirement for several experiments have led us to the design of a multiport microscope light scattering photometer to replace our current apparatus. The microscope will have three ports as seen in Figure 12: one for direct visual or video scan observation of liquid-to-glass/crystalline transformations (and kinetics thereof) under high pressure; one port for quasi-elastic light scattering (Rayleigh line) data analysis including oscillating magnetic spheres and for Brillouin and Rayleigh wing spectral analysis; and one for determining local pressure by the fluorescent spectral shift of ruby as measured with an optical scan spectrometer.

For the diamond anvil high pressure cell, surface scattering can be a serious problem. As will be discussed in the next section, ON THE HIGH PRESSURE DIAMOND ANVIL CELL, we have been able to adjust geometry to reduce the surface

scattering contribution by several orders of magnitude. In addition, the triple pass feature of our Fabry-Perot reduces overlap between Rayleigh and Brillouin spectra.

2. The Fabry-Perot Interferometer

A major system component is the Fabry-Perot interferometer for Brillouin shift and line width measurements. After comparison of specifications of Tropel and Burleigh units, the Burleigh Fabry-Perot Interferometer Model RC10 with multipass option was selected. Aside from stability, we concluded that the multipass feature of this unit will be very helpful in the reduction of the contribution of scattering from the surfaces of the diamond cell.

The unit has been set up and interfaced to the computer. The electronics for individual adjustment of the three piezoelectric drivers and the high voltage sweep circuit have been constructed and interfaced to the digital-to-analog drives from the computer (Figure 10). The present computerized data acquisition and analysis (autocorrelation) system as seen in Figure 12, continues to work well. A computer algorithm for tuning the interferometer and for automatic frequency drift correlation has been written, but has yet to be implemented. Next we discuss details of the theory of the Fabry-Perot interferometer and some preliminary results obtained with it.

(a) Theory of Fabry-Perot

A discussion of the theory of the Fabry-Perot interferometer has been included as Appendix C.

(b) Experimental Results by Photographic Method

Our first Brillouin scattering results have been obtained for several liquids of interest at atmospheric pressure and with the photographic mode of operation of the Fabry-Perot interferometer. It was deemed useful to survey several liquids with this less sensitive and less precise photographic mode of operation prior to use of the computerized photoelectric detection mode in order to obtain an overview of the comparative liquid characteristics.

The following liquids were examined:

1) Benzene
2) Ethanol
3) Methanol
4) Cyclohexane
5) Acetone
6) Toluene
7) Lubricant Oil ML071-6
8) Lubricant ATL5066
9) Lubricant ATL5067.

The results for the first seven fluids are illustrated in Figures 1 through 7. Detailed analyses on some of these results have been performed and summarized in Table 1. The following cursory observations can be made: (1) Lubricants ATL5066 and 5067 are highly fluorescent (yellow) for incident wavelengths of 4880A and 5145A, so that no Brillouin spectrum was obtained. The experiment will be repeated after we obtain an appropriate narrow bandpass filter. (2) Lubricant MLO-71-6 exhibits moderately weak Brillouin lines and may give us some problems for high pressure measurements. (3) In each photograph several orders are seen. The Rayleigh line (more intense) for each order has a Stokes and anti-Stokes line associated with it, apparent at somewhat smaller and somewhat larger radii. The triplet is repeated for several orders. (4) The overall apparatus stability is now shown to be very good, as evidenced by the fact that some of the exposures extended for one hour.

B. HIGH PRESSURE DIAMOND ANVIL CELL

1. Description

The basic design [23] of the rheo-optic light scattering high pressure cell instrument is centered on microscopic observation of the fluid under high pressure. The use of a tiny volume as in the diamond cell (see Figure 11) seems essential if one is to achieve pressures in the 300,000 psi range, since the transition from liquid-like to glass-like behavior of the sample would resist the pressure build-up. Furthermore, the cell volume becomes orders of magnitude closer to the volume in EHD contacts, so that one brings the laboratory experiment much closer to the real contact situation. The process of generating high pressures (and impulses) becomes simplified, a single band

TABLE 1

BRILLOUIN FREQUENCY SHIFTS FOR SEVERAL LIQUIDS
AT 22°C USING PHOTOGRAPHIC METHOD

Sample	Observed Brillouin Shift at 90° in GHz	Published Values	Reference
Toluene	6.04 (4880 Å)	6.08 (4880 Å)	Kato et al.
Ethanol	4.90 (4880 Å)	5.10 (4416 Å)	Gustafsson et al.
Benzene	6.37 (4880 Å) 6.16 (5145 Å)	6.59 (4880 Å)	Kato et al.
Cyclohexane	5.60 (4880 Å)		
Acetone	5.37 (5145 Å)		
Methanol	5.61 (5145 Å)		
MLO-71-6			

screw is sufficient to generate the desired pressures. The additional complexities that arise from the microscopic volume are connected with sample loading, measurement of pressure, and surface scattering. Furthermore, microscope optics are required for the small sample volume, and were described above.

A diamond anvil cell designed by Dr. A. Van Valkenberg, while at the National Bureau of Standards, was ordered and delivered from High Pressure Diamond Optics, Incorporated. Both optical and sample handling procedures are currently being developed for these samples of volume circa 10^{-4} cc.

Pressure and pressure distribution measurement can be determined by the shift in the fluorescence spectra of ruby crystals suspended in the fluid [24,25] and locally monitored by the microscope optics. Design is underway for the fast pressure pulse triggering device.

Fabrication of Washers

As can be seen in Figure 1, the liquid sample is contained in a small hole (shaded area) within the washer (or spacer) B. The hole diameter must be sufficiently smaller than the hexagonal surfaces of the diamond anvils in order to provide adequate interface contact. This interface overlap region provides the normal stress σ_{11}, to force the washer material into a plastic domain, and provide the shearing traction σ_{12} required for a liquid seal. Thus. typically the diamond surfaces are circa 1 mm diameter, while the sample hole is about 0.5 mm diameter. The initial thickness of the spacer depends on choice of material but is approximately 0.5 mm.

The procedure for fabricating the spacers is as follows: discs of diameter from 1/4" to 1" were punched out of the material, then placed into the cell between the anvils. Sufficient pressure was applied to leave an impression of the diamond surfaces. With the aid of a binocular microscope, holes of 1/2 mm diameter could be punched by hand at the center of the diamond impression using a dental tool. Alternatively, the spacers were cemented to a block and a high speed steel or carbide circuit board drill were used to drill the 1/2 mm hole.

Several materials were tested to see if they could withstand the high pressures. Liquids used for this test were usually water, benzene or cyclohexane. These were chosen because high pressure crystallization could readily be observed. Thus far the most satisfactory materials for the spacers were

Inconel and stainless steel. These could be used repeatedly with little degradation. Berylium copper was also found to withstand the high pressures, but could not withstand repeated cycling without bursting. An aluminum alloy was tested, but could not withstand the high pressure.

Some nonmetals were also tested. Plexiglass, polymethylmethacrylate, were able to withstand pressures sufficient to freeze cyclohexane even though crazing and cracking developed external to the "sandwiched" region. Epoxy (Eccobond) spacers shattered, and a more flexible Epoxy was unable to contain the high pressures. Mica spacers have not yet been examined. It would be useful to have spacers of transparent material so that the scattered light could also be observed at 90^{o}.

2. Microscopic Measurements

Experimental Results

Several fluids were examined in the high pressure diamond cell under the microscope in order to study the morphological properties and to gain visual experience in the use of the cell. The results for crystal transitions in water, benzene and cyclohexane are shown in the photographs of Figures 2, 3 and 4. The phase diagram of Kennedy and Holser [26], Figure 5, for water provided identification of the pressures at which the phase transitions occur. The lubricant, a perfluoroalkylpolyether, Krytox 143AC (MLO-71-6) was examined in this way; no crystallization was observed, rather the sample underwent a transition to the glassy state.

3. Resolution of the Surface Scattering Problem

The primary technical limitation of the diamond anvil cell for light scattering measurements has been the severe surface scattering at the diamond interfaces. We have successfully resolved this problem by bringing the incident light into one of the side facets of the diamond. The refracted laser beam will then enter and exit the sample area (the hole in the washer) at points on the diamonds that can readily be spatially resolved; hence these image points are readily blocked off by an adjustable aperture. Full discussion of the cell geometry will follow. Fluorescent sodium fluorescein solutions have been utilized to demonstrate this effect visually - the point surface scatters are seen spatially separated from the sample fluoroescence.

Description of Cell Geometry

The geometry of the diamond can be seen in Figures 1 and 2, which show the cross-sectional and top and bottom views, respectively. Notice that the area of the anvil end (gasket end) of the diamonds are smaller than the support end so that the pressure developed in the support will not force plastic deformation of the stainless steel holder.

Limiting examples of refraction at the diamond surfaces are shown in Figure 1. The refractive index of the lubricant is taken to be 1.4, and the indices of diamond and air are 2.42 and 1.0, respectively. Rays pass through the center of the liquid sample (center of the gasket). Thus, in principle, rays incident at 70° with respect to the normal of the major surface, enter the liquid at 42°. By symmetry, the scattered light observed through the second diamond, would appear externally at 140° with respect to the incident beam, and the scattering angle in the liquid would be 84°. For a ray striking a 30° facet (see also facet A of Figure 2), that is at normal incidence to the facet but 30° with respect to. The window axis, the scattered beam could be observed at 60° with respect to incident, and the scattering angle could then be twice 59° or 108° in the liquid. Thus in principle, a range of scattering angles is possible.

In addition to refraction, the diffraction limitation of beam size must also be considered. The laser beam diameter is 1.5 mm, and assuming that we use a 15 cm focal length lens to focus the beam, then the diameter of the beam at the geometrical focal point is given by the Airy diffraction equation

$$d = 2.44 \frac{f\lambda}{D} \tag{6}$$

where d is beam diameter at the geometric focus - called the "waist" diameter, D is the laser beam diameter, f is the focal length and λ is the wavelength of light. Thus the beam diameter would be 100 microns (about 0.005"). This is a small restriction on entrance (and exit) position. The length of the "waist" of the beam is given by

$$\ell = 4.88 \frac{f^2}{D^2} \lambda \tag{7}$$

Thus the beam diameter would be 2.4 cm, sufficiently small and long to make it through the diamonds.

Notice that with this choice of a 15 cm lens, the incident beam is no longer parallel but converges in a core of angle 0.01 radians (0.57°). This becomes the "uncertainty" in the geometrically defined scattering angle.

In practice, the choice of incident beam angle is limited by mechanical constraints. As seen in Figure 3, the diamond must be mounted in a support plate A, which in turn is held in alignment chuck B. The diamond is cemented into a small recess (not shown) in the support plate. The diamond support area, and the thickness of the backing of the support plate must be sufficient to accommodate a few thousand pounds of force without excessive deformation or plastic flow. Hitherto we have used a 1 mm hole through this plate to pass the light beam. This has restricted the angle of incidence to about 10° with respect to the normal.

In the diamond-anvil cell modification that is currently being machined we will slit the support plate, so that a rectangular aperture the <u>full width</u> of the diamond surface will be exposed. We believe that the area of support will remain adequate. Thereby the range of entrance angle for the incident beam will be extended to about 40°. The mechanical obstacle then becomes the configuration of the alignment chuck. This configuration can be changed, but this will be done at a later time.

The alignment chuck B, is seen in cross-section in Figure 3, and in top view in Figure 4. As seen in these figures, there are two screws which protrude from the chuck B to act as pivots for the support plate A. Two additional screws adjust the angle of tilt about the pivot axis and lock the plate to the chuck. The tilt axes of the opposing anvil assemblies are perpendicular. The two anvil assemblies fit into the holder part E of Figure 5. Not shown in this figure is the pressure plate, and the spring and lever assembly by which the pressure is actually applied.

The purpose of these changes is to extend the range of scattering angle, and thereby extend the effective frequency range of the Brillouin light scattering measurements. In addition, these changes will provide greater flexibility in separation of transmitted and scattered beams.

C. MAGNETO-MECHANICAL VISCOMETRY

In order to cover the extensive frequency range of interest in viscoelastic response, techniques must also be developed for measurement of steady state and low frequency dynamic shear viscosity measurements of lubricants at high pressures. Inasmuch as a diamond anvil cell is required to generate pressures in excess of 200,000 psi; the working volume is restricted to a liquid cylinder of 0.5 mm diameter by 0.5 mm long - a volume of 10^{-4} cc. The following technique is being developed here to accommodate viscosity measurement in this small volume: a tiny magnetic sphere, diameter 0.1 mm, is placed into the sample fluid. An external magnetic field is then applied to force steady state or oscillatory motion of the sphere. The motion is then measured by optical means through the diamond windows. This method is analogous to our previous one in which nonmagnetic spheres were subjected to Brownian forces and observed optically. The primary difference is that we will be able to supply the large forces required as the viscosity becomes very high at high pressures. The viscosity η, of the liquid is determined from the Stokes relation

$$F = 6\pi\eta v r \tag{8}$$

where the sphere is known, and the force and velocity must be measured.

In order to quantitatively determine the force F, that will produce a translation, requires an understanding of the interaction between the magnetic sphere and the external field.

The effect of an external magnetic field $\vec{B}$ on an iron sphere is two-fold: (1) The field induces a magnetic polarization $\vec{M}$ into the sphere. The magnitude of the polarization (or dipole moment) $\vec{M} = \vec{M}(\vec{B})$ is a function of $\vec{B}$ and increases with $\vec{B}$ until saturation. (2) The force acting on a magnetic dipole is proportional to the spatial gradient of magnetic field. Thus the force can be written as

$$\vec{F} = a\vec{M}(\vec{B})\ \nabla\vec{B} \tag{9a}$$

or considering only the x-direction

$$F_x = a\vec{M}(\vec{B})\ \frac{\partial B_x(x)}{\partial x} \tag{9b}$$

This nonlinear relationship is only meaningful provided the field generated by the sphere can be neglected. For example, the sphere should not come close to

another magnetic material such as the pole of the main magnet. Equation (2.1) is not only nonlinear but $\vec{M}(\vec{B})$ will exhibit magnetic hysteresis. To resolve these considerations and still obtain the maximum force F_x, one should make B large enough so that M approaches its saturation (maximum) value, and where it is least sensitive to changes in B. Thus in a region where the magnetic field is described by

$$B(x) = B_o + \frac{\partial B(x)}{\partial x} \Delta x \tag{10}$$

we then approximate

$$M(B) = M\left(B_o + \frac{\partial B}{\partial x} \Delta x\right) \approx M(B_o) \tag{11}$$

and Eq. (9b) becomes

$$F_x(t) = aM(B_o) \left.\frac{\partial B(x,t)}{\partial x}\right|_{x=x_o} \tag{12}$$

Under these conditions the force would become a linear function of the gradient $\left.\frac{\partial B(x,t)}{\partial x}\right|_{x=x_o}$; this gradient could then be made a time varying function.

In order to test the range of validity of Eq. (12) and obtain an estimate of the forces that can be developed, the experimental arrangement shown in Figure 1 was employed. A small iron sphere of diameter 0.1 mm was used as a test probe in a plastic cell filled with oil. Motion was observed with a telemicroscope. The magnetic field B_o, between the poles of a large electromagnet, could be set to various strengths by adjusting the current i_o. The gradient $\frac{\partial B}{\partial x}$ could be adjusted by the current i, through a small coil fixed near one pole piece. The gradient between pole pieces was not uniform, and the first objective was to determine the dependence of the gradient as a function of position. This is accomplished by finding the current through the gradient coil required to "just lift" the sphere at each position. Lift-off corresponds to a force = mg, m is the mass of the sphere.

The test procedure worked well and the experimental results are tabulated in Table 1 and presented graphically in Figures 2 and 3. The procedure was to position the cell with the sphere a measured distance above the lower pole piece, to set the current through the electromagnet to the desired fixed values of

magnetic field B_o. The field strength is approximately 500 gauss per ampere of current through the electromagnetic. The pole pieces were 3" diameter and 1" gap. Next, the current was adjusted until the iron sphere lifted off the surface of the cell as observed with the telemicroscope. Scatter in the lift-off current is primarily due to irregularities of the cell-sphere interface associated with this crude test cell.

One restriction imposed by our test apparatus was that we were unable to traverse the full magnet gap. Because of the physical restrictions introduced by the cell and the gradient coil instead of the full range of 0 to 1", we were only able to traverse the range 0.125" to 0.5"; hence our conclusions apply only to this range.

The first conclusion can be drawn from Figure 32. That is, the static field B_o, should be greater than 14 amperes, that is, 7000 gauss, to bring the iron spheres tested here into a saturated condition where the linearized Eq. (12) becomes applicable.

The second conclusion can be drawn from Figure 33. Over the range of position 0.12" to 0.5", the gradient $\frac{\partial B}{\partial x}$ is not independent of x, but has the smallest variation at the position 0.5".

The third conclusion from Figure 33 is that at the same position of minimum slope in the gradient, the magnitude of the gradient is greatest, that is, the least current is required for lift-off. Inasmuch as about 20 ma through the gradient coil is required for lift-off, as seen in Figure 33, and we are able to pass more than 300 ma without heating, the force that we can generate is about 15 times gravity.

We have also explored a variety of colloidal magnetic particles and tiny iron spheres for use in the high pressure cell dynamic viscosity technique. The colloidal suspensions compatible with the lubricants to be studied have shown a tendency to aggregate. The tiny iron spheres seem to work well in the lubricants. These were available from Whittaker Corporation in 250 μ and 50 μ diameters, suitable for our experiments. They can be individually handled. We are testing a variety of magnetic field drive geometries.

TABLE 2

LIFT-OFF CURRENT THROUGH GRADIENT COIL

Position Inches	Current Setting of Electromagnet							
	2.5 A	5.0 A	7.5 A	10 A	12.5 A	15	17.5	20
.125	-	-	-	-	83	69	72	61
.150	-	-	-	-	61	60	50	48
.175	-	-	99	74	53	51	46	39
.200	-	-	79	72	48	43	38	32
.225	-	-	77	58	43	43	34	31
.250	-	90	64	57	38	32	34	28
.275	-	83	60	44	35	31	24	25
.300	-	74	51	42	31	28	29	24
.325	-	69	51	39	28	26	21	21
.350	-	68	43	34	27	25	19	19
.375	-	57	42	32	23	21	19	21
.400	100	54	40	29	23	19	17	17
.425	99	51	39	25	21	19	16	17
.450	90	54	37	29	20	17	16	16
.475	87	49	33	25	19	17	18	18
.500	84	47	33	25	18	19	20	18

D. ULTRASONIC SHEAR WAVE APPARATUS

1. Description of Apparatus and Results

There are several atmospheric pressure reference state measurements that are required for proper interpretation of higher pressure data. One of the more important is the high frequency limiting shear viscosity and modulus (transverse wave) and relaxation time(s). Steady-state shear viscosity (low frequency limit) data is available for the test fluids, however, the directly measured high frequency limiting shear modulus appears to be lacking. Since Brillouin scattering from shear waves is difficult to observe, the high frequency limit G'_∞ and η'_∞ must be calculated from the longitudinal modulus with some assumptions. Therefore, we assembled auxiliary ultrasonic delay line apparatus [27,28] for direct measurement of G' and η' even though it is only useful at 1 atmospheric pressure. This apparatus has been calibrated in the frequency range 2 to 50 MHz and over a temperature range from $-10^\circ C$ to $+70^\circ C$. Thus this apparatus serves two purposes: (i) to provide the high frequency shear moduli and relaxation times mentioned above for bulk lubricants and (ii) to provide the limiting shear relaxational behavior for lubricants with polymer additives (i.e., a measure of the configurational relaxation contribution of the polymer additive).

This apparatus has been constructed, tested, calibrated, and we are now in the process of measuring Krytox 143.

Calibration curves have been obtained for several fluids which we believe to be Newtonian up through the frequencies of interest.

Preliminary results have also been obtained on solutions of polystyrene in a di-2-ethyl-hexyl phthlate fluid. These results are relevant to the role of polymer additives, and indicate that at high frequencies the viscosity of the solution does not become that of the solvent. Namely, theory has assumed that when conformational relaxation of the polymer has been "frozen out", then only the viscosity of the solvent would remain. This picture is incomplete. Extensive data and analysis of this phenomenon, called the η_∞ problem, together with apparatus description and calibration are detailed in Appendix B.

2. Relevance to Lubricants

The aforementioned results led us to a very important conclusion as to the roles of the polymer additive in a lubricant. Addition of the polymer, naturally, enhances the viscosity, but the mechanism of enhancement may be through the traditionally accepted "backbone conformation relaxation", or alternately may be through interaction with the lubricant (solvent) such as to increase the solvent orientation relaxation time, and thereby the viscosity. While these two mechanisms are indistinguishable in steady state viscosity measurements, the effectiveness of the additive can be dramatically different in a high-speed lubrication situation. The apparent viscosity enhancement due to the polymer additive operating by the first mechanism will disappear at high speeds (frequency), whereas the contribution of the additive operative by the second mechanism will be maintained at high speeds.

Clearly this represents a new criterion for characterization and evaluation of polymer additives.

E. CAPILLARY TUBE VISCOMETRY

We have also measured the temperature dependence of viscosity and density of the test sample MLO-71-6 at atmospheric pressure, in contrast to the pressure dependent measurements of Cameron [29] and Winer [30,31]. The viscosity data has been plotted as log η vs. $\frac{1}{T - T_o}$, where the value T_o was determined so as to linearize the plot. The temperature T_o was found to be -120°C. On the basis of free volume concepts, this is the temperature at which free volume disappears, and viscosity becomes infinite. Extrapolation of the curve to a "glassy" viscosity of 10^{12} poise, would place the glass transition temperature at -80°C. These data only extend down to -33°, the lower limit of the bath; our revised dewar set-up is now capable of temperatures down to -70°C.

TABLE 3

FLUID: MLO-71-6

COMPOSITION: PERFLUOROALKYL POLYETHER

PRESSURE: 1 ATMOSPHERE

Temperature °C	Viscosity (Poises)	Density g/cc
25°	11.96	1.89
20°	16.60	1.90
15°	23.53	1.90
10°	34.47	1.91
* 25.0	11.43	1.90
* 37.8	5.33	1.88
* 98.9	.488	1.78
* 148.9	.160	1.69

* This data has been supplied by Mr. F.C. Brooks of the Air Force Materials Laboratory, but not on the identical sample.

TABLE 4

FLUID: ATL-5066
(Emery 2958)

COMPOSITION: DI-2-ETHYLHEXYL AZELATE

PRESSURE: 1 ATMOSPHERE

Temperature °C	Viscosity (Poises)	Density g/cc
25°	.156	0.908
20°	.189	0.911
15°	.232	0.915
10°	.287	0.918

TABLE 5

FLUID: ATL-5067
(Stauffer 704)

COMPOSITION: TRI-METHYLOL PROPANE TRIHEPTANOATE

PRESSURE: 1 ATMOSPHERE

Temperature °C	Viscosity (Poises)	Density g/cc
25°	.239	.958
20°	.286	.959
15°	.355	.962
10°	.449	.963

SECTION III

CONCLUSIONS

1. Separately, the technical problems concerning the diamond anvil cell and the Fabry-Perot optics have been solved and tested; we are now prepared to couple the two. But we still feel that the development of the Diamond Light Scattering Apparatus will provide an optimum and unique facility whereby extensive data about the phenomenological and molecular properties of the lubricant can be obtained under laboratory conditions that come closest to stimulation of actual EHD bearing lubrication.

2. The utilization of colloidal spheres for measurement of viscosity at high pressures by technique of quasi-elastic light scattering has been demonstrated as in the revised manuscript of Appendix A.

3. An initial study for utilization of single magnetic spheres for steady state and dynamic measurements has been completed.

4. A high frequency ultrasonic shear apparatus has been completed, tested and utilized to study the role of additives.

5. A new criterion for characterizing and understanding the role of additives to high speed lubricants has been proposed based on the above results.

6. Steady-state reference data on the test fluids are reported.

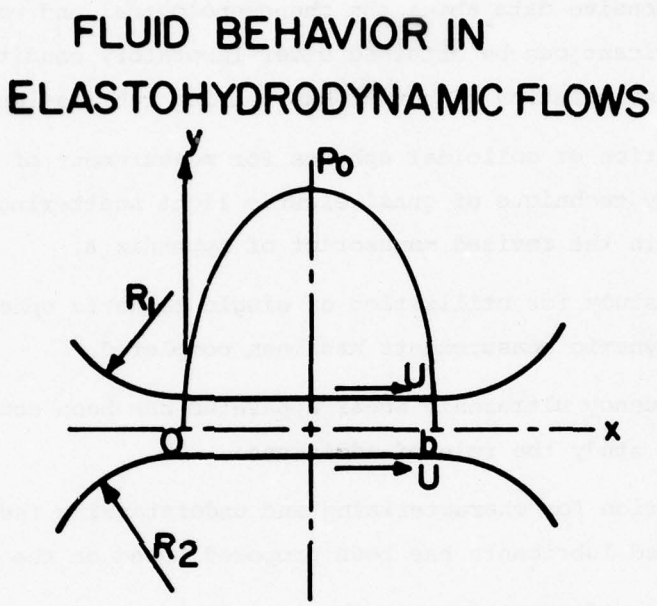

Figure 1(a) Stress/Deformation History in the EHD Problem (Contact Zone)

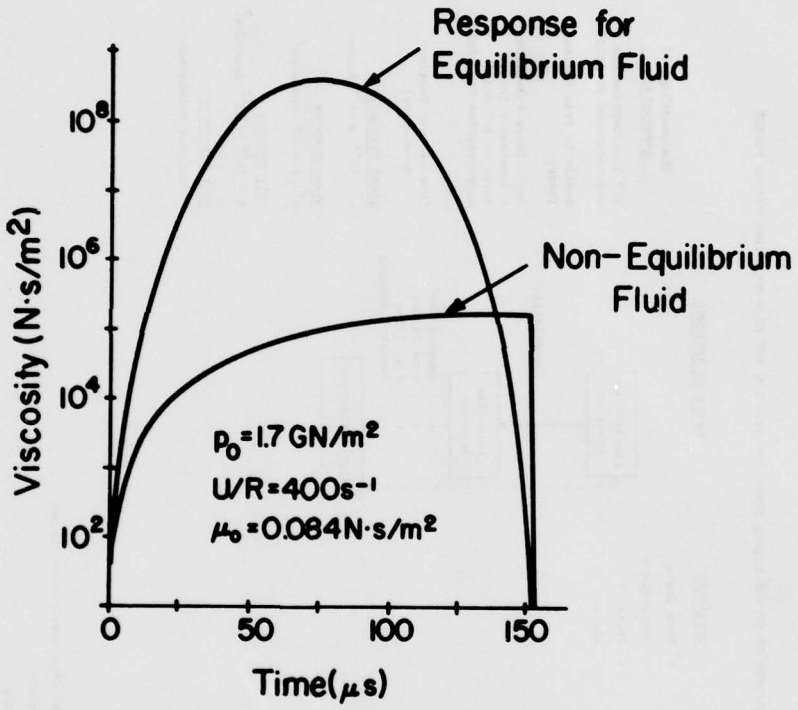

Figure 1(b) Stress/Deformation History in the EHD Problem

PROPERTIES OF THE LIQUID STATE FOR BOTH LOW AND HIGH MOLECULAR WEIGHT FLUIDS

*EXPERIMENTAL TECHNIQUES**

I. Wide Frequency Range Viscoelastic for Mechanical Relaxation Spectroscopy:

- ◒ Magnetic Suspension Viscometer DC → 10^3Hz
- ● Multiple Lumped Resonator 50 - 5000Hz
- ● Mason Torsion Crystals 20 - 200KHz
- ● Torsional Wire Delay Line 500KHz - 4MHz
- ◒ Meitzler Mode Surface Delay Line 0.5 - 50MHz
- ● Bragg Diffraction Cell (Bulk Modulus) 0.5 - 50MHz

II. Laser Light Scattering Techniques for Optical Relaxation Spectroscopy:

- ● Rayleigh Scattering (Quasi-elastic Light Scattering)
- ● High Pressure Cell for Scattering - Includes High Pressure Viscosity by Diffusion of Spheres
- ◒ Brillouin Scattering
- ○ Depolarized Scattering
- ○ Rayleigh Wing Scattering

VARIABLES

- Time Scale
- Temperature
- Pressure
- History

MATERIAL RESPONSE

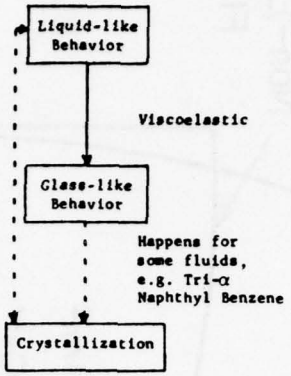

NEEDS

Phenomenological Description

WLF Time/Temperature Superposition Principle

Doolittle Free Volume Theory

Basic Three-dimensional Viscoelastic Theory Based on Boltzmann Superposition Principle

[Macroscopic Physical Parameters]

Shear Viscosity
η: $10^{-1} \rightarrow 10^{12}$ poises

Shear Modulus
G: $0 \rightarrow 10^{11}$ dynes/cm^2

Bulk Modulus
B: $10^{10} \rightarrow 10^{12}$ dynes/cm^2

Bulk Viscosity

Structural Relaxation

Microscopic Model Interpretation

Relevant Molecular Theories:

- Free Volume Theory
- Gibbs Statistical Model
- Turnbull
- Landau-Placzek
- Rouse/Zimm/Kirwood/Fixman
- Zwanzig
- Litovitz
- *Fluery*

*All of above interface existing on-line computer data acquisition system.

● Currently available in Viscoelasticity Laboratory.

◒ Under development in Viscoelasticity Laboratory.

○ Proposed acquisition to Viscoelasticity Laboratory.

Figure 2 Survey of Properties of the Liquid State

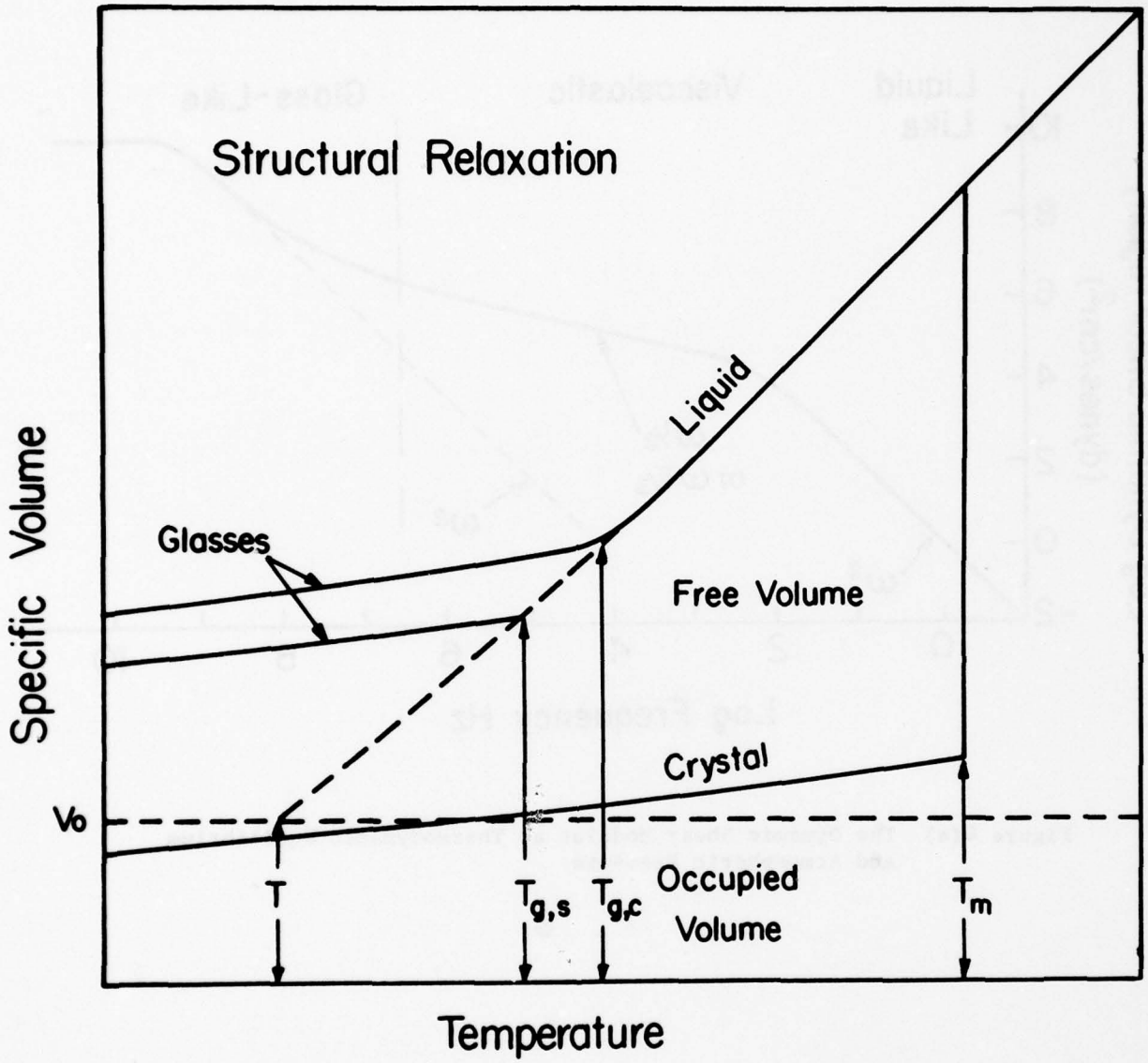

Figure 3 The Volume-Temperature Curves with Reference to: Equilibrium, Nonequilibrium, Glass/Liquid to Glass Transition

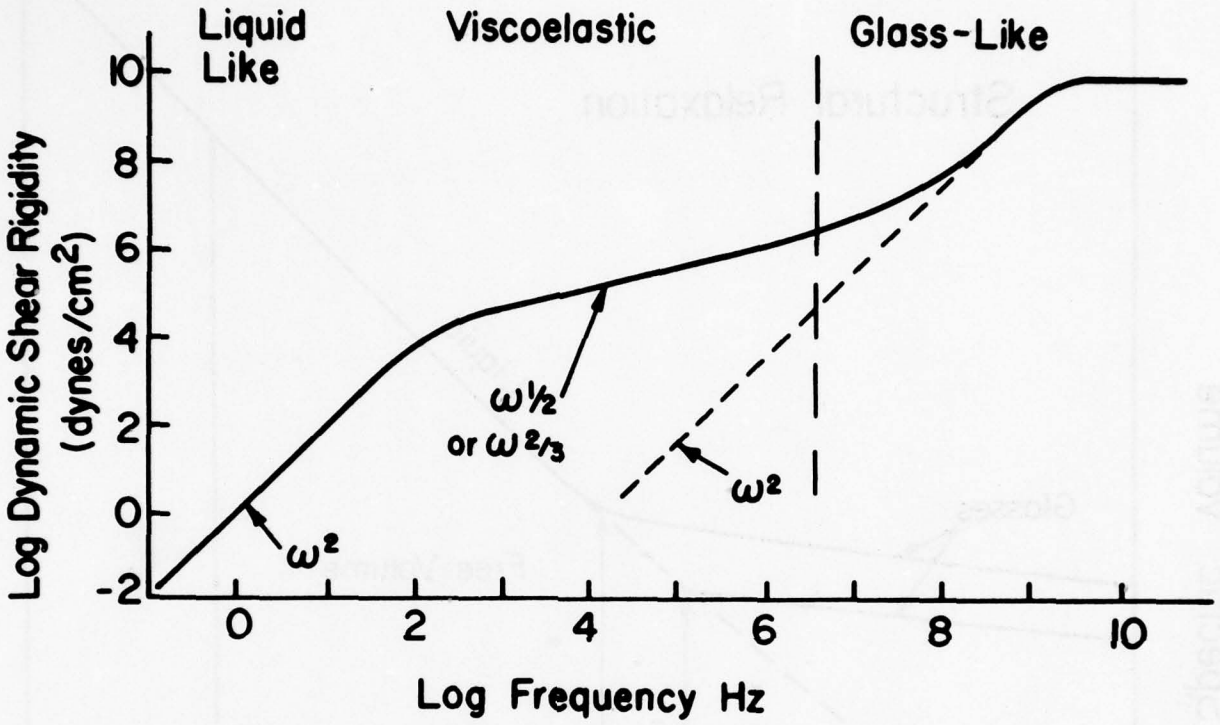

Figure 4(a) The Dynamic Shear Modulus at Thermodynamic Equilibrium and Atmospheric Pressure

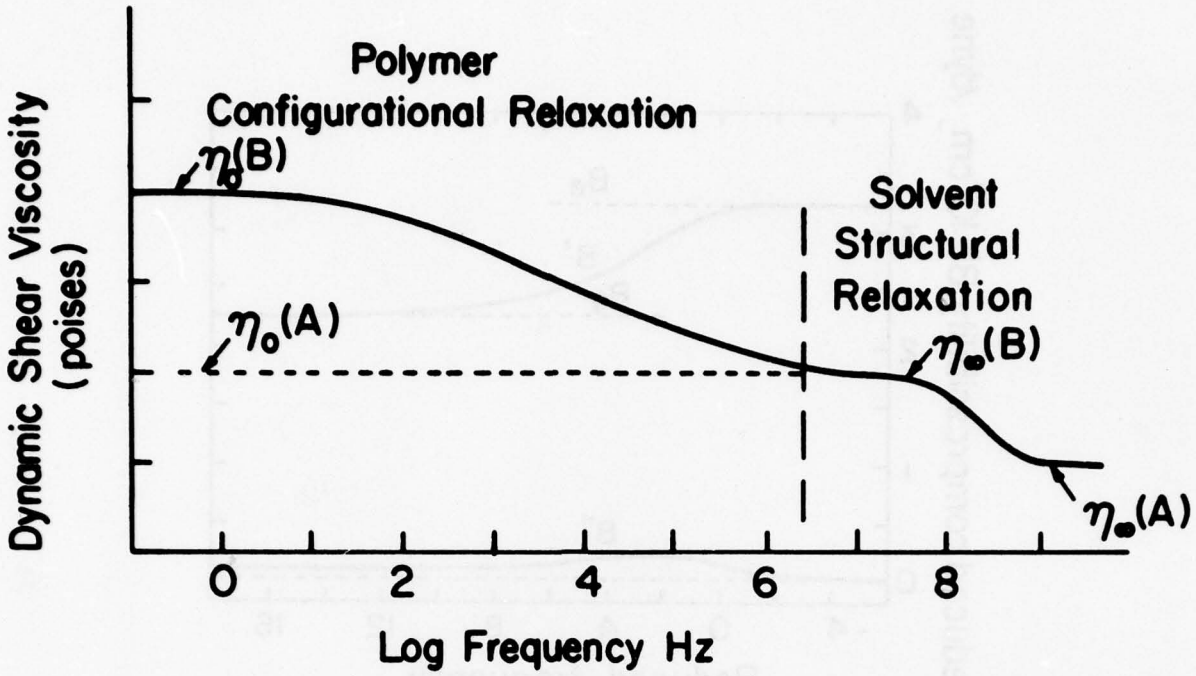

Figure 4(b) The Dynamic Shear Viscosity at Thermodynamic Equilibrium and Atmospheric Pressure

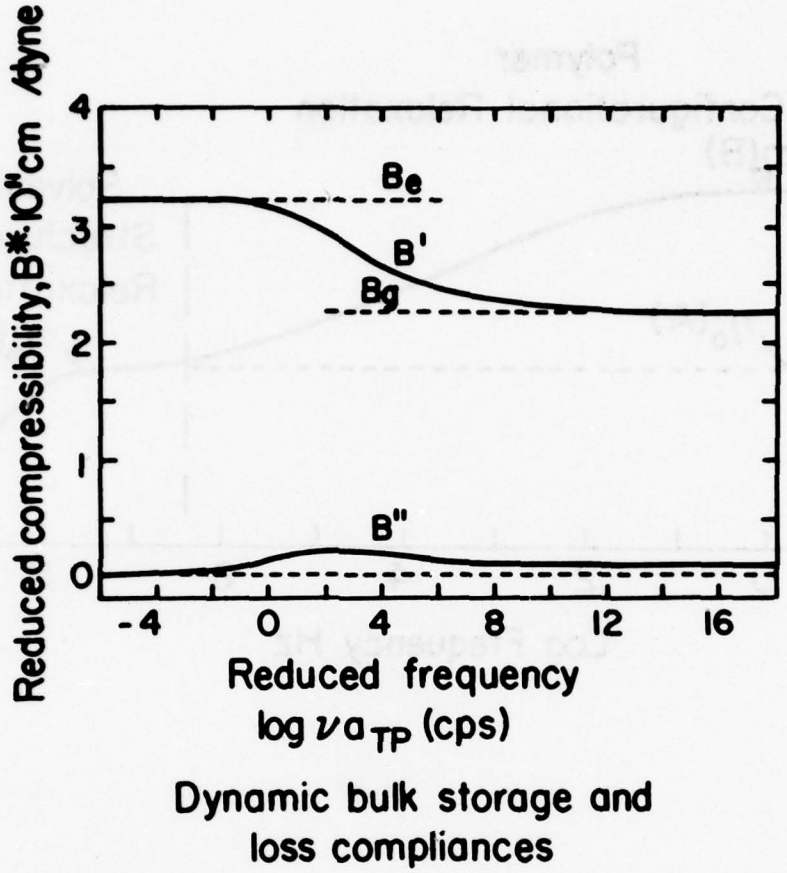

Figure 5(a) The Dynamic Compressibility: Viscosity and Modulus

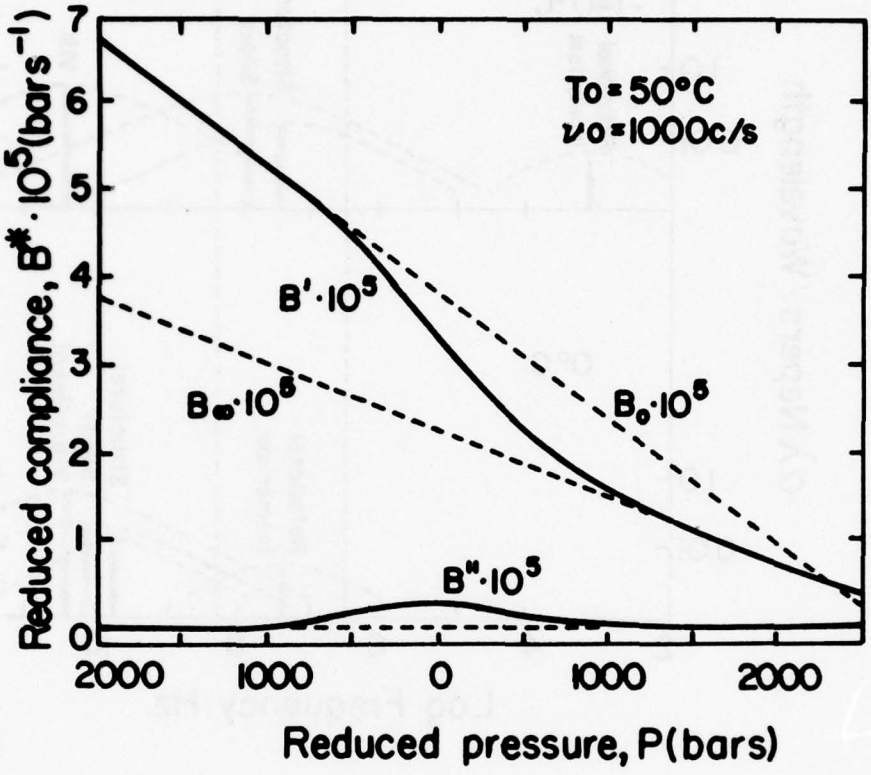

Figure 5(b) The Dynamic Compressibility: Viscosity and Modulus

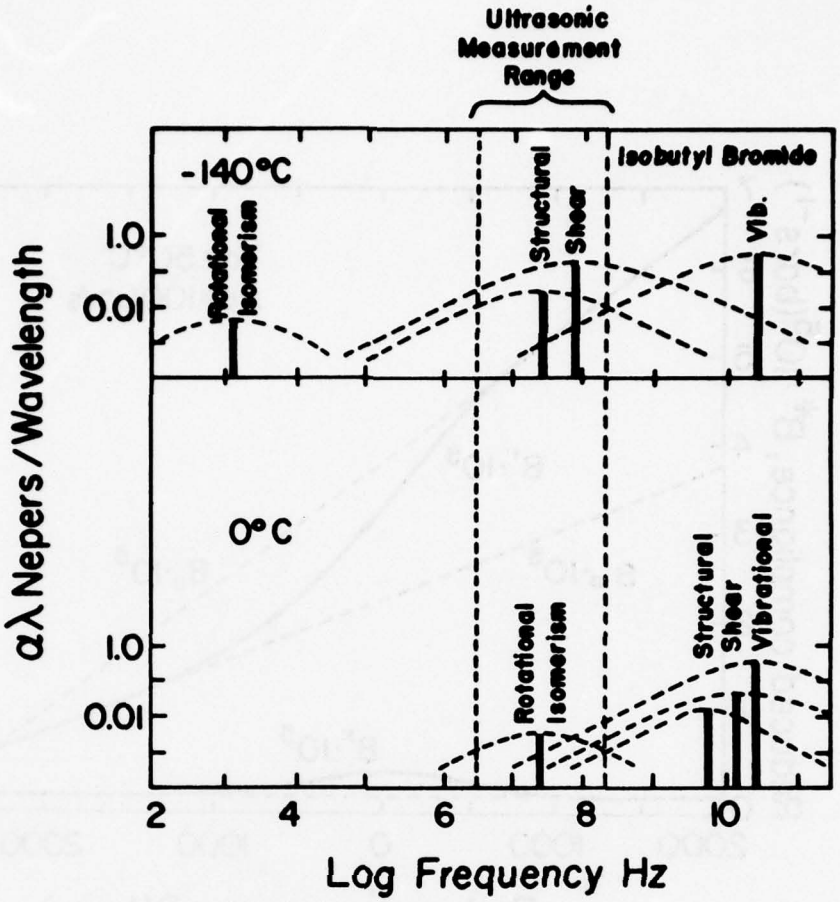

Figure 6 Summary of Mechanical Relaxation Spectra

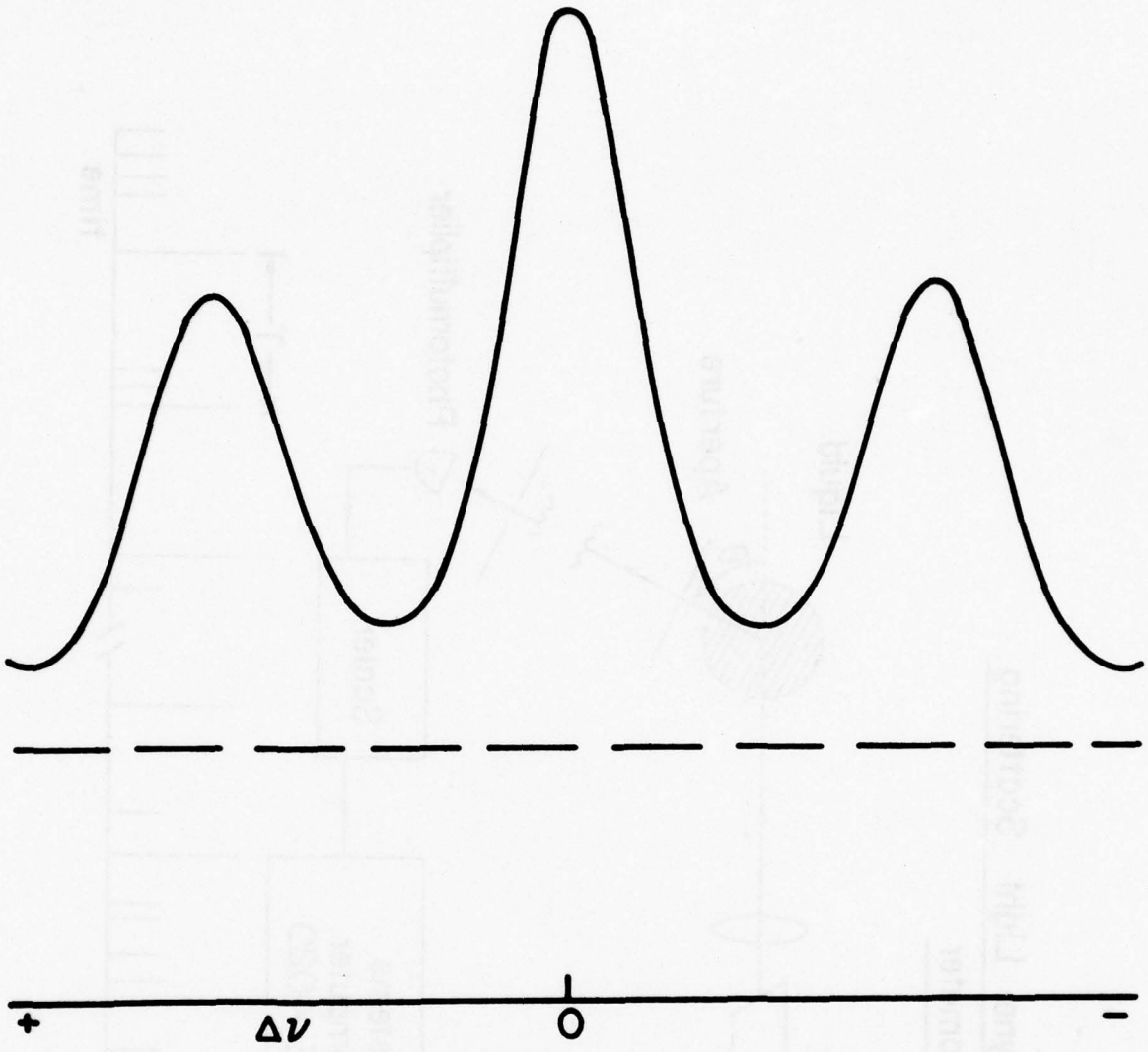

Figure 7 Light Scattering Spectrum with Rayleigh (Central and Brillouin Peaks for Benzene

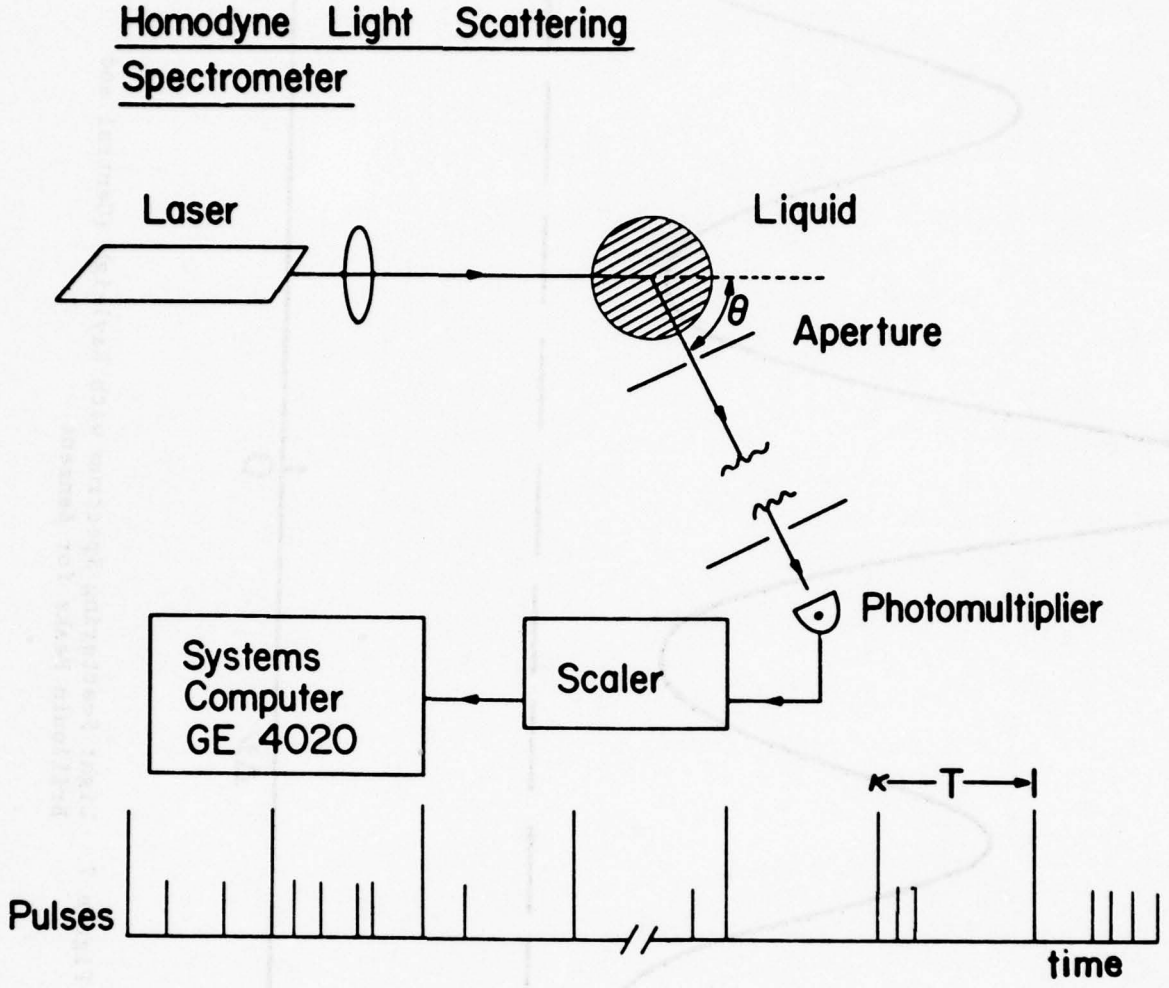

Figure 8 Light Scattering Apparatus

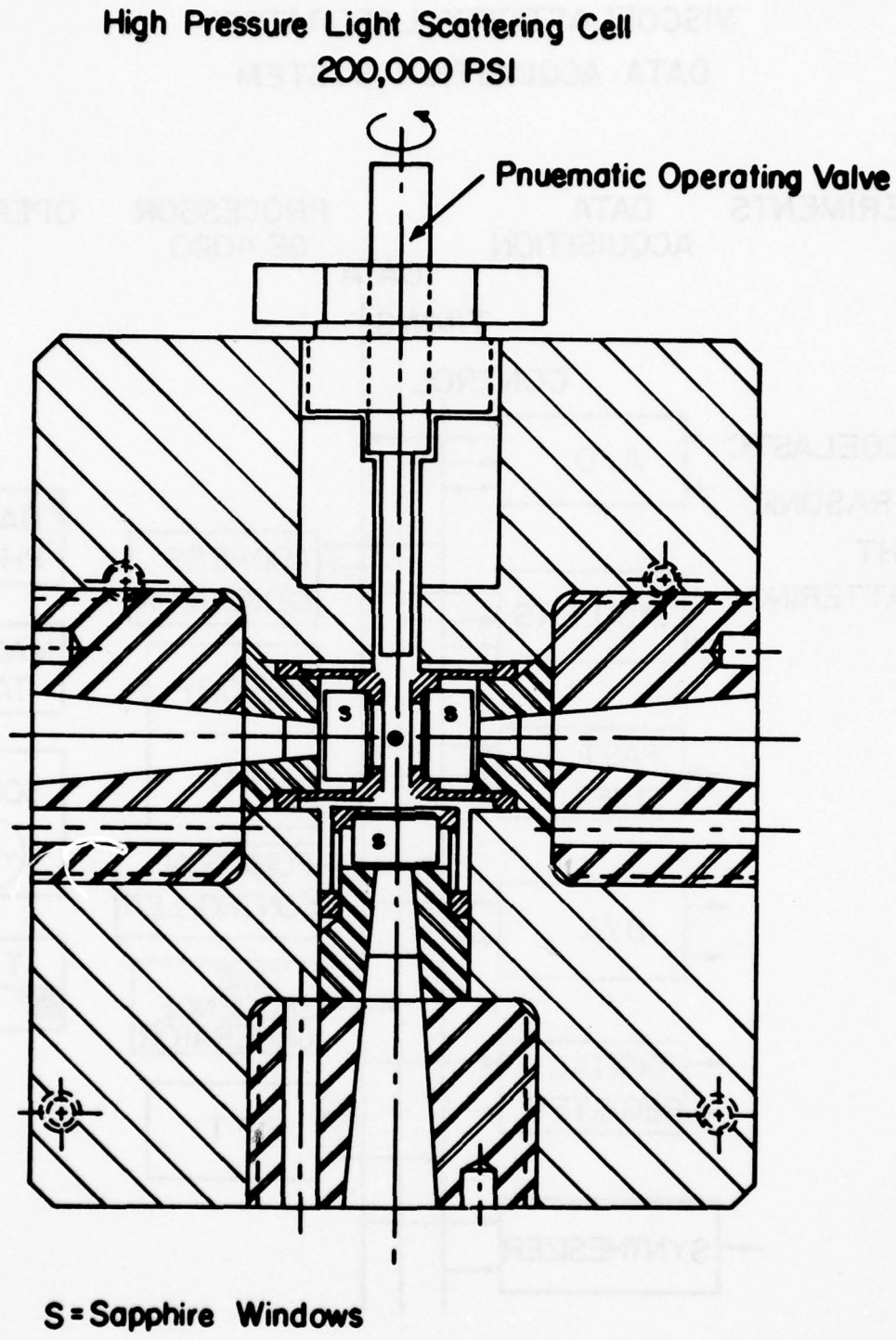

Figure 9 The New High Pressure Cell

VISCOELASTICITY LABORATORY
DATA ACQUISITION SYSTEM

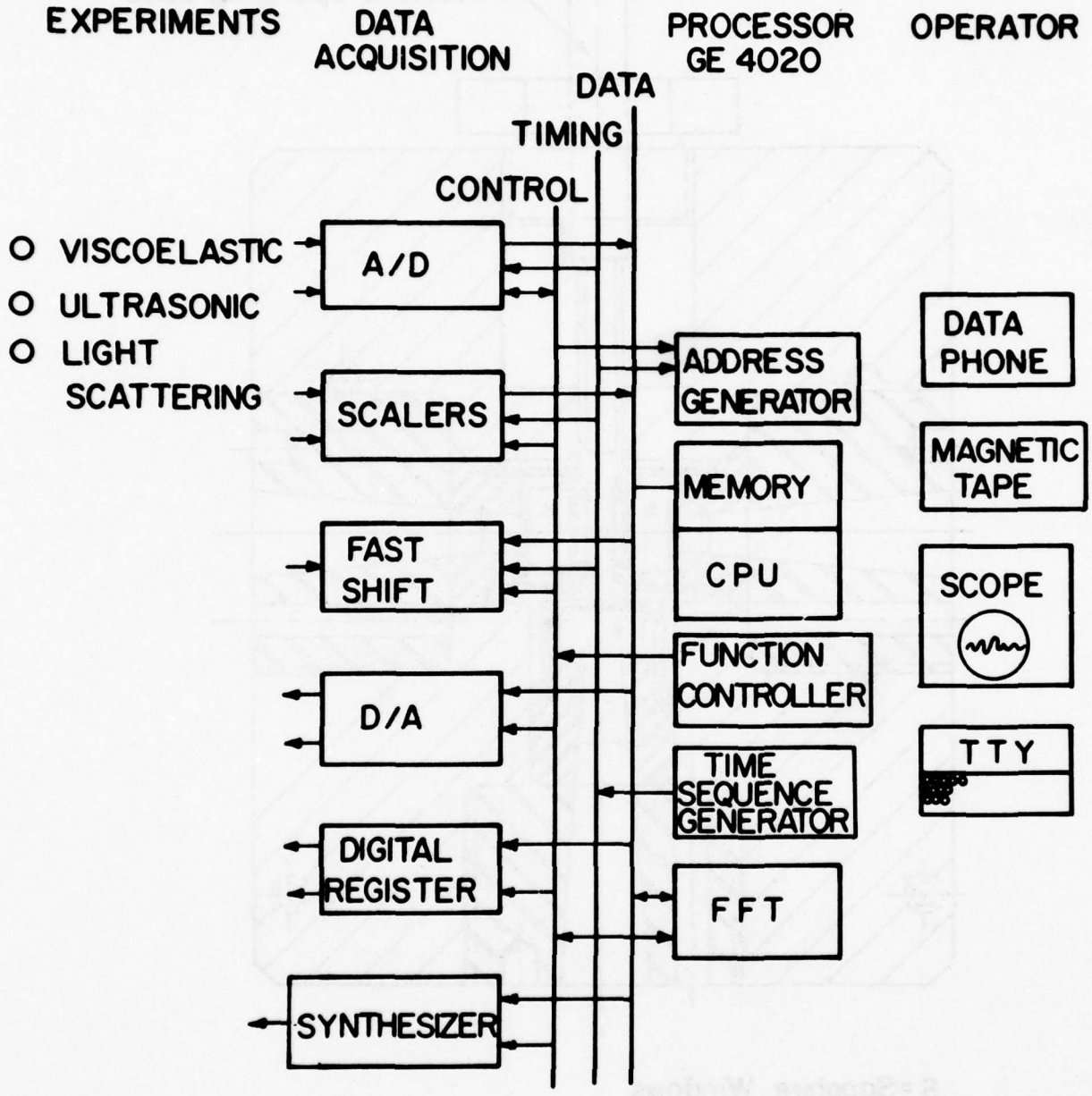

Figure 10 Viscoelasticity/Light Scattering Data Acquisition System

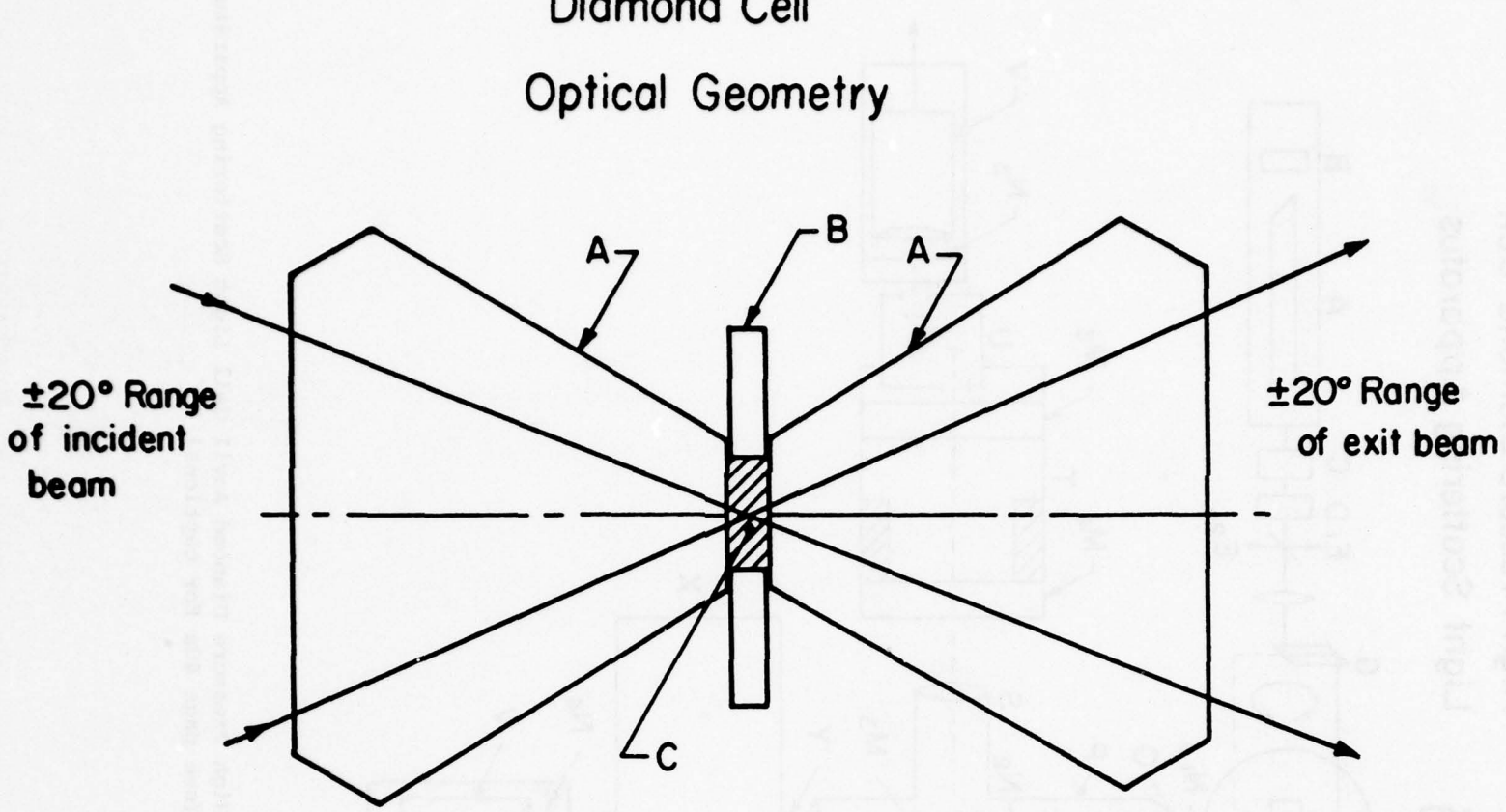

Figure 11 Diamond Cell Optics
A - Diamonds; B - Spacer; C - Liquid Sample
Note that refraction corrections have been neglected

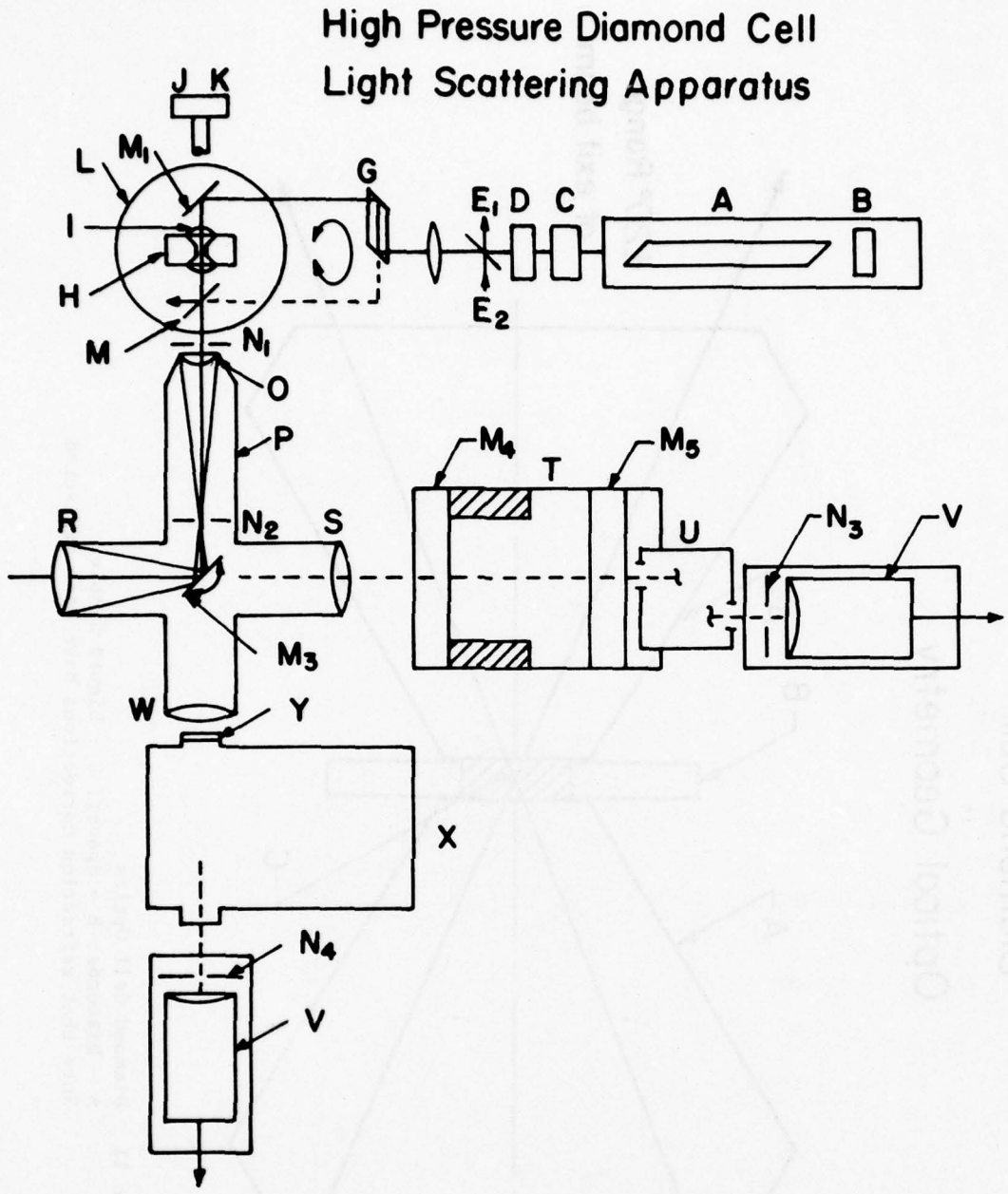

Figure 12 High Pressure Diamond Anvil Cell Light Scattering Apparatus
(see page 40a for captions)

Figure 12 - Captions

A - Argon ion laser, B - Single frequency etalon, C - Polarization rotator, D - Spatial filter, E - Partial (5%) reflector - for beam intensity monitor or alternately E_2 entrance point for HeNe (red) laser (second source), F - Lens to focus beam into "waist" diameter of 50 microns, G - Prism. Rotate 180° to displace beam from "forward to backward scattering" illumination, H - Diamond anvil cell, I - Cell clamp with cell orientation adjustment, J - Pressure adjustment screw (only partly shown), K - Pneumatic impact relay, (not shown), L - Primary goniometer to adjust scattering angle, M_1 - Mirror for beam steering in forward scattering regime, M_2 - Partially reflecting mirror for beam steering in back scattering regime, N - Adjustable slits or apertures, O - Microscope objective, P - Three port microscope body attached to Table L, M_3 - Rotatable and removable mirror for beam steering to R, S; R - Eyepiece or Vidicon port, S - Lens, T - Piezoelectrically driven Fabry Perot interferometer of adjustable free spectral range, U - Multipass corner cube reflector and an Iodine filter (not indicated), V - Photomultiplier, W - Lens, X - Double grating spectrometer, Y - Filter for fluorescence.

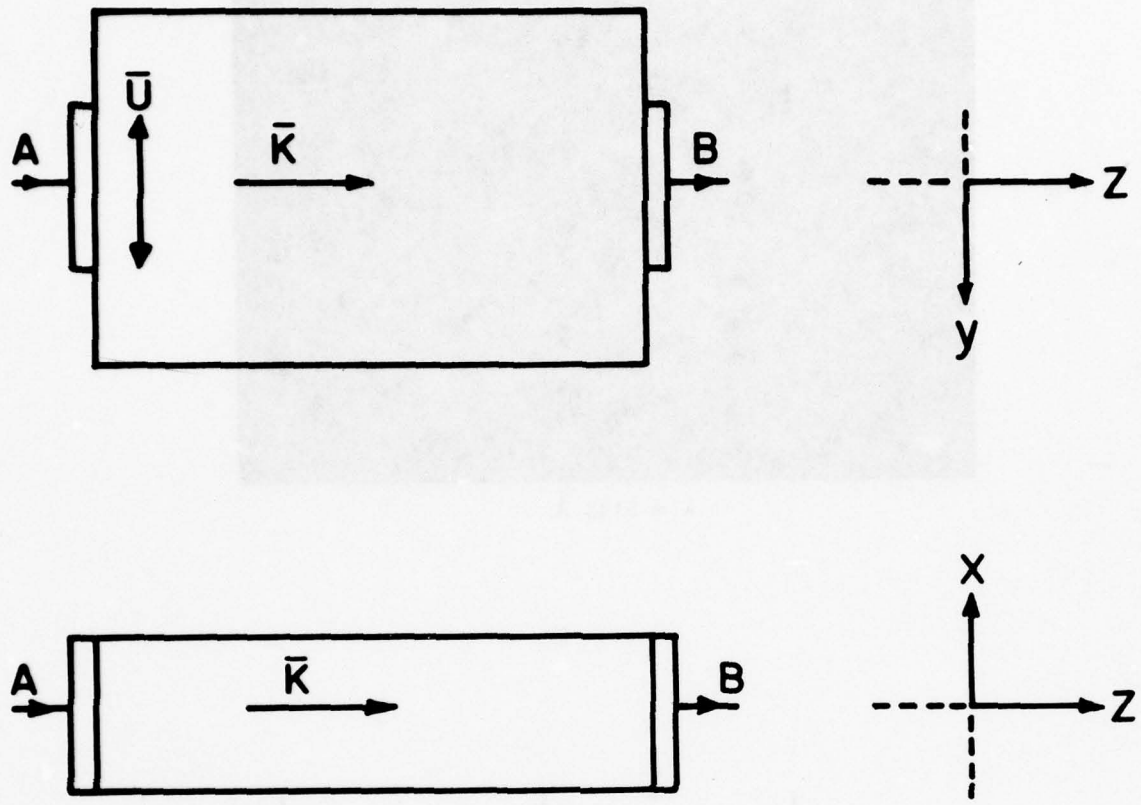

Figure 13 Delay Line

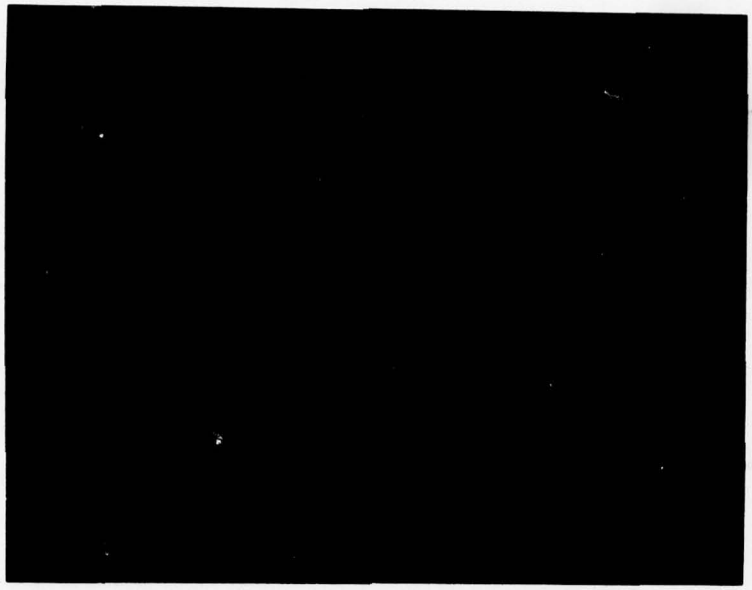

λ = 5145 Å

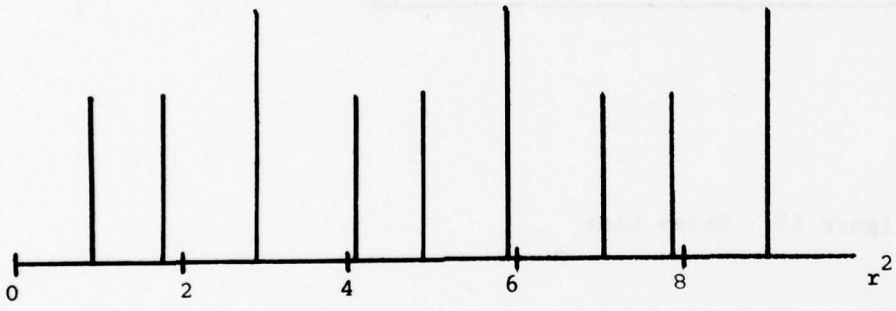

λ = 5145 Å

Figure 14 Brillouin Scattering from Benzene at 90°.
d = 1.545 cms

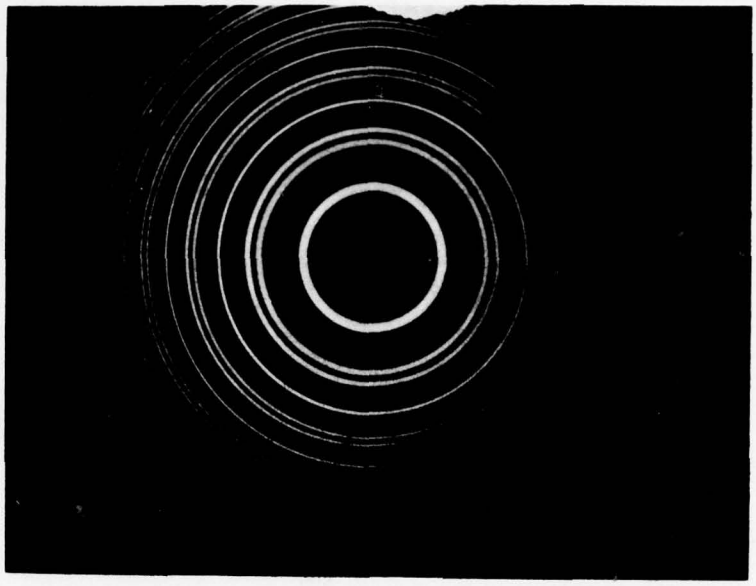

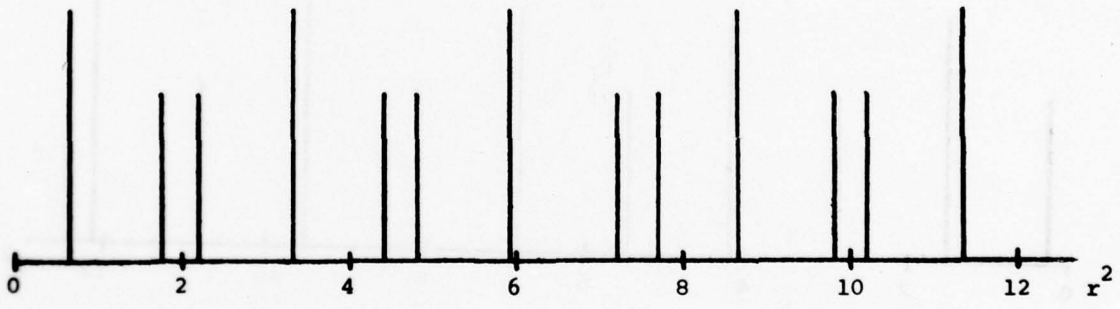

Figure 15 Brillouin Scattering by Photographic Method from Methanol at Scattering Angle $\theta = 90^{\circ}$, Temperature 22°C, Laser Wavelength 5145 Å. Free spectral range 9.68 GHz. The spectral order is identified by symbol M.

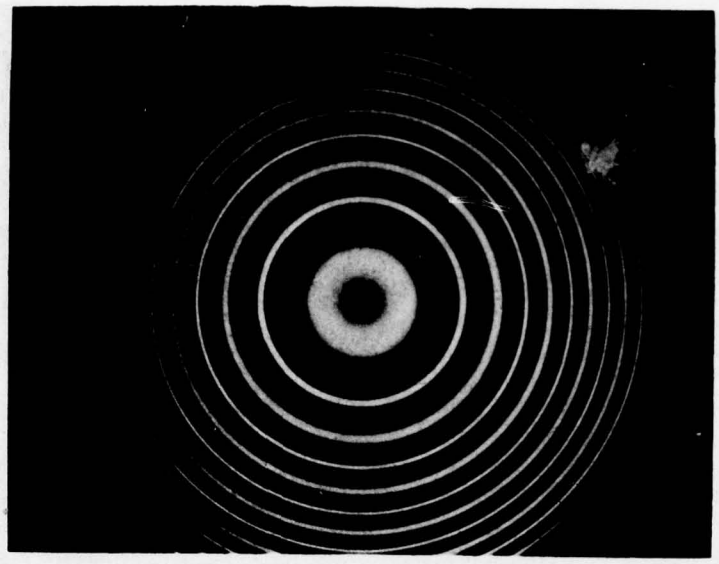

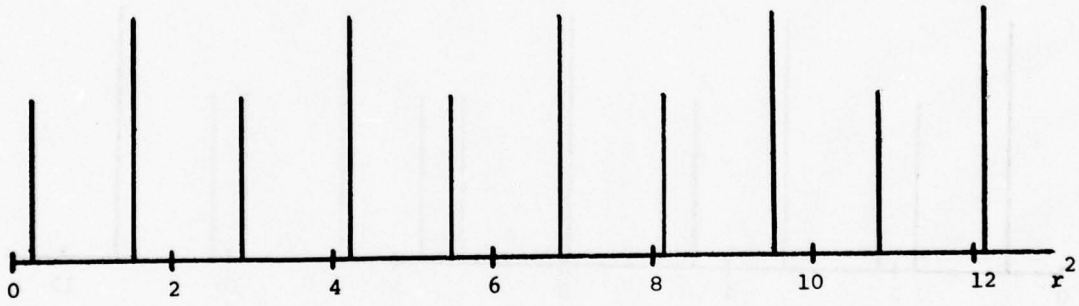

Figure 16 Brillouin Scattering by Photographic Method from Ethanol at Scattering Angle $\theta = 90^{\circ}$, Temperature $22^{\circ}C$, Laser Wavelength 4880 Å. Free spectral range 9.68 GHz. The spectral order is identified by symbol M.

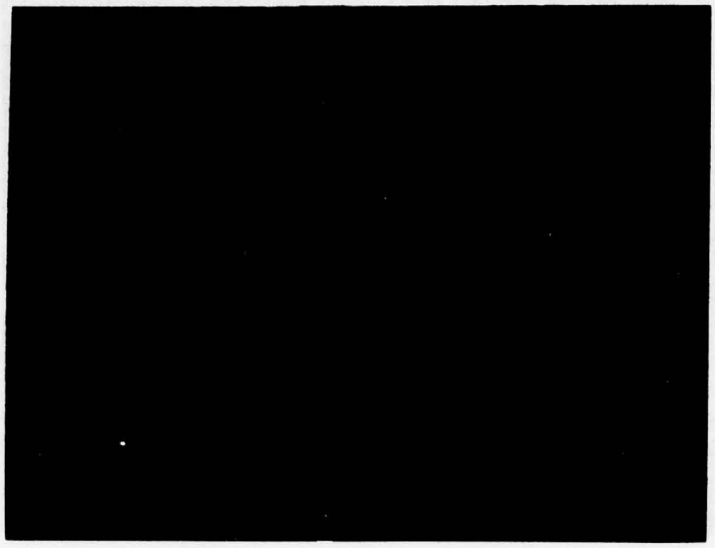

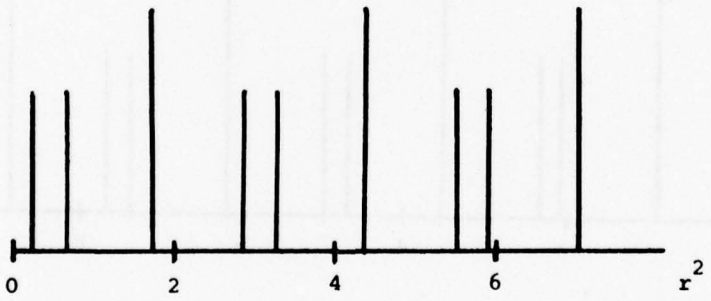

Figure 17 Brillouin Scattering by Photographic Method from Cyclohexane at Scattering Angle $\theta = 90^{\circ}$, Temperature 22°C, Laser Wavelength 4880 Å. Free spectral range 9.68 GHz. The spectral order is identified by symbol M.

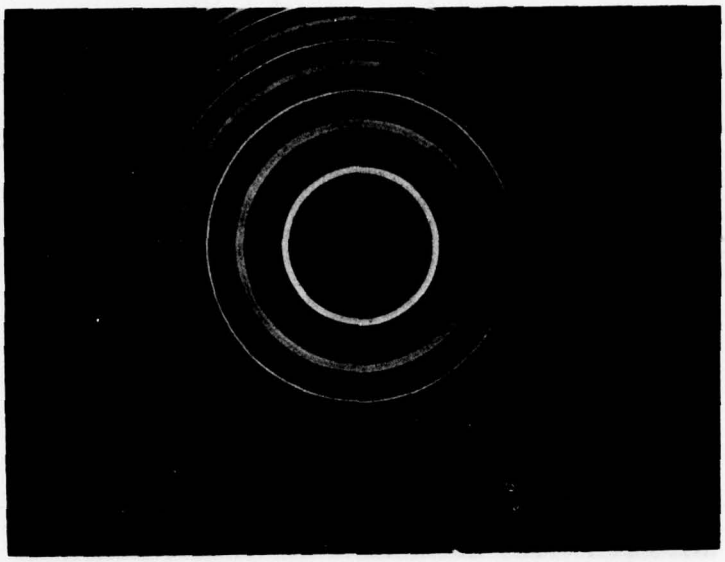

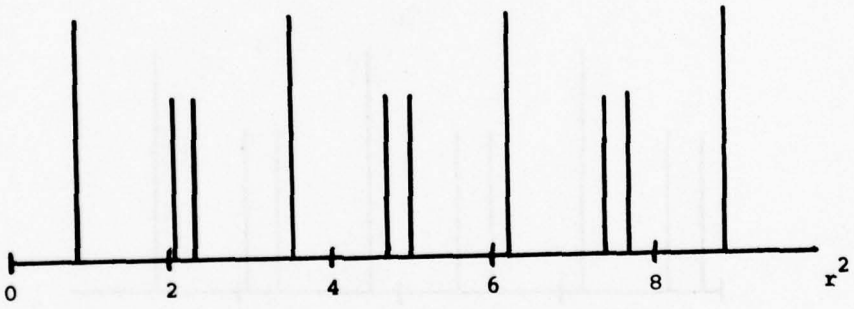

Figure 18 Brillouin Scattering by Photographic Method from Acetone at Scattering Angle $\theta = 90^{\circ}$, Temperature 22°C, Laser Wavelength 5145 Å. Free spectral range 9.68 GHz. The spectral order is identified by symbol M.

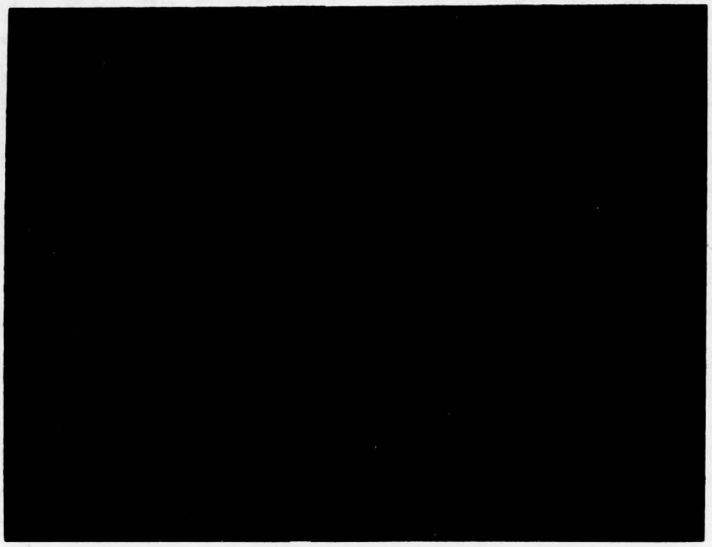

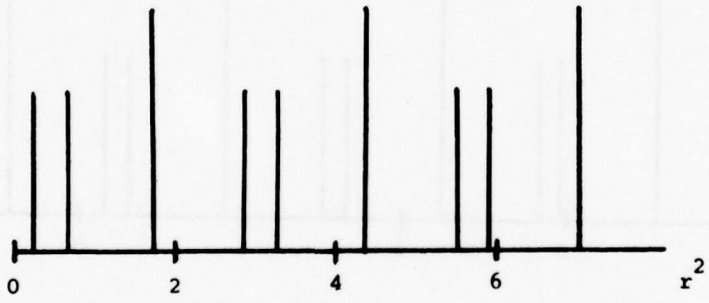

Figure 17 Brillouin Scattering by Photographic Method from Cyclohexane at Scattering Angle $\theta = 90^{\circ}$, Temperature $22^{\circ}C$, Laser Wavelength 4880 Å. Free spectral range 9.68 GHz. The spectral order is identified by symbol M.

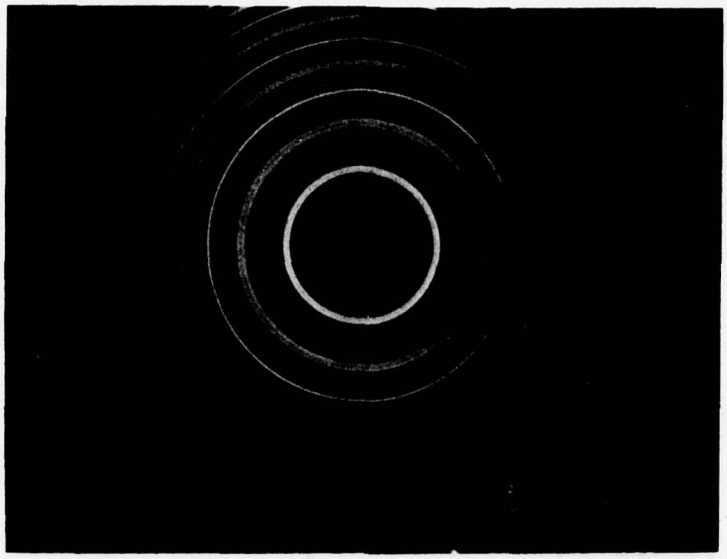

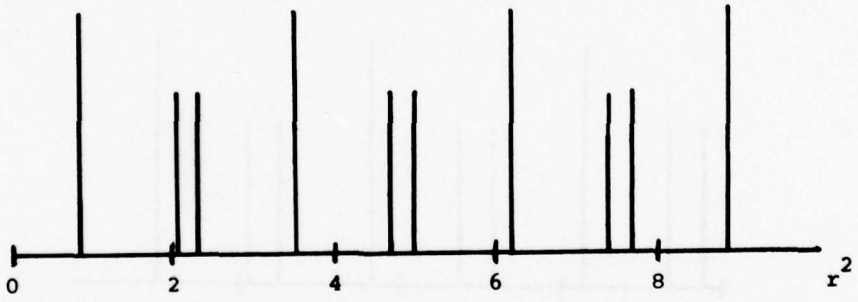

Figure 18 Brillouin Scattering by Photographic Method from Acetone at Scattering Angle $\theta = 90^{\circ}$, Temperature $22^{\circ}C$, Laser Wavelength 5145 Å. Free spectral range 9.68 GHz. The spectral order is identified by symbol M.

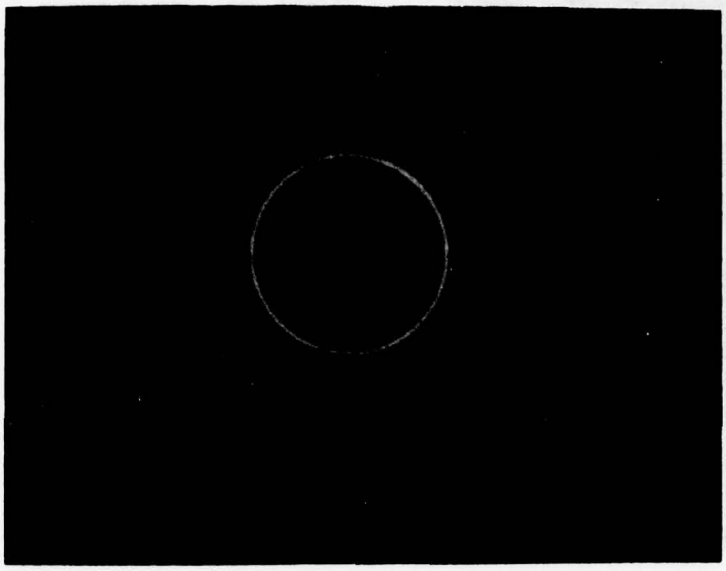

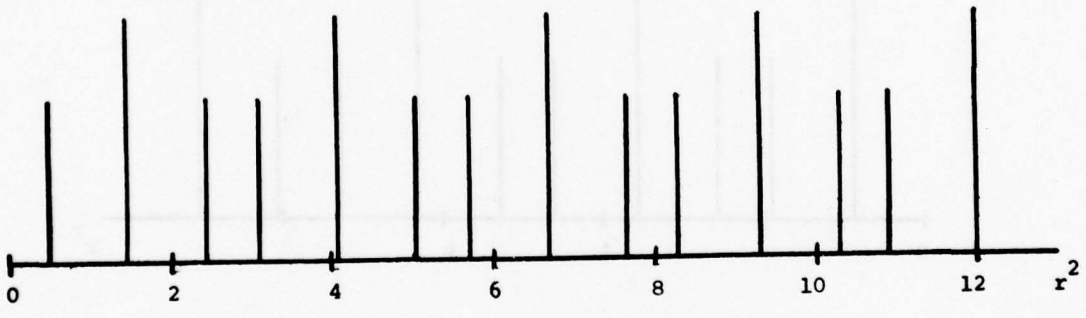

Figure 19 Brillouin Scattering by Photographic Method from Toluene at Scattering Angle $\theta = 90^{\circ}$, Temperature $22^{\circ}C$, Laser Wavelength 4880 Å. Free spectral range 9.68 GHz. The spectral order is identified by symbol M.

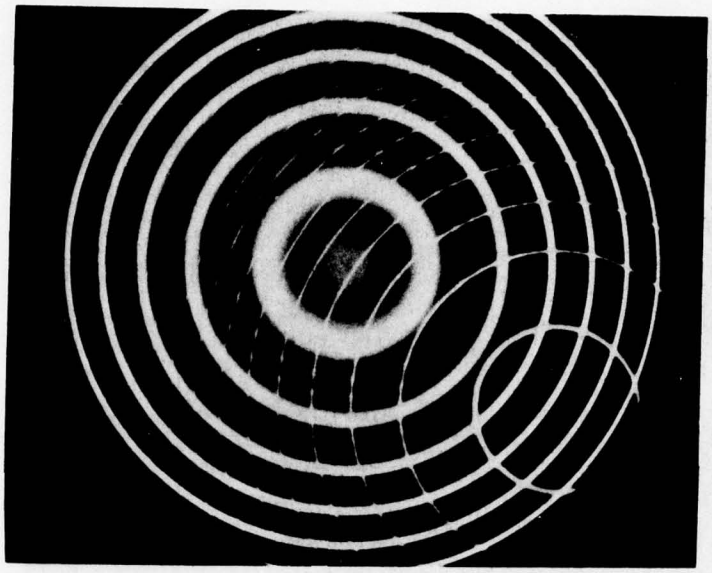

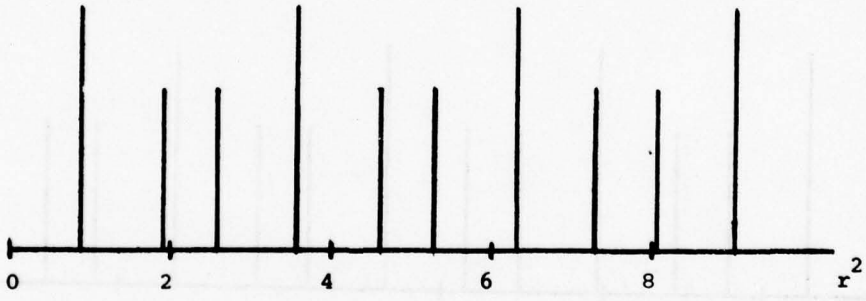

Figure 20 Brillouin Scattering by Photographic Method from MLO 71-6 at Scattering Angle $\theta = 90^{\circ}$, Temperature $22^{\circ}C$, Laser Wavelength 5145 Å. Free spectral range 9.68 GHz. The spectral order is identified by symbol M.

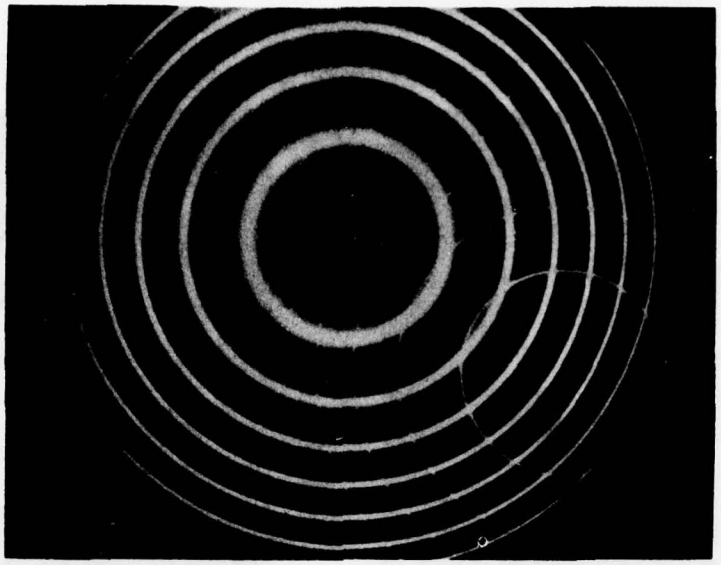

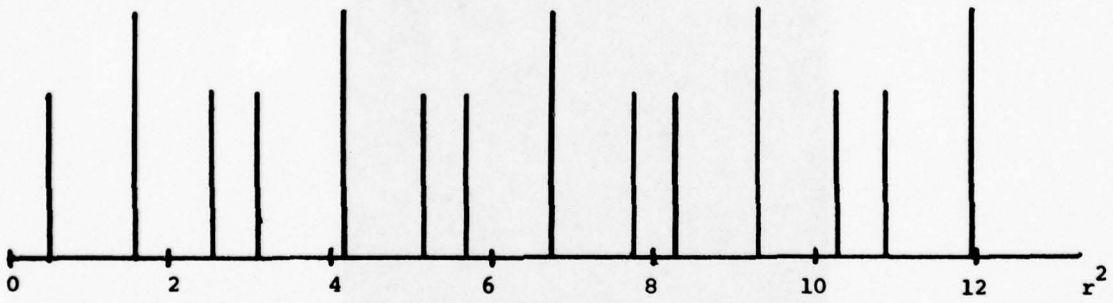

Figure 21 Brillouin Scattering by Photographic Method from MLO 71-6 at Scattering Angle $\theta = 90^{\circ}$, Temperature 22°C, Laser Wavelength 4880 Å. Free spectral range 9.68 GHz. The spectral order is identified by symbol M.

WATER

Exp 1/2 sec

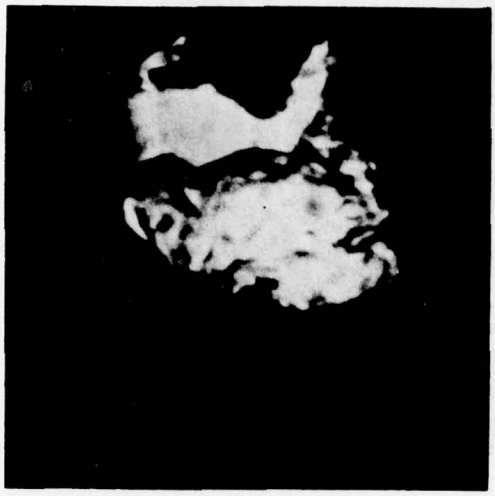

Ice VII (Darker)
Encroaching on Ice VI
≈ 22 kbar

Exp 1/2 sec

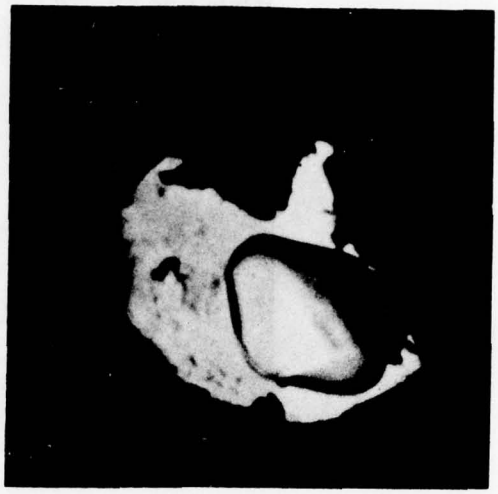

Ice VI Single Crystal

Exp 2 sec

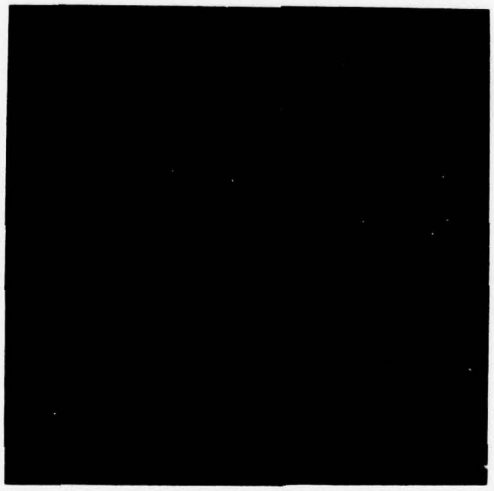

Ice Vi Single Crystal
(higher mag.)

Figure 22 Microphotographs of Water in the Diamond Anvil Cell

BENZENE

Exp 1/2 sec

Exp 1/4 Sec

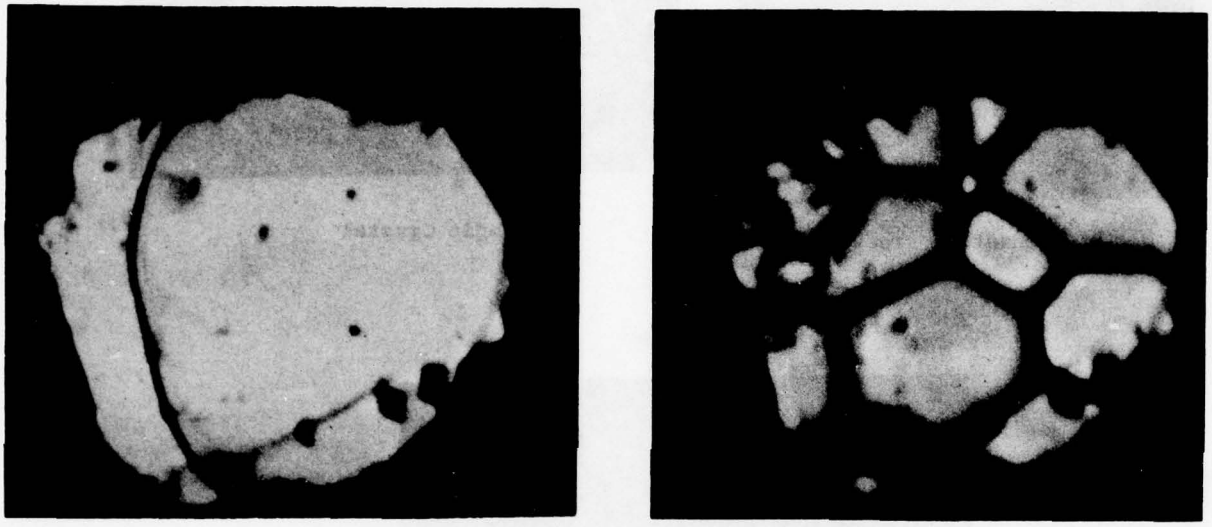

Single Crystal

Onset of Freezing

Figure 23 Microphotographs of Benzene in the Diamond Anvil Cell

CYCLOHEXANE

Exp 1/2 Sec

Onset of Freezing

Exp 1/4 Sec

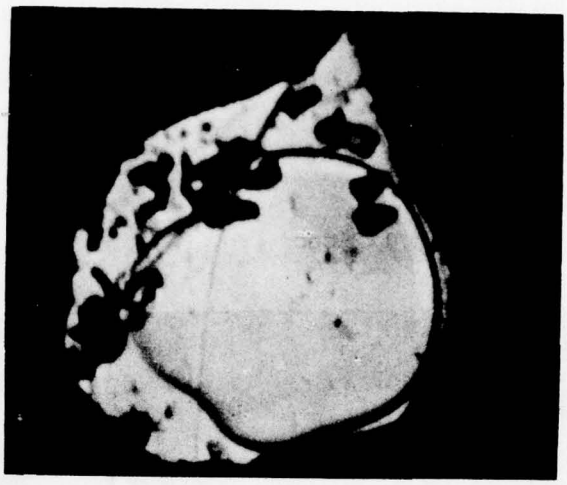

Single Crystal

Exp 2 Sec

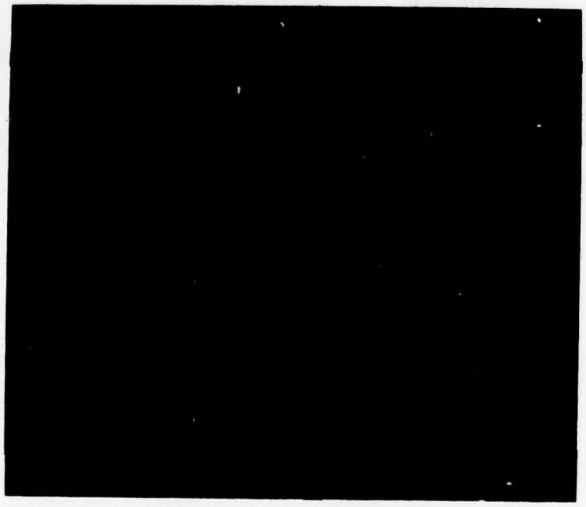

Single Crystal
(as above)

Figure 24 Microphotographs of Cyclohexane in the Diamond Anvil Cell

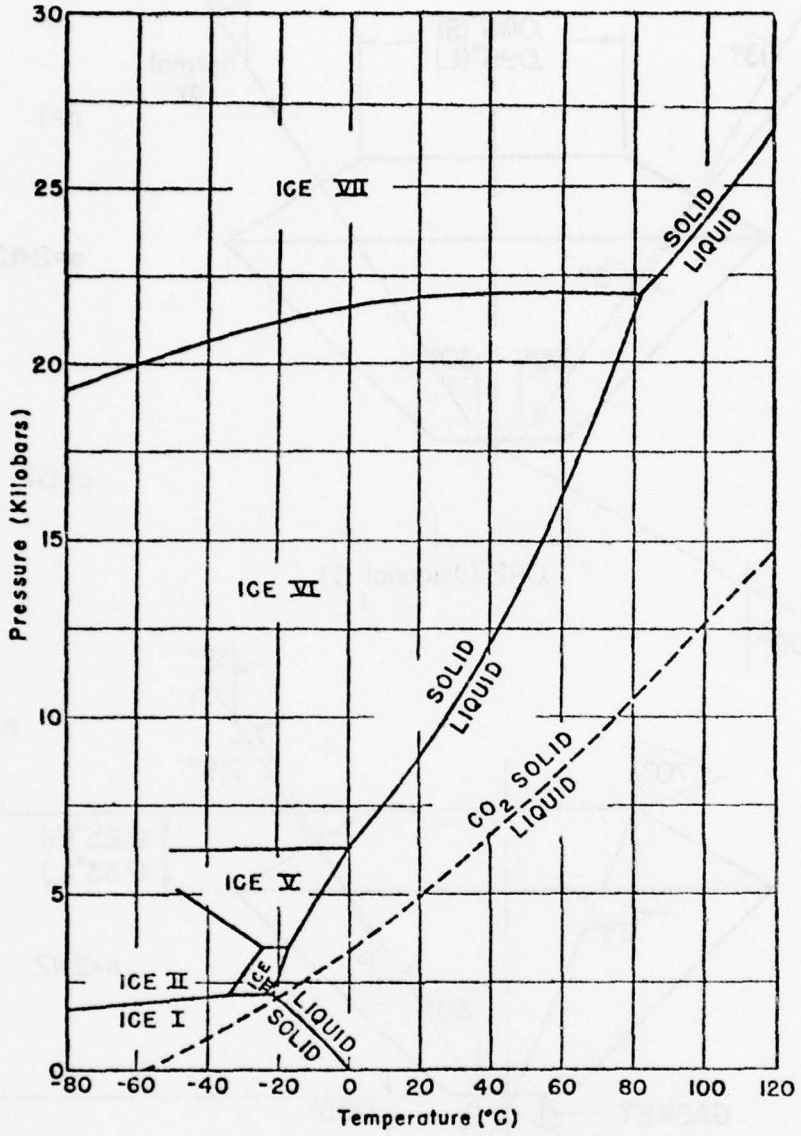

Figure 25 Phase Diagram of Water and the Melting Curve of Carbon Dioxide

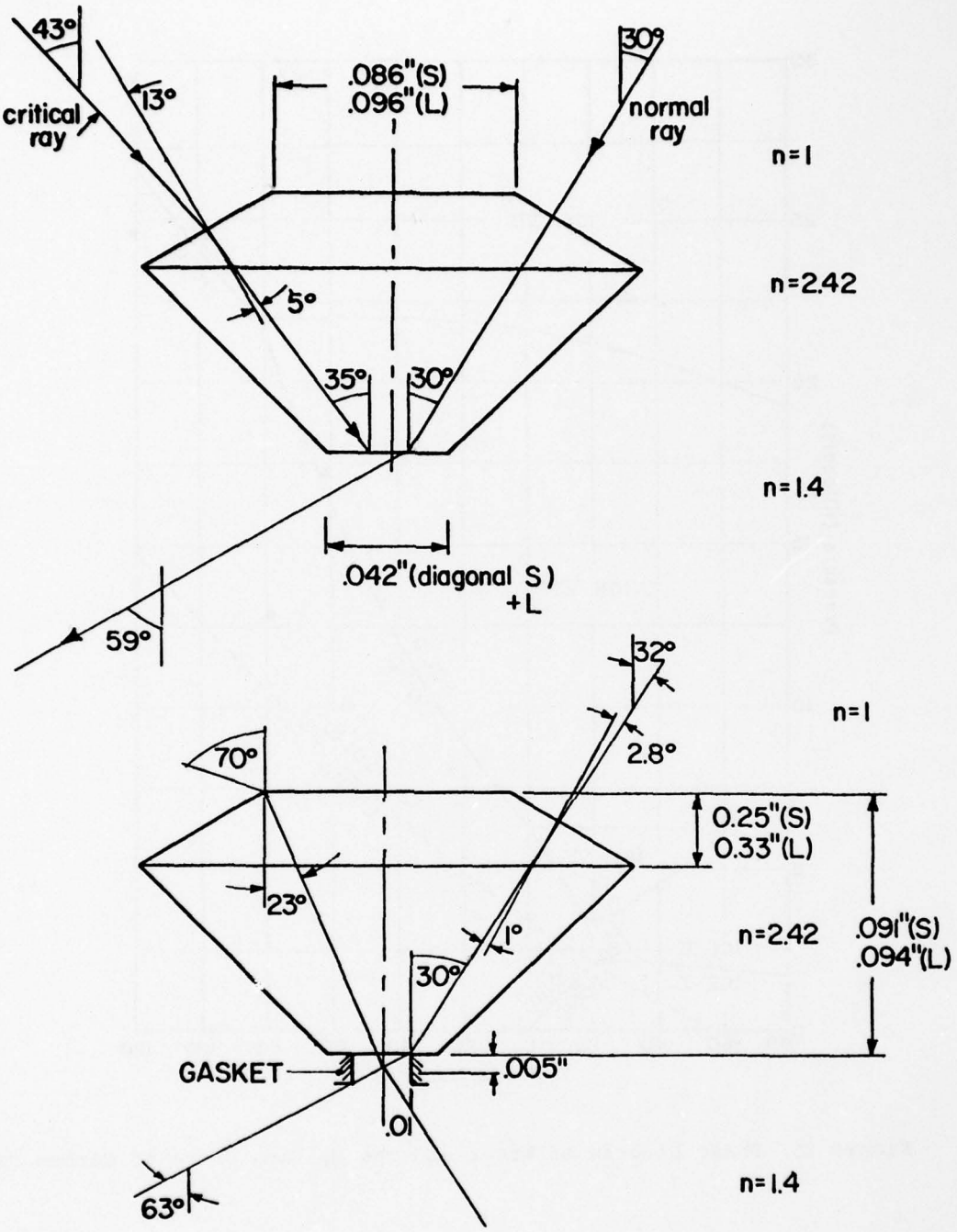

Figure 26 Cross-Sectional View of the Ground Type I Diamonds. Several examples of refraction of light rays are shown; the symbol n is the index of refraction.

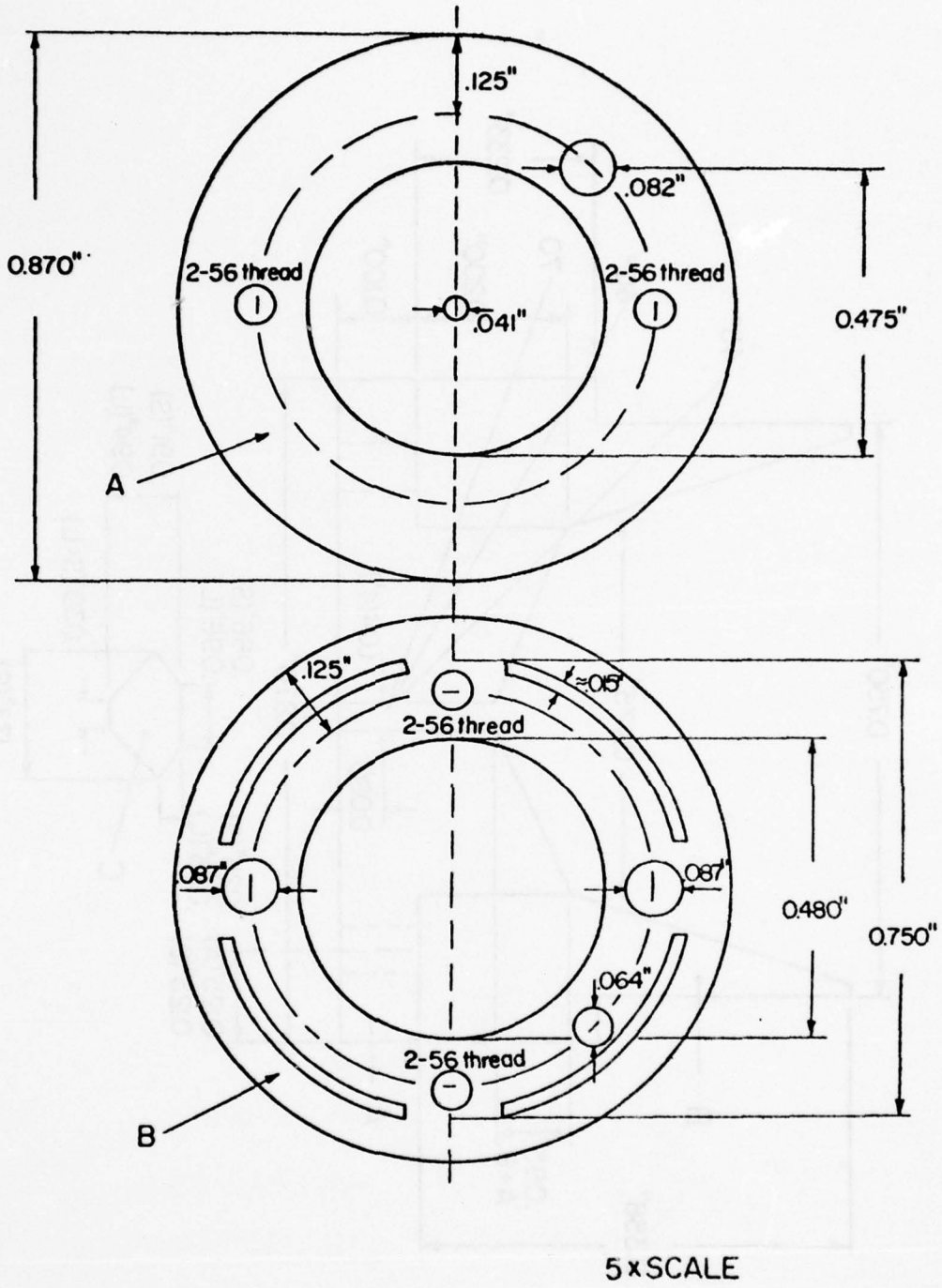

Figure 27 Top View of Support Plate A and Alignment Chuck B

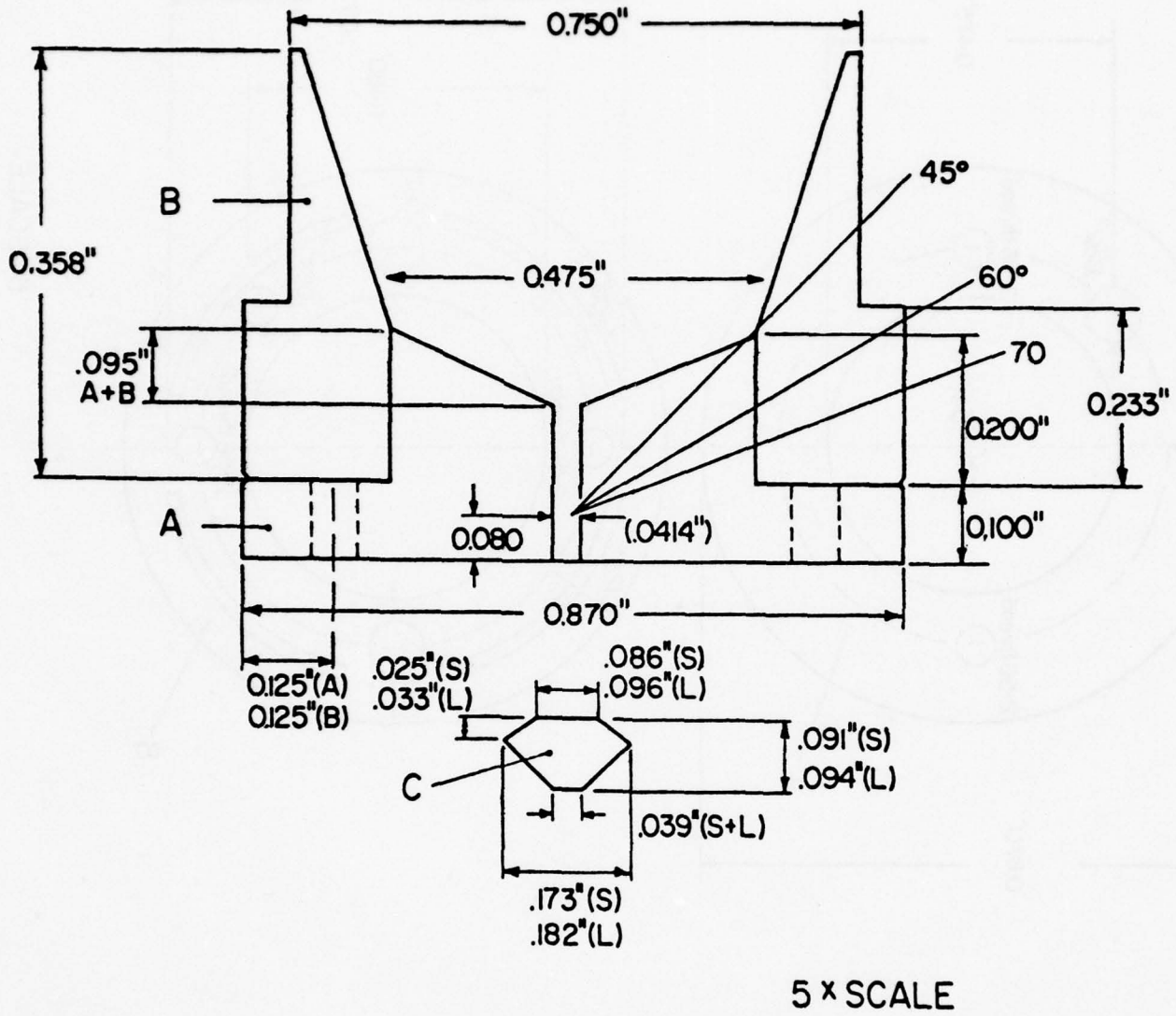

Figure 28 Cross-Sectional View of the Diamond Support Plate A, and Alignment Chuck B

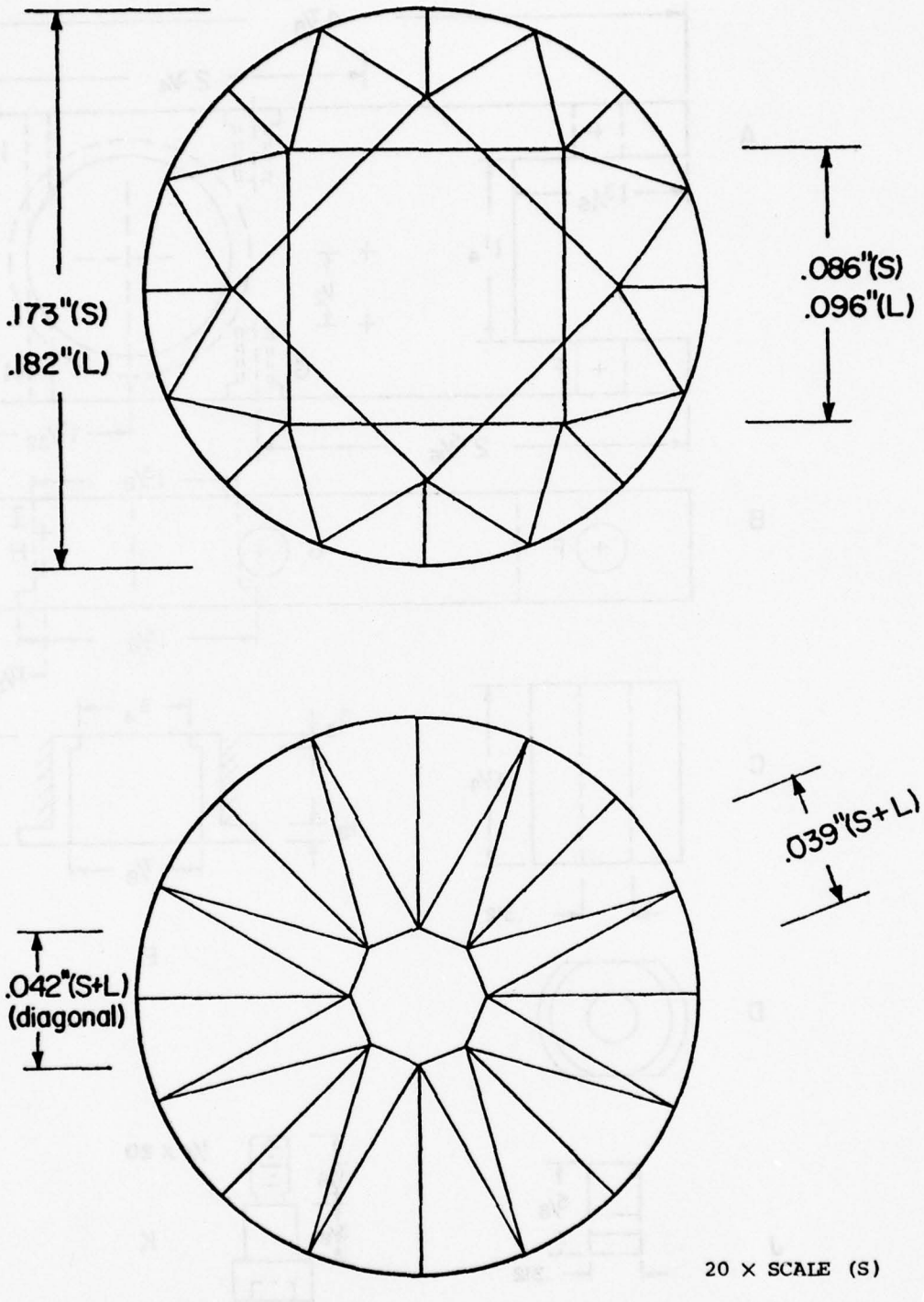

Figure 29 The Top View (Support End) and Bottom View (Anvil End) of the Ground Diamonds. Symbols S and L refer to the smaller and larger diamonds.

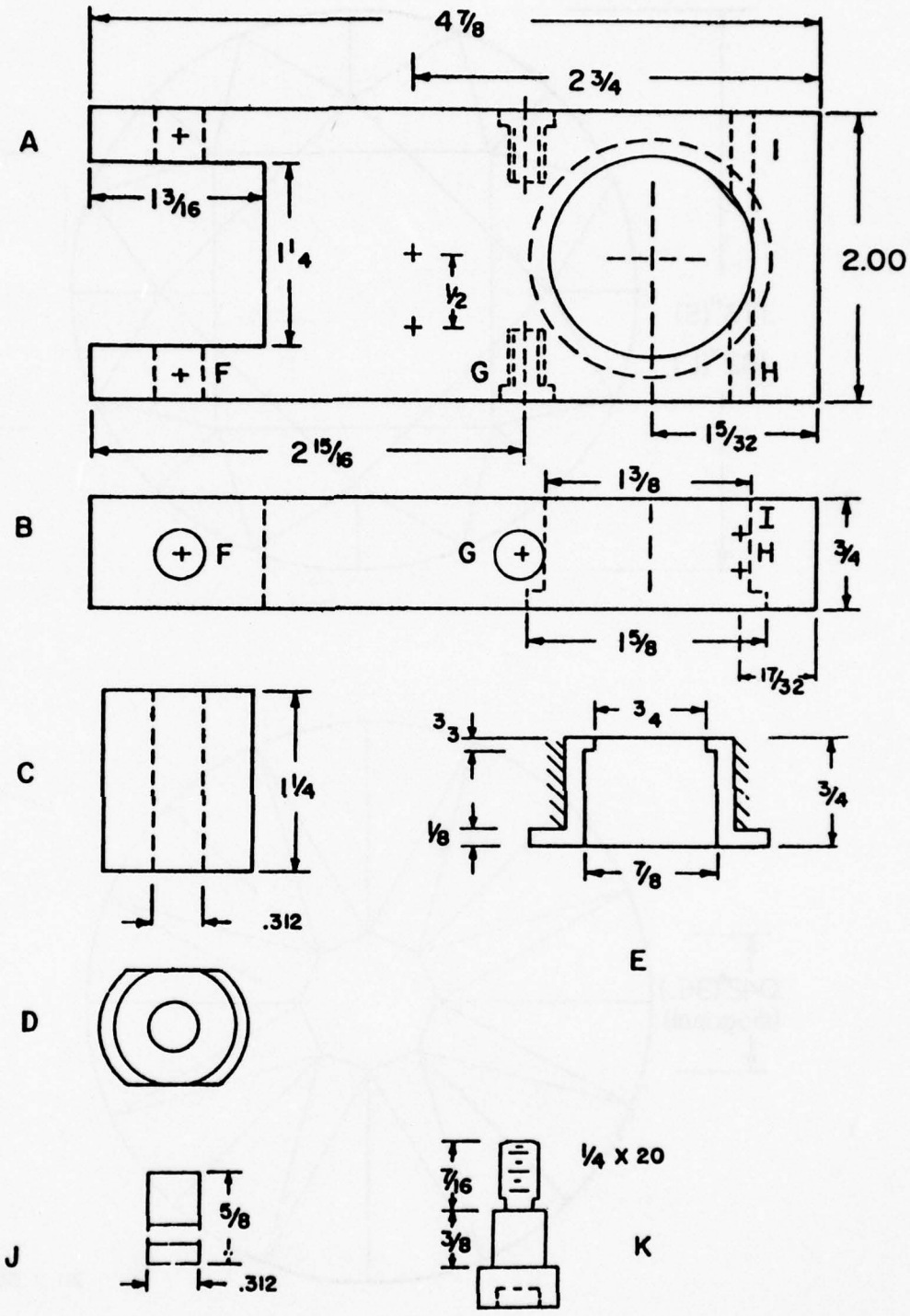

Figure 30 Diamond Anvil Cell Holder and Pressure Generating Assembly

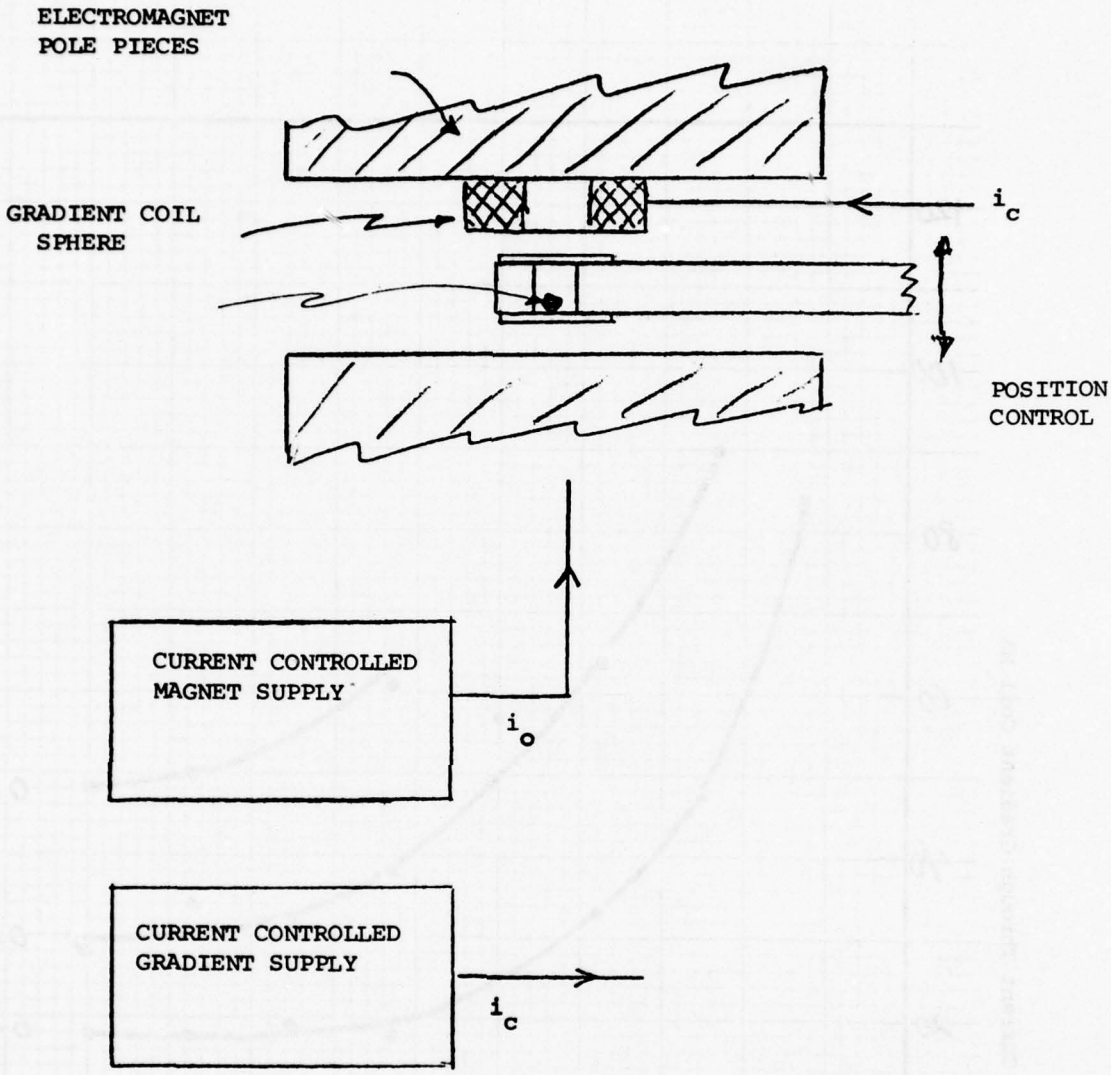

Figure 31 Apparatus to Evaluate Magnetic Lifting Force for High Pressure Viscometry Measurements

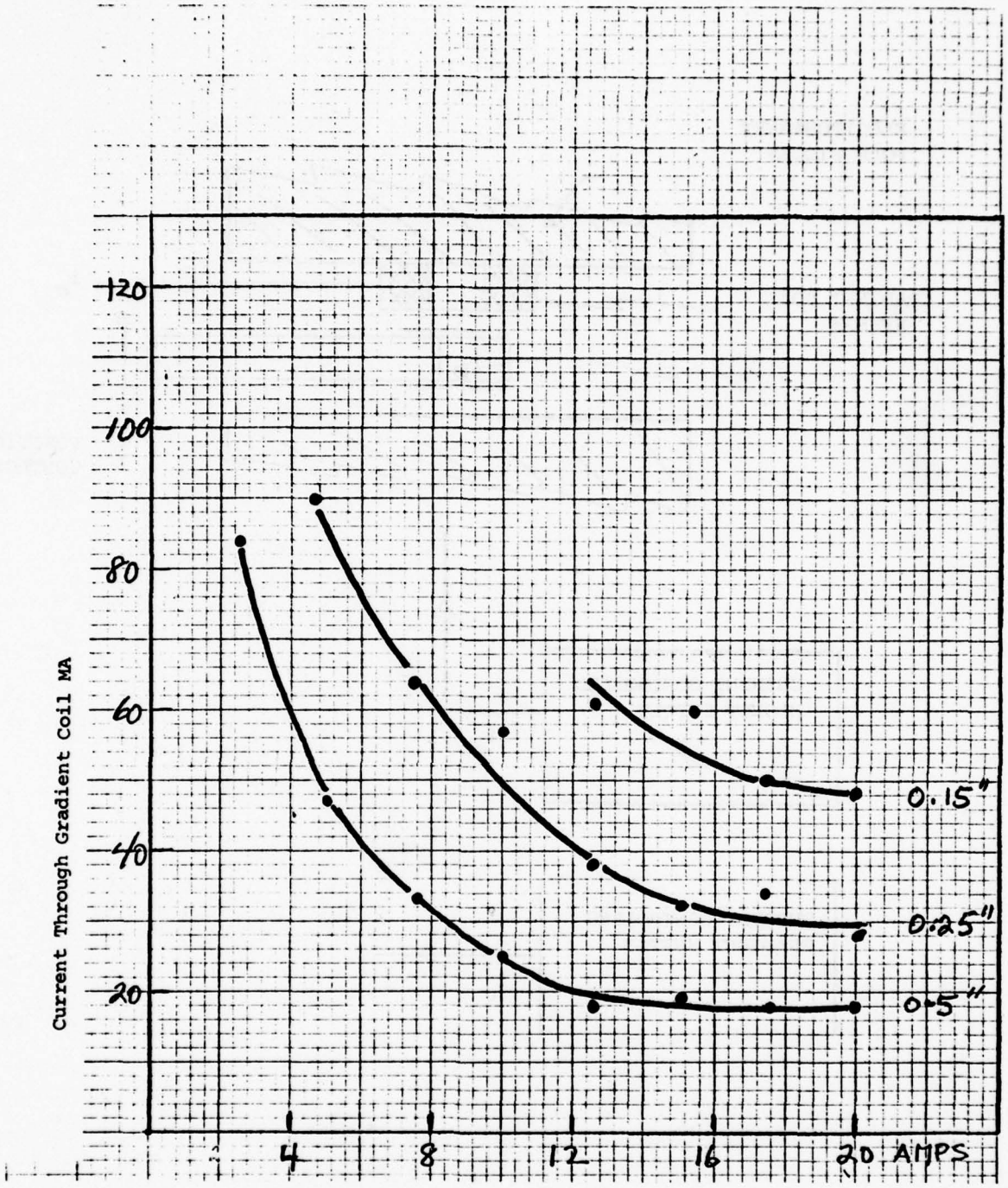

Figure 32 Curves of Constant Magnetic Lifting Force F = mg. (Parameter = position).

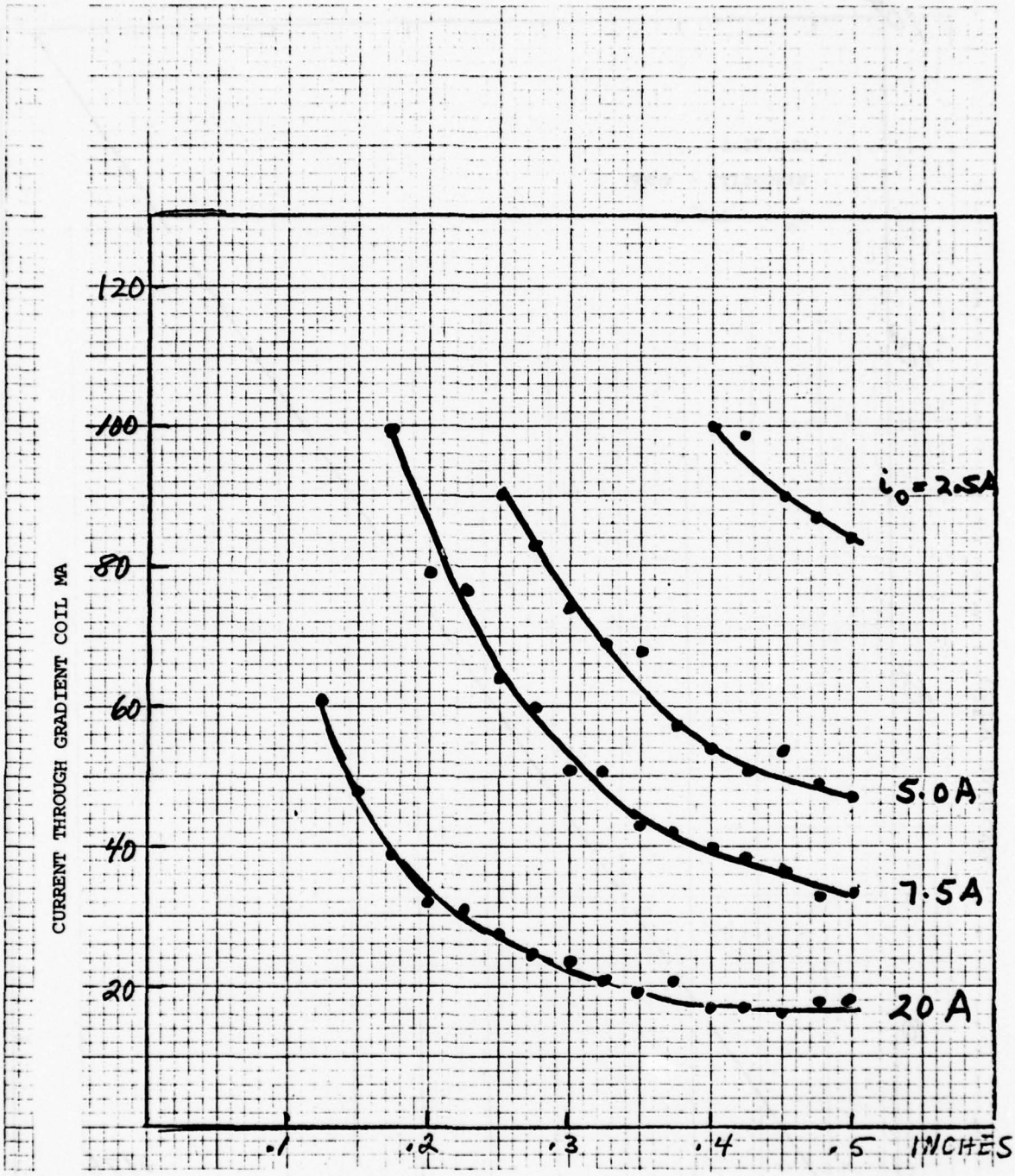

Figure 33 Curves of Constant Magnetic Lifting Force F = mg. (Parameter = i_o).

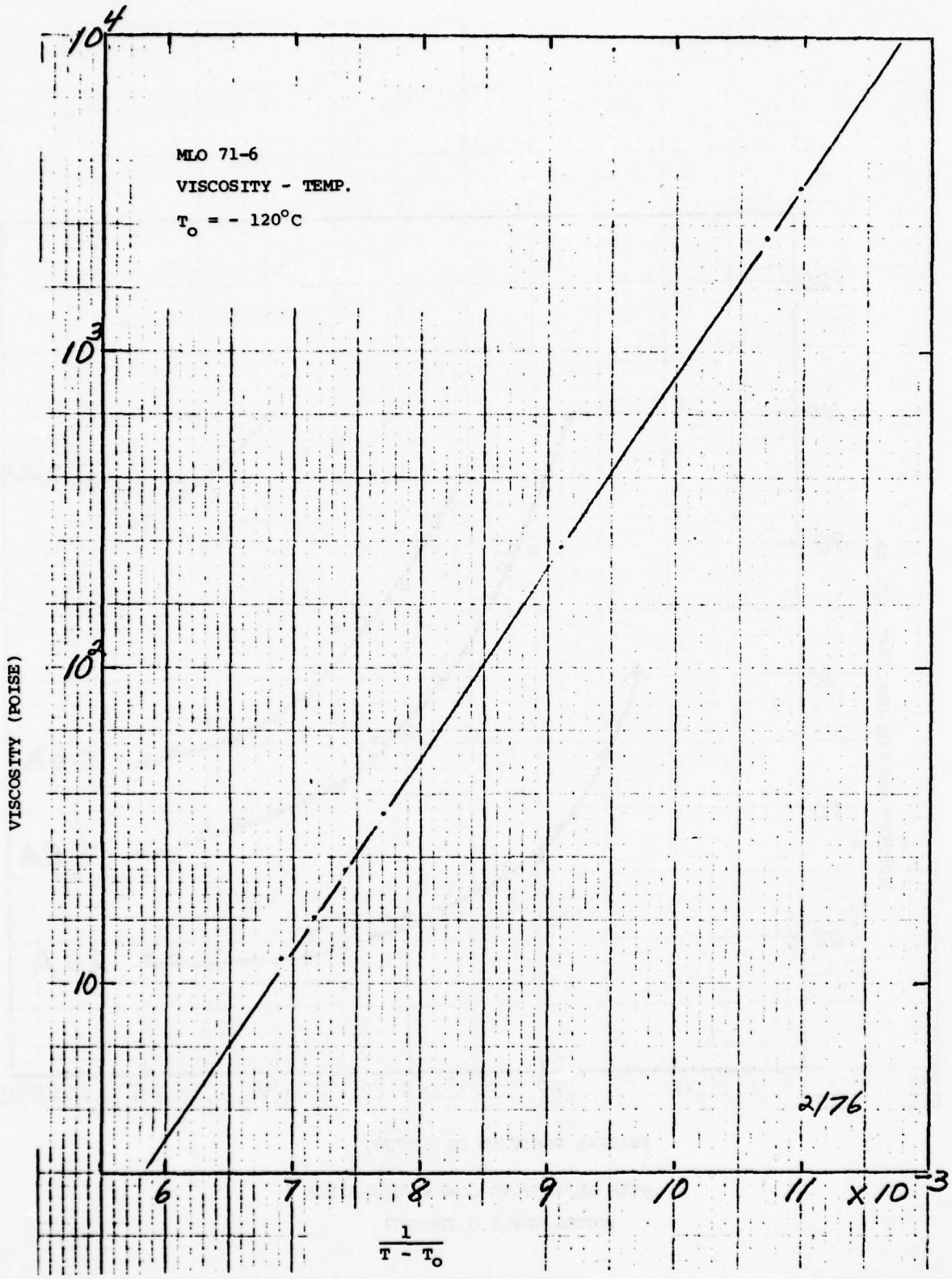

Figure 34 Temperature Dependence of Steady-State Viscosity of Oil MLO 71-6 at Atmospheric Pressure

REFERENCES

1. D. Dowson and G.R. Higginson, Elastohydrodynamic Lubrication, Pergamon Press, New York 1966.

2. T.E. Tallian, Elastodynamic Hertzian, Mechanical Engineering, p.14, November 1971.

3. E.G. Trachman, The Short-Time Viscosity Behavior of a Lubricant in a Hertzian Pressure Zone, J. Lub. Tech., Trans. ASME, &4 Lub-8.

4. D.J. Plazek and J.H. Magill, Physical Properties of Aromatic Hydrocarbons IV. An Analysis of the Temperature Dependence of the Viscosity and the Compliance of 1, 3, 5 Tri-α-naphthylbenzene, J. Chem. Phys., 49, 3678 (1968).

5. R.S. Marvin and J.E. McKinney, Volume Relaxation in Amorphous Polymers, Physical Acoustics, Vol.IIB, p.165, Warren P. Mason, ed., Academic Press, 1965.

6. A.K. Doolittle, Studies in Newtonian Flow. III. The Dependence of the Viscosity of Liquids on Molecular Weight and Free Space (in Homologous Series), J. Appl. Phys., 23, 236 (1952).

7. J.D. Ferry, Viscoelastic Properties of Polymers, John Wiley & Sons, 1970.

8. M. Cohen and D. Turnbull, Molecular Transport in Liquids and Glasses, J. Chem. Phys., 47, 2185 (1967).

9. J.H. Gibbs and E.A. DiMarzio, Nature of the Glass Transition and the Glassy State, J. Chem. Phys., 28, 373 (1958).

10. G. Harrison and E.G. Trachman, The Role of Compressional Viscoelasticity in the Lubrication of Rolling Contacts, J. Lub. Tech., Trans. ASME, F94, 306 (1972).

11. A.J. Barlow and E. Erginsav, Viscoelastic Relaxation in a Series of Short Chain Polydimethyl Siloxanes, J. Acoust. Soc. Am., 56, 83 (1974).

12. J. Lamb, Thermal Relaxation in Liquids, Physical Acoustics, IIA, 203, Warren P. Mason, ed., Academic Press, 1965.

13. P.A. Fleury, Light Scattering as a Problem of Phonons and Other Excitations, Physical Acoustics, Vol.VI, p.2, Warren P. Mason, ed., Academic Press, 1970.

14. H.Z. Cummins and E.R. Pike, Photon Correlation and Light Beating Spectroscopy, Plenum Press, New York 1974.

15. M.H. Birnboim and H. Weiss, A Novel Method for Viscosity Measurements at High Pressures, Presented in part, American Physical Society.

16. M.A. Lowenstein and M.H. Birnboim, A Method for Measuring Sedimentation and Diffusion of Macromolecules in Capillary Tubes by Total Intensity and Quasi-Elastic Light-Scattering Techniques, Biopolymers, 14, 419 (1975).

17. H.Z. Cummins and R.W. Grammon, Rayleigh and Brillouin Scattering in Liquids: The Landau-Placzek Ratio, J. Chem., 44, 2785 (1966).

18. Y. Kato and G.A. Zdasiuk, Absolute Measurements of Brillouin Scattering Efficiencies of Molecular Liquids, J. Opt. Soc. Am., 65, 995 (1975).

19. S.E. Gustafsson, H.E. Gunilla Knape and L.M. Torell, Brillouin Spectra of Ethyl Ether and Ethyl Alcohol, J. Phys. D: Appl. Phys., 7, 389 (1974).

20. J.F. Dill, P.W. Drake and T.A. Litovitz, The Study of Viscoelastic Properties of Lubricants Using High Pressure Optical Techniques, ASLE Preprint 74 LC-5B-2.

21. H.J. McSkimin, Ultrasonic Methods for Measuring the Mechanical Properties of Liquids and Solids, Physical Acoustics, 1A, 271, Warren P. Mason, ed., Academic Press.

22. T.A. Litovitz and C.M. Davis, Structural and Shear Relaxation in Liquids, Physical Acoustics, IIA, 281, Warren P. Mason, ed., Academic Press, 1965.

23. Modern Very High Pressure Techniques, R.H. Wentorf, editor, Butterworths, 1962.

24. J.D. Barnett, S. Block and G.T. Piermarini, An Optical Fluorescence System for Quantitative Pressure Measurement in the Diamond Anvil Cell, Rev. Sci. Inst., 44, 1 (1973).

25. J.L. Lauer and M.E. Peterkin, Analysis of Infrared Spectra of Fluid Film in Simulated EHD Contacts, ASLE Preprint 74 LUB-34.

26. G.C. Kennedy and W.T. Holser, Pressure-Volume-Temperature, p.373.

27. T.R. Meeker and A.M. Meitzler, in Physical Acoustics, Vol.IA, W.P. Mason, ed., Academic Press 1964.

28. D. Hunston, Ph.D. Thesis, Determination of Viscoelastic Constants for Polymers, Chemistry Dept., Kent State University, December 1969.

29. G.R. Paul and A. Cameron, An Absolute High Pressure Microviscometer Based on Refractive Index, Proc. Roy. Soc.A, London, 1 (1972).

30. J. Jakobsen and W.O. Winer, High-Shear Stress Behavior of Some Representative Lubricants, ASLE Preprint, 74 Lub-41.

APPENDIX A

A NOVEL METHOD FOR VISCOSITY MEASUREMENTS AT HIGH PRESSURES

Meyer H. Birnboim and H. Weiss
Mechanics Division
Rensselaer Polytechnic Institute
Troy, New York 12181

A NOVEL METHOD FOR VISCOSITY MEASUREMENTS AT HIGH PRESSURES

The technique of quasi-elastic light scattering is utilized as a method to determine the viscosity of fluids subjected to large hydrostatic pressures. In this method, a small concentration of insoluble polystyrene spheres of known diameter, 0.109 microns, were added to the fluid. The high pressure cell in which the fluid is contained has three optical windows. The laser light scattered from the suspended spheres is analyzed to determine the diffusion coefficient of the spheres. Since, by Stokes law,

$$\eta = \frac{kT}{8\pi rD} \tag{1}$$

the viscosity of the fluid is determined from the measured diffusion coefficient and known particle radius r. A small correction is required for the contraction of the sphere and for refractive index change of the water under pressure. Results on the viscosity of water at 25°C up to pressures of 2.5 kilobars is reported and compared to published results.

The high pressure system and scattering cell (1) is illustrated in Figure 1. The system is assembled from standard* high pressure components. The scattering cell consists of a high pressure cross; three blank conical plugs are drilled out and fitted with sapphire cylinder windows which are epoxied in place. Windows from 1/8" to 1/4" diameter by 3/4" long have been used successfully to pressures of 35,000 psi. The fluid is filled through the reservoir to overflow at the window to ensure that no air is trapped, then the window plug is tightened. Pressure is generated by hand, by compression

---

* American Instrument Company, Silver Springs, Maryland.

of fluid in the valves. The sequence is: close all valves, open valves A, B. close A, open C, close B, C, then repeat sequence from open valves A, B. Three repetitions of the sequence will bring the pressure to 35,000 psi for the case of a water sample.

The light scattered by the polystyrene spheres is observed at a scattering angle of 90° to the main beam. The intensity of scattered light is monitored by a photomultiplier which is operated in a photon counting mode, thus the number of photoelectric events (photocounts) per second $n(t)$ is proportional to the intensity of light. The intensity is not constant on short time scales but exhibits fluctuation associated with the Brownian motion of the scattering particles. The sequence of "instantaneous" intensities are stored in real time in the memory of a computer, then the autocorrelation function is calculated.

The photocount rate autocorrelation function $c(\tau)$ is defined in terms of the sequence $n(t)$; and in turn $c(\tau)$ is related (2) to the translational diffusion coefficient D:

$$c(\tau) \equiv \langle n(t)n(t+\tau)\rangle_t = \langle n(t)\rangle\, \delta(\tau) + \langle n(t)\rangle_t^2 + Ae^{-2DK^2\tau} . \qquad (2)$$

The brackets $\langle\ \rangle_t$ denote the average overall starting times t; $\delta(\tau) = 1$ for $\tau = 0$ and $\delta(\tau) = 0$ otherwise.

For our computer method, the real time t and delay time τ are always a multiple of T, that is $t = jT$ with $j = 0,1,2 \ldots$; A is a coefficient related to the intensity of light scattered from the macromolecules; and the magnitude of the scattering vector $\vec{K}$ is obtained from

$$K^2 = \left(\frac{4\pi n_o}{\lambda_o}\right) \sin^2 \frac{\theta}{2} \qquad (3)$$

where n_o and λ_o are the refractive index of the solution and wavelength of the light in vacuum. In this experiment, the scattering angle θ was kept at 90°. The correlation time $\frac{1}{2DK^2}$, and therefore D, is calculated from the slope of $\ell n[c(\tau) - \langle n(t)\rangle^2]$ vs. τ, where the shot noise, the first term of Eq. (2) may be neglected since it is zero except at $\tau = 0$, and $\langle n(t)\rangle_t$ is the average count rate.

Water was taken as the first sample to test the technique. An example of the autocorrelation function is seen in Figure 2, taken at a pressure of 15,000 psi. The diffusion coefficient determined from the slope of this curve in conjunction with Eq. (1) yields the viscosity at 15,000 psi. Our results for the limited pressure range of 0 to 35,000 psi (2.5 kilobars) taken at a temperature of 23°C are shown by the points in Fig. 3. These points are superposed on the extensive data of Butt and Capi (3) as represented by the solid lines. The results are only intended as an illustrative example of the method.

This method is applicable to lubricants where the viscosity is many orders of magnitude greater than water. The correlation time for 0.1 micron spheres in water is circa 37×10^{-6} seconds. The apparatus is capable of determining correlation times some six or seven orders of magnitude longer, hence for correspondingly higher viscosities. It may also be possible to use spheres of about 1 order of magnitude smaller to extend the method to even higher viscosities.

Acknowledgement

The authors gratefully acknowledge the valuable suggestions of Mr. W.E. Hake of American Instrument Company, Inc. in the design of the high pressure cell. This work was supported by the National Science Foundation and the Air Force Materials Laboratory, Wright-Patterson Air Force Base.

References

1. Bridgman, P.W., Proc. Amer. Acad. Sci., 61, 57 (1926).

2. Cummins, H.Z. and Swinney, H.L., in "Progress in Optics," ed. E. Wolf, North Holland Publishing Company, pp.135-200 (1970).

3. Bett, K.E. and Cappi, J.B., Nature, 207, 620 (1965).

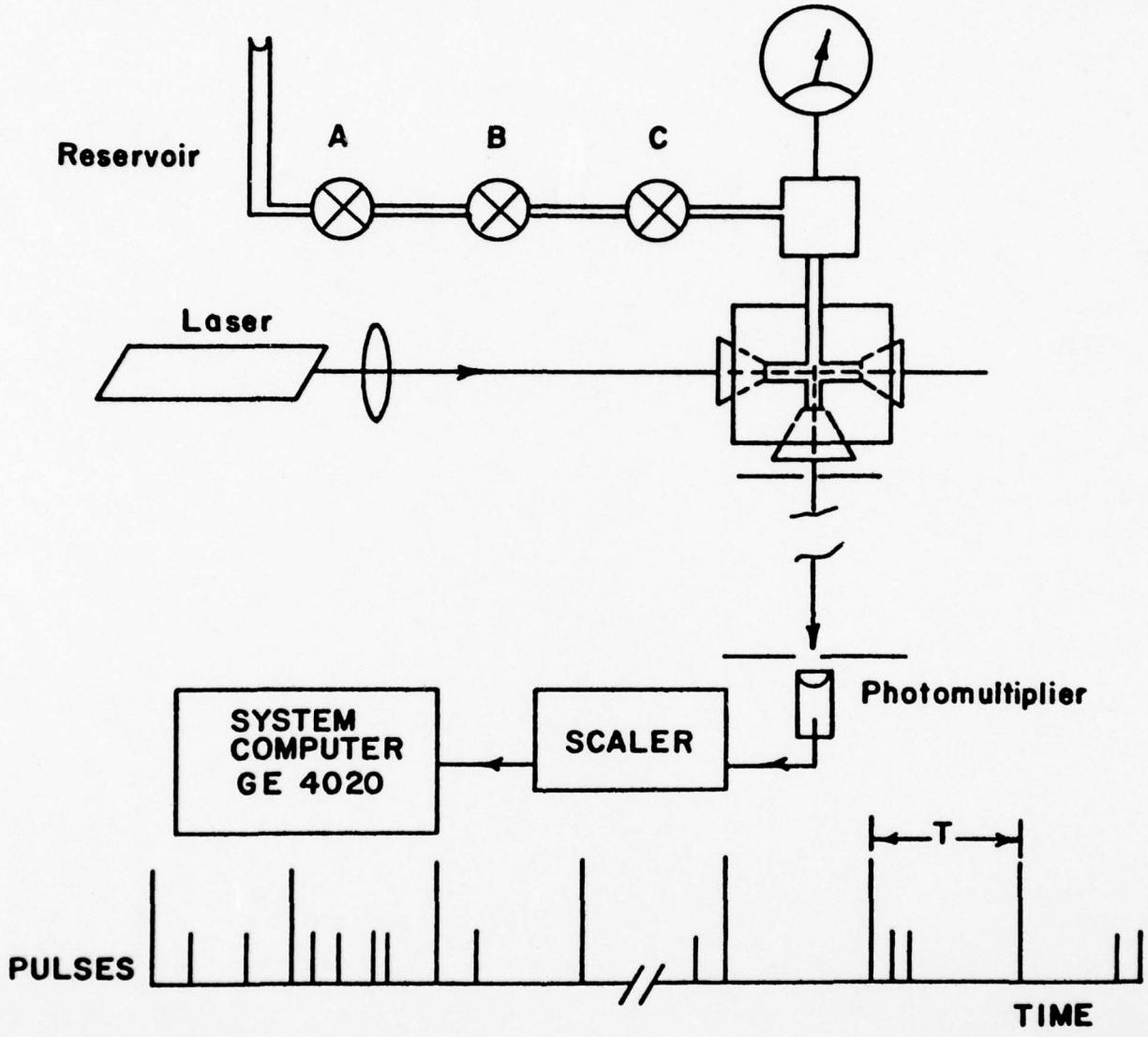

Figure 1 Block Diagram of the Homodyne Spectrometer.

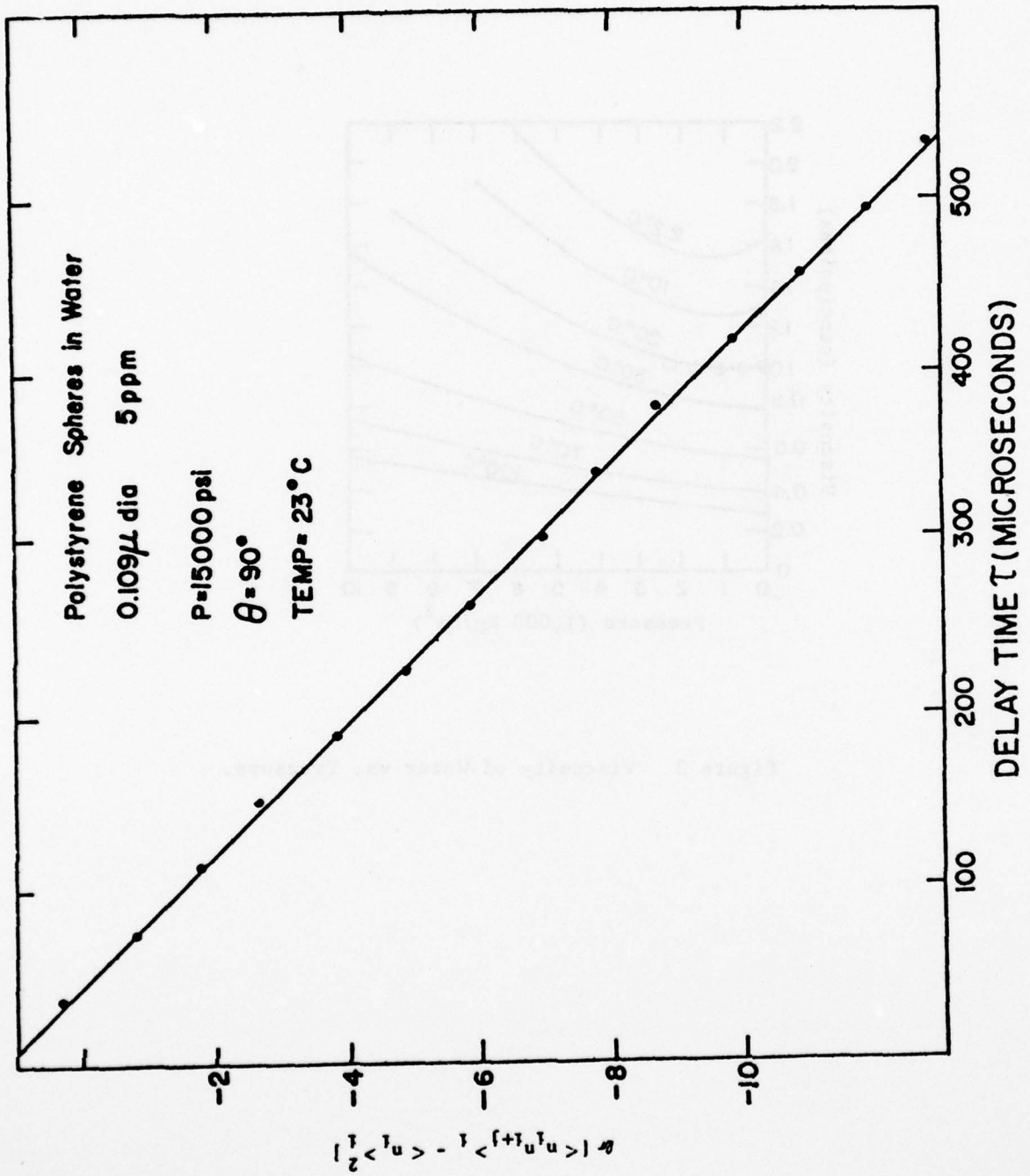

Figure 2 Plot of $\ln [\langle n_i n_{i+j} \rangle_i - \langle n_i \rangle_i^2]$ vs. Delay Time τ_j

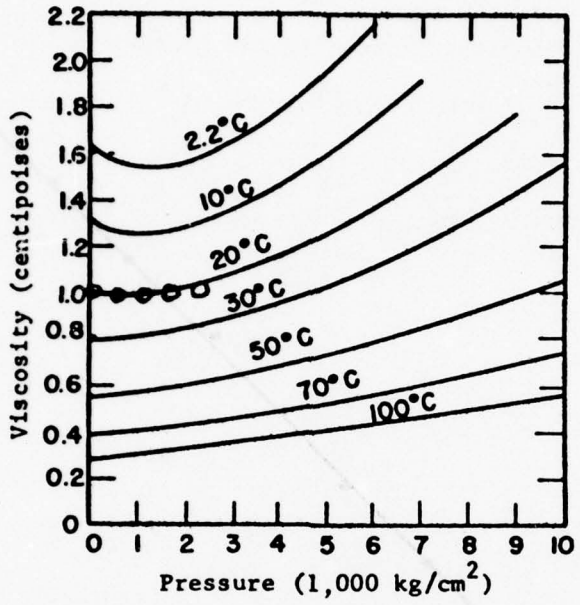

Figure 3 Viscosity of Water vs. Pressure.

APPENDIX B

AN ULTRASONIC METHOD FOR MEASUREMENT OF VISCOELASTIC PROPERTIES OF POLYMERIC SOLUTIONS

by

In-Young Koh

A Thesis Submitted to the Graduate

Faculty of Rensselaer Polytechnic Institute

in Partial Fulfillment of the

Requirements for the Degree of

DOCTOR OF PHILOSOPHY

Major Subject: Mechanics

Approved by the
Examining Committee:

_____
Meyer H. Birnboim, Adviser

_____
Frederick F. Ling, Member

_____
Van C. Mow, Member

_____
Harry F. Tiersten, Member

Rensselaer Polytechnic Institute
Troy, New York

August 1977

CONTENTS

LIST OF TABLES

LIST OF FIGURES

ACKNOWLEDGEMENT

ABSTRACT

It has been shown experimentally by various investigations that the dynamic viscosity of a dilute polymer solution in the limit of high frequency does not become the viscosity of the solvent. To study this limiting behavior, a high frequency surface delay line device has been developed. The pulsed ultrasonic shear wave propagated into the liquid over the frequency range from 3 MHz to 30 MHz and has been used to determine the viscoelastic properties of polymer solutions. A computerized data acquisition system has been interfaced with this device to determine wave attenuation and phase shift even for pulsed radio frequency signals. The method of data acquisition is based on adaptation of a conventional high-speed sample and hold circuit, the generation of precise synthesizer locked trigger pulse train, and the utilization of "walking frequencies"[1,23]. Data analysis is based on cross-correlation[2] among echoes to yield phase and amplitude. Differences in phase and amplitude with and without solutions are converted to the viscoelastic properties.

The results of the high frequency limiting behavior of several polystyrene solutions (5%, 10%, 20%, 40%) together with steady-state viscosity results are reported. With these results the possible explanation of the contribution of polymer molecules to the total steady-state viscosity is presented and compared to the theories of Rouse,[4,25], Zimm[5] and others[20].

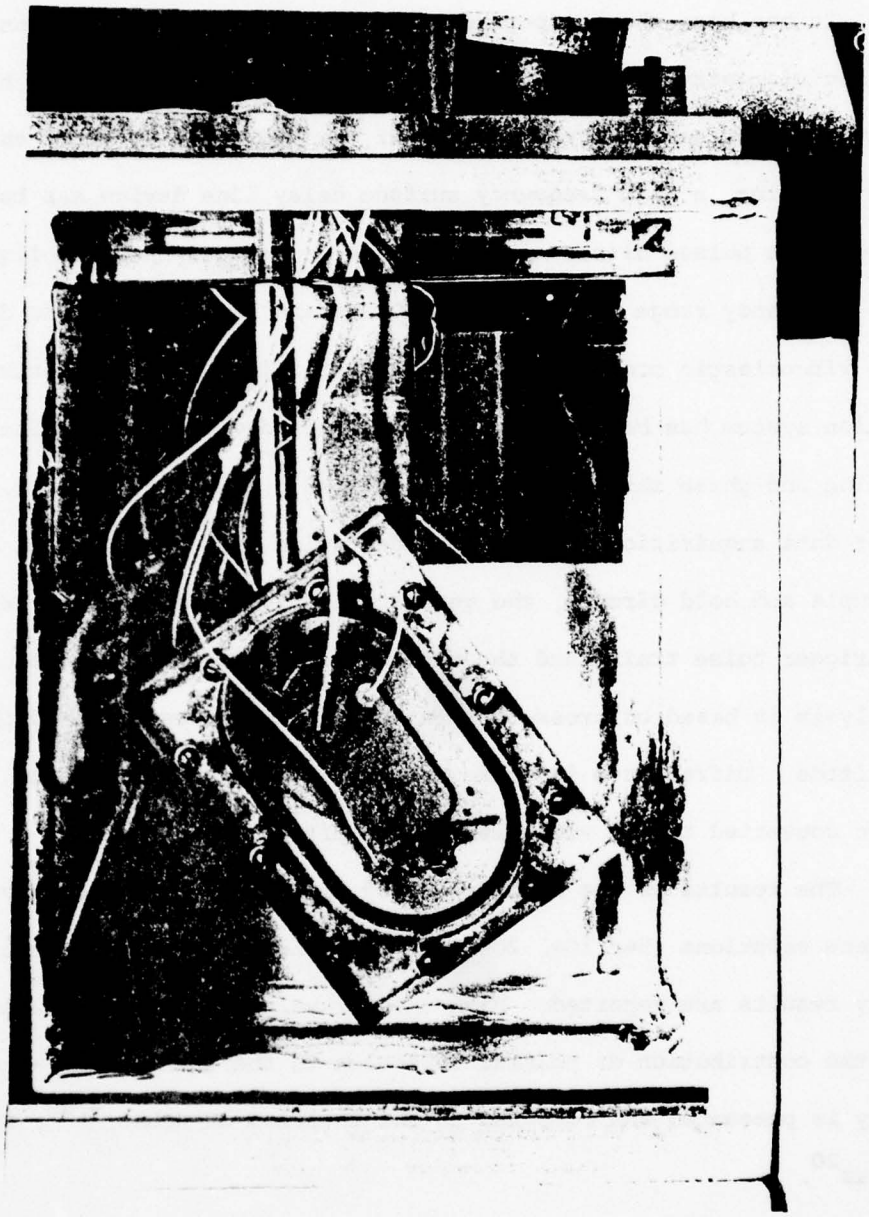

Photograph of the Apparatus in the Temperature Bath

PART I

INTRODUCTION

The viscoelastic response of dilute polymer solution is usually separated into two parts, the polymer and solvent contributions. The theories of Rouse, Zimm and others attribute the polymer contribution to internal relaxational modes of the macromolecules.

At low frequencies, the long-range correlated segmental motions dominate the viscoelastic response. The low-frequency dynamic response has been investigated by a number of people using the Birnboim apparatus. Thereby, it has shown that the behavior can be described rather well by the theories of Rouse, Zimm and others as well as experimentally by Birnboim and Ferry[6].

The high frequency response in dilute polymer solution has been explored by several investigators recently. On the basis of the theories of Rouse and Zimm one might expect the polymer contribution, evident at lower frequencies, to drop to zero in the limit of high frequencies, and thus the viscosity of the solution to approach the viscosity of the solvent in the limit of high frequency. However, it has been found experimentally that this assumption is not borne out and the difference between the limiting solution viscosity and that of the solvent has been attributed to internal friction within the polymer molecule. Since the higher frequency modes of motion are short range in nature, they could be greatly influenced by the internal viscosity of the submolecules. This interpretation has been brought into question by Schrag[3,4,5,27] and the problem remains open. This discrepancy between theory and experiment in the high frequency limit is called the η_∞ problem.

The experimental techniques that have been used to investigate this phenomena have mainly been in the frequency range from 0.01 Hz to 10 KHz. This means that it has been necessary to use highly viscous solvents in order to shift the η_∞-phenomenon into experimentally accessible regimes. This shifting normally requires an assumption of applicability of the principle of time-temperature superposition.

We now present a brief discussion on the historical development of shear property measurements in liquids. A great deal of attention has been given to lower frequency experiments by using a quartz crystal vibrating in torsion[24]. This was used to measure the complex shear viscosity of the liquid surrounding the crystal. The change in resonant frequency and half width due to adding the liquid are measured in terms of impedance change by a bridge. When the shear impedance of the liquid is quite high, a different pulse method employing torsional waves traveling along a delay rod can be used. The phase and amplitude of waves reflected back from the bottom end or the rod are then measured. A liquid sample is then placed around a rod and then the change of the phase and amplitude is determined. In another technique, the first thickness shear modes of an infinite plate were used in a nondispersive delay line by Meitzler[9]. This mode was propagated in a thin rectangular strip delay line. The edges were taped with absorbing tape to damp edge generated modes, and the SSO mode was excited piezoelectrically. Also, Meitzler demonstrated that the shear mode could be propagated in a finite plate 10 to 20 wavelengths in width if absorbing material is placed on a minor surface. These lines are constructed of a metal strip with piezoelectric transducers bonded to the ends. The crystals can excite

AD-A062 612 RENSSELAER POLYTECHNIC INST TROY NY LAB FOR VISCOELA--ETC F/G 11/8
MEASUREMENT OF PROPERTIES AND RESPONSE FUNCTIONS OF LIQUID LUBR--ETC(U)
JUN 78 M H BIRNBOIM F33615-76-C-5101

UNCLASSIFIED AFML-TR-78-69 NL

2 OF 3
ADA
062612

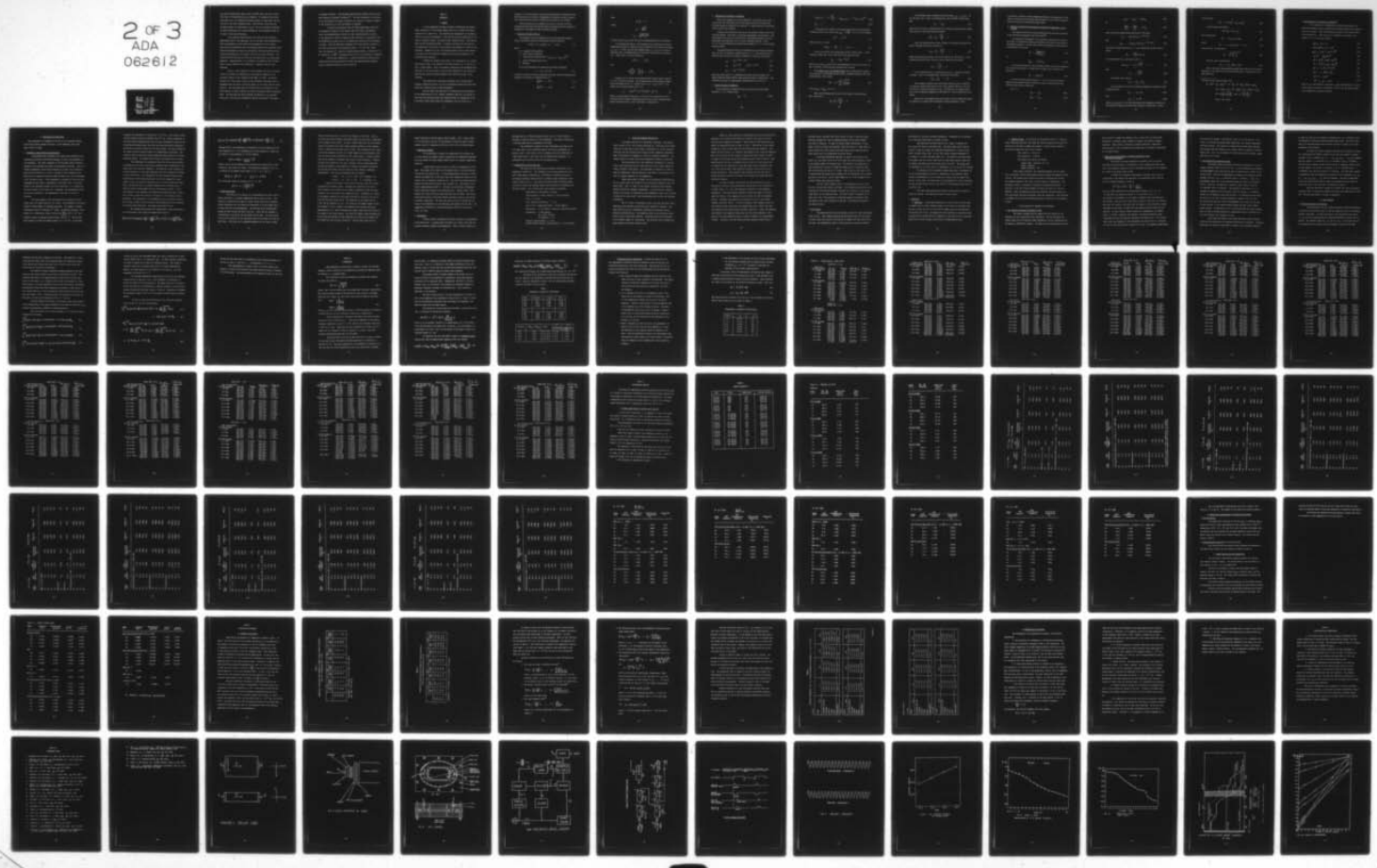

only the thickness-shear mode, which is zeroth mode, and thus a delay line free of unwanted modes can be achieved. In designing the zeroth mode delay line, the frequency-thickness product is kept below that for cut-off of the first dispersive mode. This cut-off occurs when the thickness equals one wavelength or $V_s/2f$ and as the resonant frequency of these transducers has no width dependence, the transducer width can be equal to the strip thickness.

The polygonal delay material was tried for high frequency measurement here in the laboratory, but it has been found experimentally that the assumption of only shear wave propagation was not correct. There existed longitudinal wave contributions which were generated at the reflecting boundaries, since the cut angle of the delay material at the reflecting boundary did not satisfy the critical angle condition. The critical angle is the angle at which only the shear wave can continuously propagate. Experimentally, it is difficult to fabricate this critical angle in delay substrate with perfection. Therefore this has been abandoned.

Hence, a major objective in this research has been to develop a device and method for measuring the viscoelastic response of low viscosity liquids in the frequency range 2MHz to 30 MHz. The device consists of a glass plate in which an RF ultrasonic transverse wave is propagated down the plate, while the liquid is in contact with the major surfaces. The transverse mode of vibration which is polarized in the same direction as major surfaces is called the Meitzler mode as mentioned above. The same mode was used by Meeker and Meitzler in an aluminum strip delay line that was subsequently applied by Hnuston[11] and Meyers

to polymer solutions. The technique described here differs also from the high frequency technique of McSkimin[10]. The wave propagates in the plane of the solid/liquid interface instead of at a normal or oblique incidence to the interface as in the two methods of McSkimin.

It should be understood that all these measurements deal with the mechanical response of the sample under very small deformations where the phenomenological theory of linear viscoelasticity is valid. In the apparatus we shall be measuring the difference in attenuation (ΔA) and difference in phase (ΔB) in the absence of liquid and in the presence of liquid. Then the mechanical impedance Z^* of the liquid is related to the above ΔA and ΔB by the following formula: $Z^* = 2b\rho V (\Delta A + i\Delta B)$. Also, the quantity G^*, called the complex shear modulus, is related to Z^* by equation $Z^* = \sqrt{\rho G^*}$. The quantities Z^* and G^* are functions of frequency.

For the data acquisition, a cross-correlation and walking frequency method has been utilized to obtain the phase/amplitude measurements on pulsed RF echoes to yield ΔA and ΔB.

PART II

APPARATUS

A. Theory

In this experiment the main interest is measuring the dynamic shear viscosity η' of the liquid sample which is in contact with major surfaces of the delay line. The equations for propagation of ultrasonic waves in a plate are developed in this section and then restricted to the case of interest, namely, the lowest order transverse mode. This mode is often called the Meitzler mode[6]. We obtain solutions for the velocity and attenuation of this wave in the presence and absence of liquid at the interface. Equations for the relationship between velocity and attenuation change and the mechanical impedance and the shear modulus of the liquid are also obtained.

Consider an infinite plate (Fig.1) of thickness 2b in a coordinate system, where it is bounded by the major planes at $X = b$ and $X = -b$ with a liquid sample. When an ultrasonic transverse wave propagates down the plate in the Z-direction, a wave is also generated in the liquid because of the no-slip condition between solid plate and liquid at the interface.

The steady-state sinusoidal excitation with the appropriate boundary conditions results in a set of homogeneous equations whose solutions have discrete modes of wave propagation.

For the delay line used here, the dimensions and polarization of the piezoelectric (P.Z.T. ceramic transducer material) are chosen so that only the principal shear mode (Meitzler mode) of propagation is excited while higher shear modes are suppressed (when the plate is in

vacuum). It is very useful to have only the nondispersive Meitzler mode SS (O) because its velocity is independent of frequency and the complication of having several modes of different velocities can be avoided.

Even in the presence of liquid on the major surfaces it will be assumed that only the same SS (O) mode is present since the mechanical impedance of the liquid is much less than the solid.

1. Equations for Shear Waves

The equation of wave propagation for an isotropic homogeneous linear viscoelastic material is generally written as follows:

$$\mu^* \Delta^2 \underset{\sim}{u} + (\lambda^* + \mu^*) \underset{\sim}{\Delta}(\underset{\sim}{\Delta} \cdot \underset{\sim}{u}) = -\rho\omega^2 \underset{\sim}{u} \qquad (1)$$

where

μ^* - complex shear modulus

λ^* - other Lame coefficient

u - total particle displacement $U_{(x, y, z, t)} = u_{(x, y, z)} e^{i\omega t}$

$\underset{\sim}{u}$ - particle displacement vector

ρ - density.

If one uses Hamilton's decomposition method by defining

$$\underset{\sim}{u} = \Delta\phi + (\underset{\sim}{\Delta} \times \underset{\sim}{W}) \qquad (2)$$

in terms of scalar and vector potentials ϕ and $\underset{\sim}{W}$, then the following wave equations in ϕ and $\underset{\sim}{W}$ are obtained from (1):

$$V_D^2 \Delta^2 \phi = -\omega^2 \phi \qquad (3)$$

$$V_S^2 \Delta^2 \underset{\sim}{W} = -\omega W \qquad (4)$$

with

$$\underline{\underline{\Delta}} \cdot \underline{\underline{W}} = 0 \tag{5}$$

where

$$V_S = \sqrt{\frac{\mu^*}{\rho}}$$

$$V_D = \sqrt{\frac{2\mu^* + \lambda^*}{\rho}}$$

in which V_S and V_D are the transverse and dilatational wave velocities.

In our delay line device, the transducers are polarized to provide displacements with a component in the y-direction only, hence we assume $u_x = u_z = 0$. Thus, the wave has displacement $u_y = u_y(x, 0, z, t)$ in the y-direction only; the displacement is assumed to be the same everywhere in y. Thus, Eqs. (3) and (4) reduce to:

$$\mu^* \Delta^2 u_y = -\rho\omega^2 u_y \tag{6}$$

and

$$\mu^*\left(\frac{\partial^2 u_y}{\partial x^2} + \frac{\partial u_y}{\partial z^2}\right) = -\rho\omega^2 u_y \tag{7}$$

Equation (7) is a shear wave equation with complex shear modulus μ^* (one of Lamés constants). By the application of the method of separation of variables to Eq. (7), namely $U_y(x, 0, z, t) = U_y(x, 0, z)e^{i\ t}$, one obtains for the total solution of Eq. (7)

$$U_y = A(Ce^{mz} + De^{-mz})(Ee^{nx} + Fe^{-nx}) \tag{8}$$

where ω is the angular frequency, A, C, D, E, F are constants to be determined by the boundary conditions and m and n are the complex propagation constants in the z- and x-directions, respectively.

2. Displacement Boundary Conditions

This same equation can now be applied to each of the three regions of interest: the solid delay line and the upper and lower liquid layers; then the boundary conditions are matched. In steady state the frequencies are the same in all regions.

Consider the transverse wave in the viscoelastic medium above and below the plates. This wave is traveling unbounded in the positive z- and x-directions and since it is traveling in an attenuating medium, the displacement must approach zero as z and x approach infinity. Then $C = E = 0$ in the liquid above the plate and similarly $C = F = 0$ in the liquid below the plate.

In the plate itself the waves are bounded in the x-direction and thus there is only one boundary condition that is $C = 0$. The solutions can be obtained with symmetric boundary condition in x-direction as follows:

$$u_{yo} = H_o e^{-m_o z} e^{-n_o x} \tag{9a}$$

$$u_{y1} = H_1 e^{-m_1 z} \left(e^{n_1 x} + e^{-n_1 x}\right) \tag{9b}$$

$$u_{y2} = H_o e^{-m_o z} e^{n_o x} \tag{9c}$$

where the subscripts 0, 1, 2 designate the region above the plate, the region within the plate and the region below the plate, respectively. The symbols H_o and H_1 are appropriate combinations of A, C, D, E, F.

3. Stress Boundary Conditions

In the presence of liquid the stress continuity across the plane boundary, $x = \pm b$, requires that

$$\sigma_{xx} = 0 \tag{10a}$$

$$\sigma_{xy(\lambda, y, t)} = \mu^* \frac{\partial U_y}{\partial x} = \sigma_{\lambda y(s, y, z, t)} = \bar{\sigma}_{\lambda y(x, y, z)} e^{i\omega t} \tag{10b}$$

$$\sigma_{xz} = 0. \tag{10c}$$

If the plate is in vacuum, all component stresses across the plate surface must be zero, hence from $\sigma_{xy} = \mu^* \frac{\partial u_y}{\partial x} = 0$ at $x = \pm b$ one obtains

$$e^{n_1 b} = e^{-n_1 b} \tag{11}$$

Thus real $[n_1] = 0$ and

$$IM[n_1] = \frac{\pi I}{b}, \quad I = 0, 1, 2, \cdots\cdots \tag{12}$$

If we now restrict our consideration to the solution with I = 0 (the Meitzler mode), Eq. (10) for the wave in the plate becomes

$$U_{y1} = 2H_1 e^{-m_{1V} Z} \tag{13}$$

where m_{1V} and m_{1L} will refer to the propagation vector in the solid, in the z-direction, in the absence and presence of liquid.

If the plate is in a viscoelastic liquid, the complex shear modulus of the liquid μ^* is obtained from the stress continuity equation (10b) combined with Eq. (9b) to yield

$$\mu_o^* = \mu_1 \frac{n_1(1 - e^{2n_1 b})}{n_o(1 + e^{2n_1 b})} \tag{14}$$

since $(\sigma_{xy})_o = (\sigma_{xy})_1$, at $x = b$.

Next, the following wave vector for the liquid is obtained from Eqs. (9z) and (7)

$$m_o^2 + n_o^2 + \frac{\omega^2 \rho_o}{\mu_o^*} = 0 \tag{15}$$

From displacement continuity across the plate, $u_{y_o} = u_{y_1}$ at $x = +b$ for all values of z. Thus, by equating Eqs. (9a) and (9b), one conclues that

$$m_o = m_{1L} \tag{16}$$

Hence Eq. (15) can be combined with (16) to obtain an equation that couples wave vectors in the liquid and in the solid.

$$m_{1L}^2 + n_o^2 + \frac{\omega^2 \rho_o}{\mu_o^*} = 0 \tag{17}$$

Next, the following wave vector relation for the plate (in liquid contact) is obtained from Eqs. (9b) and (7)

$$m_{1L} + n_1^2 + \frac{\omega^2 \rho_1}{\mu_1} = 0 \tag{18}$$

While for the plate <u>in</u> vacuum, we have shown by Eq. (12) that $n_1 = 0$ for the Meitzler mode, thus, the wave vector relation (18) becomes

$$m_{1V} + \frac{\omega^2 \rho_1}{\mu_1} = 0 \tag{19}$$

In our experiment m_1 is measured in air (i.e., vacuum) and again in liquid. Thus, by combining Eqs. (18) and (19) we obtain

$$m_{1L}^2 - m_{1V}^2 = - n_1^2 \tag{20}$$

The complex modulus of the viscoelastic liquid μ_o^* can be obtained by using the experimental values of Eq. (20) together with Eqs. (14) and (17) to give a quadratic equation for μ_o^*. Alternatively, an ezplicit relation to the mechanical impedance of the liquid z*, can be obtained as seen below.

Notice some assumptions that were made in the preceding discussion: (1) Motions are steady-state sinusoidal of small amplitude so that

no nonlinear response of the propagating media can be neglected; (2) the plate is assumed to be isotropic and homogeneous and (3) the transducer will only excite the nondispersive SS(0) mode.

4. Relation of Mechanical Impedance of Liquid to Propagation Vector in Solid

The equations derived in the preceding section can also be related to the mechanical impedance Z_o^* of the liquid[26].

The mechanical impedance of a material is defined as the ratio of the stress to the particle velocity produced by that stress at any surface through the material. For the shear stress components of interest here in the liquid we can write

$$Z_o^* \equiv \frac{\bar{\sigma}_{xyo(x,z)}}{i\omega U_{yo(x,z)}} \tag{21a}$$

or

$$\bar{\sigma}_{xyo} = i\omega Z_o^* U_{yo} \tag{21b}$$

It can be shown that the characteristic (shear) mechanical impedance for an unbounded liquid is related to the complex shear modulus and density by

$$Z_o^* = (\rho_o \mu_o^*)1/2 \tag{22}$$

Across the liquid-plate interface, $x = +b$, we have seen that displacement and stress must be continuous, hence velocity and stress/velocity must also be continuous.

At $x = b$

$$U_{y1} = U_{yo} \tag{23a}$$

$$\dot{U}_{y1} = \dot{U}_{yo} \tag{23b}$$

$$\sigma_{xyl} = \sigma_{xyo} = Z_o^* U_{yo} \tag{23c}$$

or

$$\frac{\sigma_{xyl}}{U_{yl}} = \frac{\sigma_{xyo}}{U_{yo}} = i\omega Z_o^* \tag{23d}$$

Since we had for displacement and stress in the plate

$$U_{yl} = 2H_1 \cosh n_1 x \, e^{-m_1 Z} e^{i\omega t} \tag{24}$$

and

$$\sigma_{xyl} = -2H_1 \mu_1 n_1 \sinh n_1 x \, e^{-m_1 Z} e^{i\omega t} \tag{25}$$

the values of these functions at $x = b$ are substituted into Eq. (23d) to obtain

$$Z_o^* = i \frac{\mu_1 n_1}{\omega} \tanh n_1 b \tag{26}$$

If we expand $\tanh n_1 b$, and take $|n_1 b| \ll 1$,

$$\tanh n_1 b = n_1 b + \frac{(n_1 b)^3}{3} + \cdots\cdots \tag{27}$$

then

$$Z_o^* = i \frac{\mu_1 n_1^2 b}{\omega} \tag{28}$$

We had Eq. (20), that is,

$$-n_1^2 = m_{1L}^2 - m_{1V}^2 \tag{20}$$

It is convenient to write the complex propagation constants in their component form:

$$m_{1V} \equiv A_o + iB_o \tag{29a}$$

and

$$m_{1L} \equiv A + iB \tag{29b}$$

where A_o, B_o and A, B are the attenuation and propagation constants in the plate in the absence and presence of liquid, respectively. Hence,

from Eq. (20)

$$- n_1^2 = (A + iB)^2 - (A_o + iB_o)^2 \tag{30}$$

For the usual case* where

$$(B + B_o) >> (A + A_o) \tag{31}$$

Eq. (30) becomes

$$- n_1^2 = 2B_o(- \Delta B + i\Delta A) \tag{32}$$

where

$$\Delta A = A - A_o \text{ and } \Delta B = B - B. \tag{33}$$

and from Eqs. (19) and (29a)

$$B_o = \left(\frac{\rho_1 \omega^2}{\mu_1} \right)^{1/2} \tag{34}$$

Now Eq. (28) is rewritten as

$$Z_o^* = 2V_{s\ 1} b(\Delta A + i\Delta B) \tag{35}$$

This is the basic experimental equation that relates the mechanical impedance of the liquid to the measured differences in attenuation in the plate delay line.

---

*Assume $B_o \approx B$, and from Eqs. (31),

$$(A + iB)^2 - (A_o + iB_o)^2 = A^2 - A_o^2 - B^2 + B_o^2 + 2i(AB - A_oB_o)$$

$$= (A - A_o)(A + A_o) - (B - B_o)(B + B_o) + 2i(AB - A_oB_o)$$

$$= (B + B_o)\left(\Delta A \frac{A + A_o}{B + B_o} - \Delta B + 2i \frac{\Delta A - B_o}{B + B_o}\right)$$

$$\approx 2B_o(- \Delta B + i\Delta A)$$

5. Relationships of Viscoelastic Constants[22]

It is convenient to summarize the interrelation between the mechanical impedance and the complex shear modulus parameters for description of the liquid. These relationships are based on the linear theory of viscoelasticity. Also note that in viscoelastic convention, the symbol $G^* \equiv \mu^*$ for the shear modulus:

$$Z^* \equiv R + iX \tag{36}$$

$$G^* \equiv \mu^* \equiv G' + iG'' \tag{37}$$

$$|G| \equiv (G'^2 + G''^2)^{1/2} \tag{38}$$

$$Z^* = (\rho_0 G^*)^{1/2} \tag{39}$$

$$R = \rho_0^{1/2} (|G| - G')^{1/2} \tag{40}$$

$$X = \rho_0^{1/2} (|G| - G'')^{1/2} \tag{41}$$

$$G' = (R^2 - X^2)/\rho_0 \tag{42}$$

$$G'' = 2RX/\rho_0 \tag{43}$$

$$G^* = i\omega\eta^* \tag{44}$$

$$\eta^* \equiv \eta' - i\eta'' \tag{45}$$

where R and X are mechanical resistance, ρ_0 the liquid density, G' and G'' are the shear storage and loss moduli, η' and η'' are the real and imaginary components of dynamic viscosity.

B. Description of Delay Line

This instrument is intended for the use of low viscosity samples, particularly dilute polymer solutions, in the frequency region from about 3 MHz to 30 MHz.

1. Transducer, Delay Material and Equations

The piezoelectric transducer will vibrate when subjected to an alternating electrical field whose frequency is within the bandwidth of the transducer. The center frequency of the thickness shear transducer depends on its thickness and choice of piezoelectric material. The P.Z.T. ceramic transducers, whose center frequency is 20 MHz, are rectangular bars with the width 2b (b = 0.030"), the same as the thickness of the delay line, of length one third the width of delay line, and of thickness 0.007" as shown in Fig.1. This transducer is designed to drive only the nondispersive SS(O) mode of propagation in the delay line. The polarization of the transducer motion is in the y-direction, i.e., parallel to the major surface of the delay line. Therefore, the displacement exists only in the y-direction. The propagation of the wave is in the z-direction.

The delay medium of low loss fused silica (quartz) is three inches long, two inches wide and .060" thick. The smoothness of the major surface of delay medium is extremely important. For example, consider a Newtonian liquid of viscosity 10^{-2} poise. The damping length in centimeters for a viscoelastic liquid is given by $\left[\frac{\omega^2\rho}{2|G''|^2}\left(|G^*| - G\right)\right]^{-\frac{1}{2}}$; for a Newtonian liquid the damping length becomes $(\omega^2\rho/2G'')^{-\frac{1}{2}}$. Thus for the above liquid at 30 MHz the damping length is 1×10^{-5} cm. At the same

frequency the wavelength in the solid is 1×10^{-2} cm. The surface irregularities should be kept much smaller than 10^{-5} cm. Surface smoothness of the delay medium reported herein have not been established in spite of the claims made by manufacturers that they have done high quality mechanical polishing on the major surfaces of the delay medium. The small streaks of the random lines are observed under 20 × magnification microscope. The streak of lines on the major surface might have been caused by a careless polishing process. The nominal delay time of the delay line is 20 μ sec.

The transducers are mounted at both ends of the delay material. A transducer at one end is the driving transducer and a transducer at the other end is the receiving transducer. The mounting of the transducer to the delay material is critically important since the transducer thickness is only 0.007" thick. The thickness of the bond between transducer and cross-section of the delay material has to be thin compared to a wavelength (0.014") so that wave reflection will not occur between the interfaces; the adhesive has to be spread uniformly over the whole area in order to produce uniform phase shift of the mechanical signal. A thin lead backing is also important for reflection consideration and is necessary in order to make the electrical connection to the backside of the transducer. The connection to the transducer is by a very thin flexible wire so that it does not exert stress on the transducer and also minimize the acoustic wave reflection. The details are shown in Fig. 2.

The coupled wave solutions for displacement in the y-direction u, in the solid and in the liquid are respectively given by

$$U_s(x,z,t) = H_s \exp\left[-i\left(\frac{\omega^2}{V^2} - i\frac{\omega Z^*}{b\rho V^2}\right)^{1/2} Z + i\omega t\right] \cos\left(\frac{i\omega Z^*}{b\rho V^2}\right)^{1/2} X \quad (46)$$

$$U_L(x,z,t) = H_L \exp\left[-i\left(\frac{\omega^2}{V^2} + i\frac{\omega Z^*}{bpV^2}\right)^{\frac{1}{2}} z + i\omega t\right] \exp\left[-i\frac{\omega \rho_L}{Z^*} x\right] \quad (47)$$

Through Eq. (46), the difference in attenuation ΔA and in phase ΔB of the wave measured at $Z = \ell$ in the absence and in the presence of liquid can be related to the mechanical Z^* of the liquid by

$$\Delta A + i\Delta B = \frac{1}{2bpV} Z^* \quad (48)$$

where ρ and ρ_L are the density of the solid and the liquid and V is the velocity in the solid with liquid. The mechanical impedance $Z^* \equiv R + iX$ is related to the dynamic shear moduli $G^* \equiv G' + iG'' \equiv i\omega\eta'$ by

$$\rho_L G' \equiv R^2 - X^2 \quad ; \quad \rho_L G'' = 2RX \quad (49)$$

For a Newtonian liquid of viscosity η, $G' = 0$, thus

$$R = X = \left(\frac{\rho\omega\eta}{2}\right)^{1/2} \quad (50)$$

2. Delay Line Holder

The delay line is mounted in a polycarbonate cell which can be easily inserted in a constant temperature bath as shown in Fig. 3. The electrical connections are made of coaxial cables which have waterproof teflon insulation, and the cables are terminated in o-ring clamps (Fig. 3) to seal them into the polycarbonate. Two one-inch thick polycarbonate plates are used to make the delay line cell. There are two recessed o-ring grooves in one plate, and one groove in the other. The large outer o-ring is for isolation of the electrical part of the delay line from the bath water. The delay line is suspended between the two inner o-rings.

These o-rings also serve to isolate the samples to be tested. That is, the delay line major surfaces and holder inside the wall form a compartment for the sample to be tested. To form a liquid tight seal with the brittle fused silica delay line at the lowest possible stresses (o-ring compression), a rather soft silicone o-ring is used. The thickness of the o-ring is selected carefully so that it is large enough for wave penetration and does not have any wave reflection in the liquid sample. Silicone o-rings have better durometer (softness) than those of other materials. Chemical silicone was satisfactory for water, alcohols, DOP and polystyrene-DOP solution but swells in the presence of toluene, cyclohexane and benzene. The o-rings were bought from the Irving B. Moore Company, Cambridge, Massachusetts. The sizes and durometer were as follows:

o-ring 1 I.D. = 2½, W = 1/16 #10 Durometer = 60

o-ring 2 I.D. = 4½, W = 3/16 # 3 Durometer = 70.

There are two holes in each side of the cell plate for filling and emptying the sample liquid. Syringes are connected to the end of teflon tubings which extend from the sample compartment inside the polycarbonate cell to outside of the temperature bath. Therefore, the volume of the sample injected into both major surfaces of the delay line can be read off from the syringe scale. The thickness of the sample cell is 0.015" and the diameter is 2.5". The volume of the sample liquid in each cell becomes 0.74 mℓ. However, the reading of the syringe scale was approximately 2 mℓ. This was because the sample liquid was also filled in the length of the teflon tubing. The holes for sample liquid exchange have to be lined up vertically so that emptying and filling of the sample can be carried out with the help of gravity. Gravity helps avoid the air

bubble forming and leaving sample liquid trapped. Also, a small weight of 1 lb was used at the end of the syringe to create the gentle steady gradual motion for emptying and filling of the cell with liquid sample.

3. Temperature Control

It is necessary to control the temperature of the delay line not only because the sample (liquid) properties are temperature dependent but also because the delay medium (fused silica) is strongly temperature sensitive.

A Neslab RTE-4 unit was used to control the temperature of the bath. The Z-pump of the control unit enables water to circulate between the bath and the control unit. It takes approximately two hours to equilibrate the sample cell in the bath water when temperature setting of the control unit is lowered or raised by 5°C. The total circulating distance between the bath and the control unit is about 6 ft. The volume of the bath is approximately 16,000 cc. The bath is constructed of thermopane double glass walls mounted in an aluminum frame. Several coats of RTV adhesive are used to seal the glass sections into the frame. The double glass walls provide an excellent thermal insulation from the fluctuation of ambient temperature. The water was used for the bath liquid and the range of the temperature in the experiment was between 10°C and 25°C. The temperature fluctuation of the bath was about 0.005°C in an hour and 0.05°C in a day.

4. Thermometry

A quartz crystal thermometer was used to measure the temperature of the bath water. A crystal quartz had been cut in such a way that the resonant frequency changes with temperature. When the quartz crystal is

adjoined with H.P. 2830A oscillator sensor, the G.R. 1192B counter is provided to read the output of this thermometer. The quartz crystal has a rod-like shape which is immersed in the bath.

The calibration constant for this thermometer was found to be 0.87 KHz/C when it was calibrated against the mercury thermometer as shown in Fig.8. This value is not in agreement with the coefficient of 0.9861 KHz/C which is the value that the manufacturers supplied. No explanation can be given for this at the present time.

5. Manufacturer of the Delay Line

The delay line was fabricated by Andersen Laboratories, Inc., Bloomfield, Connecticut. The transducer and the delay medium are P.Z.T. and a fused quartz, respectively. The method of fabrication was the multilayer transducer mounting with an optimum energy transduction technique as shown in Fig.2. The tinfoil was used between conductive epoxy in order to achieve the maximum energy couple between the transducer and the delay medium. The following data were supplied by Andersen:

Delay Medium - Fused Quartz, polished

Particle Motion - Shear, Parallel to Major Surfaces

Delay - 20 μs nom.

Loss, Terminal-to-Terminal: 1 - 2 db

Loss, in 50 Ω comparison system: - 14 db (approx.)

Reflections: - 10 db (approx.) referred to previous signals

Transducers: 20 MHz ceramic
Cp ~ 1500 - 2000 pfd
Rp (dynamic) ~ 10 Ω

Density of Delay Medium - 2.2 g/cc

Acoustic Shear Velocity of Delay Medium - 3.8×10^5 cm/sec.

C. Drive and Response Electronics

The method used here is a pulse-echo technique. This method uses a series of R.F. drive pulses generated at a relatively slow repetition rate so that when a drive pulse is generated, all of the vibration resulting from the previous drive pulse has been completely attenuated. Each of the pulses is composed of a train of sinusoidal vibration. Its nominal width is 20 μsec long and the repetition interval is 1280 μsec.

The pulse method has a very important advantage of a low duty cycle; since the pulse rate is relatively slow, only a small amount of energy is added to the system. This phenomena is important in order to keep the temperature from fluctuating in the device; the velocity of the wave is strongly dependent on the temperature.

These input pulses to delay line are generated electrically by an R.F. pulser which was designed to give the proper repetition rate and pulse width. The C.W. input to this pulser originates from a Hewlett Packard 5110A/5100A frequency synthesizer. A precise 40 μsec clocking pulse for the pulser is generated by the programmable clock; this interval is based on the same stable 1 MHz oscilliscope which drives the frequency synthesizer.

The R.F. pulser is designed in such a way that the pulse width, repetition rate and pulse delay time can be adjusted as follows: the pulse width is set by a monostable, adjusting time constant with an external potentiometer R_1. The repetition rate is set by digital multiplier of the 40 μsec pulse interval. The pulse delay is set precisely to an integral number of 1 μsec pulse. The detailed circuit diagram and pulse sequence are shown in Figs.5 and 6.

These R.F. drive pulses are transformed by the input piezoelectric transducer into acoustic waves which are echoed in the delay line until they have been completely attenuated. These echoes in the delay line will exhibit an exponential decay as shown in Fig.2. When driven at the center frequency of circa 20 MHz, more than ten echoes have been observed. The sample and hold circuit is a Tektronic 586 sampling unit, where the sampling part of the circuit and the external trigger mode were utilized in order to sample the incoming pulsed radio frequency signal from the device. This sample-and-hold circuit is triggered every 40 μsec by a fast pulse which is produced by the combination of the mark pulse from the mono ③ of the R.F. pulse and the same 1 MHz reference oscillator that drives the frequency synthesizer. These sampled analog signals are then fed into an analog-to-digital converter and stored in the memory of GE/PAC-4020 data processing computer.

In order to ensure the precise time synchronization, all the electronics involved in data acquisition process have to be referenced to a single clock, i.e., the 1 MHz reference oscillator in the frequency synthesizer. The phase change produced by adding the sample is so very small that jitter in the sampling circuit trigger can lead to erroneous results. Therefore this experiment involves the use of a very stable external electronic source. In order to sample a high frequency train of sine waves and then reconstruct the sampled data into a single sine wave, the sampling circuit must satisfy two basic conditions. First, the aperture time window of the sampling circuit must be very short compared to the period of the high frequency signal in order to measure an "instantaneous voltage". Secondly, the time interval between sampling pulses must be

precisely known, and must have little jitter in order to maintain phase coherence between the train of sampling pulses and the high frequency sine wave of interest. In order to achieve these requirements, a snap-diode is used to convert the standard 1 MHz sine wave to a 1 MHz train of narrow pulses and a gate selects each 40th pulse as the sampling pulse. These pulses are a few nanoseconds wide fast pulses.

An HP 461A broad-band amplifier is used at the output of the delay line, and either 20 db or 40 db of gain were used according to level of the output signal of the delay line. The output of the amplifier is then connected to B input of a model 4S1 plug-in unit of sampling scope with the vertical gain set at 10 mv/cm. The A input of the plug-in unit is derived from the output drive frequency of the synthesizer with vertical gain set at 100 mv/cm. This A input signal is C.W., and is tapped at the voltage divider just before the mixer.

The two "hold" outputs A and B of the sampling scope are then fed into the analog-to-digital converter. The differential amplifier input terminals of the analog-to-digital converter are connected to the single ended output of the sampling scope. The outer shield is grounded at the scope only, and a load resistor is connected between the negative side and ground of the input terminals of the ADC. The detailed electronics are shown in Fig.4.

1. R.F. Pulser

The program clock is set to produce a train of 1 μsec wide pulses every 40 μsec. Upon computer program initialization signal to the pulser 16 clock pulses are counted in the pulser to produce one gate pulse after 640 μsec, and subsequently every 32 clock pulses are counted to produce

gate pulses at 1280 μsec intervals thereafter. Monostable #1 is adjusted to set the gate pulse width to nominal 20 μsec.

The gate pulse is mixed with the R.F. signal to produce the R.F. pulse for input to the delay line. The same output pulse from the counter is used to trigger the adjustable monostable #2 in order to produce a variable delay time. In turn this output triggers monostable #3 to produce a 0.9 μsec wide mask pulse (P3). The width of this mask pulse will permit only one of the 1 MHz train of snap diode pulses to pass and to trigger the sample and hold circuit every 1280 μsec. The pulse width of monostable #3 is set by the R.C. combination of 1.271 kΩ and 10^{-3} μ farad.

The purpose of the (variable) delayed mask pulse, (adjustment of the 50 kΩ potentiometer of the R.C. combination in the external timing circuit of monostable #2) is to enable us to select only one delay line echo at a time; thus, the delay time of the monostable #2 is set accurately so that the mask pulse occurs at the center of the selected output echo of the delay line.

The reset pulse produced by program initialization is used to reset the counter. The details are shown in Figs.5 and 6.

2. Detection

2.1 Amplifier. A broad-band amplifier, H.P. 461 20 dB - 40 dB was used to amplify the low level response signal at the output of the delay line. The gain control was set to 20 dB and the output signal of the amplifier was greater than 40 mv. We assumed that this amplifier is linear and that the phase shift introduced by the amplifier is the same for all the pulses regardless of their voltage level within our experimental range.

2.2 Sampling Scope. As indicated in the previous section, a sampling scope (Tektronix model 661 with model 461 vertical amplifier and model 5T3 timing unit) was used to sample the signals, A channel and B channel of the vertical amplifiers were set as follows:

Gain control A: 100 mv/cm

Gain control B: 10 mv/cm

5T3 timing unit was set as follows:

trigger mode: external, DC, 50 Ω
slope: negative
sample points/cm: 100.

Under these conditions, the staircase generator of the timing unit is inactive, and the input pulse directly triggers the sampling bridge circuit. The vertical gain controls are used to attenuate the driving and response signals at the input A and the input B, respectively. The smoothness control is adjusted to minimize the sampling hysteresis. In practice, it has been found necessary to select one echo at a time for sampling. When the sampling circuit was constantly switched between one echo and another excessive hysteresis noise was introduced. This phenomena is probably due to the long discharging time of capacitor at the sampling circuit.

D. Data Acquisition (Hardware and Software)

1. ADC (Analog to Digital Converter) to CPU

The output voltages from the sample and hold circuit of the sampling unit are available for ADC conversion. The ADC digitizes the analog signal and the digitally coded information will be transferred into the memory of GEPAC-4020 computer. The same pulse recurring every 40 μsec,

that is used to trigger the sampling unit, is also used to initiate ADC conversion, to execute a data transfer to memory, and causes a computer interrupt. Each interrupt initiates a program subroutine, "READ DATA" whose function it is to organize the incoming data into memory as described in the next section.

2. Selection and Development of Walking Frequencies from Synchronous Frequency

The method of walking frequencies as shown in Fig.7 has been developed for the purpose of transforming a high frequency periodic signal into a low frequency signal that can be digitized and read into the computer at a rate of one point every 40 μsec.

In order for a complete and separate sinusoidal wave to be reconstructed in the memory from each echo, the synthesizer must always be set to a walking frequency f given by

$$f = f_N + \Delta f = \frac{N}{T} + \frac{1}{32nT}$$

where $f_N = \frac{N}{T}$ corresponds to any synchronous frequency (e.g., $f_N = N \times$ $\times$ 25 KHz since the sampling interval T = 40 μsec and N = 1, 2, 3, ...). The integer 32 corresponds to the number of samples taken following each drive pulse. Thus the cyclic repetition interval is 1280 μsec (32 × 40 μsec). Note that the length of the delay line was chosen so that successive echoes are about 40 μsec apart in order that the sampling pulse overlap the echo duration. We then choose n memory location to correspond to 2π radians. Since n = Δf/32T = constant, then choose n to provide sufficient phase resolution for sine wave storage consistent with memory size. At the same time, since the frequency of the synthesizer can only be set to a multiple of 0.01 Hz, then Δf must be a multiple of 0.01 Hz. The possible combinations

of n and Δf are either n = 125 and Δf = 6.25, or n = 625 and Δf = 1.25. Since n = 625 gives the better phase resolution, this latter combination has been selected. The values of n larger than 625 have been neglected even though there are solutions for n larger than 625, because of limited memory size. As it is, we require 625 locations for each sinusoid, namely each echo, to be stored.

3. Data Acquisition Software Outline

The memory region associated with data is initially set to zero (memory locations from 21,000 to 37,777). In the initialization procedure, the programmable reset pulse must be sent to reset the R.F. pulser to its initial state. This was accomplished by an output to the external control register "XA" bit (i.e., B = 2504 1004 with A = 0000 3000). Next, the programmable clock "XC" in the interface module is reset by B = 2504 1004 with A = 0000 3000, and then set to produce a pulse every 40 μsec by B = 2504 1004 with A = 0014 2400. The purpose of this pulse is: 1) to activate the repetition rate counter in the R.F. pulser, 2) to enable a trigger to the sampling scope every 40 μsec, 3) to initiate the ADC every 40 μsec and 4) to send a program interrupt to computer every 40 μsec. The same instruction that sets the programmable clock also sets the mode of data transfer to the computer memory through the DMA, direct memory access channel. By setting bit 10 = 1, we have selected the single address mode, so that new output from ADC is transferred directly to memory location 20,000 every clock interval, 40 μsec.

This means that every 40 μsec fresh data enter memory location 20,000 and the instruction at interrupt location 265 is executed. A program instruction of "Branch to read data" is stored in the interrupt location

in order to carry out the sequence of reading data (i.e., 1400/3027) into the sequential locations as each interrupt comes along. The first interrupt is in synchronization with the start of the R.F. pulser, as is each subsequent 32nd interrupt.

By using the initial interrupt and every 32nd interrupt or after, as a synchronization method, sequence of the data that appears at memory location 20,000 is numbered b_o, b_1 .... b_{14}, b_{15}, b_{16} .... b_{31} and repeated. When ADC channel 1 is selected (i.e., B = 25041004 with A = 00142400), then the data at memory location 20,000 are the b (response) signal; whereas when channel 2 of the ADC is selected (i.e., B = 25041004 with A = = 00142400), then the drive signal A is selected. The "Read Data" program is designed so that the sequences at location 20,000 correspond to b_o, b_1, b_2 ... b_{14}, a_{15}, b_{16} .... b_{31} and this repeated. The entire "READ Data" routine is recycled 456 times in order to preaverage the data points to reduce the noise in the sine wave reconstruction process.

When the "Read Data" program is finished, the digital-to-analog converter (DAC) is utilized to display the stored data sequentially on the CRT. The detailed program is listed in Appendix A.

E. Data Analysis

1. Cross-Correlation and Averaging

The determination of the relative amplitude and phase difference of the drive and response signal is the most important part of the dynamic analysis experiment. As indicated earlier, the sinusoidal drive signal $A = a_{15} \sin \omega t$ is generated by the frequency synthesizer through the R.F. pulser. The response signals $B_i = b_i \sin (\omega t + \varphi_i)$ + noise from the output transducer of the delay line are sinusoidal echoes with the same

frequency but have noise components in addition. The subscript i designates the echo number; the first response signal has traveled the length of the delay line without reflection, but it will be still called the zeroth echo for the sake of convenience.

The method of walking frequencies enables sampling of the amplitude of each analog signal in real time at intervals of 40 μsec. The digitized amplitude of the sampled signal is then stored into the data region of the memory (i.e, locations 22200 - 36600) as mentioned in "Read Data" section. For each individual echo and the drive signal, the sampled and digitized values are stored sequentially according to their phase of $2\pi/n$, where there are n = 625 locations for each period for each echo and the drive signal. Thus, a single sinusoid is reconstructed in memory for each echo; the data are accumulated in 625 × 32 × 40 μsec.

The data obtained and stored in this manner lends itself ideally to the determination of the phase difference θ and relative amplitude b_i/a_{15} through the mathematical technique of cross-correlation.

Since the signals are of known frequency ω, the following useful integrals can be formed

$$\int_0^{2\pi} a_{15} \sin(\omega t + \phi_A)\, C \sin \omega t \, d\omega t = \pi C a_{15} \cos \phi_A \tag{51}$$

$$\int_0^{2\pi} a_{15} \sin(\omega t + \phi_A)\, C \cos \omega t \, d\omega t = \pi C a_{15} \sin \phi_A \tag{52}$$

$$\int_0^{2\pi} b_i \sin(\omega t + \phi_i)\, C \sin \omega t \, d\omega t = \pi C b_i \cos \phi_i \tag{53}$$

$$\int_0^{2\pi} b_i \sin(\omega t + \phi_i)\, C \cos \omega t \, d\omega t = \pi C b_i \sin \phi_i \tag{54}$$

in which φ_A and φ_i are each phase angles of a and b_i relative to an arbitrarily chosen time t = 0 in Eqs. (51) - (54). An ideal software constructed is stored in memory and is used as a reference signal. This helps to eliminate errors due to nonzero base line in the above integrations. However, the phase angles φ of b_i relative to a is just $\varphi_i - \varphi_o$, thus independent of choice for t = 0.

The desired experimental quantities b_i/a and $\Delta\varphi$ can be obtained through the use of Eqs. (51) - (54). This technique of integration is called the method of cross-correlation. The phase shift of $\pi/2$ required for Eqs. (52) and (54) is achieved by a circular rotation of the b_i vector regions through N/4 locations, where N = 625 here. Therefore, N/4 becomes the noninteger number of 156.25; but the memory locations must be integer numbers.

In order to resolve this difficulty, the following approximations for Eqs. (51) and (52) were adopted:

$$4\int_0^{2\pi} a_{15}\sin(\omega t+\phi_A)\,C\sin\omega t\,d\omega t = 4\cdot\frac{2\pi}{625}\sum_{j=0}^{j=624} a_j c_j \tag{55}$$

$$= 4\pi a_{15} C\cos\phi_A \tag{56}$$

$$4\int_0^{2\pi} a_{15}\sin(\omega t+\phi_A)\,C\cos\omega t\,d\omega t$$

$$\approx 3\cdot\frac{2\pi}{625}\sum_{j=0}^{j=624} a_j c_{j+156} + \frac{2\pi}{625}\sum_{j=0}^{j=624} a_j c_{j+157} \tag{57}$$

$$\approx 4\pi a_{15} C\sin\phi_A \tag{58}$$

Notice that the data region is considered to have circular boundary conditions, so that $j = 625, 626, \ldots$ is equivalent to $j = 0, 1, \ldots$.

This approximation is exact to the extent that linear interpolation is valid for the value of the cosine function within an interval of $2\pi/625$ radians. The same procedure can be applied to Eqs. (53) and (54).

PART III

CALIBRATION

The calibration of the device is based on fluids, DOP and ETOH (ethanol), which we believe to be Newtonian up through the frequency range of interest, i.e., beyond 30 MHz.

For a Newtonian fluid the mechanical resistance and reactance are equal and given by

$$R = X = \sqrt{\frac{\omega \rho \eta}{2}} \tag{59}$$

where ρ and η are the density and the steady-state viscosity, respectively. The relation between measured attenuation per unit length ΔA and phase shift per unit length, ΔB, and R and X were given by equation and shown here

$$\Delta A = \frac{R}{2 V_s \rho_1 b}$$

$$\Delta B = \frac{X}{2 V_s \rho_1 b} \tag{60}$$

where V_s, ρ_1 and 2b are the wave velocity in the delay medium, the density of delay material and the thickness of delay line, respectively.

The raw experimental attenuation and phase shift data for ETOH and DOP is seen in Figs.16 and 17. This data is measured at the various indicated temperature from 25°C to 10°C and over the frequency range from 3.4 MHz to 27.1 MHz. These data are then replotted as a function of the square root of frequency in Figs.18 through 20 in order to test the linearity predicted by Eqs.(59) and (60) above.

Notice the data in Fig.18 in which the ratio of output to input of the entire delay line system including amplifiers is plotted as a function of $\sqrt{f}$. The major resonance of the transducers is evident as is the fact that the total attenuation for the more viscous DOP is greater

than for EPOH. An important secondary effect can also be observed from this curve. That is, in addition to the higher attenuation of the DOP response curve, it can be seen (by vertical and horizontal shifting) that the DOP curve is shifted slightly towards lower frequency.

The primary effect of liquid loading on the delay line is to cause an $\sqrt{f}$ bias on the magnitude of attenuation, hence some apparent distortion in the resonance curve. Beyond this, the shift in the DOP response curve is attributed to the coupling of transducer response to mechanical impedance increment of the delay line. This coupling is neglected in the analysis.

The data of Figs.16 and 17 are then replotted as a function of $\sqrt{f}$ at fixed temperatures as presented in Figs.19 and 20. Next, we calculate the theoretically predicted slope from delay line dimension, and these are drawn onto the same figures.

The theoretical calculations are as follows. From Eqs.(59) and (60), we obtained the attenuation equation:

$$(\Delta A)\ell = f^{1/2}(\rho_L \eta)\frac{\sqrt{\pi}}{2b V_s \rho_s}\ell \qquad (61)$$

where V_s is the acoustic velocity in a fused quartz (3.8×10^5 cm/sec), 2b is the thickness of the delay line (0.154 cm), ρ_s is the density of a fused quartz (2.2 g/cc), and ℓ is the length of the liquid - delay line interface region (6.7 cm).

In practice, the cell with ETOH is taken as a <u>reference state</u>, thus Eq.(61) must be modified when applied to DOP, and becomes

$$(\Delta A)\ell = (\Delta A_{DOP} - \Delta A_{ETOH})\ell = f^{1/2}\cdot\frac{\sqrt{\pi}}{2V_s b\rho_s}\left[\sqrt{\eta\rho}\Big|_{DOP} - \sqrt{\eta\rho}\Big|_{ETOH}\right]\ell \qquad (62)$$

Similarly, the phase difference of DOP with respect to ETOH is

$$(\Delta B)\ell = (\Delta B_{DOP} - \Delta B_{ETOH})\ell = (f^{1/2})\frac{\sqrt{\pi}}{2bV_s\rho_s}\left[\sqrt{\eta\rho}\Big|_{DOP} - \sqrt{\eta\rho}\Big|_{ETOH}\right]\ell \qquad (63)$$

The coefficient $\sqrt{\pi}/2V_s b\rho_s$ for a fused quartz delay material is 1.39×10^{-5}.

The slope of the calibration curves can be obtained from Eqs. (62) and (63) together with steady-state viscosity and density data for the fluids. These are summarized in Table 1 and the theoretically predicted lines are indicated in Figs. 19 and 20.

TABLE 1

THEORETICAL CALIBRATION COEFFICIENTS

ETOH	η (Poise)	ρ (g/cc)	$\sqrt{\eta\rho}$
25°	0.01	0.785	0.088
20° C	0.012	0.789	0.097
15° C	0.0133	0.793	0.0103
10° C	0.0147	0.798	0.108
DOP			
25°	0.306	0.971	0.545
20° C	0.376	0.976	0.606
15° C	0.476	0.977	0.682
10° C	0.619	0.980	0.779

DOP/ETOH	$\sqrt{\eta\rho}_{DOP} - \sqrt{\eta\rho}_{ETOH}$	Slope	$\sqrt{f}$ × Degrees/$\sqrt{f}$	$\sqrt{f}$ × Nepers/$\sqrt{f}$
			f = 25 MHz	
25° C	0.457	4.2×10^{-5}	12.15°	0.212
20° C	0.509	4.72×10^{-5}	13.5°	0.236
15° C	0.579	5.37×10^{-5}	15.4°	0.269
10° C	0.671	6.23×10^{-5}	17.9°	0.311

Conclusions about calibration. As seen from Figs.18 to 20, the experimental calibration data are consistent with the straight line predicted theoretically from first principles. Some sources for the remaining discrepancy that have not been incorporated into the theoretical analysis are as follow:

1) The coupling between the transducer and the liquid via the delay line has not been included in the analysis. The liquid changes the mechanical impedance of the delay line and in turn affects the load seen by the transducer, and hence its response.

2) It was assumed that there is no propagation loss in the delay line in the absence of liquid on the surface. That is, the propagation constant m_{v1} in Eq. (13) is purely imaginary. However, there exists a finite propagation loss in any material due to the internal friction. Therefore, the propagation vector m_{v1} in Eq. (13) becomes a complex number; and in turn both the phase ΔB and the attenuation ΔA in Eq. (28) will be coupled with this propagation loss through n_1 of Eq. (20).

3) Modes of propagation other than SS(O) are permissible inasmuch as we are above the cut-off frequency of 2.2 MHz. The magnitude of such possible modes was observed to be small. The echo amplitude as seen on the oscilloscope only oscillates by a small amount as we tune through a continuous range of frequency in the neighborhood of each operating frequency.

4) The smoothness of the surface can be of critical importance for low viscosity liquids such as ethanol since the shear wavelength $\lambda_s = 2.5 \times 10^{-3}$ cm begins to approach the magnitude of the surface irregularities.

In practice, since the experimental calibration data (Table 3) does show fluctuations from the theoretical curve, it was decided to use a separate proportionality constant for each frequency. These constants are taken as the average of the measured calibration values. Thus, for

$$R = K_1(f)\,\Delta A \tag{64}$$

$$X = K_2(f)\,\Delta B \tag{65}$$

The proportionality constants $K_1(f)$ and $K_2(f)$ were obtained from DOP and ETOH at each frequency and are shown in Table 2.

TABLE 2

EXPERIMENTAL CALIBRATION COEFFICIENTS

f (MHz)	K_1	K_2
3.4	20,000	397
6.0	23,300	382
11.2	22,529	433
14.5	22,370	358
14.6	21,508	367
19.5	15,957	360

Table 3. Experimental (Raw) Data

8232.083 - C.R.

ETOH(25°C) (40 dB preamp)	$\phi_o - \phi_A$	b_o/a_{15}	$(\phi_o - \phi_A)_{av.}$	$(b_o/a_{15})_{av.}$
3.4 MHz	263.728	3.250	263.627	3.250
	263.526	3.250		
6.0 MHz	263.070	5.142	263.442	5.156
	263.813	5.170		
8.4 MHz	321.181	6.427	321.195	6.435
	321.210	6.442		
(20 dB preamp)				
11.2 MHz	325.776	0.9578	325.736	0.9611
	325.696	0.9644		
14.5 MHz	262.165	1.605	262.245	1.605
	262.325	1.605		
14.6 MHz	248.012	1.643	248.237	1.638
	248.463	1.633		
19.5 MHz	294.359	2.071	294.447	2.071
	294.535	2.070		
25.0 MHz	276.835	0.6500	277.235	0.6531
	277.634	0.6561		
27.1 MHz	5.835	0.3792	5.842	0.3786
	5.849	0.3780		

8228.112

8228.138 - C.R.

ETOH(20°C) (40 dB preamp)				
3.4 MHz	257.365	3.267	257.044	3.272
	256.722	3.276		
6.0 MHz	251.096	5.289	251.060	5.288
	251.023	5.286		
8.4 MHz	304.365	6.546	304.762	6.536
	305.158	6.527		
(20 dB preamp)				
11.2 MHz	302.003	0.9873	302.038	0.9874
	302.072	0.9874		
14.5 MHz	230.574	1.642	230.930	1.643
	231.285	1.643		
14.6 MHz	216.187	1.692	216.329	1.685
	216.471	1.677		
19.5 MHz	252.530	2.074	252.531	2.074
	252.531	2.074		
25.0 MHz	224.650	0.6550	224.650	0.6558
	224.646	0.6565		
27.1 MHz	-51.689	0.3788	-51.740	0.3802
	-51.764	0.3816	(308.26)	

	8223.475 -C. R.			
ETOH(15°C) (40 dB preamp)	$\phi_o - \phi_A$	b_o/a_{15}	$(\phi_o - \phi_A)_{av}$	$(b_o/a_{15})_{av}$.
3.4 MHz	249.567	3.279	249.722	3.290
	249.876	3.300		
6.0 MHz	236.890	5.383	236.816	5.373
	236.742	5.362		
8.4 MHz	283.667	6.715	284.117	6.698
	284.566	6.680		
(20 dB preamp)				
11.2 MHz	274.634	1.008	274.652	1.008
	274.669	1.008		
14.5 MHz	193.780	1.689	193.934	1.686
	194.088	1.682		
14.6 MHz	179.523	1.710	179.580	1.708
	179.635	1.706		
19.5 MHz	202.150	2.081	202.127	2.082
	202.104	2.082		
25.0 MHz	161.295	0.6577	161.290	0.6554
	161.284	0.6530		
27.1 MHz	-119.982	0.3829	-120.072	0.3839
	-120.162	0.3848	(239.928)	
	8219.156 -C R			
ETOH(10°C) (40 dB preamp)				
3.4 MHz	242.156	3.301	242.251	3.304
	242.346	3.306		
6.0 MHz	222.972	5.482	223.040	5.473
	223.108	5.464		
8.4 MHz	264.368	6.756	264.305	6.785
	264.243	6.813		
(20 dB preamp)				
11.2 MHz	248.230	1.023	248.276	1.022
	248.321	1.021		
14.5 MHz	159.302	1.720	159.175	1.719
	159.047	1.717		
14.6 MHz	143.679	1.740	143.570	1.735
	143.461	1.730		
19.5 MHz	155.032	2.067	155.016	2.068
	155.000	2.069		
25.0 MHz	102.450	0.6539	102.429	0.6536
	102.408	0.6533		
27.1 MHz	-183.301	0.3875	-183.352	0.3875
	-183.402	0.3875	(176.648)	

	8232.019 -C. R.		$(\phi_o-\phi_A)_{av}$	$(b_o/a_{1,-})_{av}$
DOP(25°C)	$\phi_o-\phi_A$	$b_o/a_{1,-}$	$\Delta\phi_{DOP}$	(Ratio) ΔA
(40 dB preamp)				
3.4 MHz	259.791	3.003	259.753	3.011
	259.715	3.019	(3.874)	(0.926)
6.0 MHz	258.489	4.731	258.498	4.741
	258.507	4.750	(4.944)	(0.919)
8.4 MHz	314.752	6.187	314.828	6.166
	314.903	6.144	(6.367)	(0.958)
(20 dB preamp)				
11.2 MHz	318.957	0.8560	319.015	0.8558
	319.072	0.8555	(6.721)	(0.890)
14.5 MHz	252.650	1.380	252.442	1.383
	252.234	1.386	(9.803)	(0.862)
14.6 MHz	237.996	1.393	238.188	1.397
	238.380	1.401	(10.049)	(0.853)
19.5 MHz	283.312	1.644	283.238	1.645
	283.164	1.645	(11.209)	(0.7943)
25.0 MHz	266.524	0.5049	266.496	0.5041
	266.467	0.5032	(10.743)	(0.772)
27.1 MHz	355.322	0.2859	355.912	0.2850
	356.502	0.2840	(9.93)	(0.753)
	8227.830 -C. R.			
DOP(20°C)				
(40 dB preamp)				
3.4 MHz	252.270	3.026	252.182	3.026
	252.094	3.026	(4.862)	(0.9248)
6.0 MHz	243.911	4.781	244.173	4.791
	244.435	4.800	(6.887)	(0.9060)
8.4 MHz	296.109	6.003	296.352	5.985
	296.595	5.967	(8.410)	(0.9157)
(20 dB preamp)				
11.2 MHz	293.040	0.8686	293.045	0.8692
	293.049	0.8698	(8.993)	(0.8803)
14.5 MHz	219.343	1.413	219.215	1.413
	219.087	1.413	(11.715)	(0.8600)
14.6 MHz	204.759	1.422	204.797	1.423
	204.834	1.424	(11.532)	(0.8445)
19.5 MHz	238.305	1.612	238.333	1.606
	238.360	1.600	(14.198)	(0.7743)
25.0 MHz	211.294	0.4950	211.221	0.4961
	211.148	0.4971	(13.428)	(0.7564)
27.1 MHz	-65.547	0.2785	-65.265	0.2792
	-64.983	0.2798	(13.528)	(0.7344)

	8223.496 -C. R.		$(\phi_o-\phi_A)_{av}$	$(b_o/a_{15})_{av}$
DOP(15°C)	$\phi_o-\phi_A$	b_o/a_{15}	$\Delta\phi_{DOP}$	Ratio = ΔA
(40 dB preamp)				
3.4 MHz	244.787	2.989	244.812	0.2994
	244.836	2.999	(4.91)	(0.9100)
6.0 MHz	230.023	4.803	230.075	4.820
	230.127	4.837	(6.741)	(0.8970)
8.4 MHz	276.643	5.992	276.943	6.078
	277.243	6.164	(7.174)	(0.9074)
(20 dB preamp)				
11.2 MHz	266.472	0.8642	266.451	0.8623
	266.429	0.8603	(8.201)	(0.8554)
14.5 MHz	183.032	1.409	183.048	1.407
	183.064	1.405	(10.886)	(0.8345)
14.6 MHz	168.380	1.417	168.402	1.414
	168.424	1.410	(11.178)	(0.8279)
19.5 MHz	190.120	1.568	190.178	1.569
	190.236	1.569	(11.949)	(0.7536)
25.0 MHz	151.889	0.4762	152.130	0.4771
	152.370	0.4780	(9.16)	(0.7280)
27.1 MHz	-130.563	0.2724	-130.342	0.2723
	-130.120	0.2721	(10.27)	(0.7093)
	8219.114 -C. R.			
DOP(10°C)				
(40 dB preamp)				
3.4 MHz	236.811	2.993	236.873	2.995
	236.934	2.997	(5.738)	(0.9065)
6.0 MHz	215.229	4.828	215.483	4.831
	2.5.737	4.834	(7.557)	(0.8827)
8.4 MHz	254.678	6.056	254.655	6.041
	254.632	6.026	(9.650)	(0.8903)
(20 dB MHz)				
11.2 MHz	238.802	0.8576	238.776	0.8579
	238.750	0.8582	(9.500)	(0.8394)
14.5 MHz	147.014	1.393	147.162	1.396
	147.310	1.399	(12.013)	(0.8121)
14.6 MHz	132.566	1.398	132.558	1.399
	132.551	1.400	(11.012)	(0.8063)
19.5 MHz	141.995	1.514	142.019	1.510
	142.043	1.506	(12.997)	(0.7301)
25.0 MHz	90.726	0.4524	90.662	0.4533
	90.598	0.4542	(11.767)	(0.6935)
27.1 MHz	-195.499	0.2629	-195.193	0.2627
	-194.887	0.2625	(11.841)	(0.6779)

8232.041 -C. R.

5% PS/DOP(25°C) (40 dB preamp)	$\phi_o - \phi_R$	$b_0/a_{1,5}$	$(\phi_o - \phi_R)_{AV}$ $\Delta\phi_{(5\%PS)}$	$(b_0/a_{1,5})_{AV}$ Ratio = ΔA
3.4 MHz	259.151	2.963	259.116	2.963
	259.080	2.962	(4.511)	(.9117)
6.0 MHz	257.141	4.621	257.148	4.613
	257.154	4.604	(6.294)	(.8947)
8.4 MHz	313.615	5.766	314.182	5.763
	314.749	5.760	(7.013)	(.8956)
(20 dB preamp)				
11.2 MHz	317.642	0.8482	317.746	0.8454
	317.850	0.8426	(7.99)	(.8796)
14.5 MHz	250.229	1.392	250.485	1.390
	250.740	1.388	(11.76)	(.8660)
14.6 MHz	236.202	1.405	236.271	1.407
	236.340	1.410	(11.966)	(.8590)
19.5 MHz	280.097	1.522	280.110	1.521
	280.122	1.520	(14.337)	(.7344)
25.0 MHz	266.824	0.4532	266.802	0.4529
	266.779	0.4526	(10.433)	(.6935)
27.1 MHz	356.560	0.2543	356.516	0.2533
	356.472	0.2522	(9.326)	(.6690)

8227.895 -C. R.

5% PS/DOP(20°C) (40 dB preamp)				
3.4 MHz	252.190	2.939	251.941	2.934
	251.691	2.929	(5.103)	(.8967)
6.0 MHz	243.782	4.682	243.792	4.681
	243.802	4.680	(7.268)	(.8852)
8.4 MHz	295.115	5.941	295.044	5.955
	294.973	5.968	(9.718)	(.9111)
(20 dB preamp)				
11.2 MHz	292.216	0.8417	292.305	0.8416
	292.393	0.8414	(9.733)	(.8523)
14.5 MHz	216.303	1.385	216.495	1.388
	216.687	1.390	(14.435)	(.8448)
14.6 MHz	201.533	1.396	201.872	1.390
	202.211	1.384	(14.457)	(.8249)
19.5 MHz	234.584	1.465	234.535	1.467
	234.485	1.468	(17.996)	(.7073)
25.0 MHz	210.145	0.4343	210.187	0.4361
	210.229	0.4378	(14.463)	(.6649)
27.1 MHz	-64.954	0.2467	-65.335	0.2445
	-65.715	0.2422	(13.595	(.6430)

8223.494 -C. R.

5% PS/DOP(15°C) (40 dB preamp)	$\phi_o - \phi_A$	b_o/a_{15}	$(\phi_o - \phi_A)_{AV}$ $\Delta\phi(5\%)$	$(b_o/a_{15})_{AV}$ Ratio = ΔA
3.4 MHz	243.380	2.936	243.486	2.934
	243.591	2.931	(6.236)	(.8917)
6.0 MHz	229.257	4.628	229.249	4.628
	229.240	4.628	(7.567)	(.8613)
8.4 MHz	274.689	5.634	275.353	5.609
	275.208	5.598	(8.764)	(.8374)
(20 dB preamp)				
11.2 MHz	265.492	0.8436	265.340	0.8433
	265.187	0.8429	(9.312)	(.8366)
14.5 MHz	180.570	1.374	180.476	1.379
	180.382	1.384	(13.458)	(.8179)
14.6 MHz	166.018	1.386	165.990	1.384
	165.962	1.382	(13.590)	(.8103)
19.5 MHz	185.078	1.431	185.980	1.432
	185.981	1.432	(16.147)	(.6878)
25.0 MHz	149.833	0.4194	149.737	0.4202
	149.640	0.4210	(11.553)	(.6411)
27.1 MHz	228.269	0.2405	228.373	0.2404
	228.477	0.2402	(11.555)	(.6262)

8219.177 -C. R.

5% PS/DOP(10°C) (40 dB preamp)				
3.4 MHz	236.217	2.905	236.217	2.906
	236.216	2.906	(6.034)	(.8795)
6.0 MHz	215.056	4.617	215.232	4.619
	215.408	4.621	(7.808)	(.8440)
8.4 MHz	254.758	5.656	254.820	5.631
	254.882	5.605	(9.485)	(.8299)
(20 dB preamp)				
11.2 MHz	237.462	0.8288	237.388	0.8286
	237.314	0.8283	(10.888)	(.8107)
14.5 MHz	144.342	1.345	144.423	1.343
	144.504	1.340	(14.752)	(.7813)
14.6 MHz	129.484	1.354	129.483	1.353
	129.482	1.351	(14.087)	(.7798)
19.5 MHz	137.397	1.360	137.372	1.361
	137.352	1.361	(17.644)	(.6581)
25.0 MHz	88.857	0.4004	88.990	0.3970
	89.121	0.3935	(13.439)	(.6074)
27.1 MHz	-195.212	0.2268	-195.284	0.2268
	-195.356	0.2268	(11.932)	(.5853)

8232.044 -C. R.

10% PS/DOP(25°C) (40 dB preamp)	$\phi_o - \phi_A$	b_o/a_{1r}	$(\phi_o - \phi_A)_{av}$ $\Delta\phi_{10\%}$	$(b_o/a_{1r})_{av}$ Ratio = ΔA
3.4 MHz	258.523	2.883	258.149	2.882
	257.774	2.880	(5.478)	(.8868)
6.0 MHz	255.795	4.535	255.726	4.538
	255.656	4.541	(7.716)	(.8801)
8.4 MHz	311.984	5.708	312.294	5.704
	312.603	5.700	(81901)	(.8864)
(20 dB preamp)				
11.2 MHz	315.837	0.8119	316.019	0.8119
	316.201	0.8118	(9.717)	(.8445)
14.5 MHz	246.896	1.317	246.835	1.319
	246.774	1.322	(15.410)	(.8218)
14.6 MHz	232.734	1.328	232.779	1.329
	232.824	1.329	(15.458)	(.8113)
19.5 MHz	275.604	1.376	275.660	1.374
	275.716	1.372	(18.787)	(.6634)
25.0 MHz	264.323	0.3976	264.384	0.3958
	264.444	0.3939	(12.851)	(.6060)
27.1 MHz	355.595	0.2181	355.388	0.2180
	355.180	0.2178	(10.454)	(.5758)

8227.836 -C. R.

10% PS/DOP(20°C) (40 dB preamp)				
3.4 MHz	250.952	2.927	251.230	2.906
	251.507	2.885	(5.814)	(.8881)
6.0 MHz	243.077	4.620	242.974	4.610
	242.871	4.600	(8.086)	(.8717)
8.4 MHz	295.461	5.777	295.908	5.760
	296.355	5.743	(8.854)	(.8812)
(20 dB preamp)				
11.2 MHz	289.339	0.8121	289.436	0.8141
	289.533	0.8160	(12.602)	(.8245)
14.5 MHz	212.131	1.311	212.081	1.315
	212.031	1.318	(18.849)	(.8003)
14.6 MHz	197.827	1.325	198.037	1.329
	198.247	1.333	(18.292)	(.7887)
19.5 MHz	229.125	1.332	229.164	1.331
	229.202	1.329	(23.367)	(.6417)
25.0 MHz	206.771	0.3850	206.554	0.3845
	206.336	0.3840	(18.096)	(.5863)
27.1 MHz	-68.020	0.2104	-68.314	0.2095
	-68.608	0.2086	(16.574)	(.5510)

8223.462 -C. R.

10% PS/DOP(15°C) (40 dB preamp)	$\phi_o - \phi_A$	b·/air	$(\phi_o - \phi_A)_{AV}$ $\Delta\phi_{(10\%)}$	$(b\cdot/air)_{AV}$ Ratio = ΔA
3.4 MHz	243.202	2.835	243.172	2.837
	243.141	2.839	(6.550)	(.8623)
6.0 MHz	227.821	4.564	227.477	4.563
	227.132	4.562	(9.339)	(.8492)
8.4 MHz	272.586	5.544	272.85	5.573
	273.114	5.601	(11.267)	(.8320)
(20 dB preamp)				
11.2 MHz	261.952	0.7985	262.035	0.7989
	262.117	0.7993	(12.617)	(.7926)
14.5 MHz	176.579	1.291	176.588	1.291
	176.596	1.290	(17.346)	(.7657)
14.6 MHz	161.968	1.296	162.352	1.296
	162.736	1.295	(17.228)	(.7588)
19.5 MHz	181.210	1.273	181.161	1.273
	181.111	1.272	(20.966)	(.6114)
25.0 MHz	147.093	0.3600	147.105	0.3608
	147.117	0.3615	(14.185)	(.5505)
27.1 MHz	226.585	0.2043	226.635	0.2029
	226.684	0.2014	(13.293)	(.5285)

8219.140 -C. R.

10% PS/DOP(10°C) (40 dB preamp)				
3.4 MHz	234.339	2.757	234.272	2.755
	234.245	2.753	(7.959)	(.8338)
6.0 MHz	212.682	4.401	212.688	4.401
	212.693	4.401	(10.352)	(.8041)
8.4 MHz	251.973	5.607	251.848	5.581
	251.585	5.582	(12.457)	(.8225)
	251.986	5.553		
(20 dB preamp)				
11.2 MHz	235.027	0.7700	235.032	0.7696
	235.037	0.7693	(13.244)	(.7530)
14.5 MHz	141.557	1.238	141.558	1.238
	141.559	1.238	(17.617)	(.7202)
14.6 MHz	127.069	1.248	126.957	1.246
	126.844	1.243	(16.613)	(.7181)
19.5 MHz	133.258	1.194	133.306	1.193
	133.354	1.192	(21.71)	(.5768)
25.0 MHz	86.866	0.3322	86.709	0.3319
	86.551	0.3316	(15.72)	(.5078)
27.1 MHz	-197.774	0.1937	197.976	0.1942
	-198.177	0.1946	(14.624)	(.5011)

8232.070 - C.R.

20% PS/DOP (25°C) (40 dB preamp)	$\phi_o - \phi_A$	b_o/a_{15}	$(\phi_o - \phi_A)_{av.}$ $\Delta\phi$	$(b_o/a_{15})_{av}$ ΔA
3.4 MHz	255.338	2.674	255.633	2.665
	255.927	2.656	(7.994)	(.820)
6.0 MHz	252.842	4.145	252.978	4.144
	253.113	4.142	(10.462)	(.8037)
8.4 MHz	309.481	5.173	309.206	5.134
	308.934	5.095	(11.989)	(.7978)
(20 dB preamp)				
11.2 MHz	312.380	0.7168	312.267	0.7164
	312.153	0.7159	(13.469)	(.7453)
14.5 MHz	242.907	1.153	242.734	1.155
	242.561	1.157	(19.511)	(.7196)
14.6 MHz	228.377	1.158	228.427	1.158
	228.476	1.157	(19.810)	(.7070)
19.5 MHz	269.758	1.108	269.665	1.107
	269.572	1.105	(24.782)	(.5345)
25.0 MHz	260.455	0.307	260.317	0.3068
	260.179	0.306	(16.918)	(.470)
27.1 MHz	351.724	0.166	351.830	0.166
	351.935	0.166	(14.012)	(.439)

8227.867 - C.R.

20% PS/DOP (20°C) (40 dB preamp)				
3.4 MHz	247.842	2.612	247.622	2.617
	247.441	2.622	(9.422)	(.7708)
6.0 MHz	238.075	4.065	238.025	4.076
	237.975	4.086	(13.035)	(.7708)
8.4 MHz	287.809	5.121	288.142	5.086
	288.475	5.050	(16.620)	(.7021)
(20 dB preamp)				
11.2 MHz	285.769	0.6935	285.718	0.693
	285.667	0.693	(16.320)	(.702)
14.5 MHz	208.294	1.112	208.283	1.111
	208.272	1.109	(22.647)	(.676)
14.6 MHz	193.663	1.118	193.502	1.122
	193.340	1.125	(22.827)	(.666)
19.5 MHz	223.383	1.045	223.483	1.047
	223.583	1.048	(29.048)	(.505)
25.0 MHz	203.875	0.284	203.909	0.283
	203.942	0.283	(20.741)	(.4321)
27.1 MHz	288.299	0.157	288.865	0.155
	289.153	0.153	(19.460)	(0.407)

20% PS/DOP(15°C) 8223.525 -C. R.	$\phi_o - \phi_A$	b_o/a_{15}	$(\phi_o - \phi_A)_{av}$ $\Delta\phi_{(20\%)}$	$(b_o/a_{15})_{av}$ Ratio = ΔA
(40 dB preamp)				
3.4 MHz	238.560	2.530	238.790	2.528
	239.020	2.525	(12.906	(.7684)
6.0 MHz	223.028	3.934	223.106	3.935
	223.183	3.935	(13.710)	(.7324)
8.4 MHz	266.773	4.856	266.737	4.854
	266.701	4.852	(17.380)	(.7247)
(20 dB preamp)				
11.2 MHz	257.258	0.6557	257.620	0.6595
	257.982	0.6633	(17.032)	(.6543)
14.5 MHz	172.560	1.043	172.387	1.041
	172.213	1.039	(21.547)	(.6174)
14.6 MHz	157.992	1.049	158.016	1.049
	158.040	1.049	(21.564)	(.6141)
19.5 MHz	175.617	0.9533	175.677	0.9539
	175.736	0.9544	(26.45)	(.4566)
25.0 MHz	145.024	0.2598	145.166	0.2602
	145.307	0.2606	(16.124)	(.3970)
27.1 MHz	224.689	0.1410	224.671	0.1419
	224.653	0.1428	(15.072)	(.3696)
20% PS/DOP(10°C) 8219.150 -C. R.				
(40 dB preamp)				
3.4 MHz	229.769	2.264	229.941	2.268
	229.912	2.271	(12.310)	(.6864)
6.0 MHz	208.619	3.505	208.666	3.508
	208.713	3.511	(14.374)	(.6410)
8.4 MHz	247.315	4.344	247.219	4.379
	247.122	4.414	(17.086)	(.6454)
(20 dB preamp)				
11.2 MHz	230.958	0.5850	230.950	0.5816
	230.941	0.5783	(17.326)	(0.5691)
14.5 MHz	138.167	0.9080	137.934	0.9073
	137.700	0.9065	(21.241)	(.5278)
14.6 MHz	123.288	0.9099	123.275	0.9114
	123.261	0.9129	(20.295)	(.5253)
19.5 MHz	129.345	0.8291	129.357	0.8285
	129.368	0.8278	(25.659)	(.4006)
25.0 MHz	85.422	0.2159	85.925	0.2170
	86.459	0.2178	16.504	(.3320)
	85.895	0.2174		
27.1 MHz	-194.935	0.1234	-195.079	.1231
	-194.504	0.1246	(11.727)	(.3176)
	-195.797	0.1212		

40% PS/DOP(25°C) (40 dB preamp)	$\phi_o - \phi_a$	b/a_{1r}	$(\phi_o - \phi_a)_{av}$ $\Delta\phi(40\%)$	$(b/a_{1r})_{av}$ Ratio = ΔA
	8232.105 -C. R.			
3.4 MHz	246.189	1.871	246.385	1.878
	246.580	1.884	(17.242)	(.5778)
6.0 MHz	243.488	2.708	243.192	2.712
	242.895	2.715	(20.250)	(.5260)
8.4 MHz	297.284	3.076	296.844	3.066
	296.403	3.056	(24.351)	(.4765)
(20 dB preamp)				
11.2 MHz	304.216	0.4125	304.273	0.4125
	304.330	0.4124	(21.463)	(.4292)
14.5 MHz	237.339	0.6173	237.054	0.6175
	236.769	0.6177	(25.191)	(.3847)
14.6 MHz	223.373	0.6138	223.607	0.6175
	223.840	0.6160	(24.630)	(.3754)
19.5 MHz	268.482	0.5369	268.504	0.5374
	268.525	0.5278	(25.943)	(.2595)
25.0 MHz	266.099	0.1327	266.385	0.1371
	266.673	0.1415	(10.850)	(0.2099)
27.1 MHz	0.863	0.0701	361.630	0.0685
	2.430	0.0670	(4.212)	(.1809)
	1.596	0.0683		
40% PS/DOP(20°C)	8227.877 -C. R.			
(40 dB preamp)				
3.4 MHz	236.617	1.746	236.497	1.744
	236.376	1.741	(20.547)	(.5330)
6.0 MHz	227.231	2.484	227.303	2.468
	227.375	2.451	(23.757)	(.4667)
8.4 MHz	277.569	2.753	277.738	2.842
	277.906	2.905	(27.024)	(.4348)
(20 dB preamp)				
11.2 MHz	278.615	0.3615	278.834	0.3630
	279.053	0.3644	(23.204)	(.3676)
14.5 MHz	204.239	0.5349	204.465	0.5341
	204.689	0.5332	(26.465)	(.3251)
14.6 MHz	191.209	0.5342	191.149	0.5367
	191.089	0.5392	(25.180)	(.3185)
19.5 MHz	225.697	0.4568	225.689	0.4562
	225.681	0.4556	(26.842)	(.2200)
25.0 MHz	215.101	0.1143	215.375	0.1146
	215.649	0.1148	(9.275)	(.1747)
27.1 MHz	305.359	0.0596	304.365	0.0585
	303.075	0.0591	(3.895)	(.1539)
	304.661	0.0567		

		8223.504 -C. R.	$(\phi_o-\phi_A)_{Av}$	$(b_o/a_{15})_{Av}$
40% PS/DOP(15°C) 40 dB preamp)	$\phi_o-\phi_A$	b_o/a_{15}	$\Delta\phi(40\%)$	Ratio = ΔA
3.4 MHz	227.313	1.577	227.239	1.574
	227.165	1.571	(22.483)	(.4784)
6.0 MHz	212.655	2.188	212.696	2.187
	212.736	2.185	(24.120)	(.4070)
8.4 MHz	255.248	2.493	255.972	2.493
	255.064	2.547	(28.145)	(.3722)
(20 dB preamp)				
11.2 MHz	251.488	0.3140	251.557	0.3146
	251.626	0.3151	(23.095)	(.3121)
14.5 MHz	171.049	0.4538	171.250	0.4549
	171.450	0.4560	(22.684)	(.2698)
14.6 MHz	156.955	0.4514	157.007	0.4529
	157.059	0.4543	(22.573)	(.2652)
19.5 MHz	181.507	0.3819	181.567	0.3815
	181.626	0.3811	(20.560)	(.1832)
25.0 MHz	162.722	0.0905	162.982	0.0921
	163.242	0.0936	(-1.692)	(.1405)
27.1 MHz	246.933	0.0495	248.401	0.0497
	250.171	0.0499	(-8.473)	(.1295)
40% PS/DOP(10°C) 40 dB preamp)		8219.120 -C. R.		
3.4 MHz	217.495	1.381	217.392	1.382
	217.289	1.382	(24.859)	(.4183)
6.0 MHz	196.968	1.889	196.730	1.889
	196.491	1.889	(26.31)	(.3451)
8.4 MHz	237.122	2.130	237.135	2.124
	237.147	2.118	(27.17)	(.3130)
(20 dB preamp)				
11.2 MHz	225.838	0.2667	225.537	0.2665
	225.236	0.2663	(22.739)	(.2608)
14.5 MHz	138.514	0.3785	138.777	0.3773
	139.040	0.3760	(20.398)	(.2195)
14.6 MHz	125.035	0.3780	125.391	0.3770
	125.747	0.3766	(18.179)	(.2173)
19.5 MHz	140.830	0.3141	140.751	0.3151
	140.672	0.3161	(14.265)	(.1524)
25.0 MHz	113.235	0.0748	112.574	0.0749
	111.913	0.0749	(-10.145)	(.1146)
27.1 MHz	-161.722	0.0434	-161.063	0.0441
	-160.403	0.0448	(-22.289)	(.1138)

PART IV

EXPERIMENTAL RESULTS

The series of experimental results reported herein form the basis of a study of viscoelastic properties of low molecular weight polymer solutions based on polystyrene in di-actyl-phthalate plasticizer. The study encompassed a wide concentration range from 5% to 40% of 2200 molecular weight polystyrene over a temperature range from 10°C to 25°C.

A. Dynamic Measurement of Solvent and Solution

In this kind of experiment it is important to take into account the history of sample handling in order to minimize the effect of long term drifts. It is therefore useful to specify the complete chronology.

The measurements were done in the following temperature sequence: 25°C, 20°C, 15°C and 10°C.

The cell was cleaned with DOP, followed by a rinse with ETOH.

After each sample change or new temperature setting, it is necessary to wait at least two hours before taking data, in order for the liquid to reach thermal equilibrium. Emptying and filling were always carried out at the temperature of 25°C.

The amplifier at the output of the delay line was set to 40 db gain for frequencies of 3.4 MHz, 6.0 MHz, 8.4 MHz and to 20 db gain for 11.2 MHz, 14.5 MHz, 14.6 MHz, 19.5 MHz, 25.0 MHz and 27.1 MHz. These settings were chosen so as not to overload the sample and hold circuit.

The chronology is summarized in Table 4.

TABLE 4

SAMPLE CHRONOLOGY

Date	Liquid	Temperature	Counter Reading
5/14/76	ETOH	25°C	8232.083
5/14/76	ETOH	20°C	8228.120
5/14/76	ETOH	15°C	8223.470
5/14/76	ETOH	10°C	8219.160
5/15/76	DOP	25°C	8232.020
5/15/76	DOP	20°C	8227.830
5/14/76	DOP	15°C	8223.488
5/16/76	DOP	10°C	8219.120
5/17/76	5% PS/DOP	25°C	8232.036
5/17/76	5% PS/DOP	20°C	8227.890
5/17/76	5% PS/DOP	15°C	8223.494
5/17/76	5% PS/DOP	10°C	8219.175
5/18/76	10% PS/DOP	25°C	8232.045
5/18/76	10% PS/DOP	20°C	8227.836
5/19/76	10% PS/DOP	15°C	8223.462
5/19/76	10% PS/DOP	10°C	8219.140
5/19/76	20% PS/DOP	25°C	8232.075
5/20/76	20% PS/DOP	20°C	8227.867
5/20/76	20% PS/DOP	15°C	8223.525
5/20/76	20% PS/DOP	10°C	8219.150
5/21/76	40% PS/DOP	25°C	8232.100
5/21/76	40% PS/DOP	20°C	8227.875
5/21/76	40% PS/DOP	15°C	8223.504
5/21/76	40% PS/DOP	10°C	8219.120

Table 5. Summary of Data

Ethanol

Temp. (°C)	$\phi_o - \phi_A$ (degree)	Amplitude Ratio b_0/a_{15}	Calc. Newt. X_{Ref}
f = 3.4 MHz			
25	263.4	3.26	304
20	256.6	3.27	317
15	249.5	3.29	337
10	242.2	3.30	352
f = 6.0 MHz			
25	263.1	5.17	404
20	250.0	5.28	421
15	236.6	5.37	448
10	222.5	5.48	468
f = 11.2 MHz			
25	325.3	9.62	552
20	300.1	9.90	576
15	274.3	10.07	612
10	247.4	10.24	639
f = 14.5 MHz			
25	261.7	16.07	628
20	228.3	16.46	655
15	193.9	16.85	697
10	158.3	17.21	727

Temp. (°C)	$\phi_0 - \phi_A$ (degree)	Amplitude Ratio b_0/a_{15}	Calc. Newt. X_{Ref}
f = 14.6 MHz			
25	247.5	16.38	630
20	213.6	16.89	657
15	178.8	16.89	699
10	142.4	17.37	730
f = 19.5 MHz			
25	293.5	20.71	729
20	248.3	20.77	760
15	202.0	20.81	808
10	153.4	20.69	843
f = 25.0 MHz			
25	277.0	6.55	825
20	219.8	6.55	860
15	161.3	6.55	915
10	100.2	6.55	955
f = 27.1 MHz			
25	364.8	3.77	859
20	303.2	3.80	895
15	240.0	3.84	953
10	174.0	3.88	994

At 3.4 MHz $R = \bar{R} + R_{Ref}$; $\bar{R} = 20{,}000\ \Delta A$

$X = \bar{X} + X_{Ref}$; $\bar{X} = 397\ \Delta\phi$

Temp. (°C)	$\Delta\phi$ ** (degree)	ΔA Attenuation (nepers)	Calculated Newtonian X_L	Measured R	Measured X	RX/X_L^2
DOP - w.r.t. ETOH REF.*						
25	3.7	-.083	6780	1964	1773	1.09
20	4.3	-.083	1976	1977	2024	1.02
15	4.8	-.096	2230	2257	2242	1.01
10	5.4	-.109	2544	2332	2495	.89
NBS OIL I - w.r.t. AIR						
25	2.9	-.053	1130	1066	1151	.96
NBS OIL L - w.r.t. AIR						
25	5.0	-.120	2618	2406	1985	.70
5% Polystyrene(2200 M.W.) in DOP - w.r.t. ETOH REF.						
25	4.4	-.099	2060	2284	2051	1.10
20	5.0	-.106	2323	2437	2302	1.03
15	5.6	-.119	2711	2717	2560	.95
10	6.3	-.129	3135	2930	2853	.85

Temp. (°C)	$\Delta\phi$ (degree)	ΔA Attenuation (nepers)	Calculated Newtonian X_L	Measured R	Measured X	RX/X_L^2
10% Polystyrene (2200 M.W.) in DOP w.r.t. ETOH REF.						
25	5.4	-.124	2507	2784	2450	1.08
20	5.4	-.137	2858	3057	2460	.92
15	6.2	-.147	3300	3277	2798	.84
10	8.2	-.186	3835	4072	3607	1.00
20% Polystyrene						
25	7.9	-.207	4001	4444	3440	.95
20	9.2	-.222	4720	4757	3969	.85
15	11.8	-.263	5587	5597	5021	.90
10	12.6	-.370	6711	7747	5354	.92
40% Polystyrene						
25	17.5	-.556	14566	11424	7251	.39
20	20.0	-.642	18900	13157	8257	.30
15	22.5	-.740	24727	15137	9269	.23
10	25.3	-.857	33319	17492	10396	.16

* Reference state at same temperature as sample
**Usually smoothed temperature curves difference

At 6.0 MHz $\bar{X} = 382\ \Delta\phi$ $\bar{R} = 23,300\ \Delta A$

Temp. (°C)	$\Delta\phi$ (degree)	ΔA Attenuation (nepers)	Calculated Newtonian X_L	Measured R	Measured X	RX/X_L^2
DOP - w.r.t. ETOH REF.						
25	5.3	-.085	2366	2384	2429	1.03
20	5.9	-.095	2630	2635	2675	1.01
15	6.6	-.106	2961	2918	2969	.99
10	7.3	-.126	3380	3404	3257	.97
NBS OIL I						
25	3.4	-.060	1502	1398	1299	.80
NBS OIL L						
25	7.7	-.145	3478	3378	2941	.82
5% Polystyrene(2200 M.W.) in DOP w.r.t. ETOH REF.						
25	6.0	-.115	2736	3083	2696	1.11
20	6.7	-.123	3086	3287	2980	1.03
15	7.4	-.146	3600	3850	3275	.97
10	8.0	-.171	4164	4452	3524	.90

Temp. (°C)	$\Delta\phi$ (degree)	ΔA Attenuation (nepers)	Calculated Newtonian X_L	Measured R	Measured X	RX/X_L^2
10% Polystyrene(2200 M.W.) in DOP w.r.t. ETOH REF.						
25	7.3	-.130	3331	3433	3193	.90
20	8.2	-.138	3797	3636	3553	.90
15	9.1	-.166	4385	4316	3924	.88
10	10.0	-.201	5095	5151	4288	.85
20% Polystyrene						
25	10.6	-.222	5315	5577	4453	.88
20	12.0	-.260	6270	6479	5005	.82
15	13.5	-.310	7422	7671	5605	.78
10	14.8	-.451	8916	10976	6122	.85
40% Polystyrene						
25	20.3	-.646	19351	15456	8158	.30
20	22.1	-.768	25132	18315	8863	.20
15	24.0	-.902	32848	21465	9616	.19
10	25.9	-1.065	44262	25283	10362	.13

At 11.2 MHz $\bar{X} = 433\,\Delta\phi$ $\bar{R} = 22529\,\Delta A$

Temp. (°C)	$\Delta\phi$ (degree)	ΔA Attenuation (nepers)	Calculated Newtonian X_L	Measured R	Measured X	RX/X_L^2
DOP - w.r.t. ETOH						
25	6.3	-.118	3233	3210	3280	1.00
20	7.1	-.129	3594	3482	3650	.98
15	8.0	-.157	4046	4149	4076	1.03
10	8.9	-.178	4618	4649	4493	.98
NBS OIL I						
25	4.9	-.0831	2051	1872	2121	.94
NBS OIL L						
25	11.6	-.197	4752	4437	5022	.99
5% Polystyrene in DOP - w.r.t. ETOH REF.						
25	7.7	-.132	3738	3526	3886	.98
20	8.7	-.162	4217	4226	4343	1.03
15	9.5	-.174	4919	4532	4725	.88
10	10.6	-.214	5689	5460	5229	.88

Temp. (°C)	$\Delta\phi$ (degree)	ΔA Attenuation (nepers)	Calculated Newtonian X_L	Measured R	Measured X	RX/X_L^2
10% Polystyrene in DOP w.r.t ETOH REF.						
25	9.7	-.172	4551	4427	4752	1.02
20	10.9	-.195	5187	4969	5296	.98
15	12.0	-.231	5990	5816	5808	.94
10	13.3	-.289	6961	7150	6398	.94
20% Polystyrene						
25	13.2	-.294	7262	7175	6268	.85
20	14.6	-.357	8567	8619	6898	.81
15	16.1	-.422	10140	10119	7583	.75
10	17.8	-.572	12182	13526	8346	.76
40% Polystyrene						
25	21.6	-.855	26438	19814	9905	.28
20	22.1	-1.010	34337	23330	10145	.20
15	22.5	-1.165	44878	26858	10354	.19
10	22.9	-1.359	60474	31256	10511	.08

At 14.6 MHz $\bar{X} = 367\,\Delta\phi$ $\bar{R} = 21508\,\Delta A$

Temp. (°C)	$\Delta\phi$ (degree)	ΔA Attenuation (nepers)	Calculated Newtonian X_L	Measured R	Measured X	RX/X_L^2
DOP - w.r.t. ETOH						
25	9.3	-.142	3691	3361	4043	.99
20	9.9	-.164	4104	4184	4290	1.06
15	10.5	-.189	4619	4764	4552	1.01
10	11.0	-.216	5272	5375	4767	.92
NBS OIL I						
25	5.8	-.113	2342	2430	2128	
NBS OIL L						
25	14.5	-.276	5426	5936	5321	1.07
5% Polystyrene in DOP w.r.t. ETOH REF.						
25	11.7	-.152	4268	3899	4923	1.05
20	12.5	-.195	4814	4851	5244	1.09
15	13.4	-.209	5616	5194	5616	.92
10	14.1	-.250	6495	6107	5904	.85

Temp. (°C)	$\Delta\phi$ (degree)	ΔA Attenuation (nepers)	Calculated Newtonian X_L	Measured R	Measured X	RX/X_L^2
10% Polystyrene in DOP w.r.t. ETOH REF.						
25	15.2	-.208	5196	5103	6208	1.17
20	15.6	-.239	5922	5797	6382	1.05
15	16.1	-.274	6839	6592	6607	.93
10	16.7	-.335	7949	7278	6858	.79
20% Polystyrene						
25	19.6	-.346	8291	8071	7823	.92
20	20.5	-.417	9781	9625	8180	.82
15	20.8	-.487	11577	11173	8332	.69
10	20.3	-.649	13908	14688	8180	.62
40% Polystyrene						
25	24.8	-.988	30185	21312	9731	.22
20	23.4	-1.151	39203	25412	9244	.15
15	21.8	-1.323	51239	29154	8699	.09
10	17.6	-1.530	69045	33637	7189	.05

At 19.5 MHz $\bar{X} = 360\,\Delta\phi$ $\bar{R} = 15957\,\Delta A$

Temp. (°C)	$\Delta\phi$ (degree)	ΔA Attenuation (nepers)	Calculated Newtonian X_L	Measured R	Measured X	RX/X_L^2
DOP - w.r.t. ETOH						
25	10.5	-.228	4265	4367	4509	1.08
20	11.2	-.257	4742	4860	4792	1.04
15	12.0	-.284	5338	5339	5128	.96
10	12.6	-.315	6093	5869	5379	.85
NBS OIL I						
25	7.0	-.151	2707	2409	2520	.83
NBS OIL L						
25	15.0	-.406	6271	6478	5400	.89
5% Polystyrene in DOP w.r.t. ETOH REF.						
25	14.2	-.311	4932	5691	5841	1.37
20	15.3	-.346	5564	6281	6268	1.27
15	16.6	-.373	6491	6759	6784	.93
10	17.7	-.421	7506	7560	7215	.97

Temp. (°C)	$\Delta\phi$ (degree)	ΔA Attenuation (nepers)	Calculated Newtonian X_L	Measured R	Measured X	RX/X_L^2
10% Polystyrene in DOP w.r.t. ETOH REF.						
25	18.5	-.412	6005	7300	7389	1.49
20	19.5	-.447	6844	7892	7780	1.31
15	20.5	-.488	7904	8595	8188	1.13
10	21.5	-.551	9185	9635	8583	.98
20% Polystyrene						
25	24.5	-.627	9582	10734	9549	1.12
20	25.5	-.687	11304	11722	9940	.91
15	26.7	-.781	12280	13270	10420	.77
10	25.4	-.921	16073	15539	9992	.60
40% Polystyrene						
25	26.1	-1.357	34885	22382	10125	.19
20	22.2	-1.512	45306	24886	8752	.11
15	20.2	-1.698	59216	27902	8080	.06
10	13.4	-1.895	79794	31081	5667	.03

At 14.5 MHz $\bar{X} = 358$
$\bar{R} = 22,370$

Temp. (°C)	$\Delta\phi$ (degree)	ΔA Attenuation (nepers)	Calculated Newtonian X_L	Measured R
DOP-w.r.t. ETOH				
25	9.2	-.136	3678	3379
20	10.1	-.153	4089	4077
15	10.7	-.181	4603	4745
10	11.7	-.210	5254	5424
NBS OIL I				
25	6.1	-.108	2334	2415
NBS OIL L				
25	15.5	-.264	5407	5905
5% Polystyrene (2200 M.W.) in DOP w.r.t. ETOH REF.				
25	11.5	-.145	4253	3871
20	12.6	-.171	4797	4480
15	13.6	-.200	5597	5171
10	15.0	-.249	6473	6297
10% Polystyrene				
25	15.5	-.205	5278	5213
20	16.3	-.236	5902	5934
15	17.1	-.266	6816	6647
10	17.9	-.333	7920	8176

At 14.5 MHz $\tilde{X}=358$ $\tilde{R}=22,370$

Temp. (°C)	$\Delta\phi$ (degree)	ΔA Attenuation (nepers)	Calculated Newtonian X_L	Measured R
20% Polystyrene(2200 M.W.) in DOP w.r.t. ETOH REF.				
25	19.8	-.331	8263	8032
20	20.6	-.396	9748	9513
15	21.5	-.484	11537	11524
10	21.5	-.646	13860	15178
40% Polystyrene				
25	25.7	-.969	30002	22304
20	24.5	-1.126	39068	25843
15	22.5	-1.307	51063	29934
10	20.5	-1.521	68808	34751

At 25.0 MHz

Temp. (°C)	$\Delta\phi$ (degree)	ΔA Attenuation (nepers)	Calculated Newtonian X_L
DOP-w.r.t. ETOH			
25	9.4	-.254	4006
20	9.5	-.286	4511
15	9.9	-.326	5131
10	10.3	-.367	5947
NBS OIL I			
25	6.1	-.175	3065
NBS OIL L			
25	11.0	-.443	7100
5% Polystyrene (2200 M.W.) in DOP w.r.t. ETOH REF.			
25	10.0	-.369	4760
20	11.0	-.402	5440
15	12.0	-.440	6435
10	13.3	-.503	7545
10% Polystyrene			
25	13.2	-.506	5975
20	13.9	-.537	6890
15	14.8	-.601	8035
10	15.9	-.686	9445

At 25.0 MHz

Temp. (°C)	$\Delta\phi$ (degree)	ΔA Attenuation (nepers)	Calculated Newtonian X_L
20% Polystyrene (2200 M.W.) in DOP w.r.t. ETOH REF.			
25	17.7	-.764	10025
20	16.9	-.829	11940
15	16.5	-.916	14235
10	16.4	-1.114	17243
40% Polystyrene			
25	12.0	-1.579	38675
20	4.5	-1.664	50440
15	-1.7	-1.963	66135
10	-8.6	-2.208	89395

At 27.1 MHz

Temp. (°C)	$\Delta\phi$ (degree)	ΔA Attenuation (nepers)	calculated Newtonian X_L
DOP - w.r.t. ETOH			
25	8.9	-.280	4171
20	9.3	-.313	4695
15	10.0	-.349	5342
10	11.3	-.393	6191
NBS OIL I - w.r.t AIR			
25	5.6	-.178	3191
NBS OIL L - w.r.t. AIR			
5% Polystyrene(2200 M.W.) in DOP w.r.t. ETOH REF.			
25	8.9	-.395	4956
20	10.2	-.423	5664
15	11.0	-.470	6699
10	12.5	-.549	7856
10% Polystyrene			
25	9.4	-.516	6221
20	10.9	-.584	7174
15	12.9	-.637	8365
10	15.0	-.704	9834

At 27.1 MHz

Temp. (°C)	$\Delta\phi$ (degree)	ΔA Attenuation (nepers)	Calculated Newtonian X_L
20% Polystyrene(2200 M.W.) in DOP w.r.t. ETOH REF.			
25	14.1	-.826	10437
20	14.9	-.916	12432
15	16.0	-1.016	14820
10	17.5	-1.149	17955
40% Polystyrene			
25	5.3	-1.743	40267
20	-0.6	-1.880	52516
15	-8.5	-2.019	68856
10	-23.5	-2.200	93074

The raw experimental measurements were found in Table 3 and Figs.12, 13, 14 and 15. The summary of the results are shown in Table 5.

B. Steady State Measurements of Solvent and Solutions

1. DOP Plasticizer

The steady state viscosity of the DOP (C_6H_4 - 1,2 (COO $(CH_2)_7CH_3)_2$) plasticizer used in these experiments has been measured over a range of temperatures (25°C, 20°C, 15°C and 10°C) with a capillary viscometer; and the density was also measured over the same temperature range with volumetric flask and (Mettler H-20) analytic balance. The results are presented in Table 6.

2. Polystyrene/DOP Solutions (5%, 10%, 20% and 40%)

The viscosity and the density of the solutions were measured in the same manner as above and the results are shown in Table 6.

C. Sample Description and Preparation

The anionically polymerized polystyrene sample was obtained from Pressure Chemical Company. The weight-average molecular weight of this polymer is 2200. It is in powder form.

The DOP was purchased in liquid form from Eastman Chemical Company, and bears the chemical formula C_6H_4-1,2[COO $(CH_2)_7CH_3]_2$ and the molecular weight is 390.56. The steady state viscosities at various temperatures are shown in Table 6.

All solutions were prepared by weighing, and the weight fraction of polystyrene was converted to g/cc by multiplying by the solution density.

Solutions using polystyrene and DOP were dissolved quite readily with gentle continuous swirling over an average period of two days. The

swirling was done at 50°C with the aid of a small motor which was operated at a moderate speed to avoid any possibility of mechanical degradation.

The heating was necessary since polystyrene in powder form would not dissolve at room temperature in a 48 hour period.

Table 6. STEADY STATE DATA

TEMP. C	DENSITY g/cc	*VISCOSITY (poises)	$\sqrt{\rho\eta}$	$\sqrt{\pi\rho\eta}$
Ethanol (ETOH)				
25	0.785	0.0100	0.088	0.165
20	0.789	0.0120	0.097	0.172
15	0.793	0.0133	0.103	0.182
10	0.798	0.0147	0.108	0.191
DOP				
25	0.971	0.306	0.545	0.966
20	0.976	0.376	0.606	1.074
15	0.977	0.475	0.682	1.209
10	0.980	0.619	0.779	1.380
NBS Oil I				
25	0.828	0.100	0.346	0.613
NBS Oil L				
25	0.868	0.740	0.801	1.420
5% Polystyrene (2200 M.W.) in DOP				
25	0.975	0.407	0.630	1.117
20	0.978	0.518	0.712	1.260
15	0.982	0.701	0.830	1.470
10	0.986	0.931	0.958	1.700
10% Polystyrene (2200 M.W.) in DOP				
25	0.976	0.602	0.766	1.360
20	0.979	0.783	0.875	1.550
15	0.982	1.042	1.011	1.790
10	0.986	1.403	1.176	2.080

TEMP. C	DENSITY g/cc	*VISCOSITY (poises)	$\sqrt{\rho\eta}$	$\sqrt{\pi\rho\eta}$
20% Polystyrene(2200 M.W.)in DOP				
25	0.985	1.528	1.227	2.170
20	0.989	2.114	1.446	2.560
15	0.992	2.951	1.711	3.030
10	0.996	4.236	2.054	3.640
40% Polystyrene(2200 M.W.) in DOP				
25	1.000	19.880	4.459	7.900
20	1.010	33.200	5.791	10.260
15	1.010	56.700	7.567	13.410
10	1.010	102.96	10.197	18.070
NBS Oil D				
25	0.760			
NBS Oil N				
25	0.883	9.162	2.844	
Aroclor 1242				
25	1.381	0.6044	0.913	

* CANNON VISOMETER #300 D159

PART V

DISCUSSION OF RESULTS

A. Analysis of the Data

Experimental measurements are summarized in Tables 7 and 8. In Table 7 the ratio $\eta_s/\eta(0)$ of the solvent viscosity η_s, in the absence of the polymer to the solution viscosity in the low frequency limit $\eta(0)$, is compared to the ratio $\eta'(10)/\eta(0)$, the solution viscosity at 10 MHz to the solution viscosity in the low frequency limit. This comparison is made at different concentrations and temperatures. In this form, the value of $\eta'(10)/\eta(0) = 1$ in the limit of no relaxation at 10 MHz, and can approach $\eta_s/\eta(0)$ in the high frequency limit. Similarly, in Table 8, the same results are presented normalized by η_s, that is, $\eta(0)/\eta_s$ and $\eta'(10)/\eta_s$. In this form, the value of $\eta'(10)/\eta_s = \frac{\eta(0)}{\eta_s}$ in the limit of no relaxation, and can approach 1 in the high frequency limit. In fact, if we call the value of the high frequency limiting solution viscosity η_∞, then the limiting values become $\eta_\infty/\eta(0)$ for Table 7 and $\frac{\eta_\infty}{\eta_s}$ for Table 8.

The most significant conclusion of this present data is that $\eta'(10)/\eta(0)$ shows little evidence of relaxation of viscosity even at concentrations of 20% and temperature of 10°C. This leaves us with the primary conclusion that any relaxation mechanism responsible for the solution viscosity must occur at a frequency greater than 10 MHz, or equivalently, the relaxation time τ must be shorter than 1.6×10^{-8} sec $(1/2\pi 10^7$ Hz). Table 7 indicates that only when concentration reaches 40% or beyond does relaxation become apparent, that is, the relaxation time of the solution approaches the time scale of our measurement.

TABLE 7

NORMALIZED VISCOSITIES WITH RESPECT TO STEADY STATE SOLUTION VISCOSITY

2200 M.W. Polystyrene Soln. in DOP

	5%		10%		20%		40%	
	$\frac{\eta_s}{\eta(0)}$	$\frac{\eta'(10)}{\eta(0)}$	$\frac{\eta_s}{\eta(0)}$	$\frac{\eta'(10)}{\eta(0)}$	$\frac{\eta_s}{\eta(0)}$	$\frac{\eta'(10)}{\eta(0)}$	$\frac{\eta_s}{\eta(0)}$	$\frac{\eta'(10)}{\eta(0)}$
25°C	.75	1.1	.51	1.1	.20	.9	.015	.3
20°C	.73	1.1	.48	1.0	.18	.85	.011	.2
15°C	.68	.9	.46	.9	.16	.8	.008	.1
10°C	.66	.9	.34	.9	.11	.7	.005	.08

Ultrasonic: $\eta'(10\ \text{MHz}) \approx \langle \eta'(3.4\ \text{MHz} \rightarrow 19.5\ \text{MHz}) \rangle$

Cap. Tube $\rightarrow \eta(0)$ and η_s

TABLE 8

NORMALIZED VISCOSITIES WITH RESPECT TO SOLVENT VISCOSITY

2200 M.W. Polystyrene Solution in DOP

	5%		10%		20%		40%	
	$\frac{\eta(0)}{\eta_s}$	$\frac{\eta'(10)}{\eta_s}$	$\frac{\eta(0)}{\eta_s}$	$\frac{\eta'(10)}{\eta_s}$	$\frac{\eta(0)}{\eta_s}$	$\frac{\eta'(10)}{\eta_s}$	$\frac{\eta(0)}{\eta_s}$	$\frac{\eta'(10)}{\eta_s}$
25°C	1.33	1.467	1.96	2.16	5.00	4.50	66.66	20.00
20°C	1.37	1.51	2.08	2.08	5.55	4.72	90.91	18.18
15°C	1.47	1.32	2.17	1.96	6.25	5.00	125.00	12.5
10°C	1.51	1.36	2.94	2.65	9.09	6.36	200.00	16.00

Ultrasonic: $\eta'(10\ \text{MHz}) \approx \langle \eta'(3.4\ \text{MHz}) \rightarrow 19.5\ \text{MHz}) \rangle$

In order to account for the enhanced viscosity of the solution $\eta(0)$ over that of the solvent η_s at low frequencies, we examine the prediction of several known mechanisms of viscosity enhancement. We shall briefly discuss each of these possible mechanisms. Then, in turn calculate the contribution $\eta(0) - \eta_s$ to the viscosity enhancement. We summarize the results in Table 9. Each calculation is based on the experimental observation (Table 7 or 8) that the longest relaxation time predicted by each model must be shorter than 1.6×10^{-8} sec as long as the concentration does not exceed 20%.

Briefly, predictions of the theories for known mechanisms are as follows:

1. The rigid rod model of Kirkwood and Auer[13]:

$$\eta - \eta_s = \frac{4}{5} \frac{c RT}{M} \tau \quad ; \quad \tau = \frac{\pi \eta_s L^3}{18 kT \ln(\frac{L}{b})}$$

where c is concentration in gm/cc of the solution, M is the molecular weight, η_s is the solvent viscosity, L is the length of the molecule and b is the distance between the submolecules.

2. The prolate ellipsoid model of Cerf[14] and Scheraga[15]

$$\eta - \eta_s = \frac{21}{25} \frac{c RT}{M} \tau \quad ; \quad \tau = \frac{\pi^2 \eta_s L^3}{9 kT (2 \ln 2p - 1)}$$

where p is the axial ratio.

3. The rigid dumbbell model[17]

$$\eta - \eta_s = \frac{c RT}{M} \tau \quad ; \quad \tau = \frac{\xi L^2}{12 kT}$$

where ξ is a friction coefficient for a rigid dumbbell of length L.

4. The head-spring model with no hydrodynamic interaction among heads (Rouse model):

$$\eta - \eta_s = 1.645 \frac{cRT}{M} \tau_p \quad ; \quad \tau_p = \frac{\sigma^2 N^2 f_o}{6\pi^2 p^2 kT}$$

where p = 1, 2, 3, ..., and where N is the number of submolecules, f_o is the monomeric friction coefficient and σ is the root-mean-square end-to-end length of the submolecule.

5. The bead-spring model with dominant hydrodynamic interaction (Zimm model):

$$\eta - \eta_s = 2.369 \frac{cRT}{M} \tau_k \quad ; \quad \tau_k = \frac{0.806\, \eta_s a^3 p^{3/2}}{\lambda_k' kT}$$

and

$$a = \left[\left(r_o^2/\eta_s\right)_{\dot{\gamma}}\right]^{1/2} \lambda$$

where λ_k' are numerical coefficients (eigenvalues), whose first few values are 4.04, 12.79, 24.2 and 37.9, η_s is the solvent viscosity, p is the integer 1, 2, 3, ... At finite concentrations the value of τ in the various cases becomes:

(i) $$\tau = m(\eta - \eta_s)M / cRT$$

where m = 5/4 for rod (Kirkwood and Auer), m = 25/21 for very long ellipsoids (Scheraga) and m = 1 for rigid dumbbells (Ullman)

(ii) $$\tau = (\eta - \eta_s)M / cRT$$

where s = 1.645 for Rouse's model and s = 2.369 for Zimm's model.

From the calculated values of $\eta(0) - \eta_s$ in Table 9, it is clear that none of these models are able to account for the experimentally measured viscosity enhancement. In the absence of any other mechanism to account for polymer contribution to the total viscosity, we conclude that the primary effect of adding the polymer to the solvent is to affect the relaxation time of the solvent. Namely, the relaxation time of the solvent is moved to longer times, and hence at low frequencies the solvent viscosity itself is increased.

We have no specific model to account for this increase. One possible mechanism could be that the role of the low molecular weight polymer is to reduce the available free volume and thereby slow down the solvent re-orientation process.

In this discussion, viscosity is proportional to the relaxation time. The relaxation time is related to the free volume available for rearrangement of solvent molecules. We postulate here that the primary effect of polymer molecule is to decrease the free volume available for solvent molecule rearrangement. Thereby relaxation time is increased, so as the solution viscosity and so as the solvent viscosity.

Another possibility is that the polymer molecule plays some role in correlating motions of solvent molecules and thereby extending the relaxation time to longer times and possibly broadening the solvent relaxation spectrum.

TABLE 9

VISCOSITY DIFFERENCE $\eta(0) - \eta_s$ IN POISE EVALUATED BY ASSUMING $\tau_1 \leq 1.6 \times 10^{-8}$ Sec

$T = 10^{\circ}C$

Model / Conc.	5%	10%	20%	40%
Kirkwood and Auer	6.8135×10^{-3}	1.3627×10^{-2}	2.7254×10^{-2}	5.4508×10^{-2}
Scheraga	7.1540×10^{-3}	1.4308×10^{-2}	2.8616×10^{-2}	5.7232×10^{-2}
Ullman	8.5169×10^{-2}	1.7034×10^{-2}	3.4067×10^{-2}	6.8134×10^{-2}
Rouse	1.401×10^{-2}	2.802×10^{-2}	5.604×10^{-2}	1.12080×10^{-1}
Zimm	2.0175×10^{-2}	4.035×10^{-2}	8.070×10^{-2}	1.6140×10^{-1}
Experimental	2.189×10^{-1}	6.437×10^{-1}	2.346	7.6178

$T = 20^{\circ}C$

Model / Conc.	5%	10%	20%	40%
Kirkwood and Auer	7.0×10^{-3}	1.4×10^{-2}	2.8×10^{-2}	5.6×10^{-2}
Scheraga	7.4×10^{-3}	1.5×10^{-2}	3.0×10^{-2}	5.9×10^{-2}
Ullman	8.8×10^{-3}	1.8×10^{-2}	3.5×10^{-2}	7.0×10^{-2}
Rouse	1.45×10^{-2}	2.9×10^{-2}	5.8×10^{-2}	1.2×10^{-1}
Zimm	2.1×10^{-2}	4.2×10^{-2}	8.4×10^{-2}	1.7×10^{-1}
Experimental	1.85×10^{-1}	4.07×10^{-1}	1.421	6.26

(cont'd.)

Table 9 (cont'd.)

$T = 25^{\circ}C$

Model / Conc.	5%	10%	20%	40%
Kirkwood and Auer	7.2×10^{-3}	1.4×10^{-2}	2.9×10^{-2}	5.7×10^{-2}
Scheraga	7.5×10^{-3}	1.5×10^{-2}	3.0×10^{-2}	6.0×10^{-2}
Ullman	9.0×10^{-3}	1.8×10^{-2}	3.6×10^{-2}	7.2×10^{-2}
Rouse	1.5×10^{-2}	2.9×10^{-2}	5.9×10^{-2}	1.2×10^{-1}
Zimm	2.1×10^{-2}	4.2×10^{-2}	8.5×10^{-2}	1.7×10^{-1}
Experimental	1.42×10^{-1}	3.5×10^{-1}	1.071	5.7

$T = 15^{\circ}C$

Model / Conc.	5%	10%	20%	40%
Kirkwood and Auer	6.9×10^{-3}	1.4×10^{-2}	2.8×10^{-2}	5.5×10^{-2}
Scheraga	7.3×10^{-3}	1.5×10^{-2}	2.9×10^{-2}	5.8×10^{-2}
Ullman	8.7×10^{-3}	1.7×10^{-2}	3.5×10^{-2}	6.9×10^{-2}
Rouse	1.4×10^{-2}	2.8×10^{-2}	5.7×10^{-2}	1.1×10^{-1}
Zimm	2.0×10^{-2}	4.1×10^{-2}	8.2×10^{-2}	1.6×10^{-1}
Experimental	1.54×10^{-1}	4.6×10^{-1}	1.88	5.2

B. Assumptions and Accuracy

The development of the equations is based on the following assumptions.

1. The excitation of transducer is a steady-state sinusoidal motion, whereas a pulse-echo technique is used in this experiment. The total response approaches the steady-state sinusoidal vibration when the pulse length is comparable with 10 cycles[22] and according to Hunston's[11] results, a pulse as short as 14 cycles at 2 MHz has been used successfully. In the experiment present here, the 20 μsec pulse duration used at a frequency of 10 MHz corresponds to 200 cycles.

2. A fused quartz delay material is assumed to be homogeneous and isotropic to an acoustical wave in the frequency range of our interest. When the wavelength (.03 cm) of the propagating acoustic wave is comparable with the grain size of fused quartz, the above assumptions of the homogeneity and isotropy become invalid. However, the wave propagating in the fused quartz at 10 MHz is at least two orders larger than the grain size.

3. The mode for the delay line is infinite in width and length. This assumption is based on the fact that the length (7.62 cm) and the width (5.08 cm) are large with respect to wavelength (.03 cm) in the delay line. The transducer is also designed to excite only the principal shear mode SS(0). However, with a thickness of the delay medium = 0.152 cm, other plate modes could propagate, as seen in Meeker's analysis:

$$\frac{\omega b}{V_s} \approx 3.2$$

and therefore, the cut-off frequency for SS(1) becomes

$$f_1 = 2.2 \times 10^6 \text{ Hz}$$

where 2b and V_s are the thickness of the delay medium and the velocity, respectively. Therefore, it is possible to have SS(1) mode propagation at any frequency higher than 2.2 MHz. However, frequencies at which measurements are taken have been selected so that higher order mode contributions are not apparent.

4. It is also necessary to consider reflection from the end of the liquid if the thickness of the liquid (distance from fused quartz to plastic case) is not large compared to the damping length (1×10^{-5} cm). In our case the thickness is 0.0375 cm, which is approximated as infinite with respect to damping length.

5. Smooth surface: The fused quartz surface is much easier to polish that others, i.e., steel, aluminum. The polishing is of critical importance since for the viscoelastic liquids the wavelength or damping length begins to approach the magnitude of the surface irregularities, and for low viscosity liquids such as ethanol ($\lambda = 2.5 \times 10^{-3}$ cm). Surface smoothness of the delay medium was not well esablished, and the small streaks of random lines are observed under a 20 × magnification microscope.

6. Possible residual coating of the surface by the polymer solution can occur during the drying of the cell. In order to minimize this problem, the repeated cleaning of the cell with low alcohols were carried out.

7. The temperature of the delay line must be accurately controlled and measured, even though the temperature coefficient of acoustic velocity is smaller in fused quartz than in many other materials. We can see from the example of Fig.8, that at 19.5 MHz, the phase shifts by 12° per °C temperature change. Therefore, it is necessary to control temperature to

within .01°C in order to measure the phase shift to within a few tenths of a degree. It is also important that equilibrium is reached before any measurements are made.

8. The phase and amplitude response of P.Z.T. transducer will be influenced by the total mechanical impedance of the delay line; this impedance will change slightly by the presence of liquid on the delay medium, called a "loading effect". For the experiment presented here the loading effect has not been included in the analysis.

PART VI

CONCLUSIONS AND SIGNIFICANCE

1. An ultrasonic delay line device capable of measuring viscoelastic properties of liquids has been constructed and tested. The frequency range is from 3 to 30 MHz. The viscosity range is down to 0.5 centipoise, and has been used to beyond 100 poise.

2. The method of "walking frequency" has been developed to transform a high frequency signal into 1.25 Hz in order to overcome the limitation of digitizing a high frequency periodic signal in ADC, and read into the computer at a rate of one point every 40 μsec.

3. A series of measurements were performed on low molecular weight polystyrene solutions over the concentration range 5% to 40%.

4. A basic problem in the molecular theory of viscoelastic fluids was examined experimentally with this apparatus. The problem, called the "η_∞ problem", asks: "Why does the viscosity contribution of the polymer $\eta(0) - \eta_s$ not drop to zero in the high frequency limit as seems indicated by macromolecular theories?"

While some investigators have attempted to include corrections to the macromolecular theories, we conclude from these experimental results that the apparent discrepancy is due to the neglect of a polymer solvent interaction mechanism, rather than due to any basic defect in the theories for macromolecular backbone relaxation.

PART VII

LITERATURE CITED

1. Birnboim, M.H. and Koh, I.Y., Bull. Am. Phys. Soc., 18, 318 (1973).
2. Birnboim, M.H., Burke, J.S. and Andersen, R.L., Proc. Fifth Intl. Cong. Rheol., 11, 409 (1969).
3. Miller, J.W. and Schrag, J.L., Macromolecule, 8, 361 (1975).
4. Rouse, P.E., Jr., J. Chem. Phys., 21, 1272 (1953).
5. Zimm, B.H., J. Chem. Phys., 24, 269 (1956).
6. Birnboim, M.H. and Ferry, J.D., J. Appl. Phys., 32, 2305 (1961).
7. Thurston, G.B. and Schrag, J.L., J. Polymer Sci., A-2, 6, 1331 (1968).
8. Thurston, G.B. and Schrag, J.L., J. Chem. Phys., 45, 3373 (1966).
9. Meeker, T.R. and Meitzler, A.H., "Physical Acoustics," Vol.1, ed. Mason, W.P., Academic Press, NY, p.120.
10. McSkimin, H.J. and Moore, R.S., J. Chem. Phys., 47, 3 (1967).
11. Hunston, D.L., Ph.D. Thesis, Kent State University, 1969.
12. Fahmy, A.H. and Adler, E.L., Abstract, J. Acoust. Soc. Am., 1971.
13. Kirkwood, J.G. and Auer, P.L., J. Chem. Phys., 19, 281 (1951).
14. Cerf, R., Compt. Rend., 234, 1549 (1952).
15. Scheraga, H.A., J. Chem. Phys., 23, 1526 (1955).
16. Ullman, R., Macromolecules, 2, 27 (1969).
17. Pyun, C.W. and Fixman, M., J. Chem. Phys., 42, 3838 (1966).
18. Pyun, C.W. and Fixman, M., J. Chem. Phys., 44, 2107 (1966).
19. Peterlin, A., Kolloid. -Z., 209, 181 (1966).
20. Peterlin, A., J. Polymer Sci., A-2, 5, 179 (1967).
21. Peterlin, A. and Reinhold, C., Trans. Soc. Rheo., 11, 15 (1967).
22. Herzfeld, K.F. and Litowitz, T.A., "Absorption and Dispersion of Ultrasonic Waves," Academic Press, New York, p.367, 1959.

23. Koh, I.Y. and Birnboim, M.H., "The High Frequency Limiting Behavior of Polymer Solutions," Sweden Intl. Rheol. Meeting, 1976.

24. McSkimin, H.J., J. Acoust. Soc. Am., 24, 355 (1952).

25. Rouse, P.E., Jr. and Sittel, K., J. Appl. Phys., 24, 690 (1953).

26. O'Neil, H.T., Physical Review, 75, 928 (1949).

27. Osaki, K. and Schrag, J.L., Polymer Journal, Japan, 2, 541 (1971).

28. Ferry, J.D., "Viscoelastic Properties of Polymers," 2nd. ed., John Wiley and Sons, New York, 307 (1970).

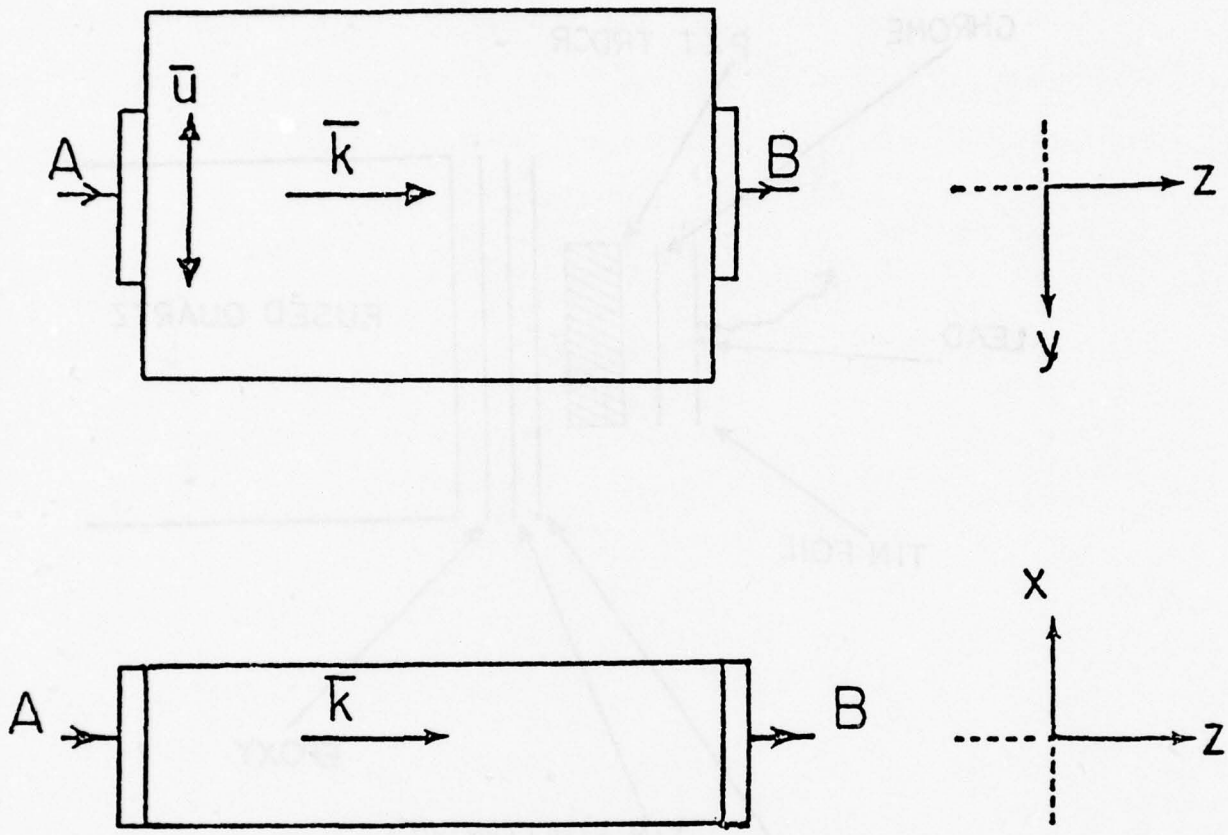

FIGURE I. DELAY LINE

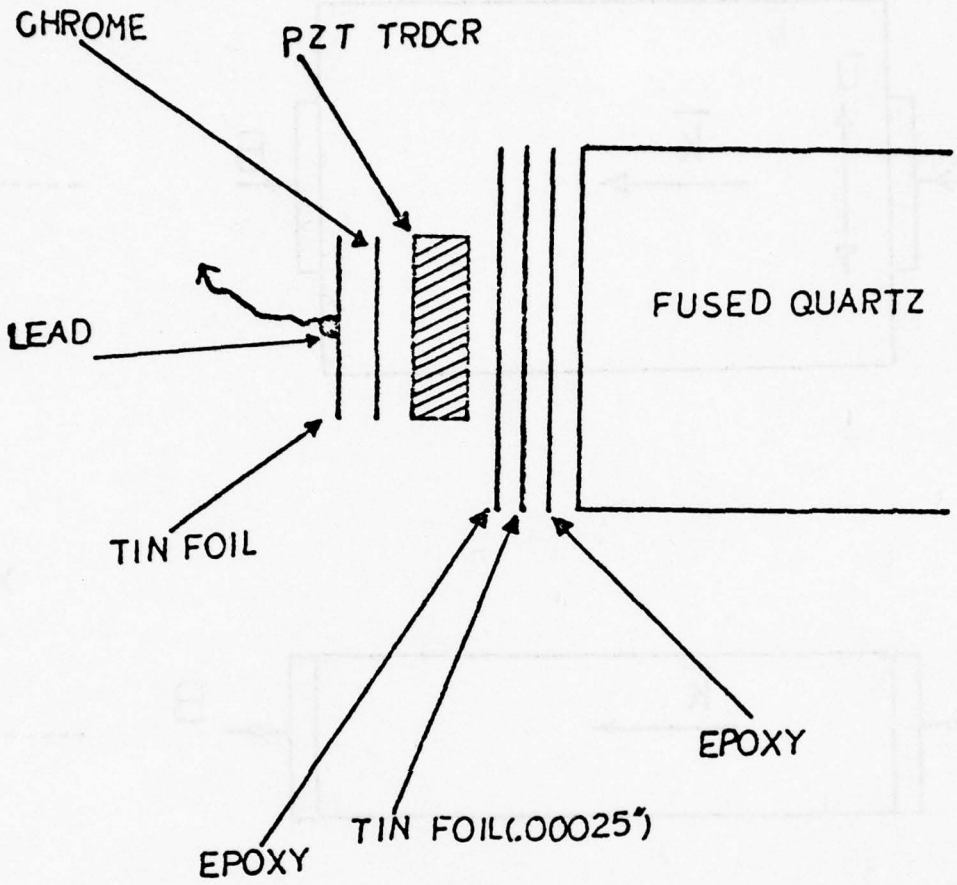

FIG. 2 DETAIL MOUNTING OF TRDCR

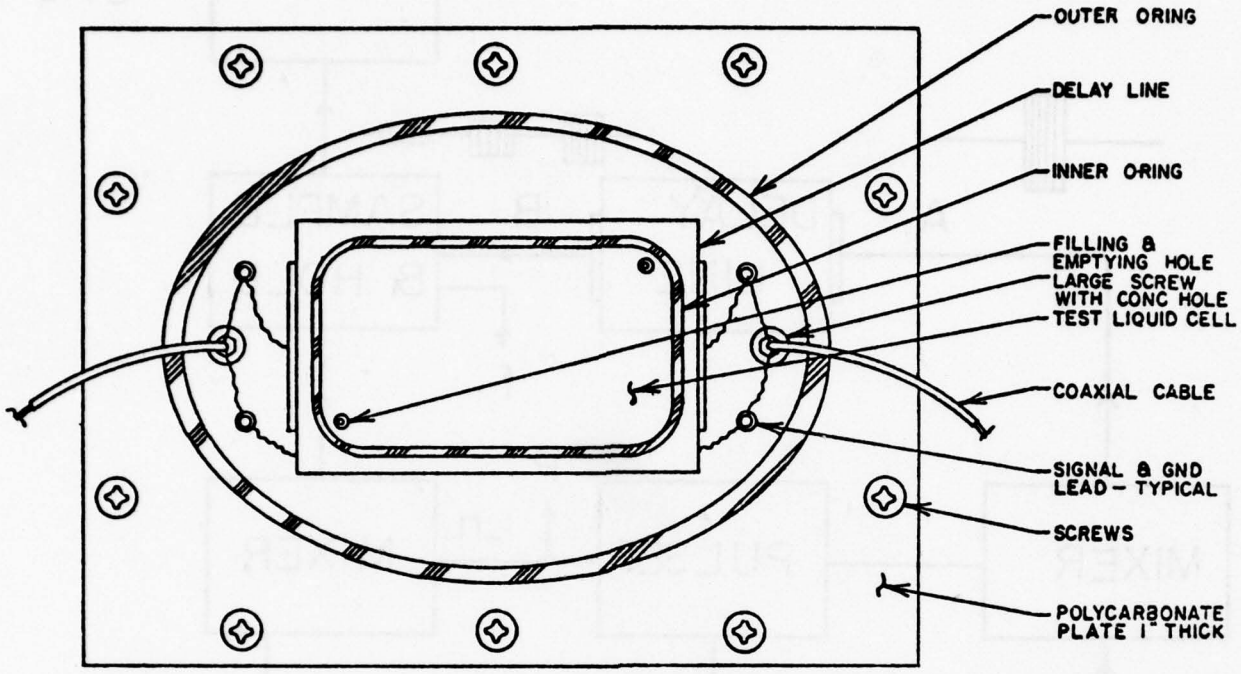

TOP VIEW

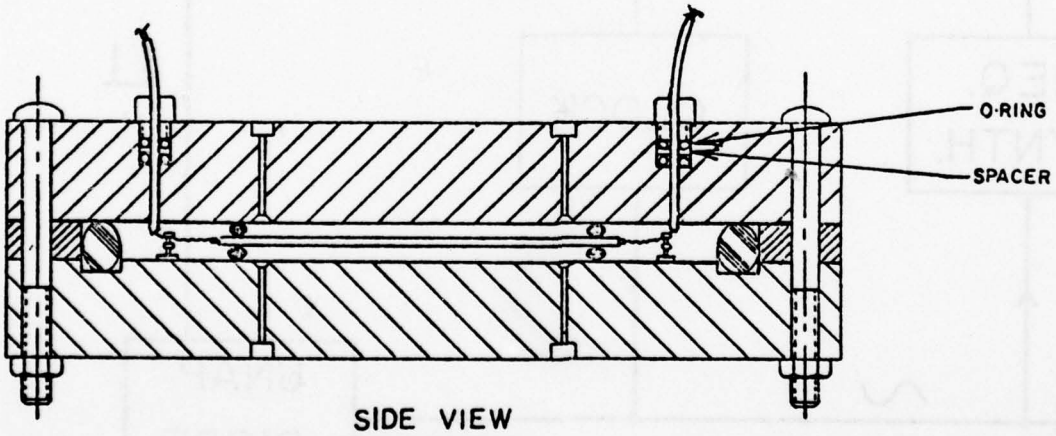

SIDE VIEW
(SECTIONED)

FIG 3. CELL ASSEMBLY

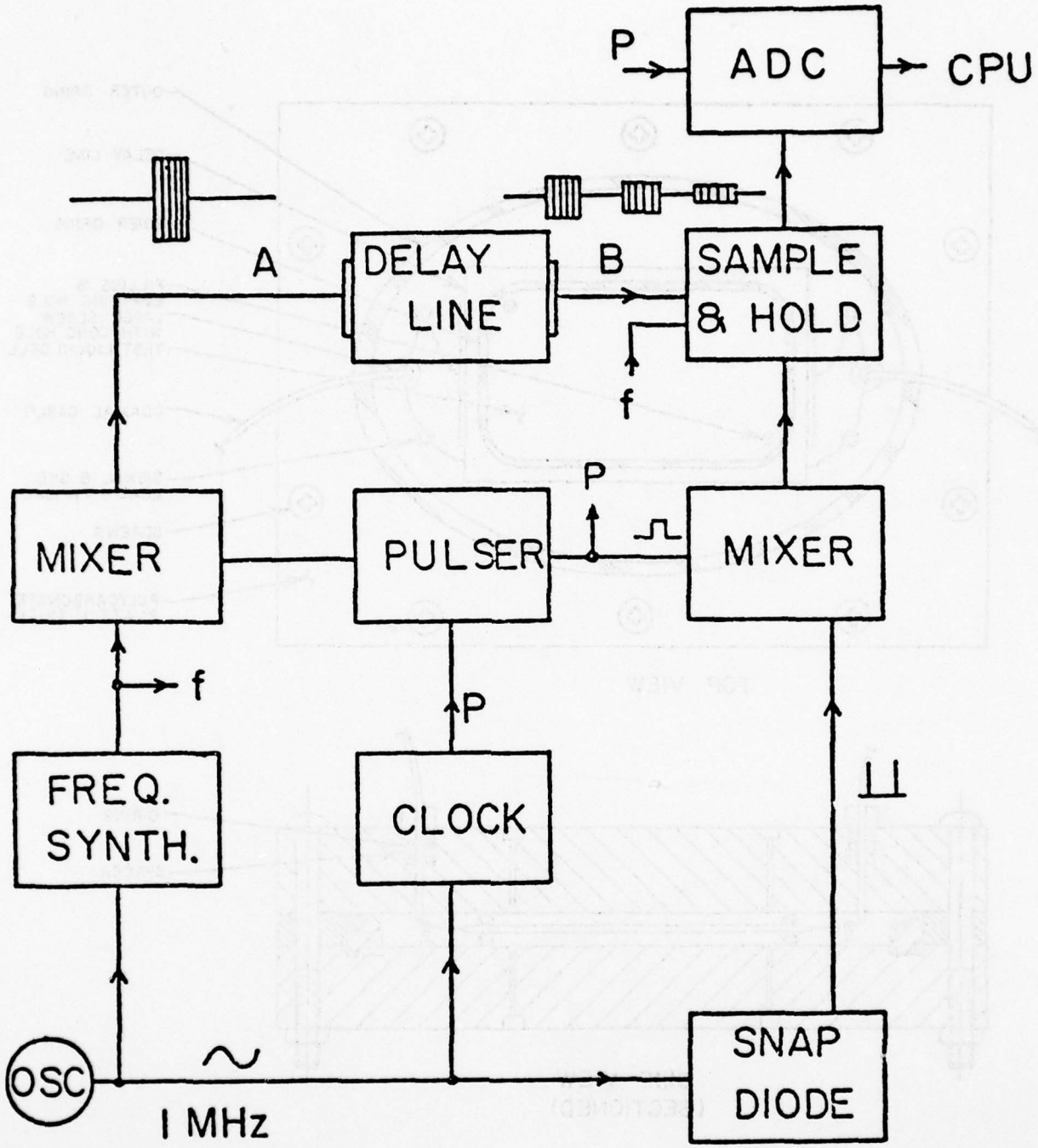

FIG.4 ELECTRONICS BLOCK DIAGRAM

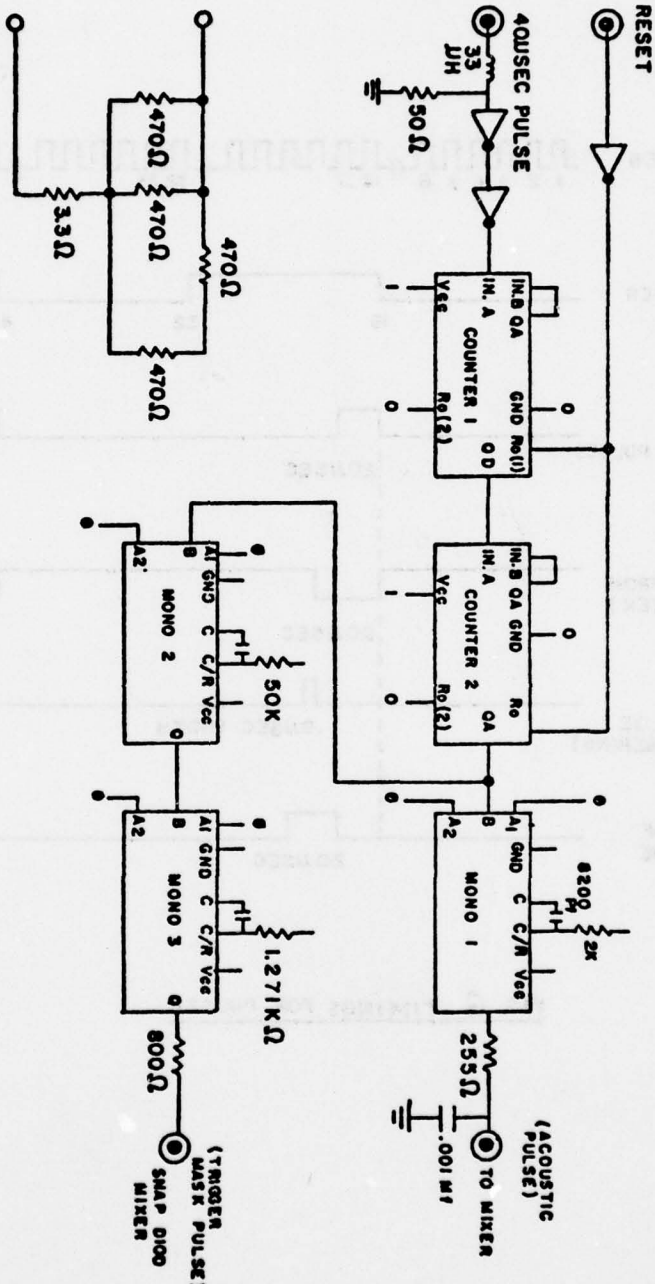

FIG. 5 SCHEMATIC DIAGRAM OF PULSER

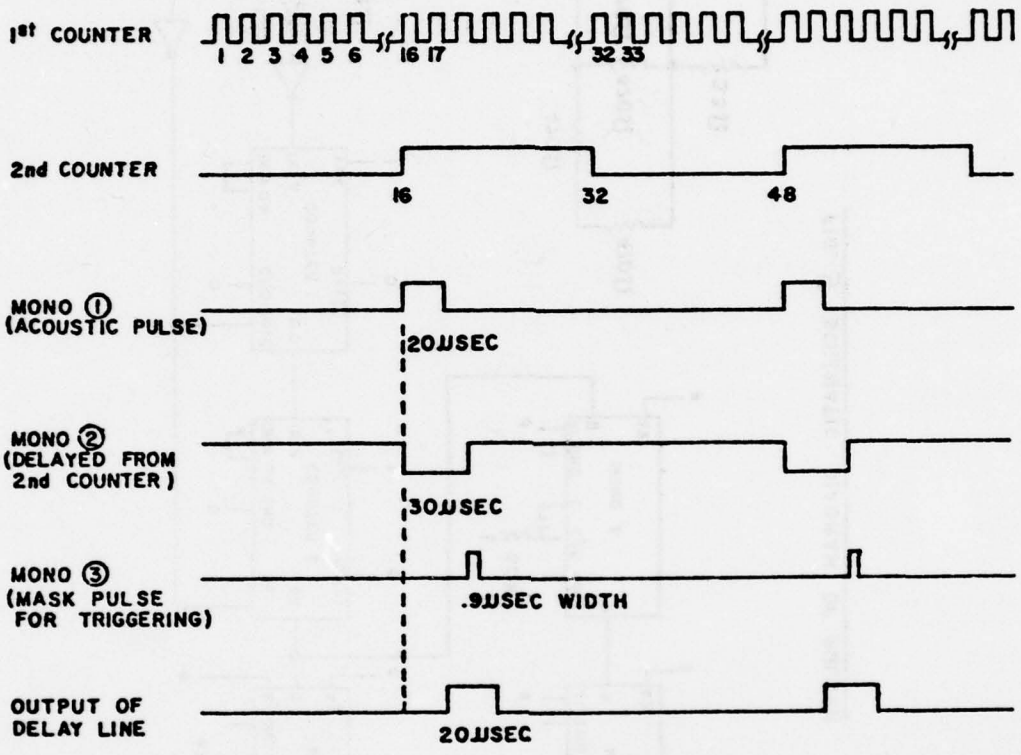

FIG. 6 TIMINGS FOR PULSER

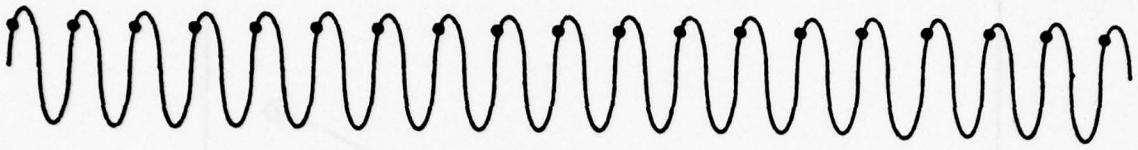

SYNCHRONOUS FREQUENCY

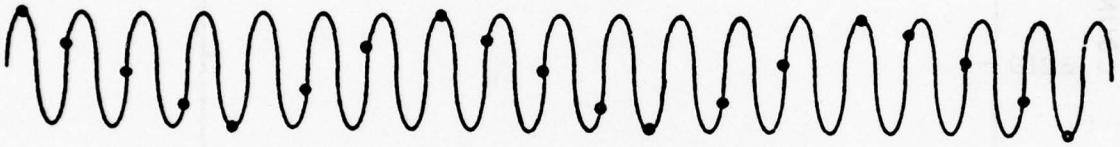

WALKING FREQUENCY

FIG. 7 WALKING FREQUENCY

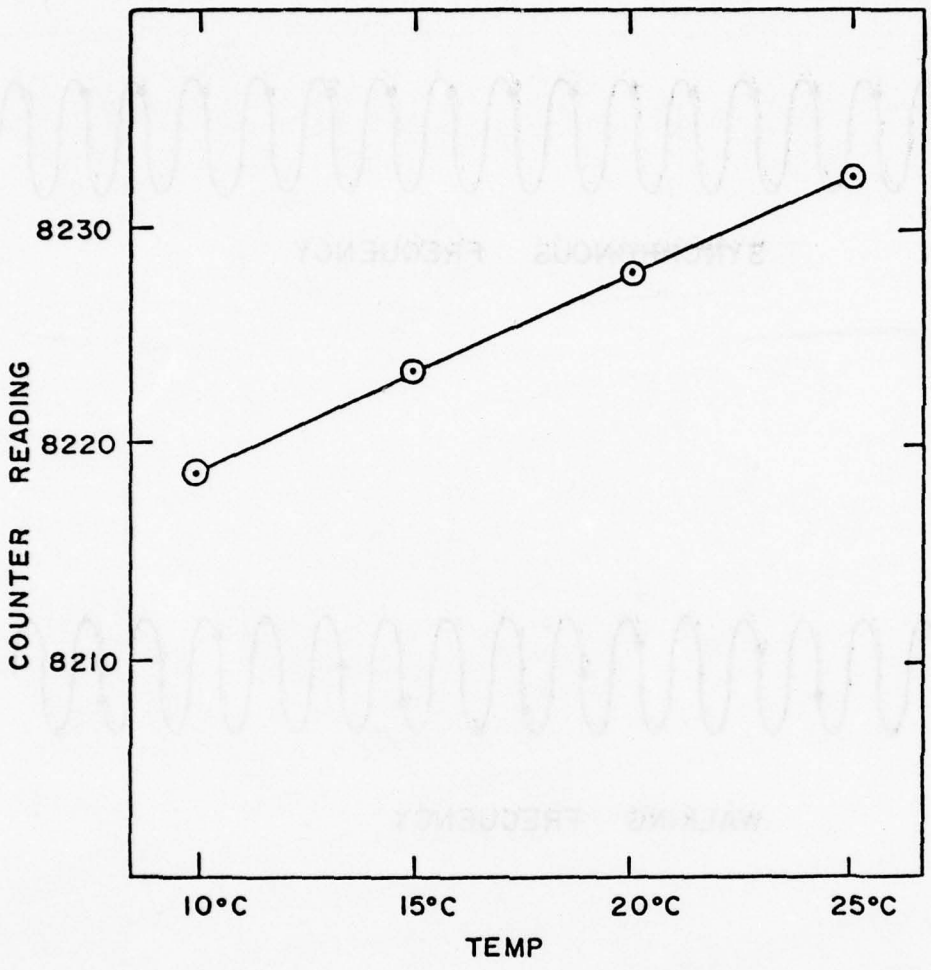

FIG. 8 G.R. COUNTER READING VS TEMPERATURE

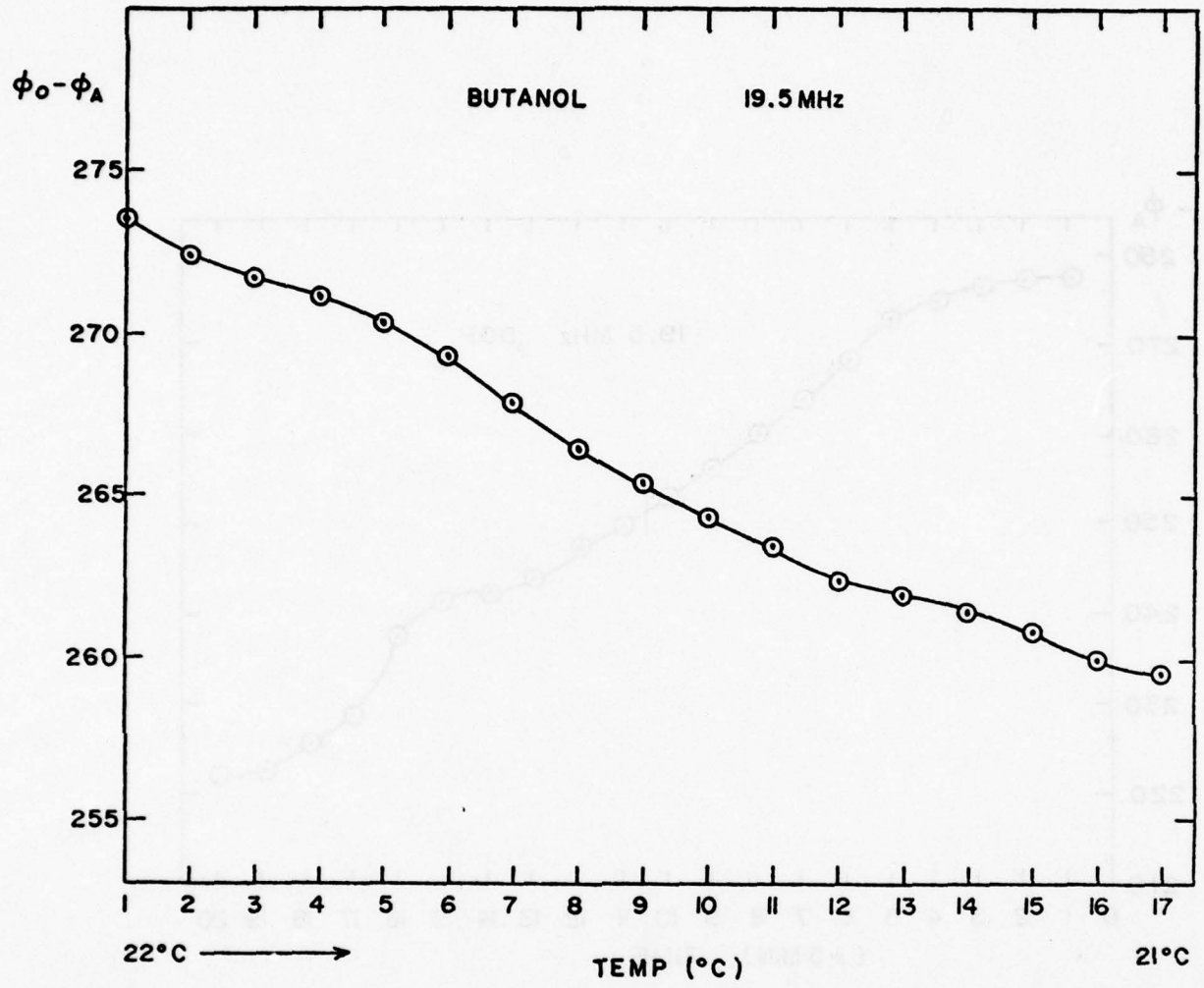

FIG. 9 PHASE vs TEMP.

(MEASUREMENTS IN 5 MINUTE INTERVAL)

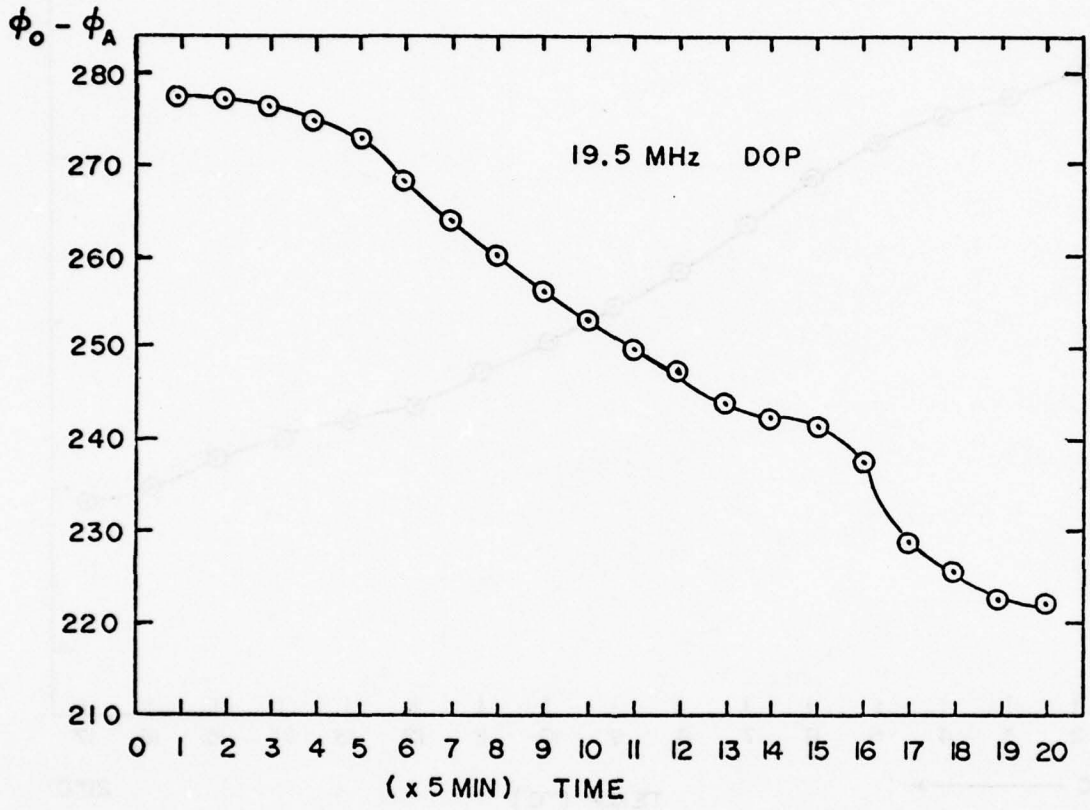

FIG. 10 TEMP 25°C — 20°C
LEFT FLOAT

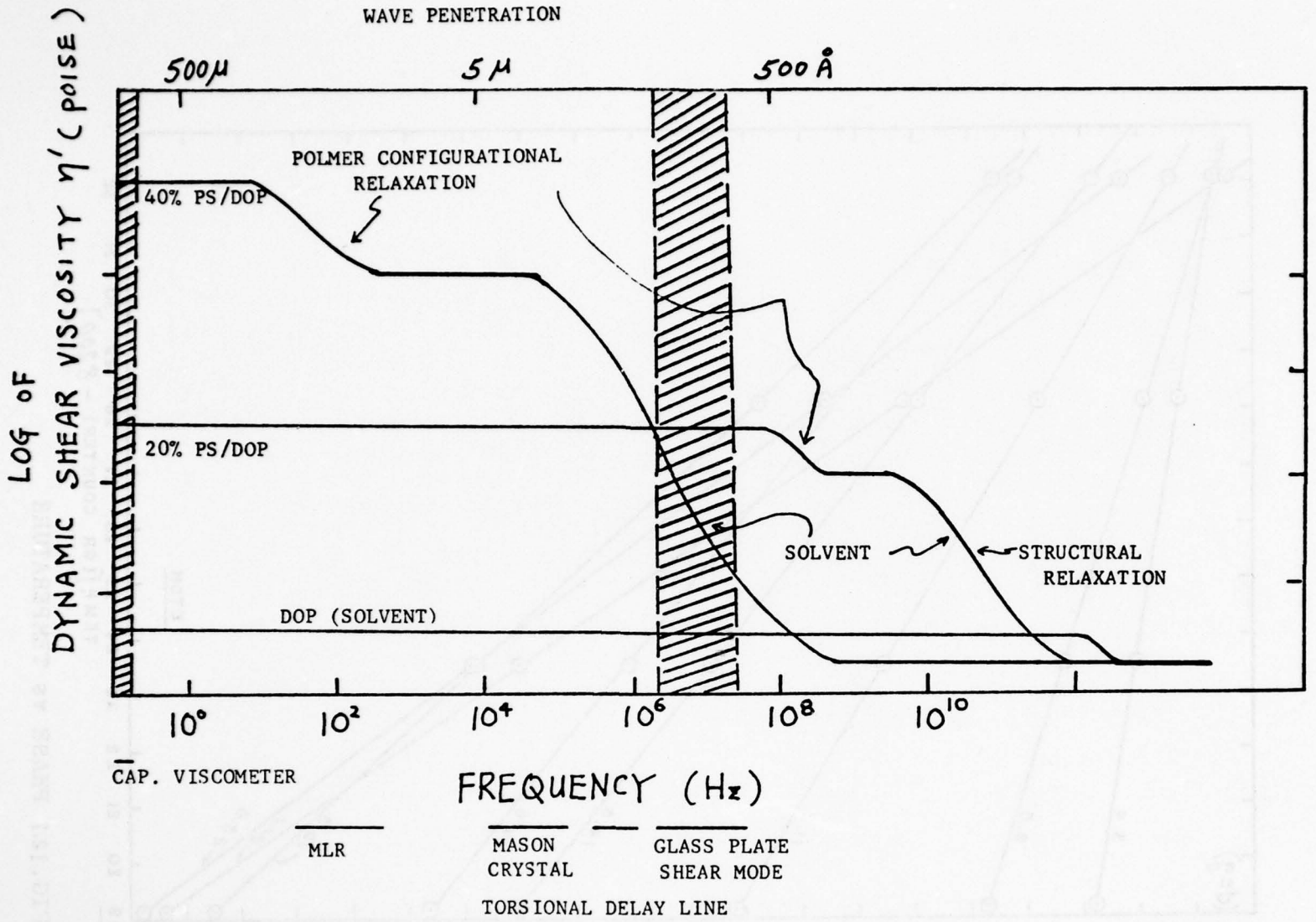

FIG. 11 DYNAMIC SHEAR VISCOSITY VS. FREQUENCY

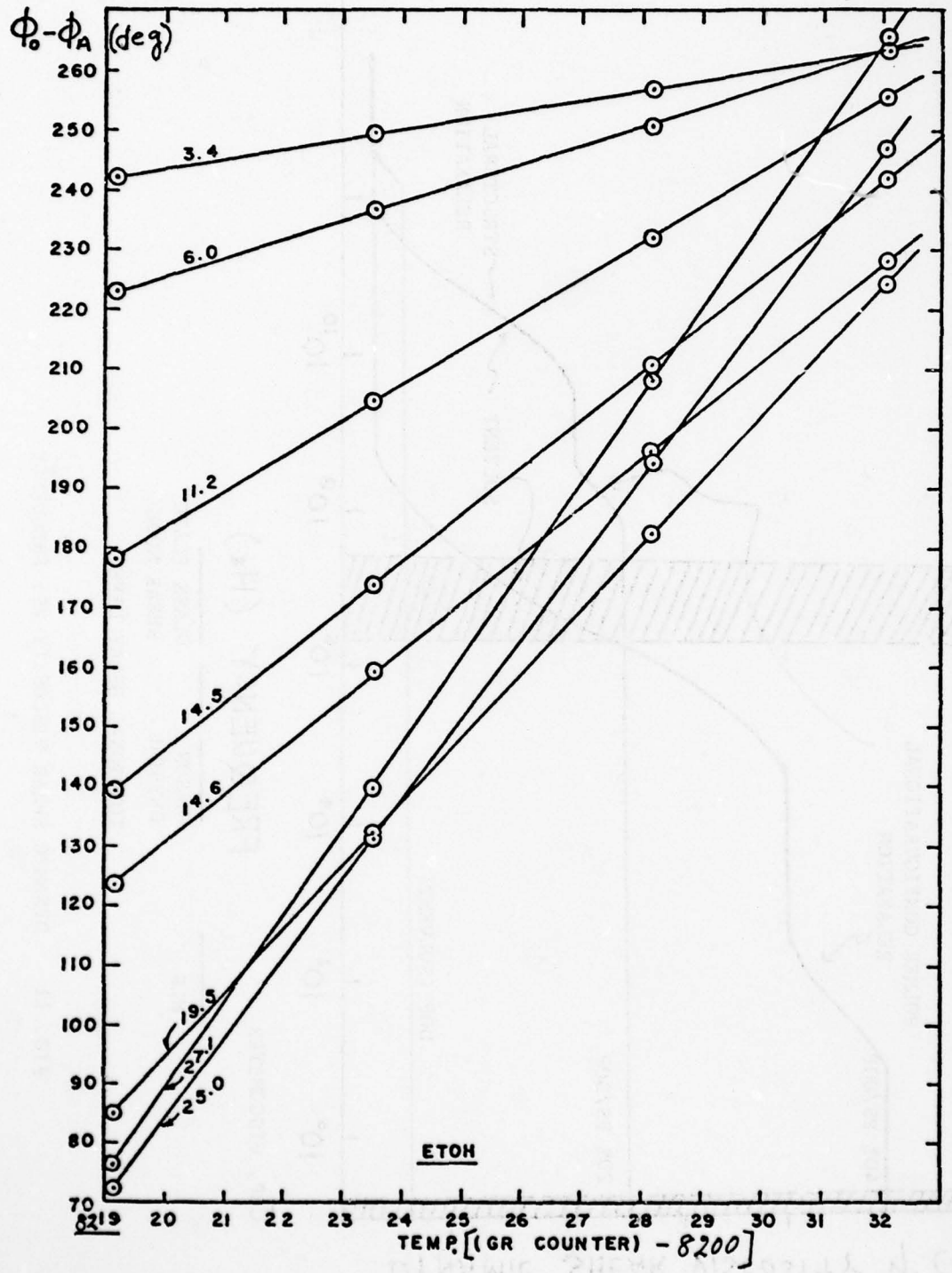

FIG. 12.1 PHASE vs TEMPERATURE

AD-A062 612 RENSSELAER POLYTECHNIC INST TROY NY LAB FOR VISCOELA--ETC F/G 11/8
MEASUREMENT OF PROPERTIES AND RESPONSE FUNCTIONS OF LIQUID LUBR--ETC(U)
JUN 78 M H BIRNBOIM F33615-76-C-5101

UNCLASSIFIED AFML-TR-78-69 NL

3 OF 3
ADA
062812

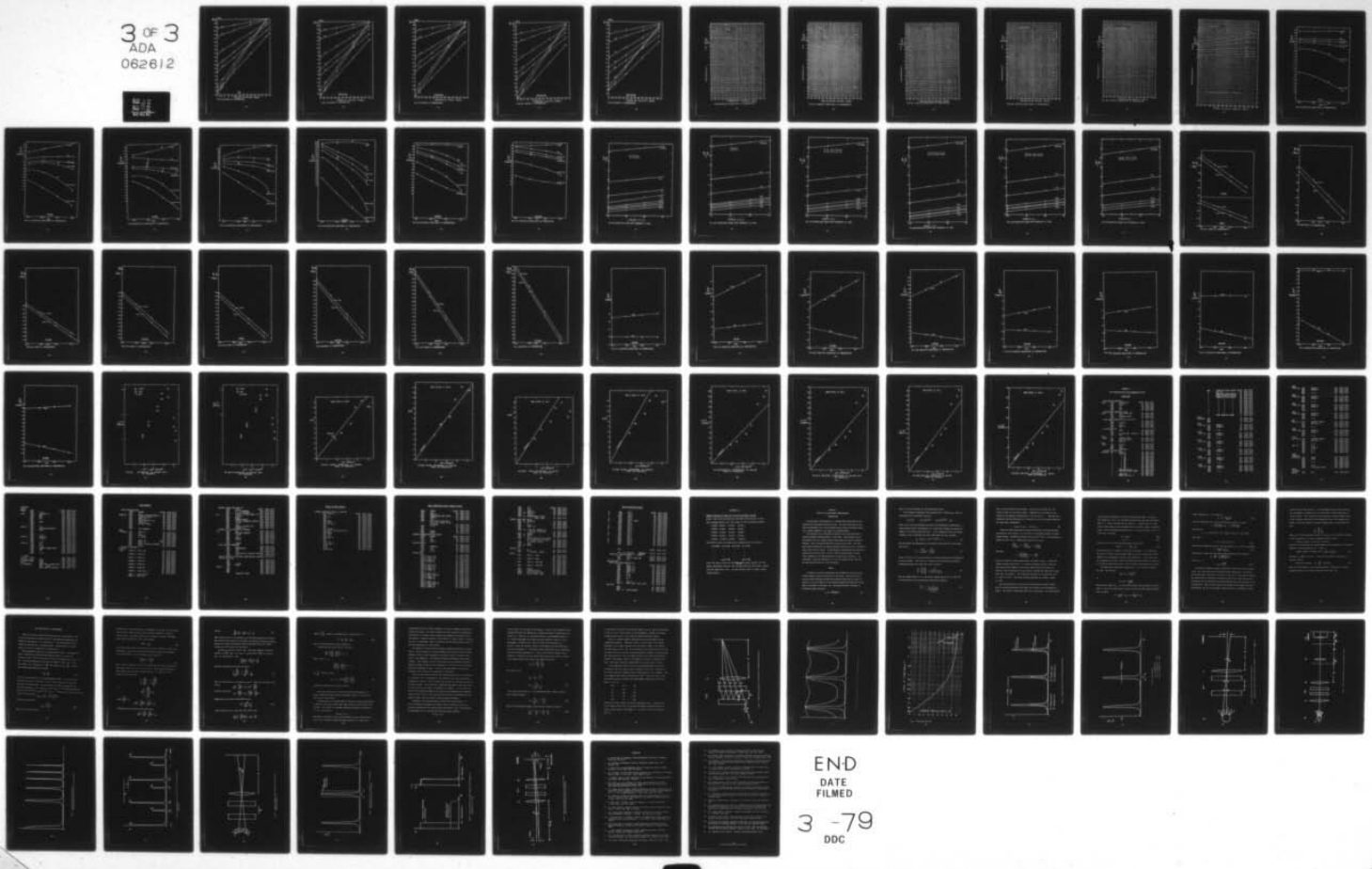

END
DATE
FILMED
3 -79
DDC

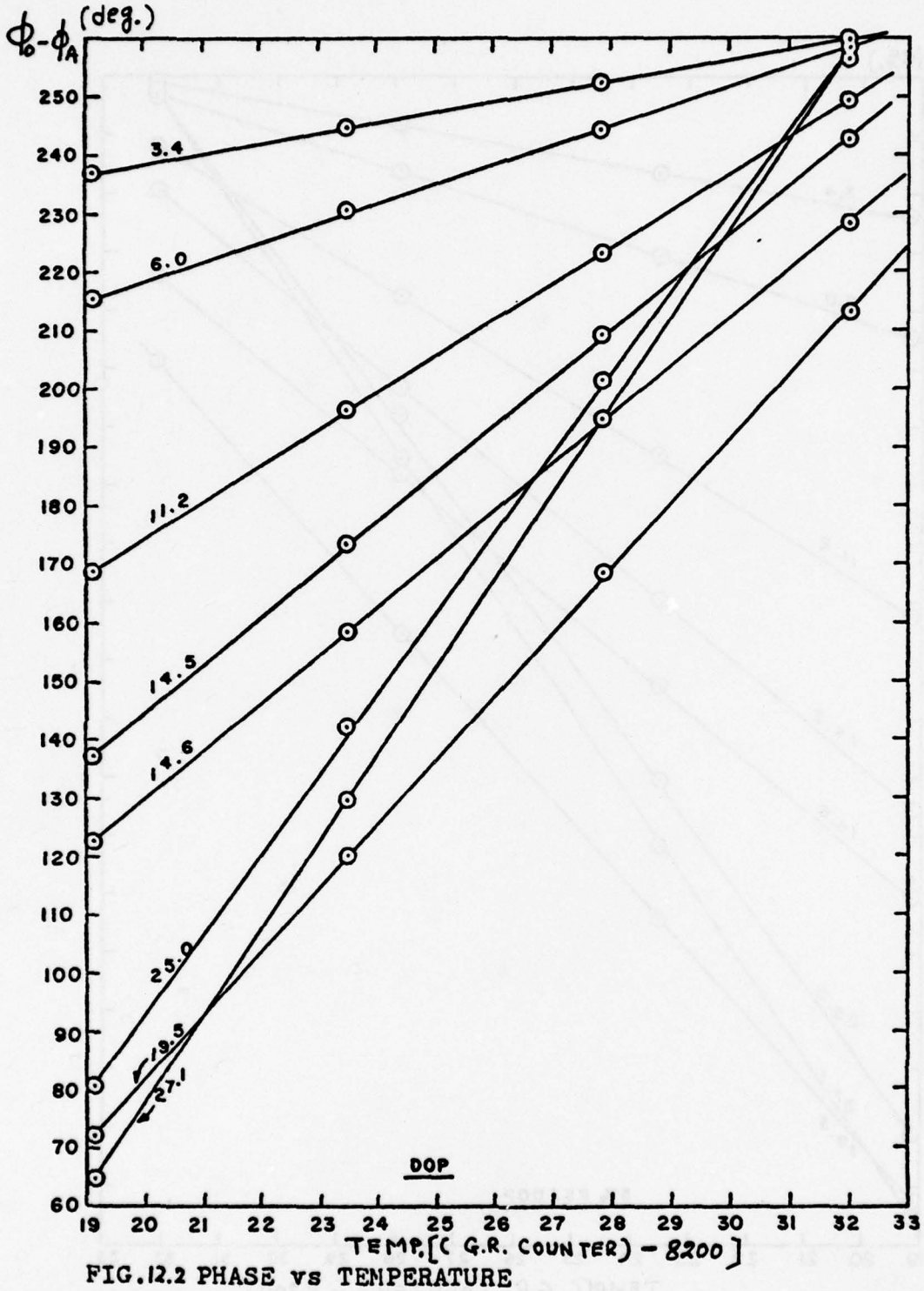

FIG. 12.2 PHASE vs TEMPERATURE

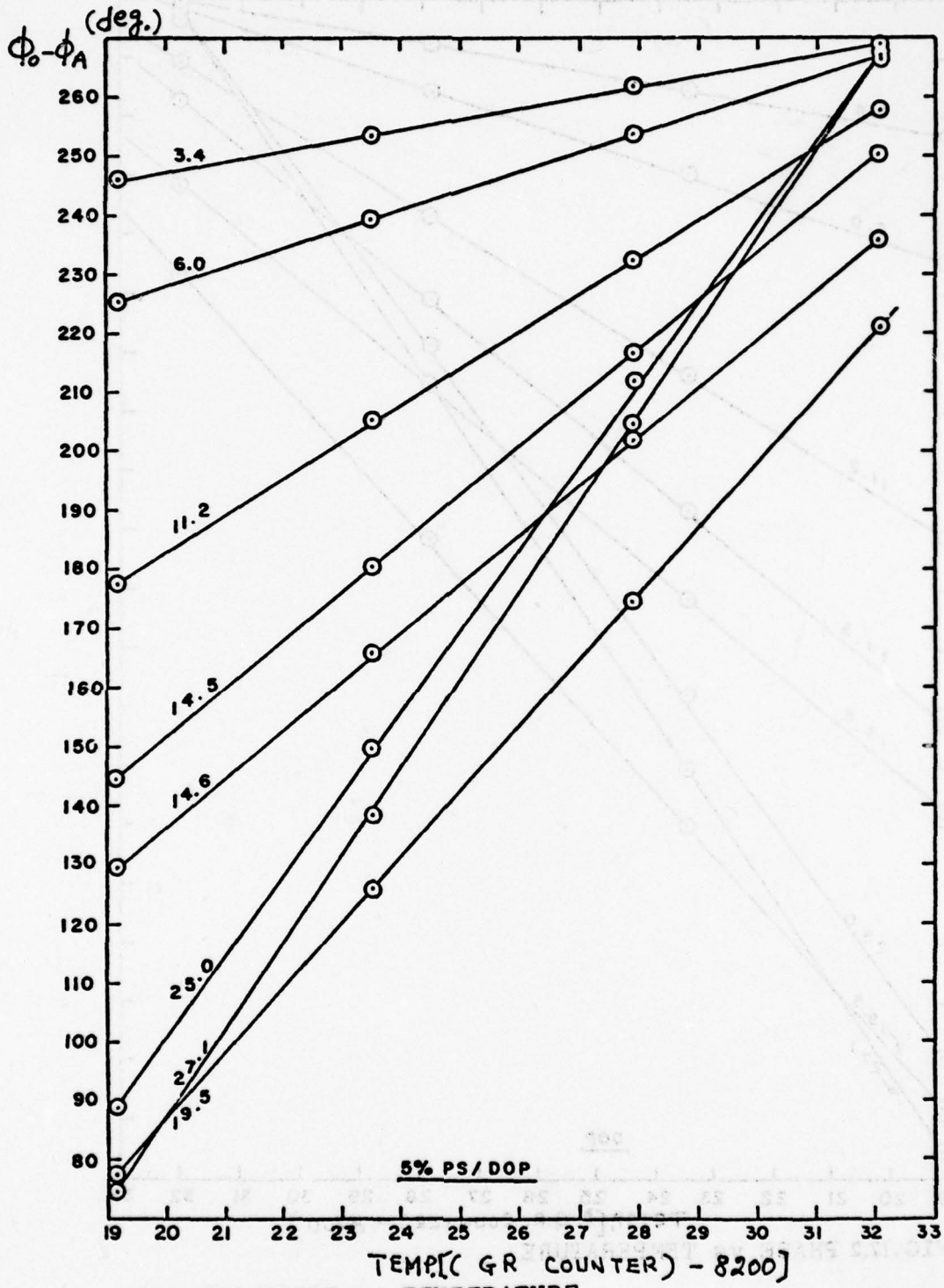

FIG. 12.3 PHASE vs TEMPERATURE

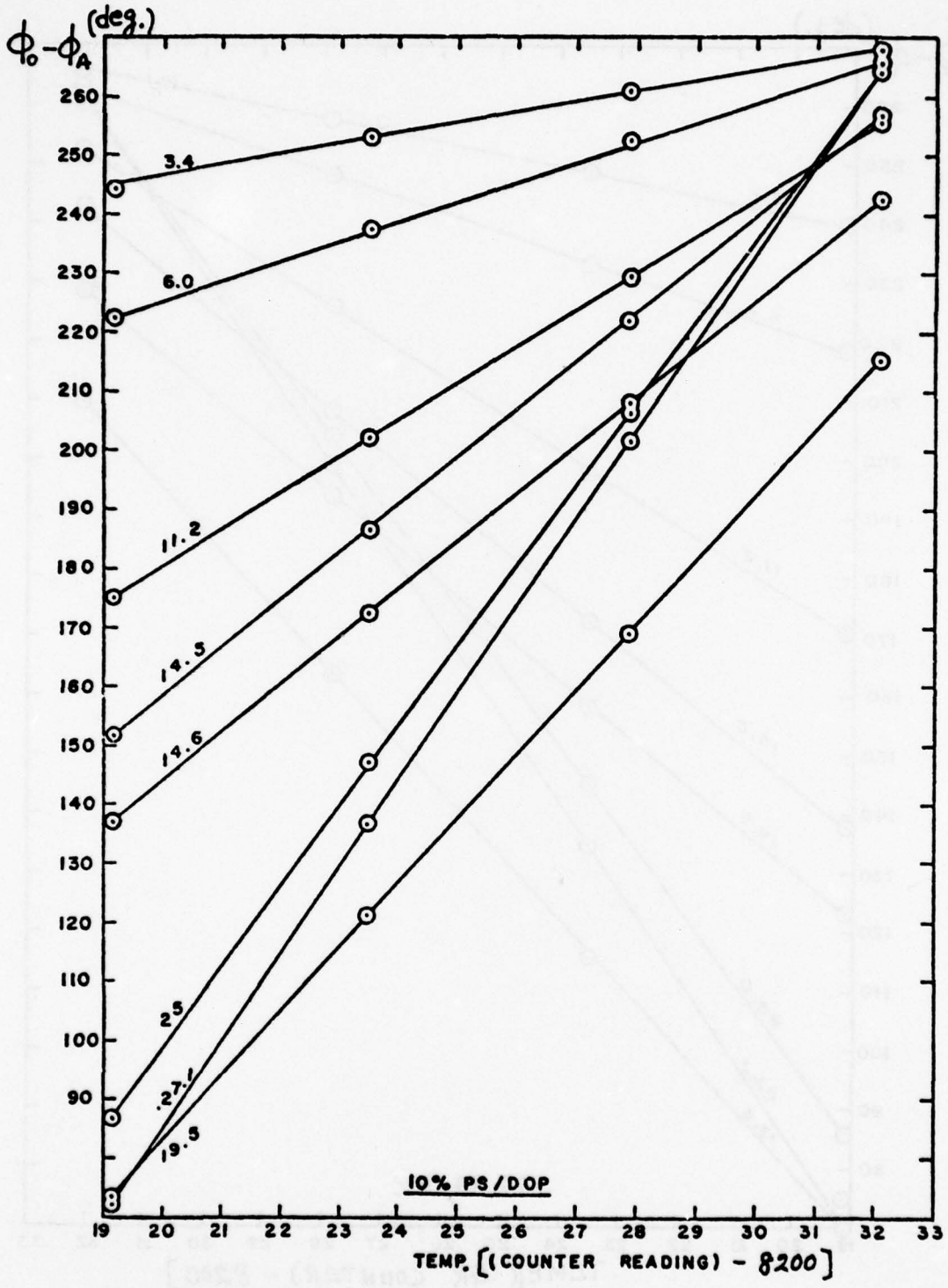

FIG. 12.4 PHASE vs TEMPERATURE

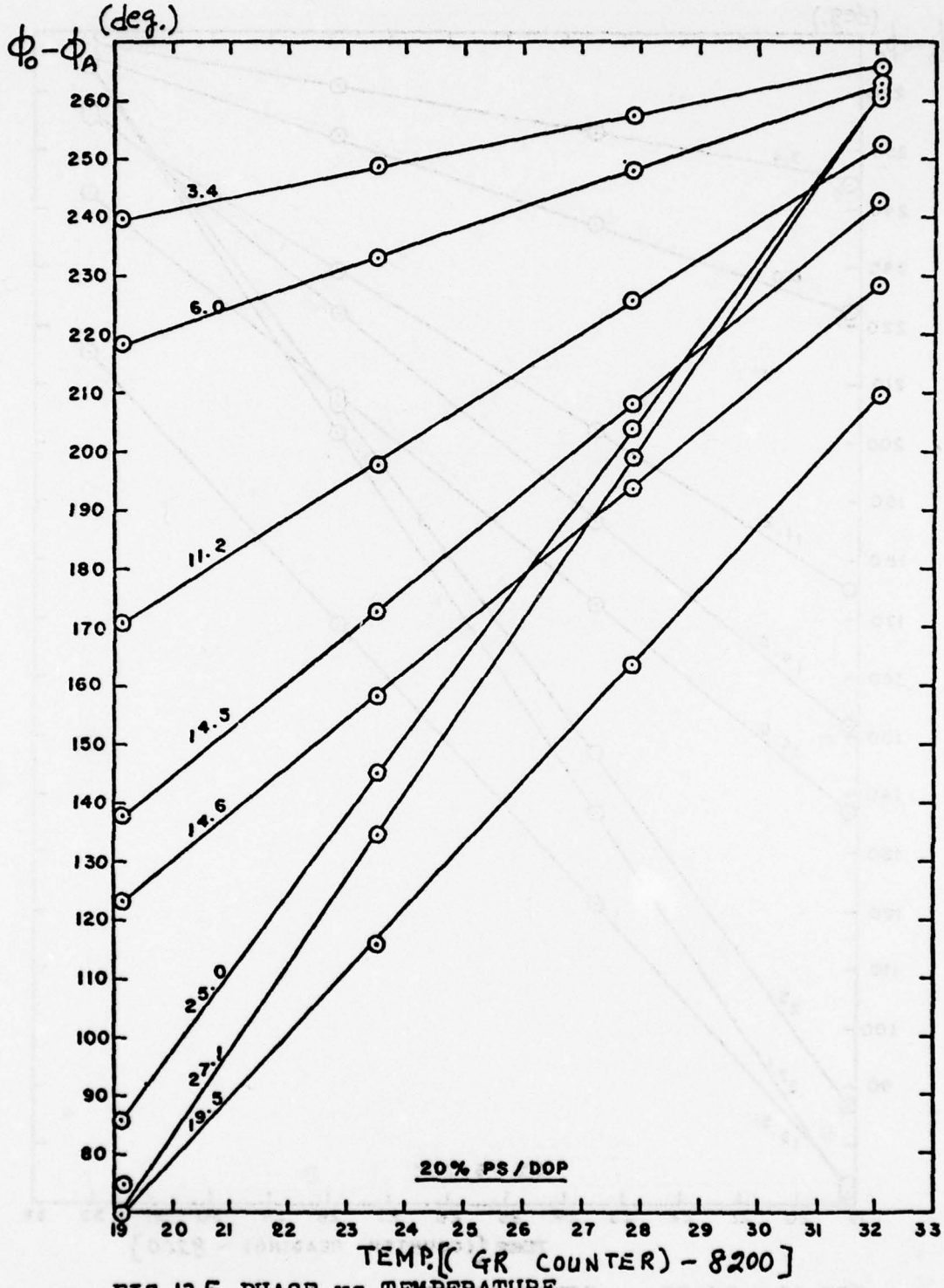

FIG.12.5 PHASE vs TEMPERATURE

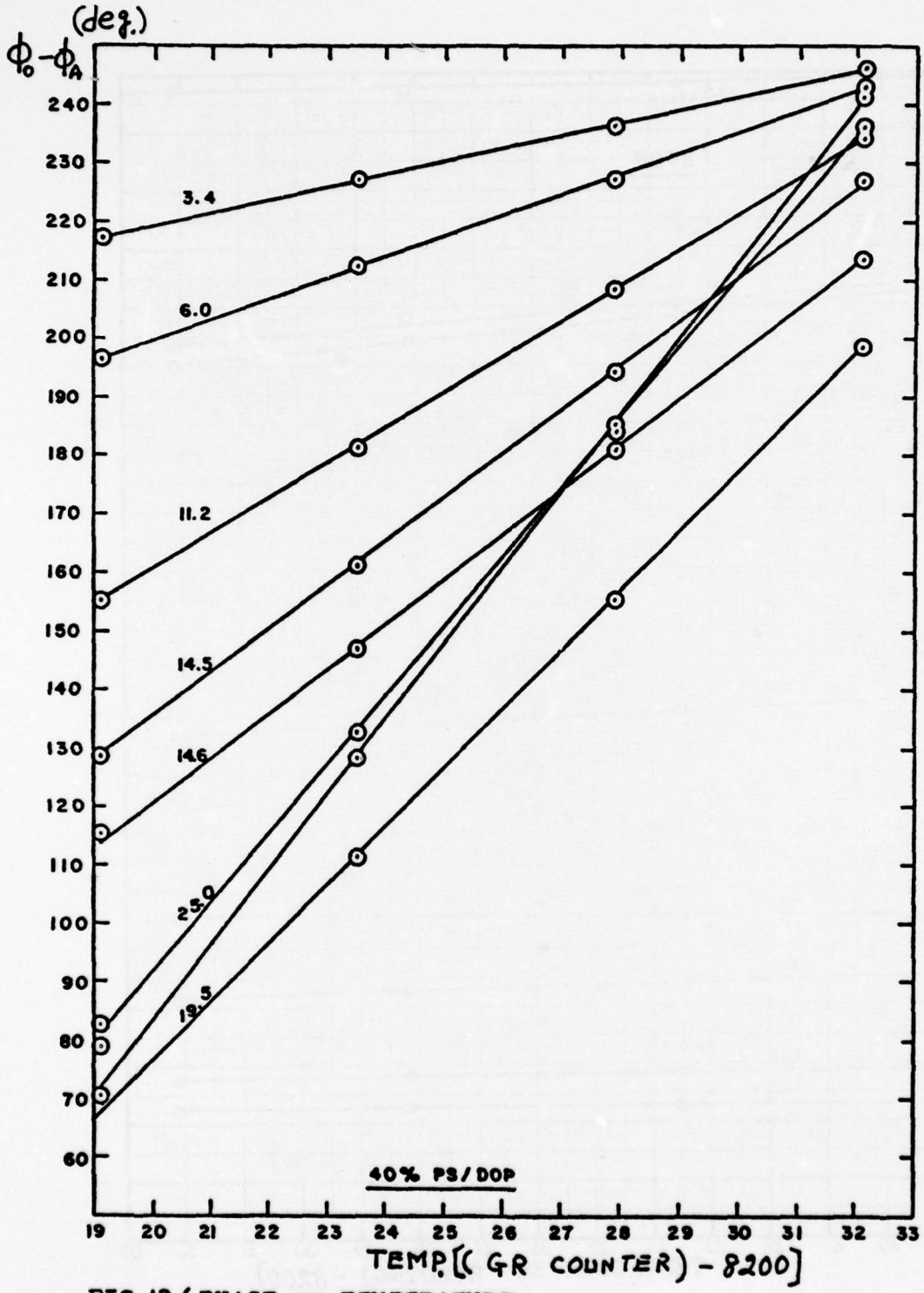

FIG.12.6 PHASE vs TEMPERATURE

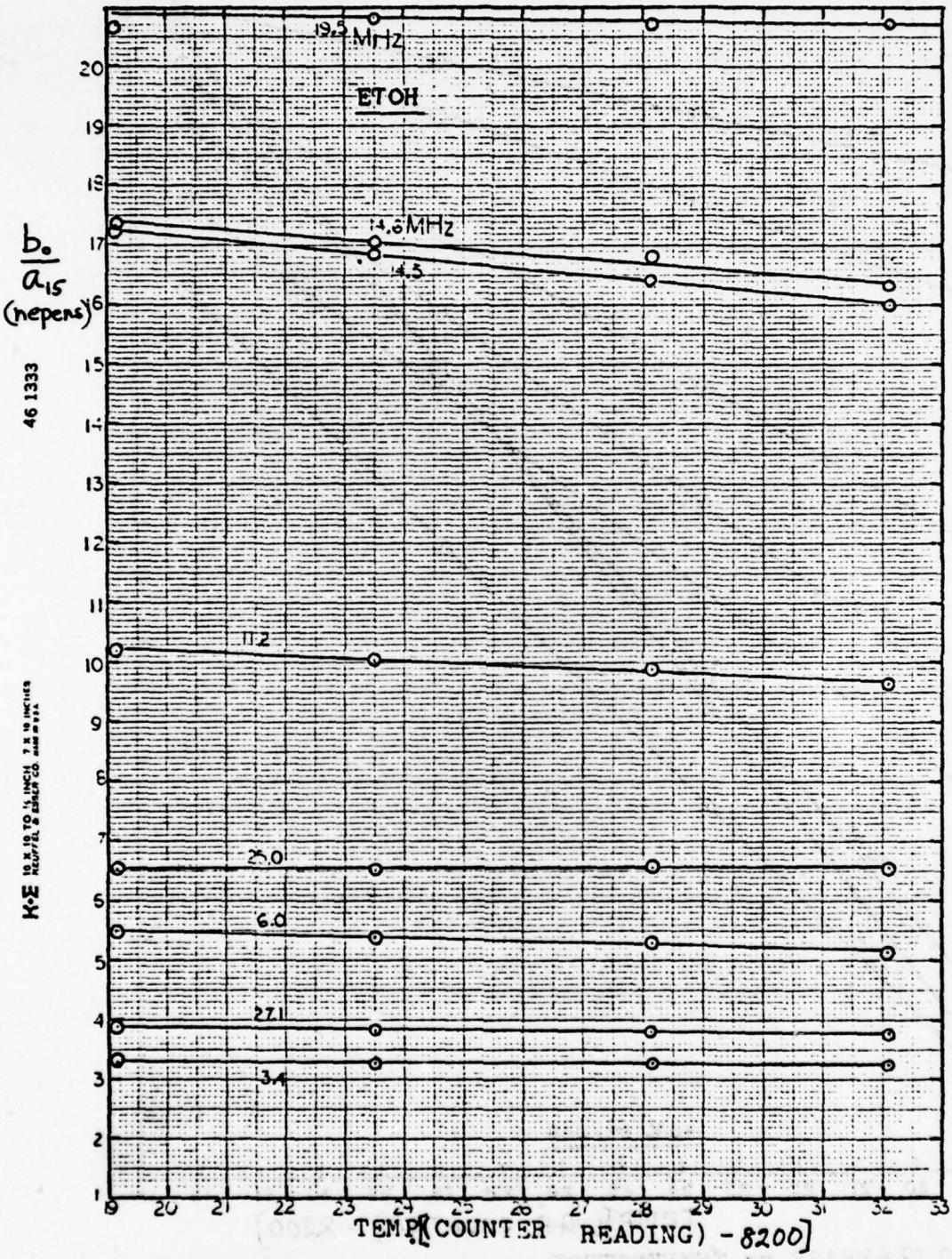

FIG.13.1 RELATIVE AMPLITUDE vs TEMPERATURE

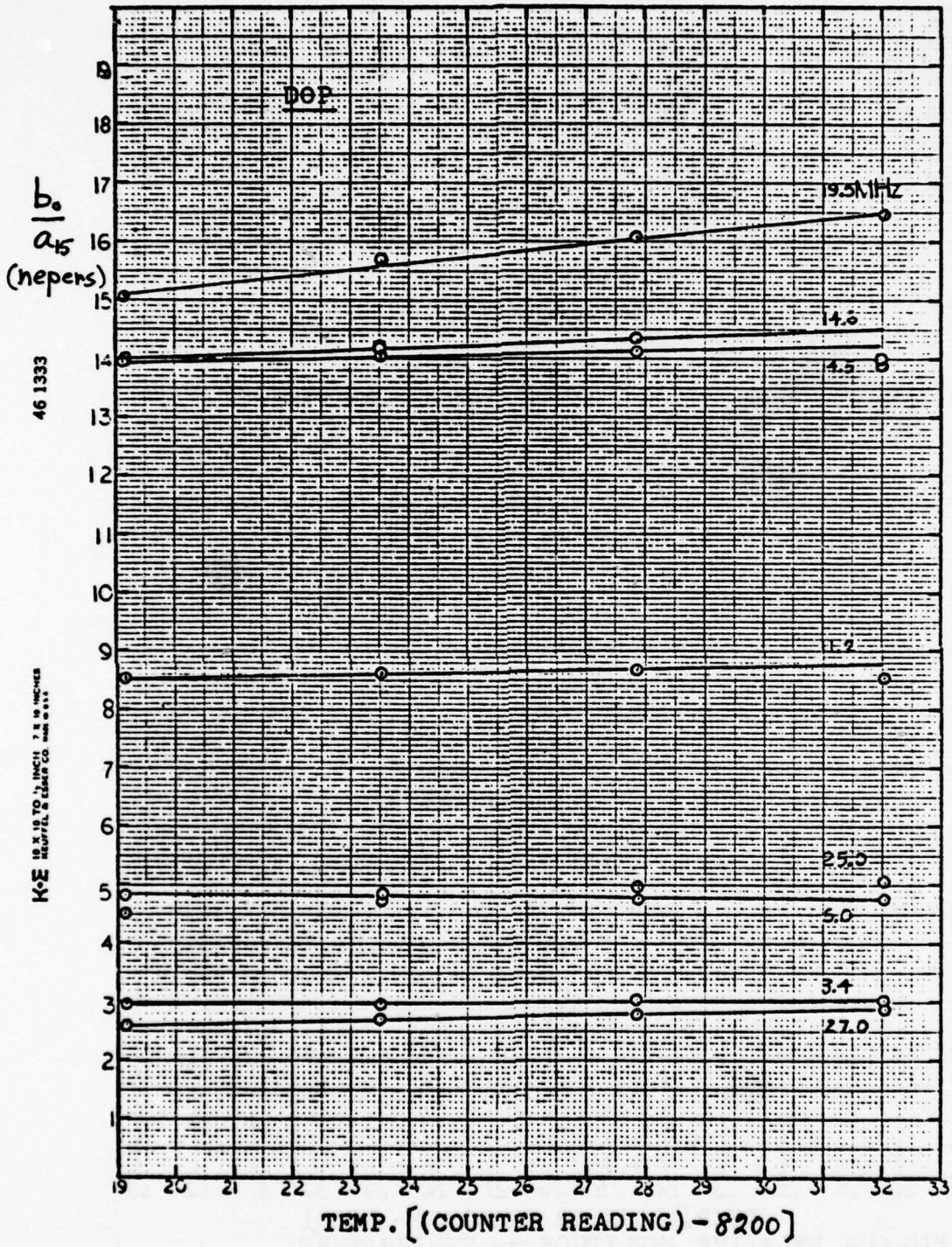

FIG.13.2 RELATIVE AMPLITUDE vs TEMPERATURE

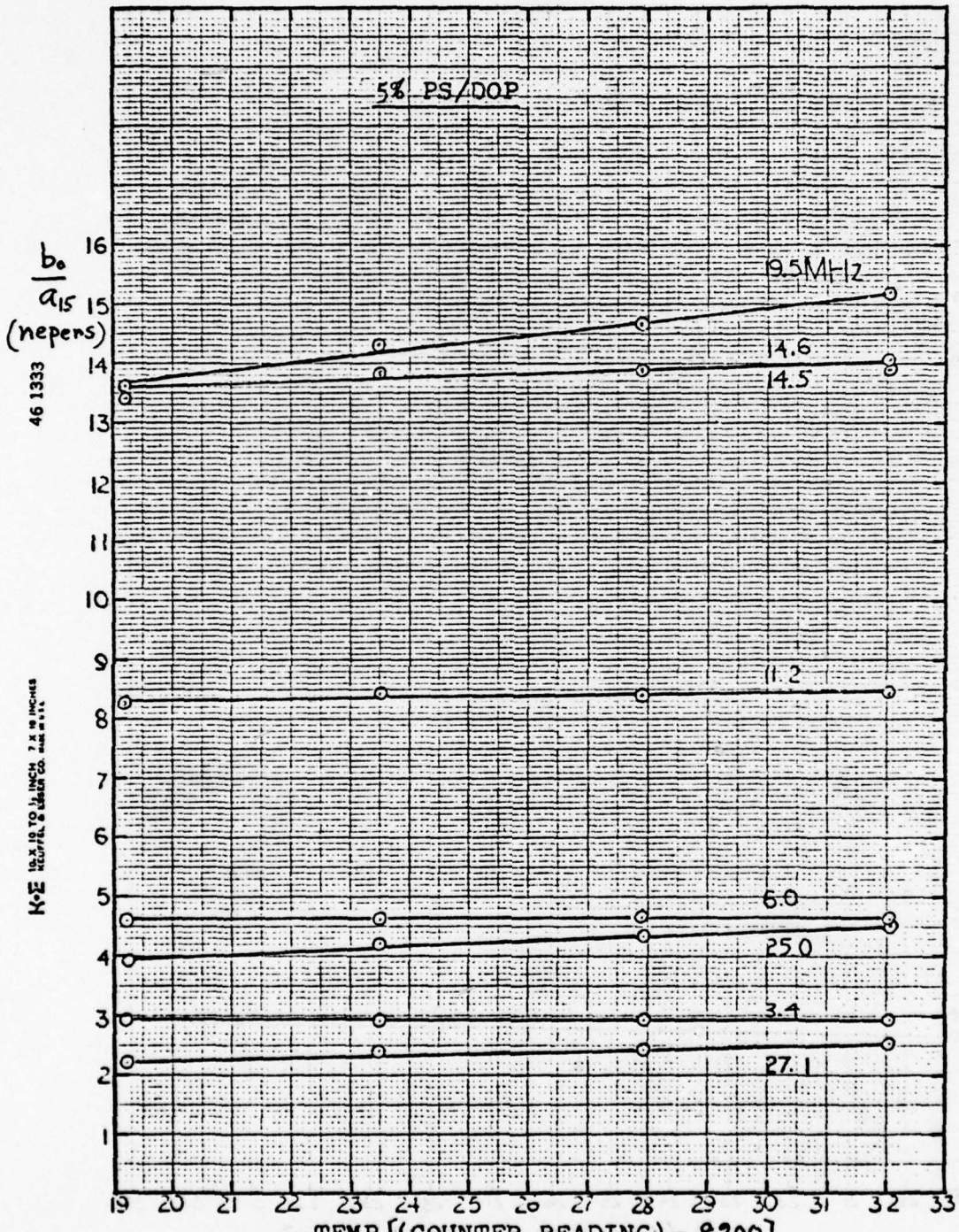

FIG.13.3 RELATIVE AMPLITUDE vs TEMPERATURE

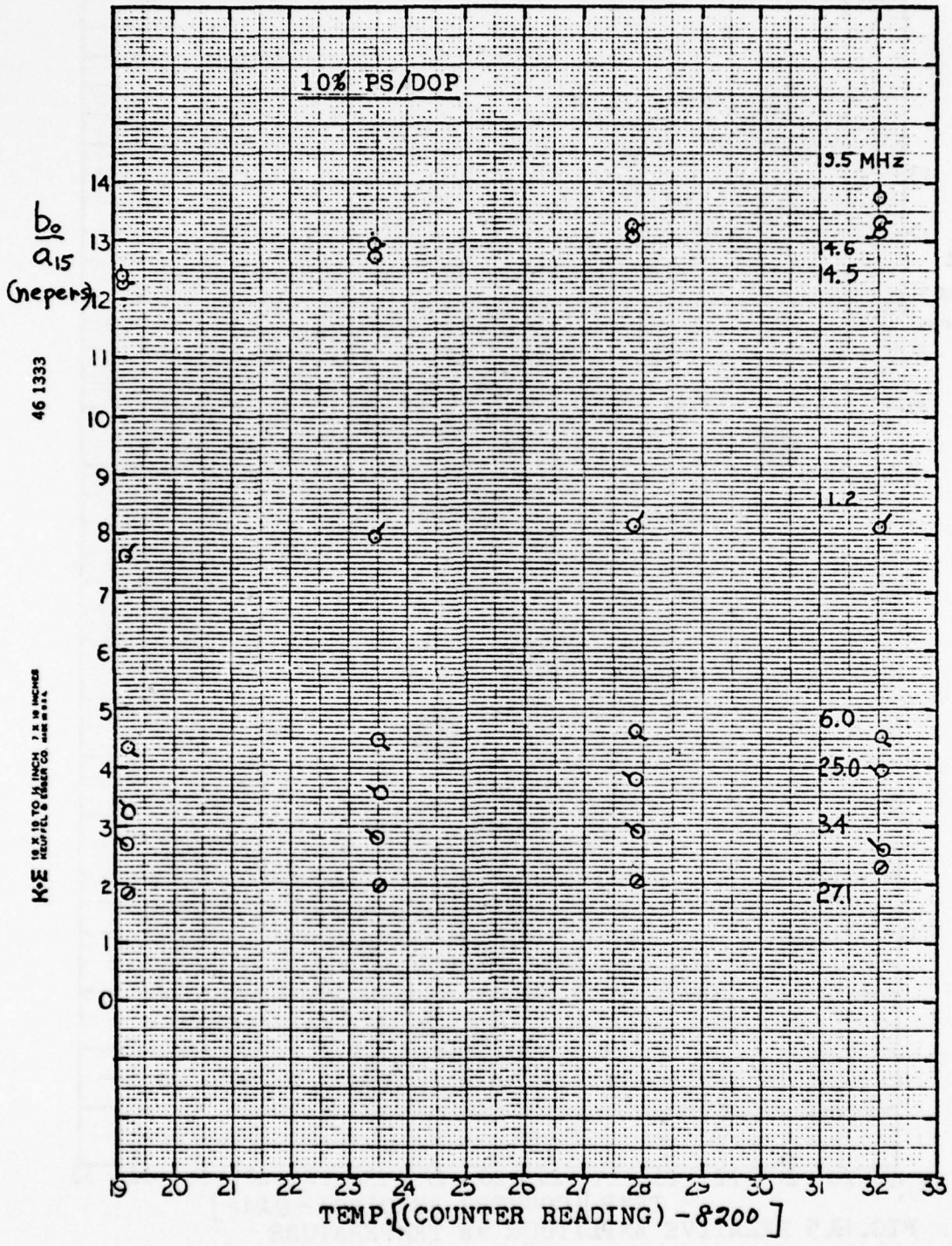

FIG.13.4 RELATIVE AMPLITUDE vs TEMPERATURE

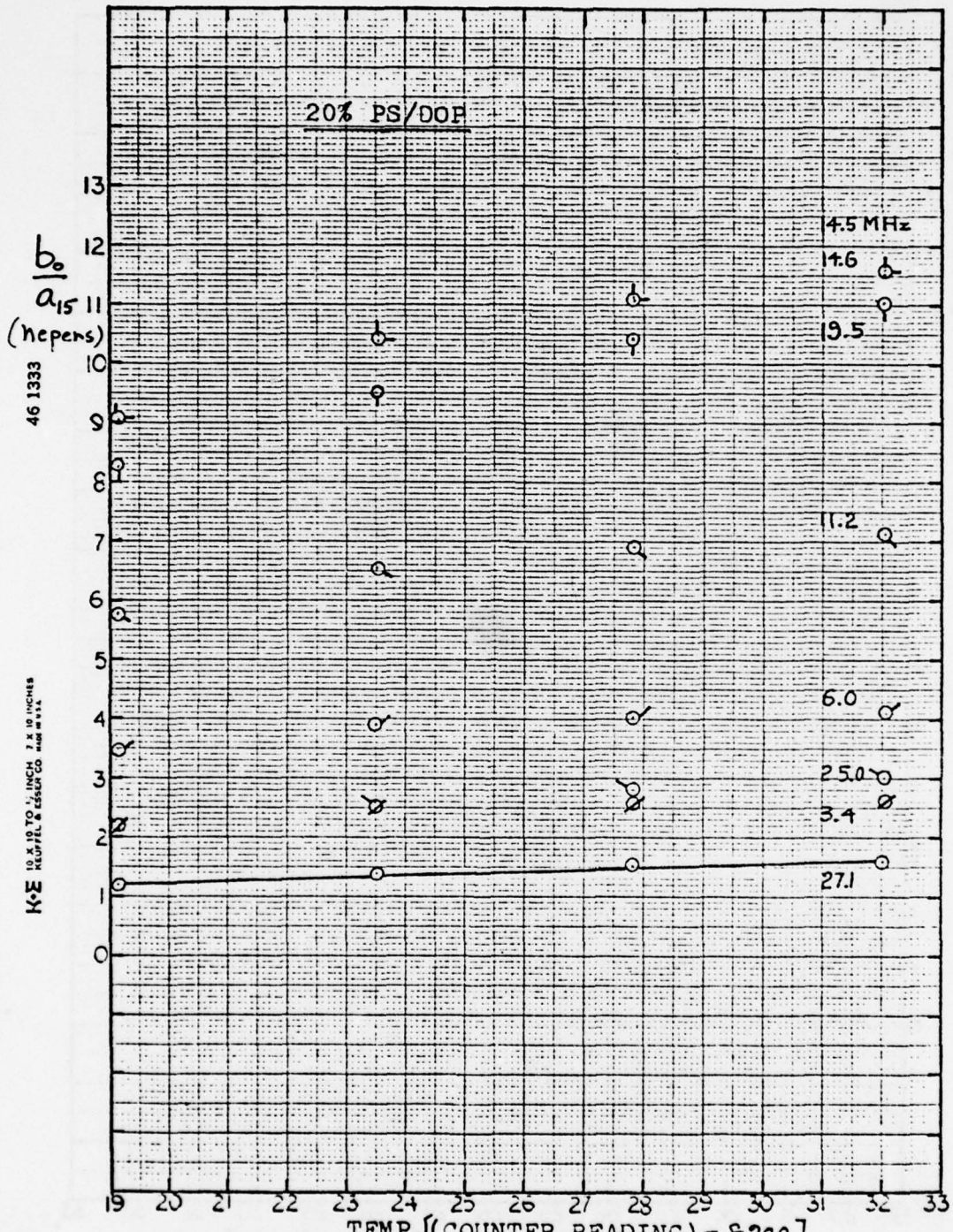

FIG. 13.5 RELATIVE AMPLITUDE vs TEMPERATURE

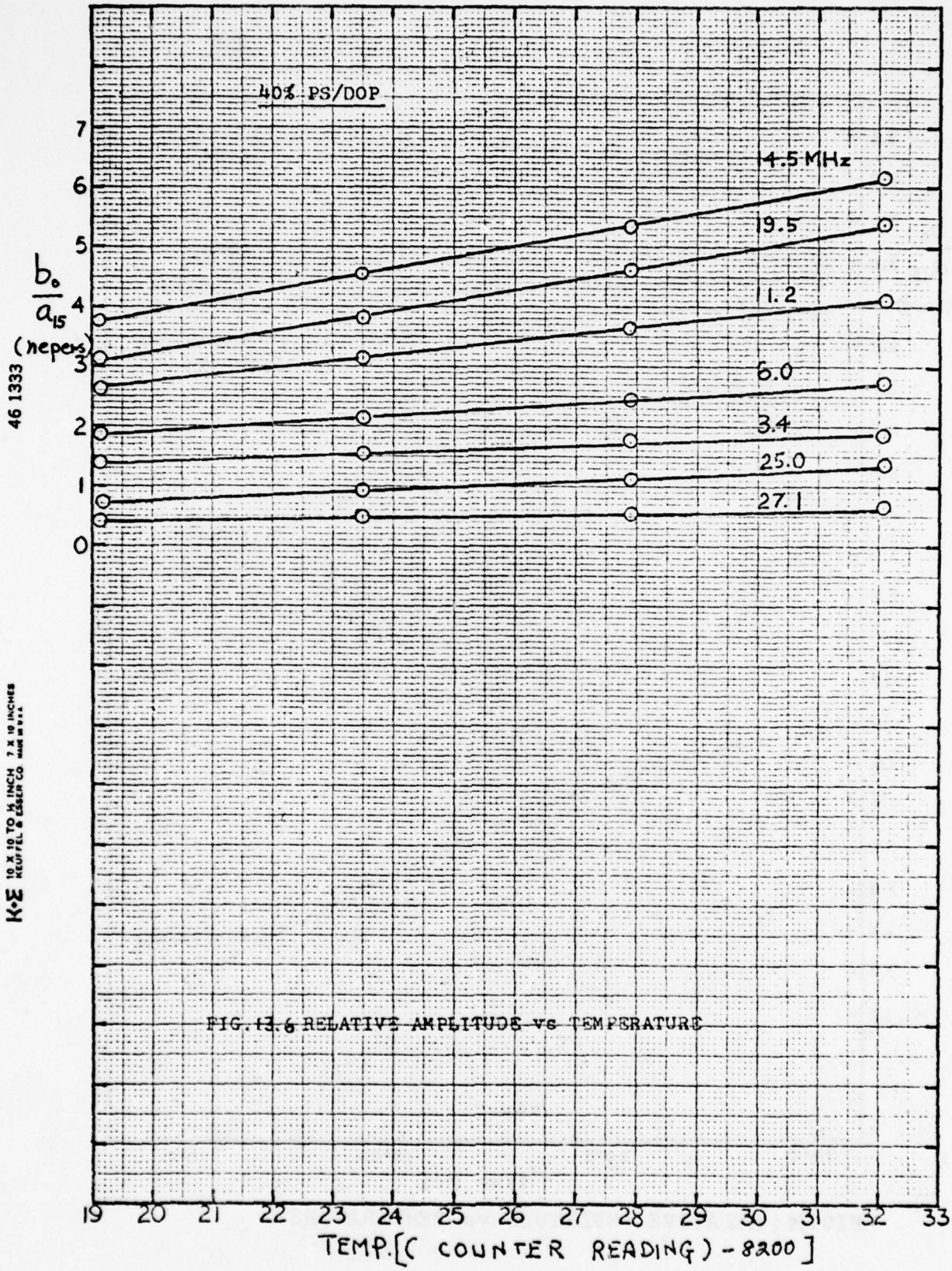

FIG. 13.6 RELATIVE AMPLITUDE vs TEMPERATURE

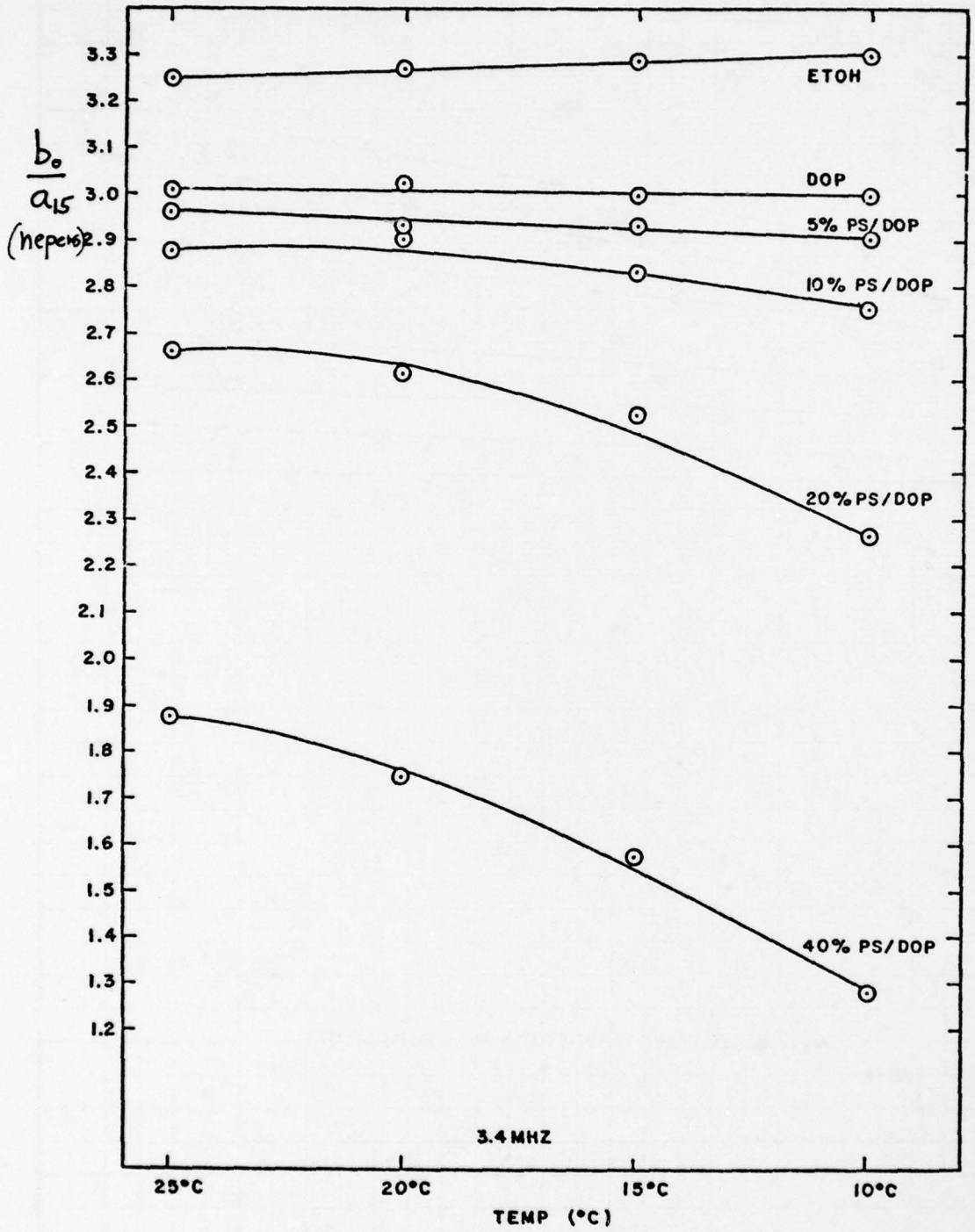

FIG. 14.1 RELATIVE AMPLITUDE vs TEMPERATURE

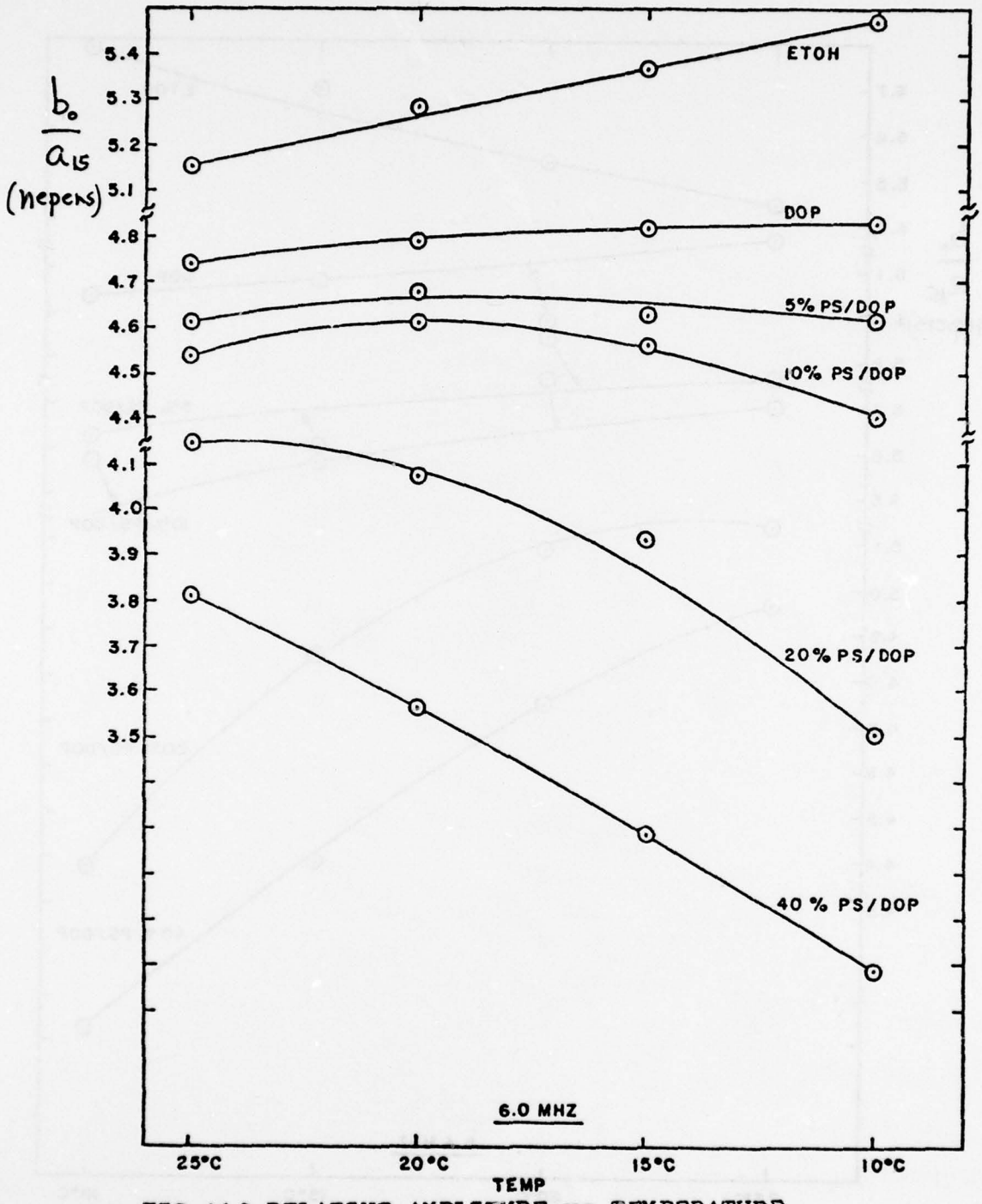

FIG. 14.2 RELATIVE AMPLITUDE vs TEMPERATURE

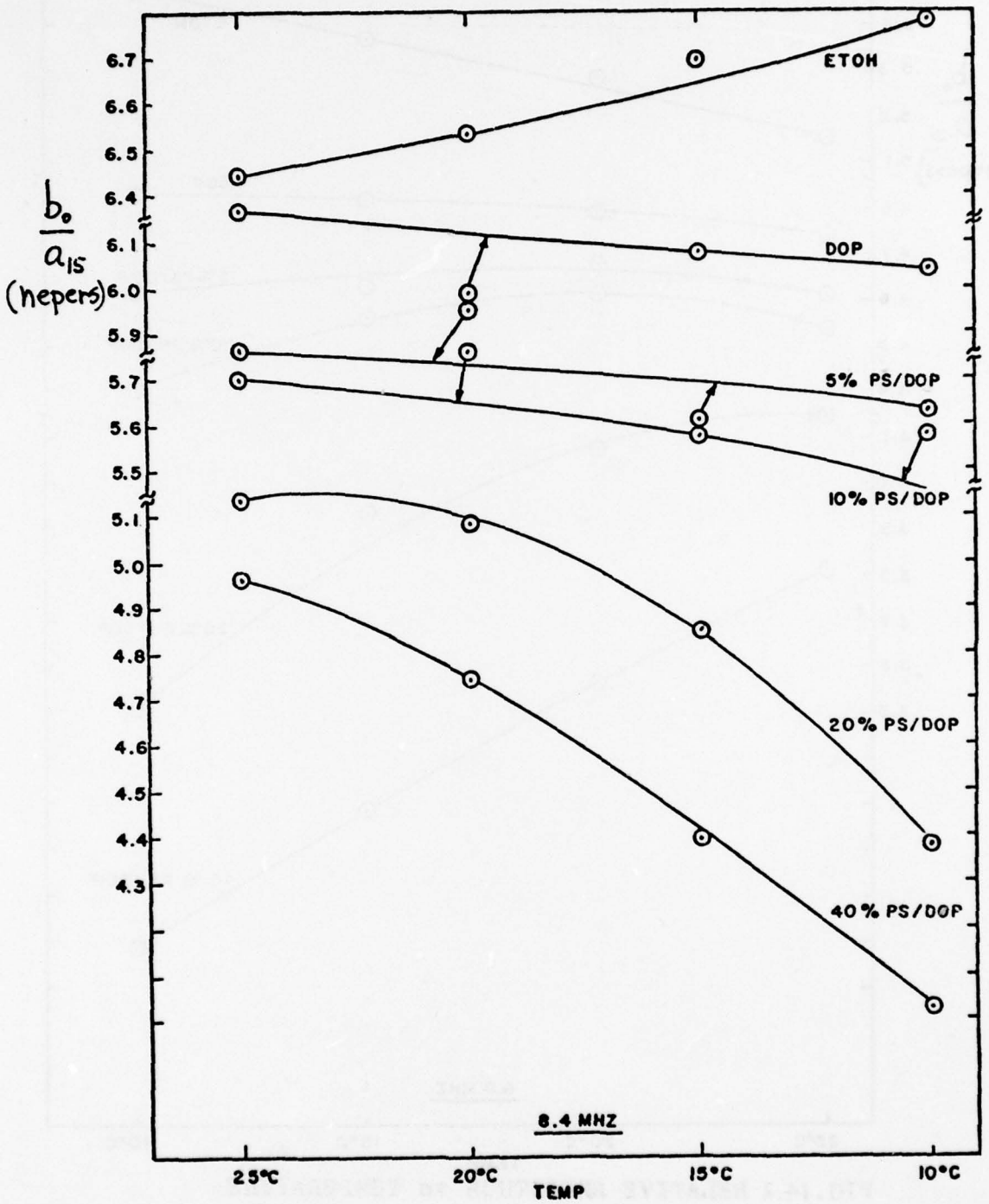

FIG. 14.3 RELATIVE AMPLITUDE vs TEMPERATURE

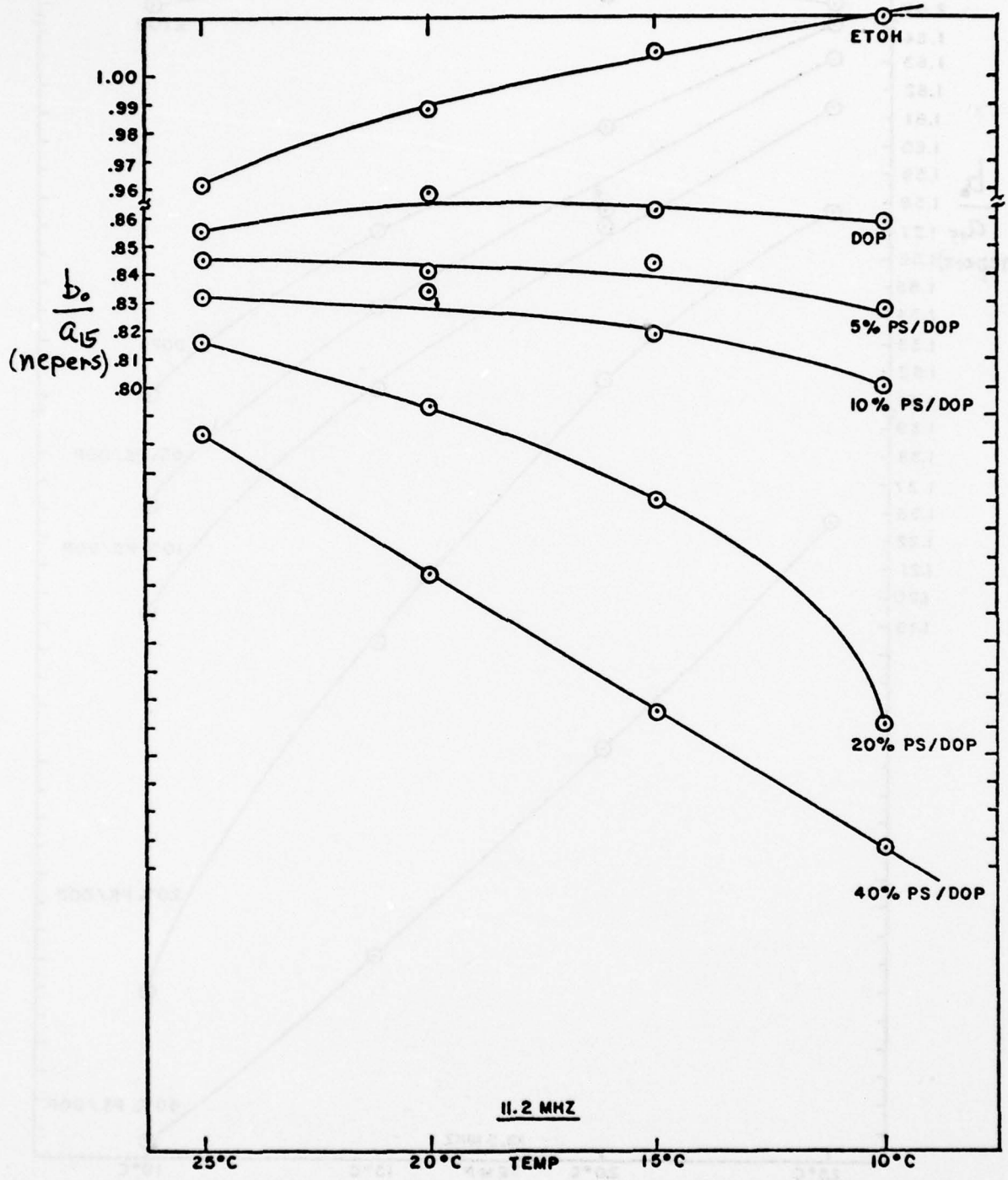

FIG. 14.4 RELATIVE AMPLITUDE vs TEMPERATURE

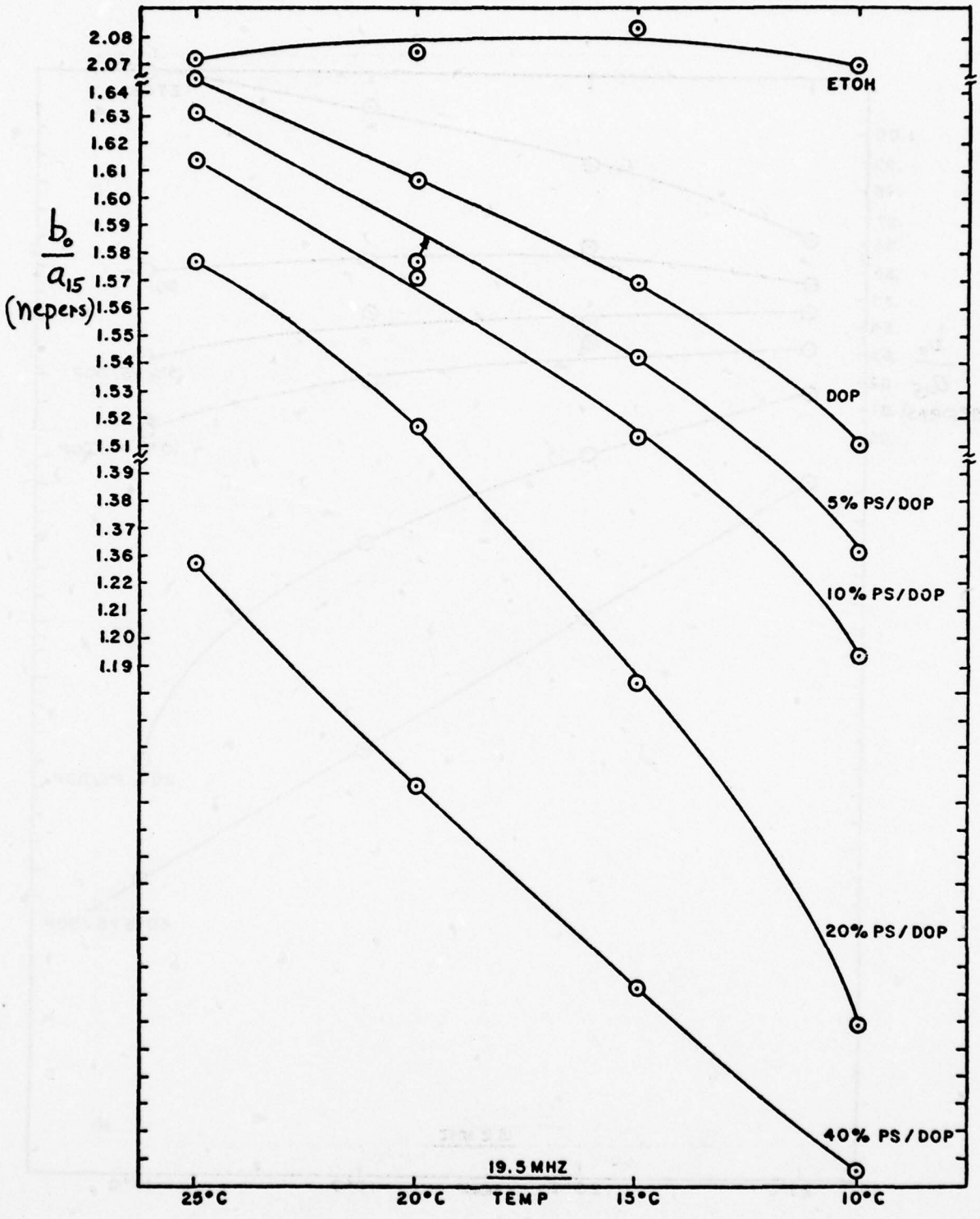

FIG. 14.5 RELATIVE AMPLITUDE vs TEMPERATURE

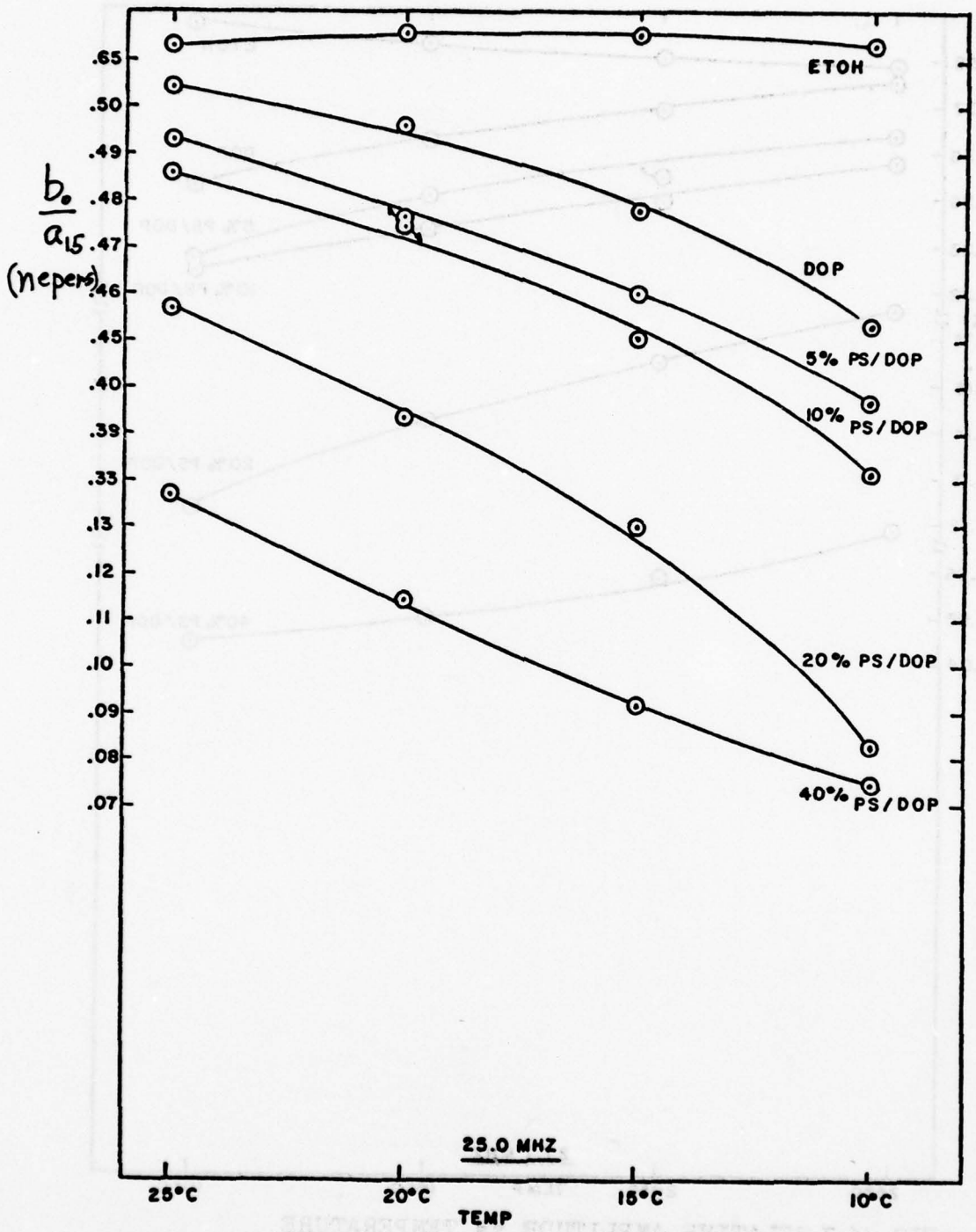

FIG.14.6 RELATIVE AMPLITUDE vs TEMPERATURE

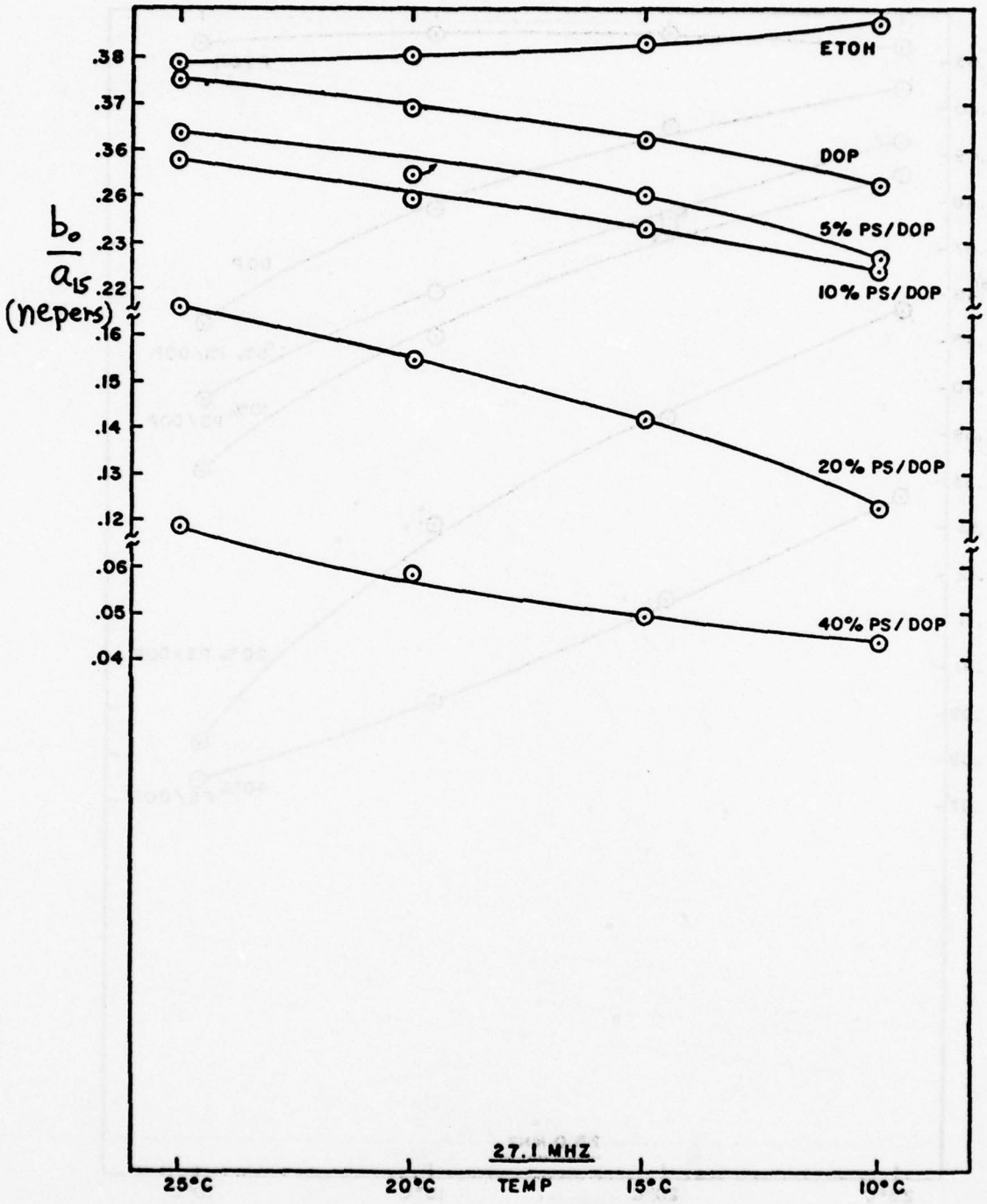

FIG. 4.7 RELATIVE AMPLITUDE vs TEMPERATURE

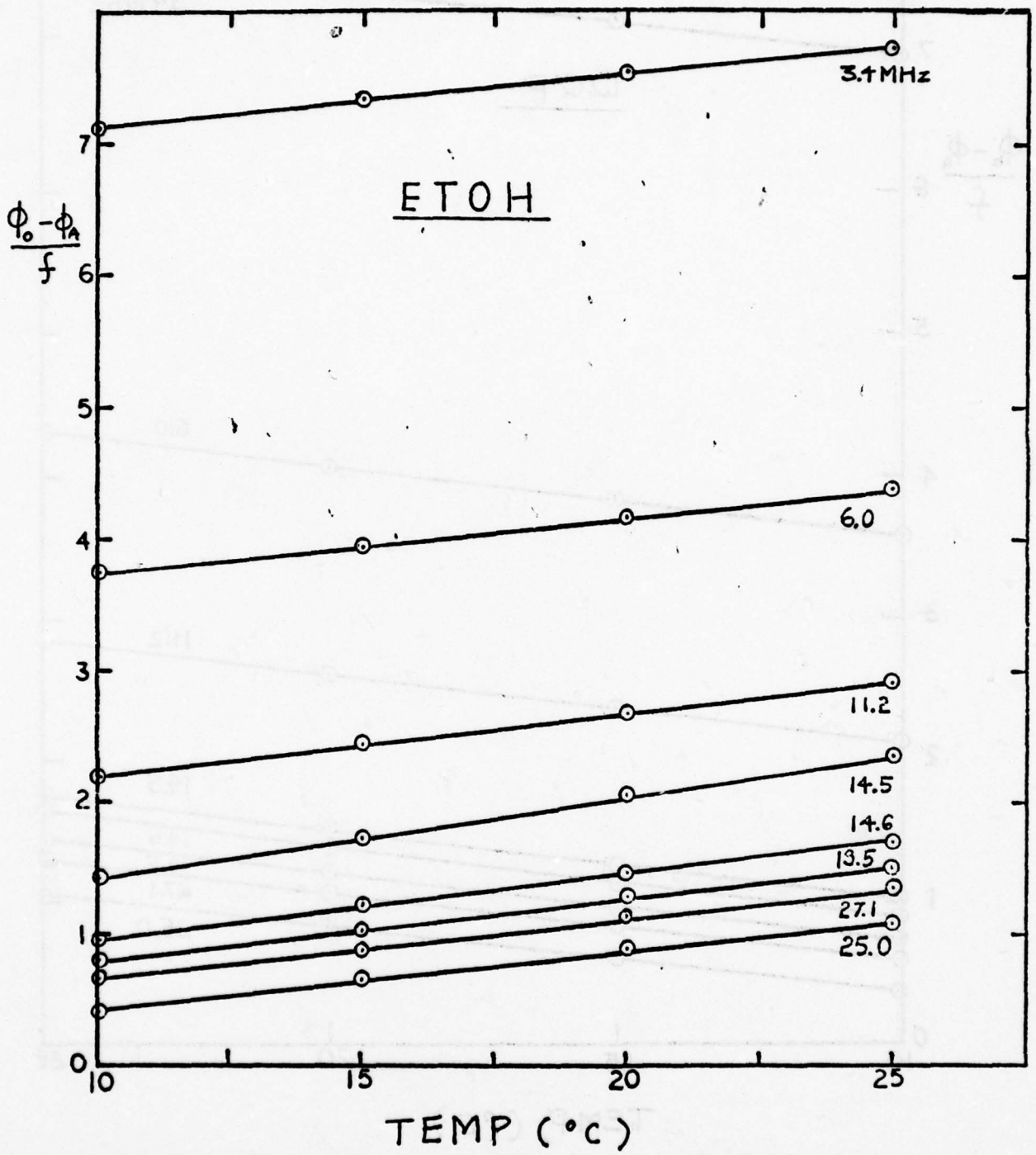

FIG.15.1 NORMALIZED PHASE WITH FREQUENCY vs TEMP.

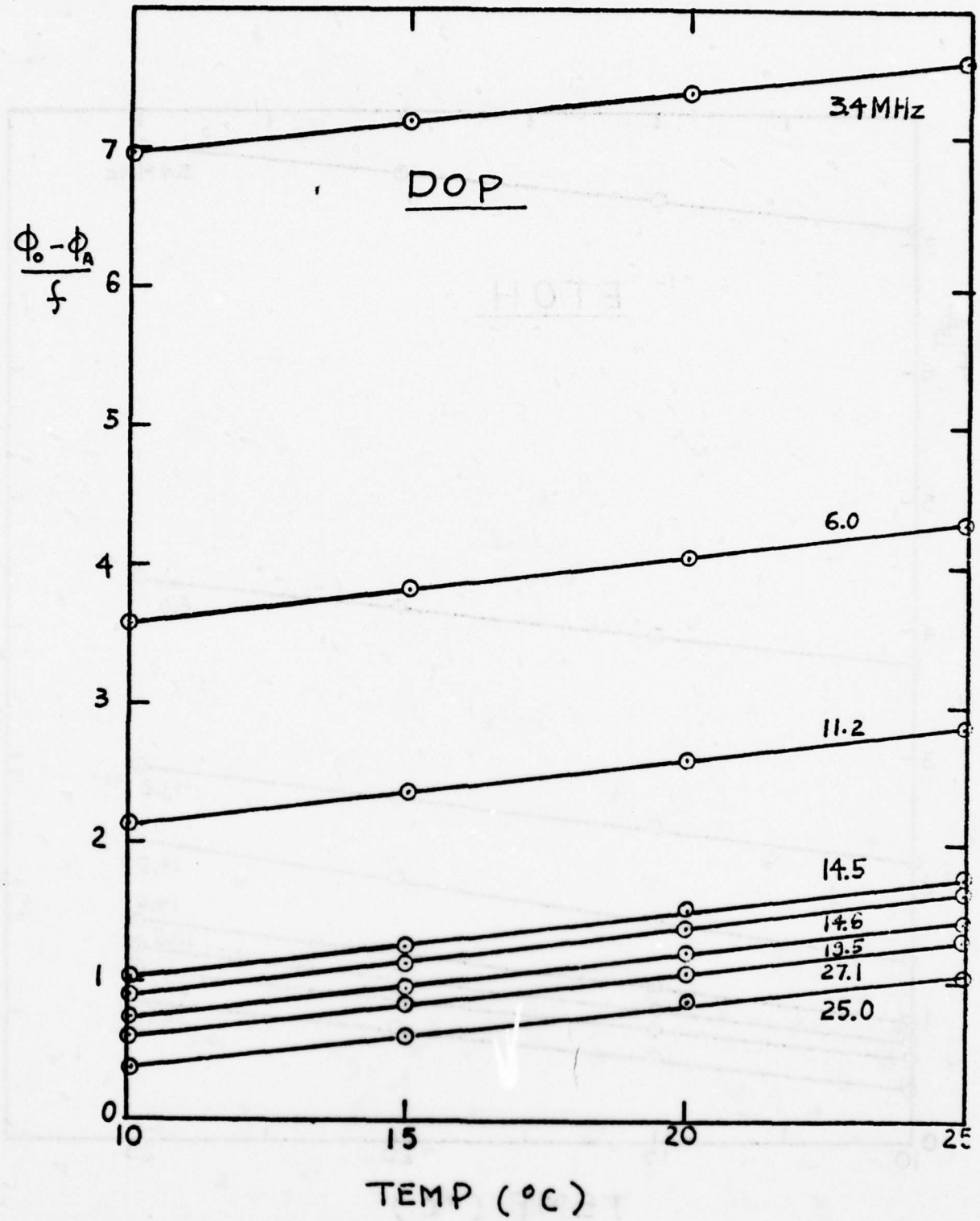

FIG.15.2 NORMALIZED PHASE WITH FREQUENCY vs TEMP.

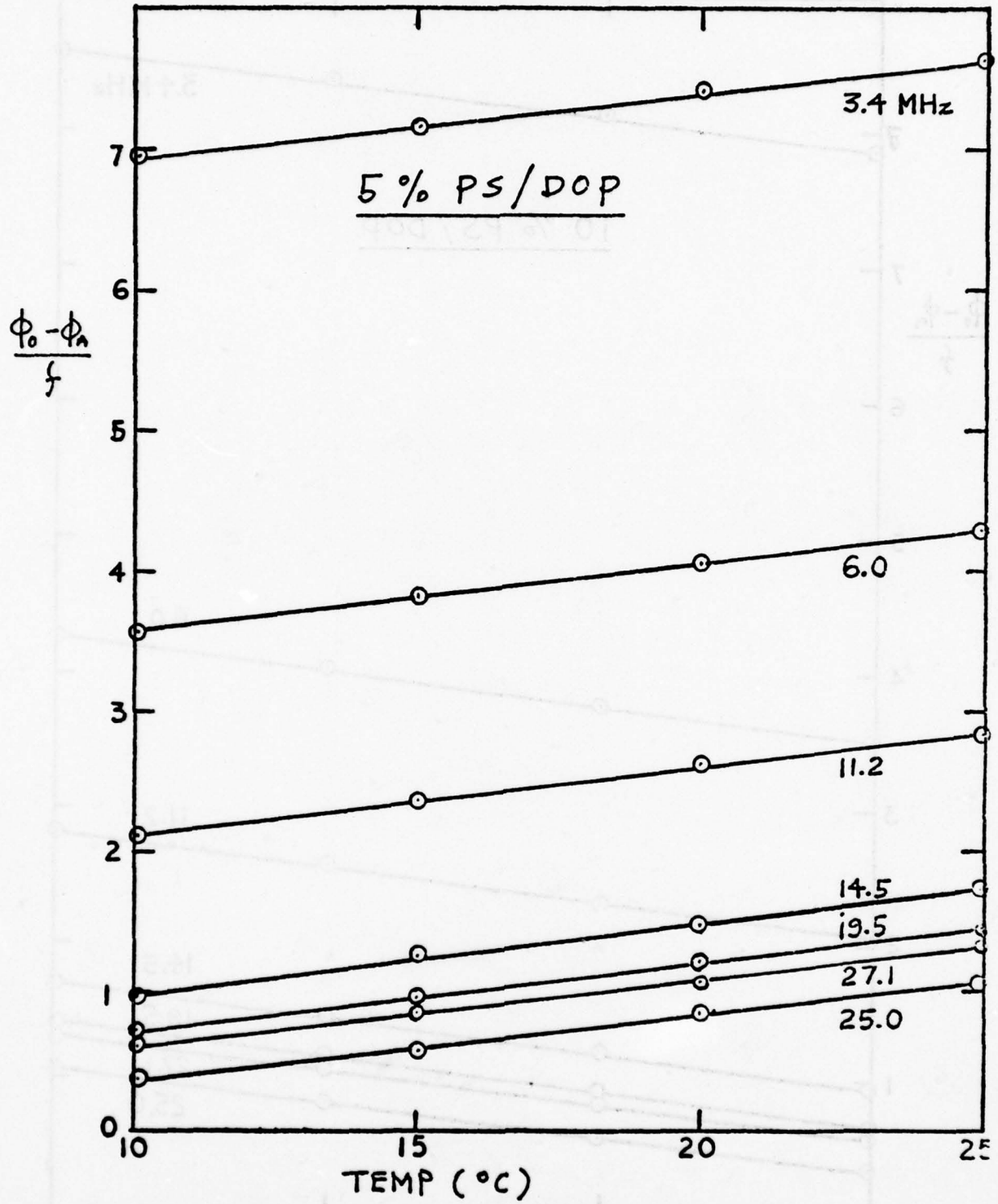

FIG. 15.5 NORMALIZED PHASE WITH FREQUENCY vs TEMP.

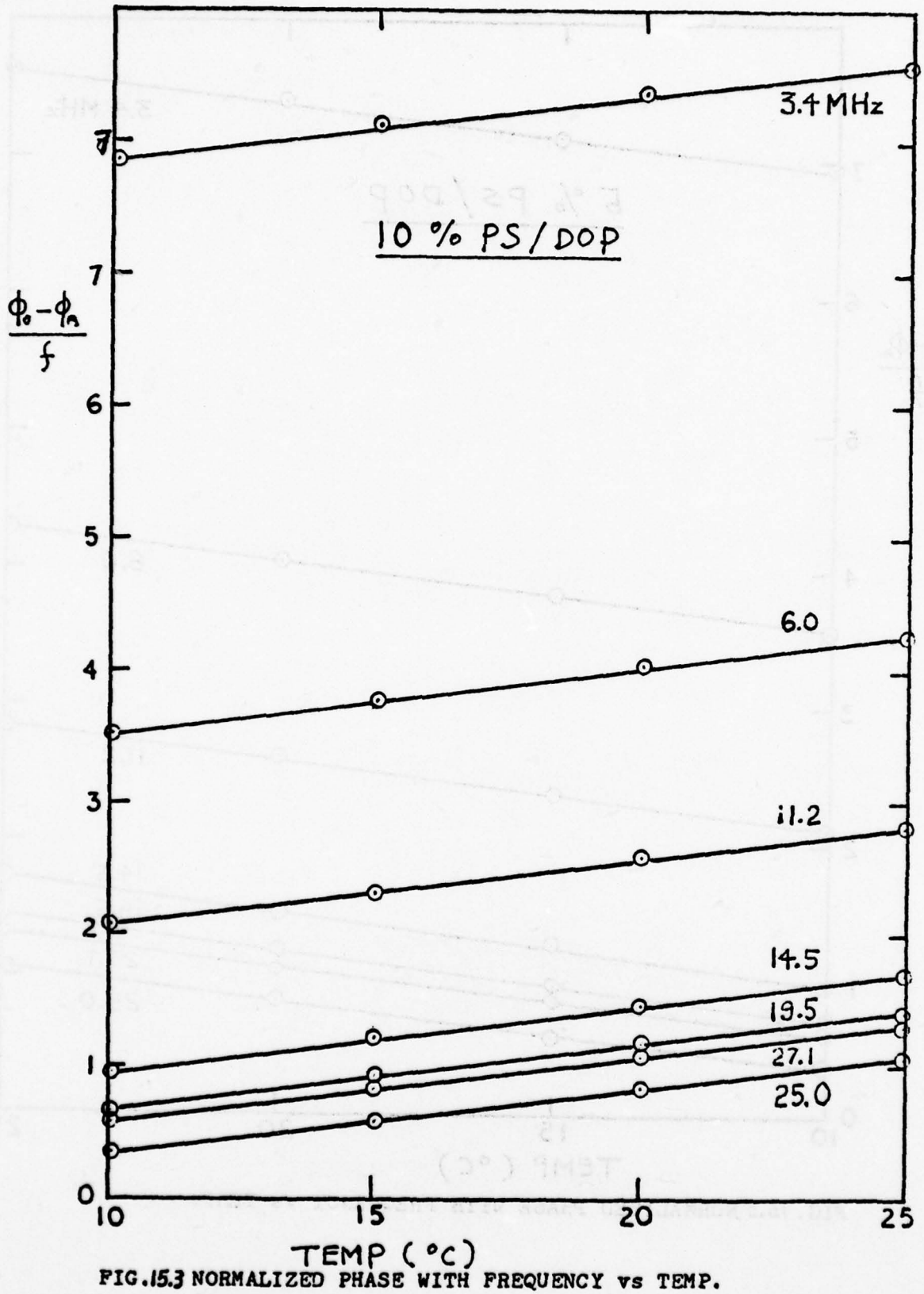

FIG.15.3 NORMALIZED PHASE WITH FREQUENCY vs TEMP.

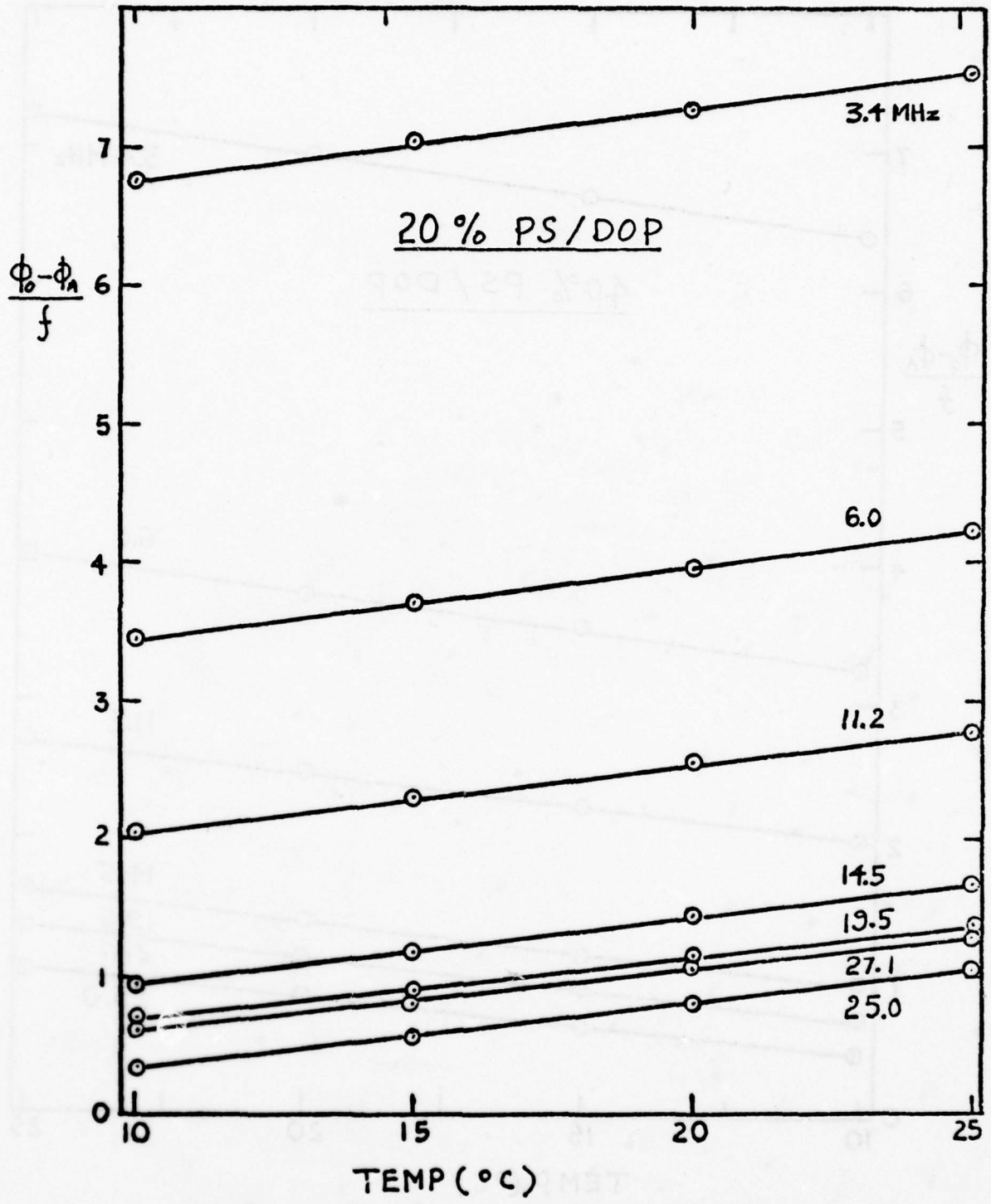

FIG. 15.4 NORMALIZED PHASE WITH FREQUENCY vs TEMP.

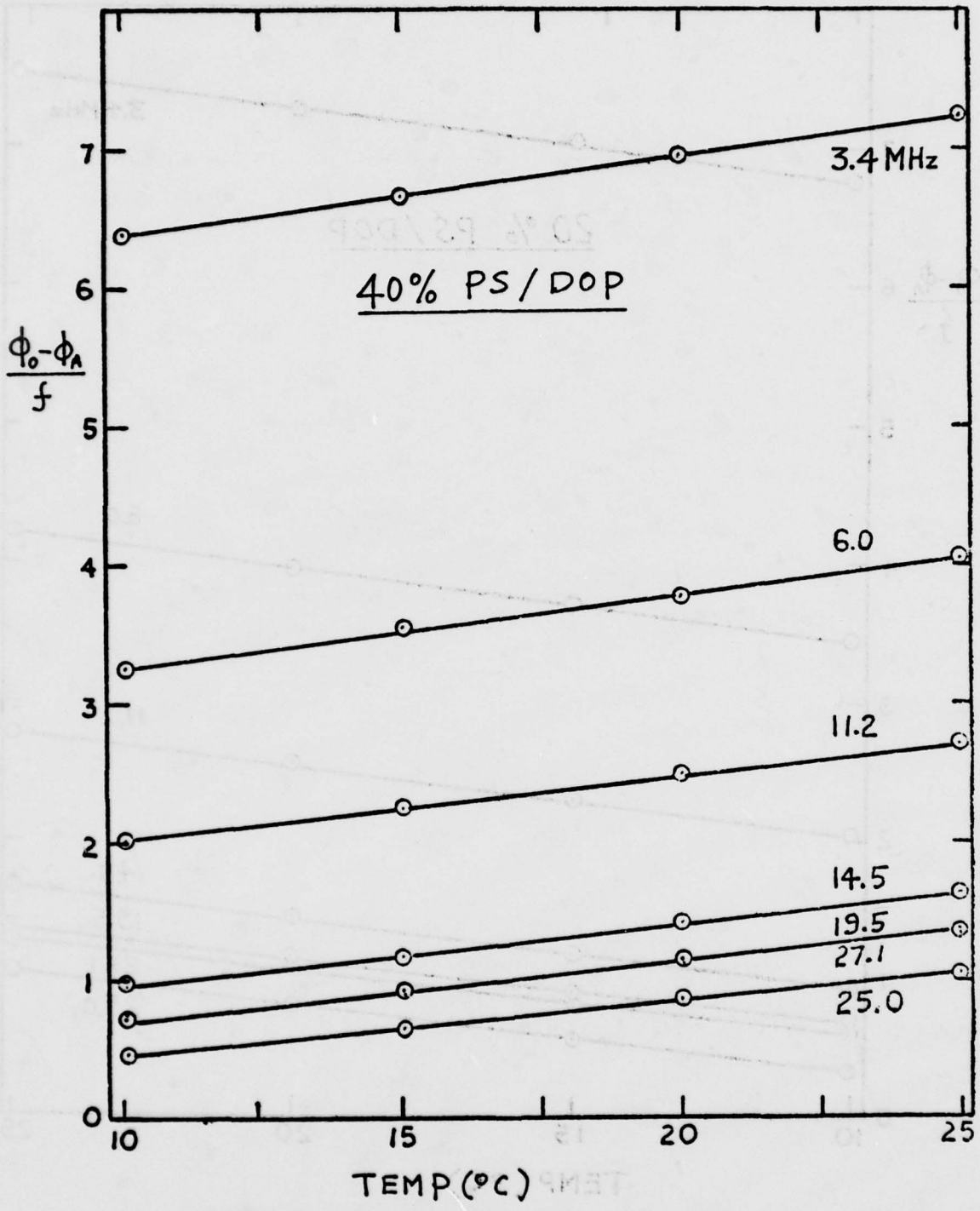

FIG. 15.6 NORMALIZED PHASE WITH FREQUENCY vs TEMP.

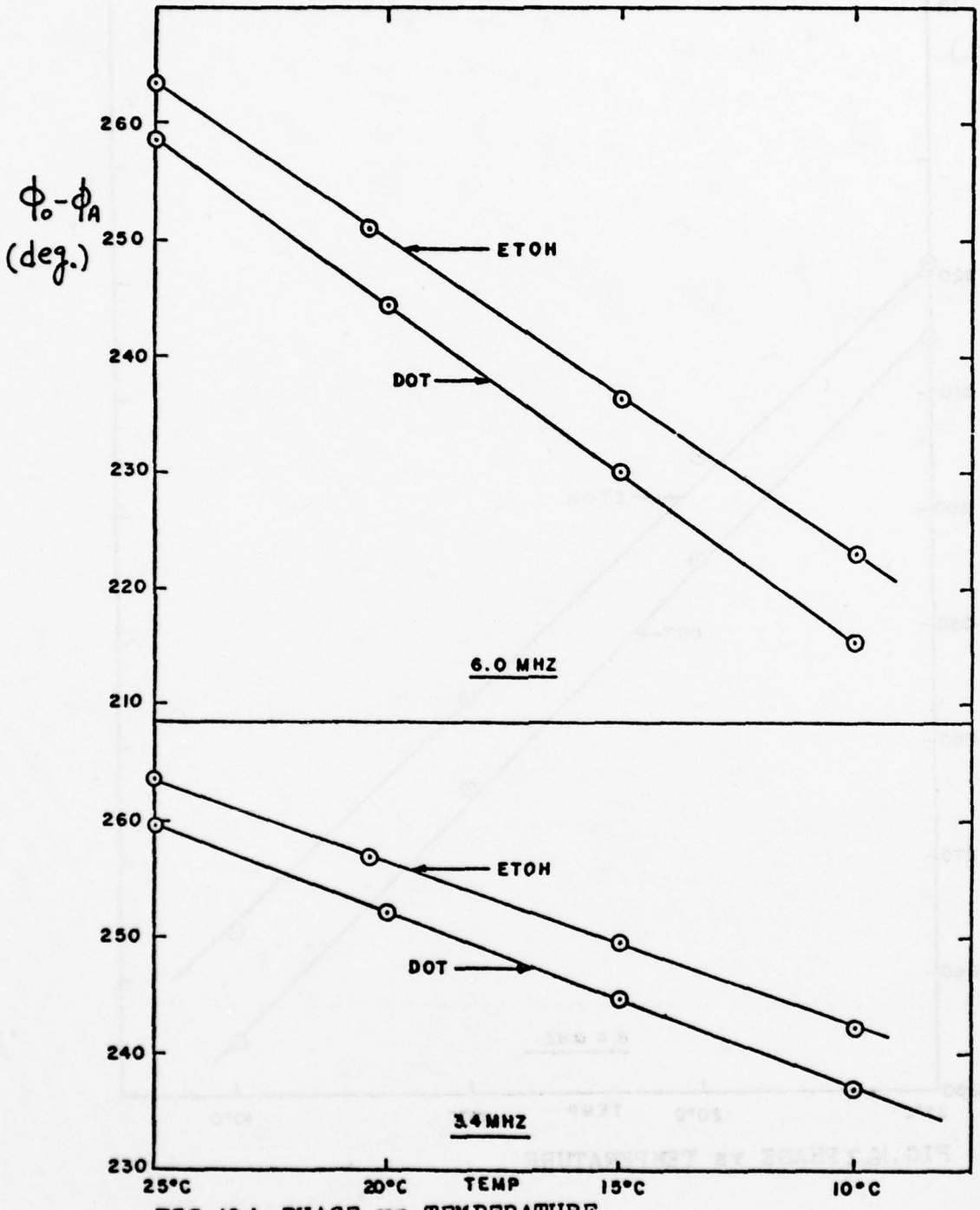

FIG.16.1 PHASE vs TEMPERATURE

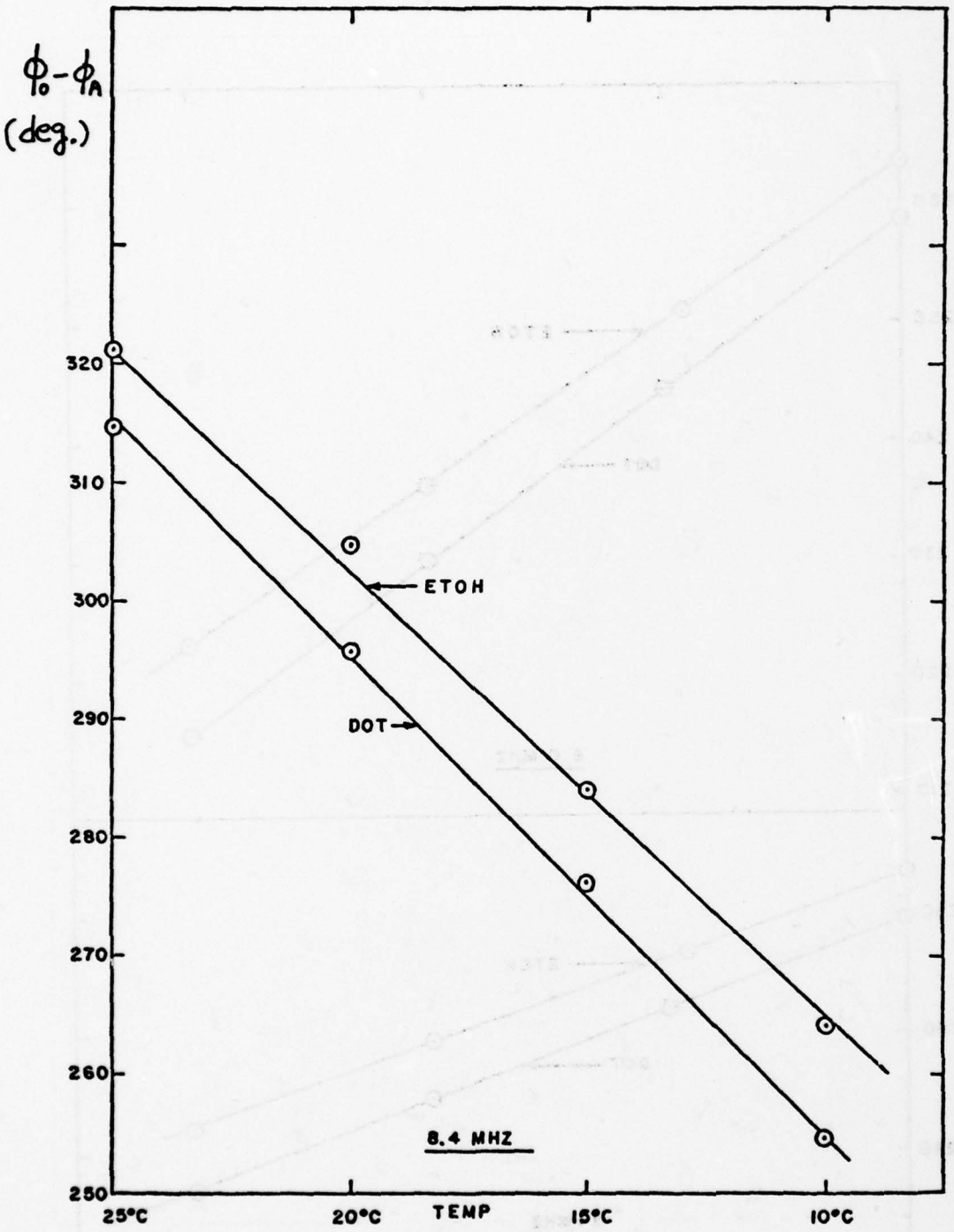

FIG. 16.2 PHASE vs TEMPERATURE

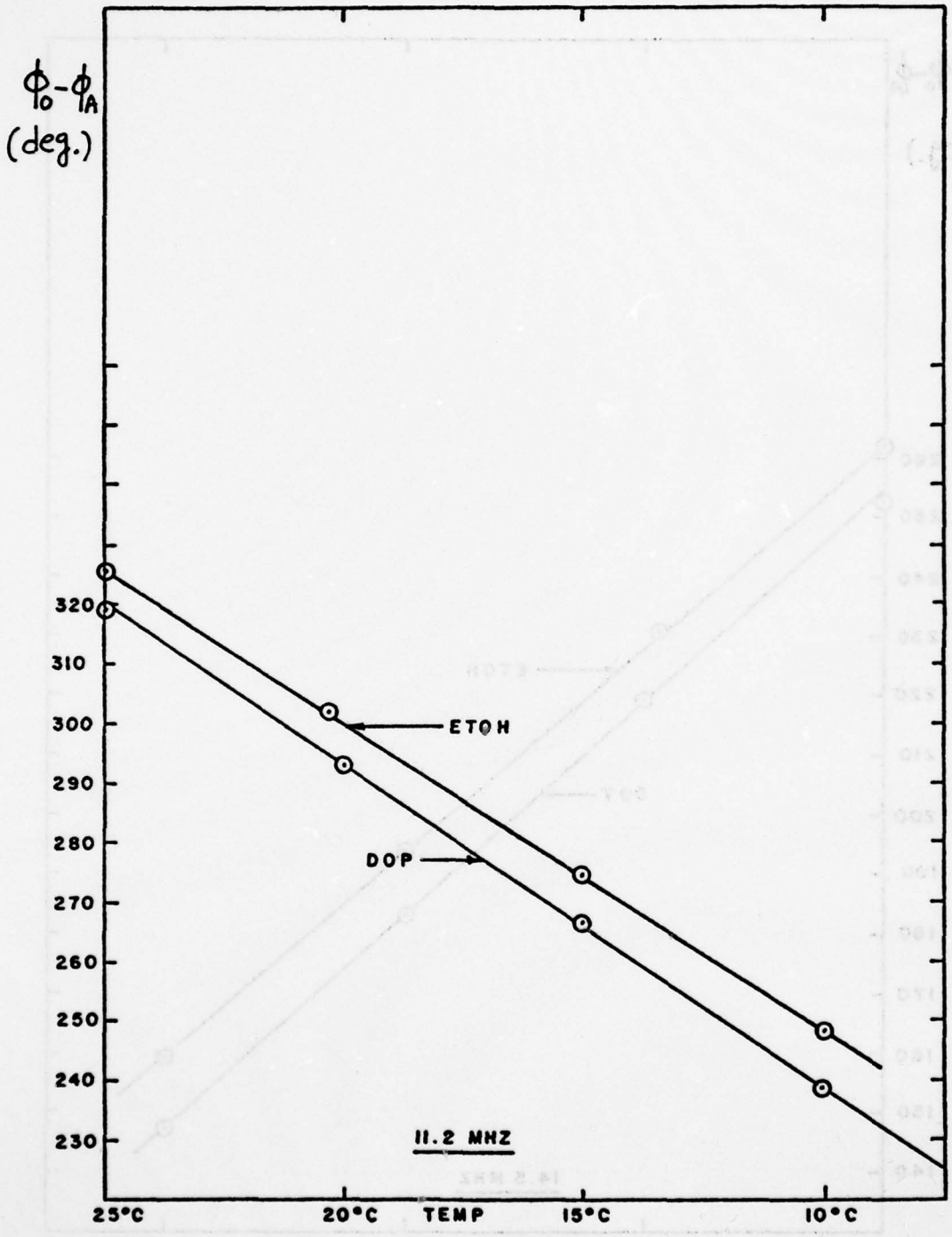

FIG.16.3 PHASE vs TEMPERATURE

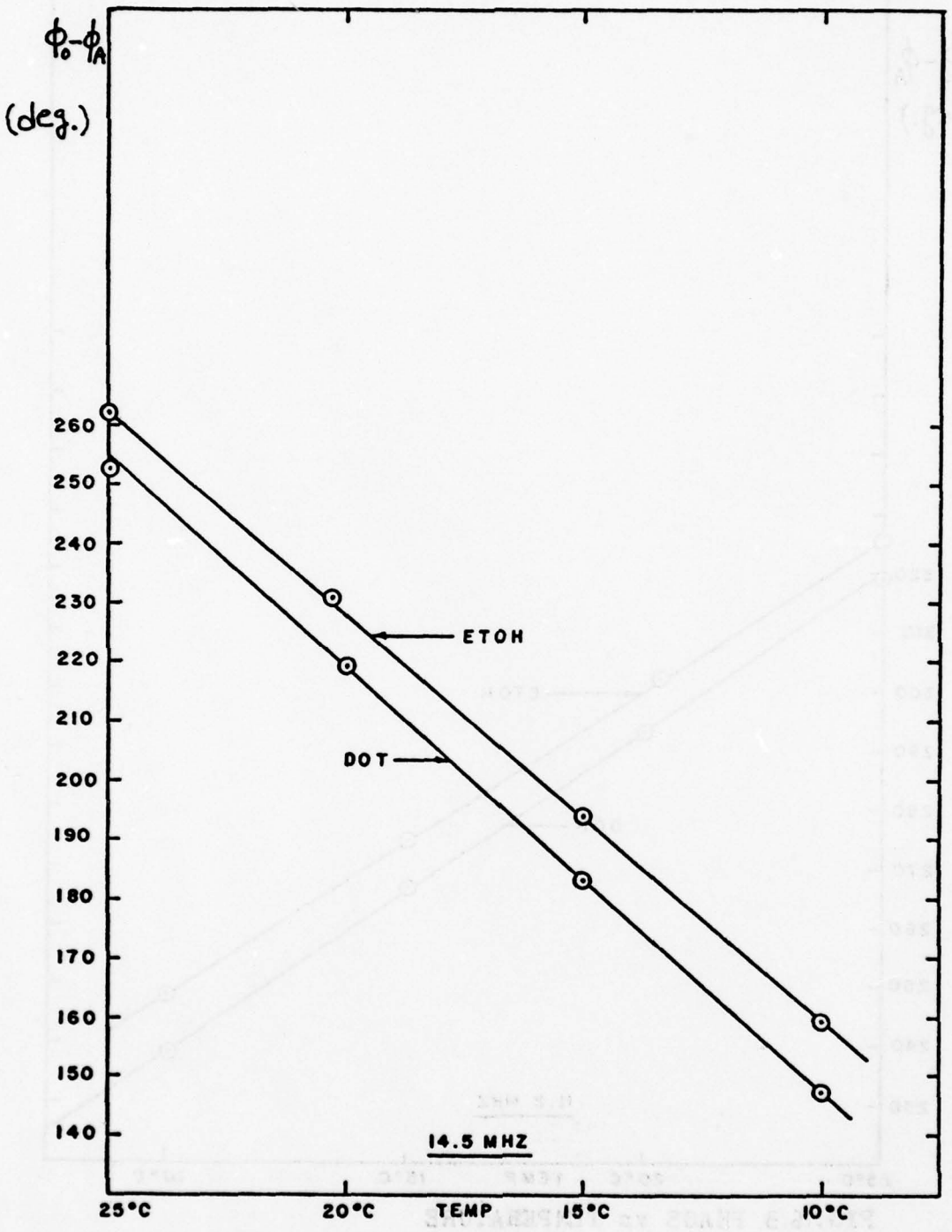

FIG.16.4 PHASE vs TEMPERATURE

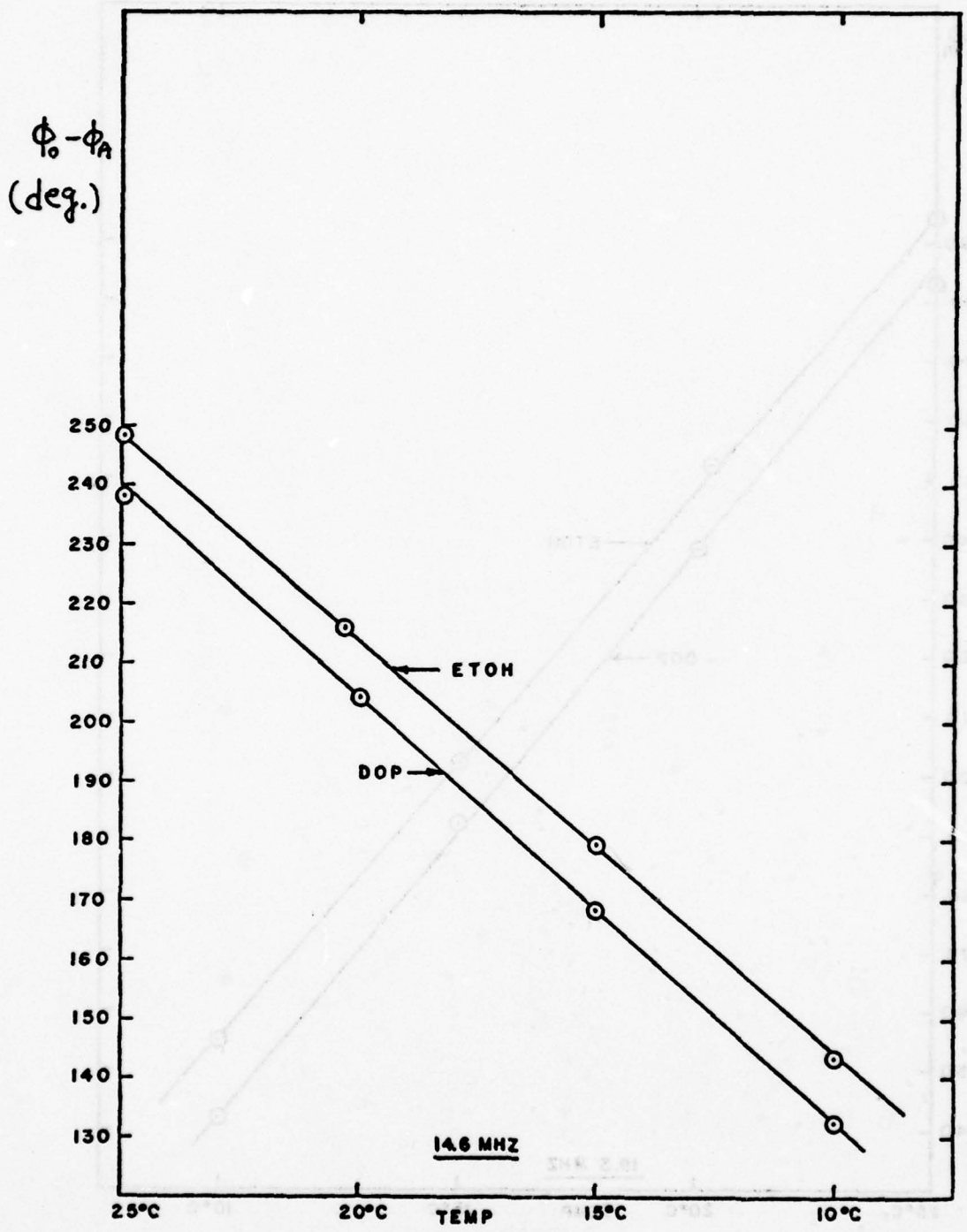

FIG. 16.5 PHASE vs TEMPERATURE

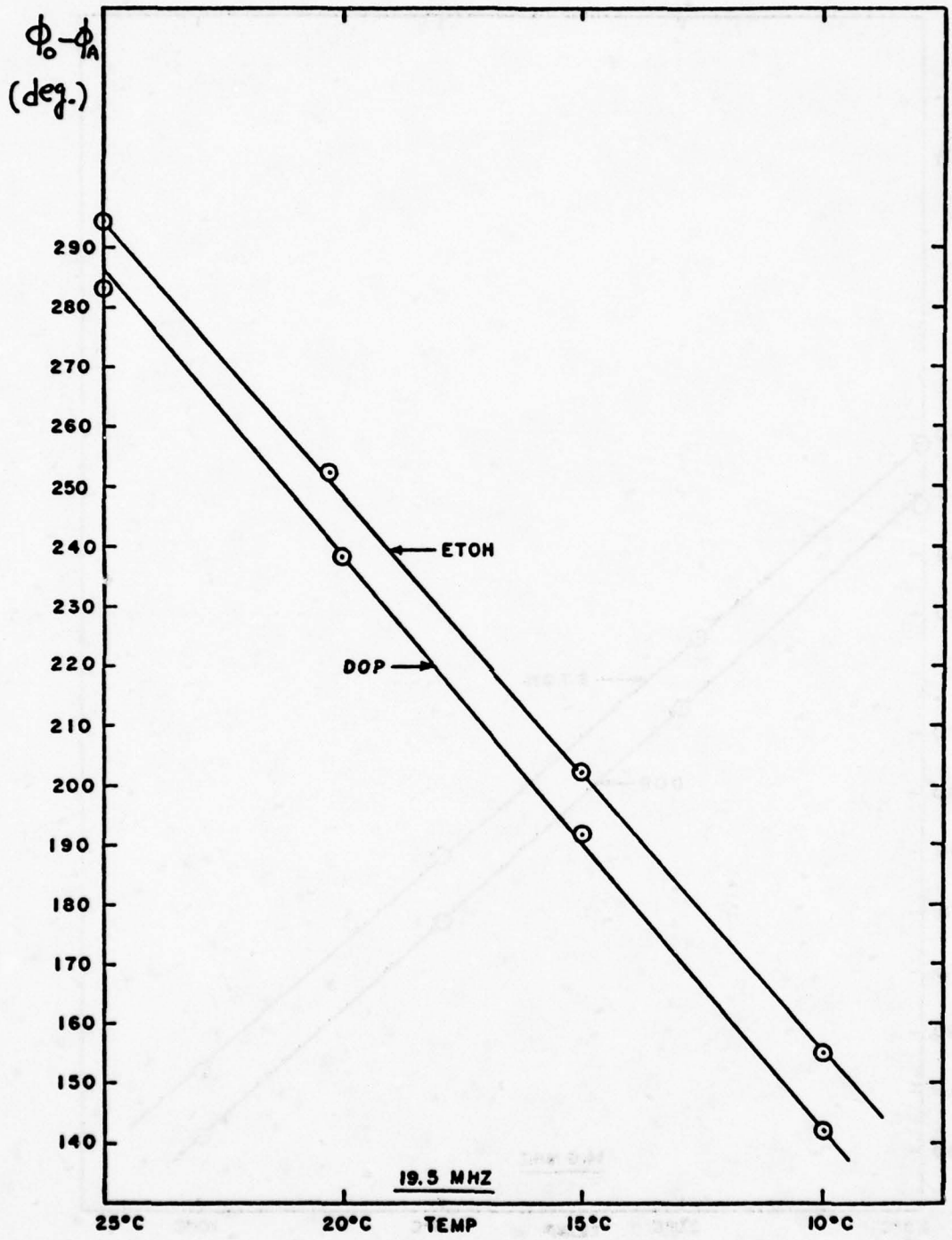

FIG. 16.6 PHASE vs TEMPERATURE

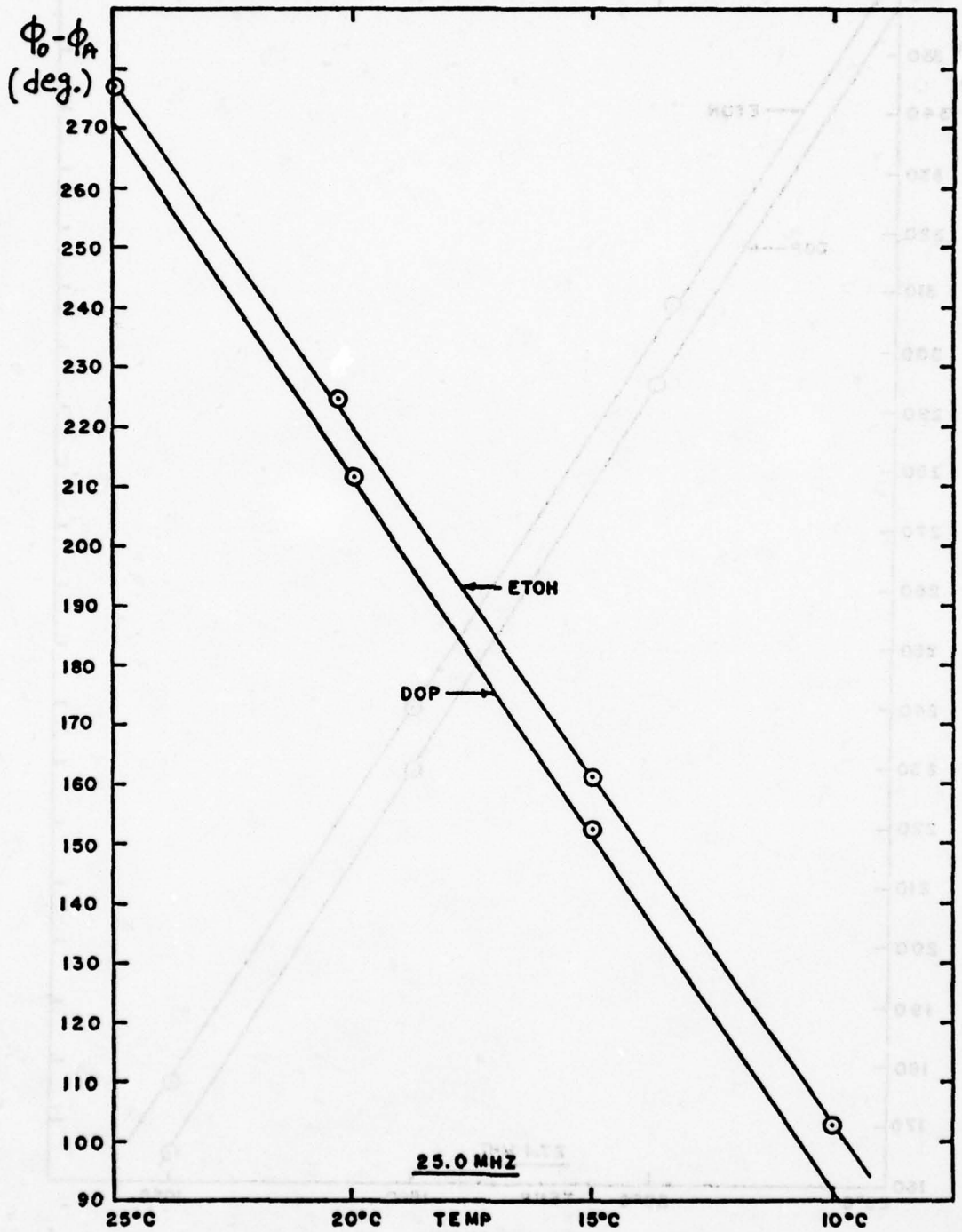

FIG. 16.7 PHASE vs TEMPERATURE

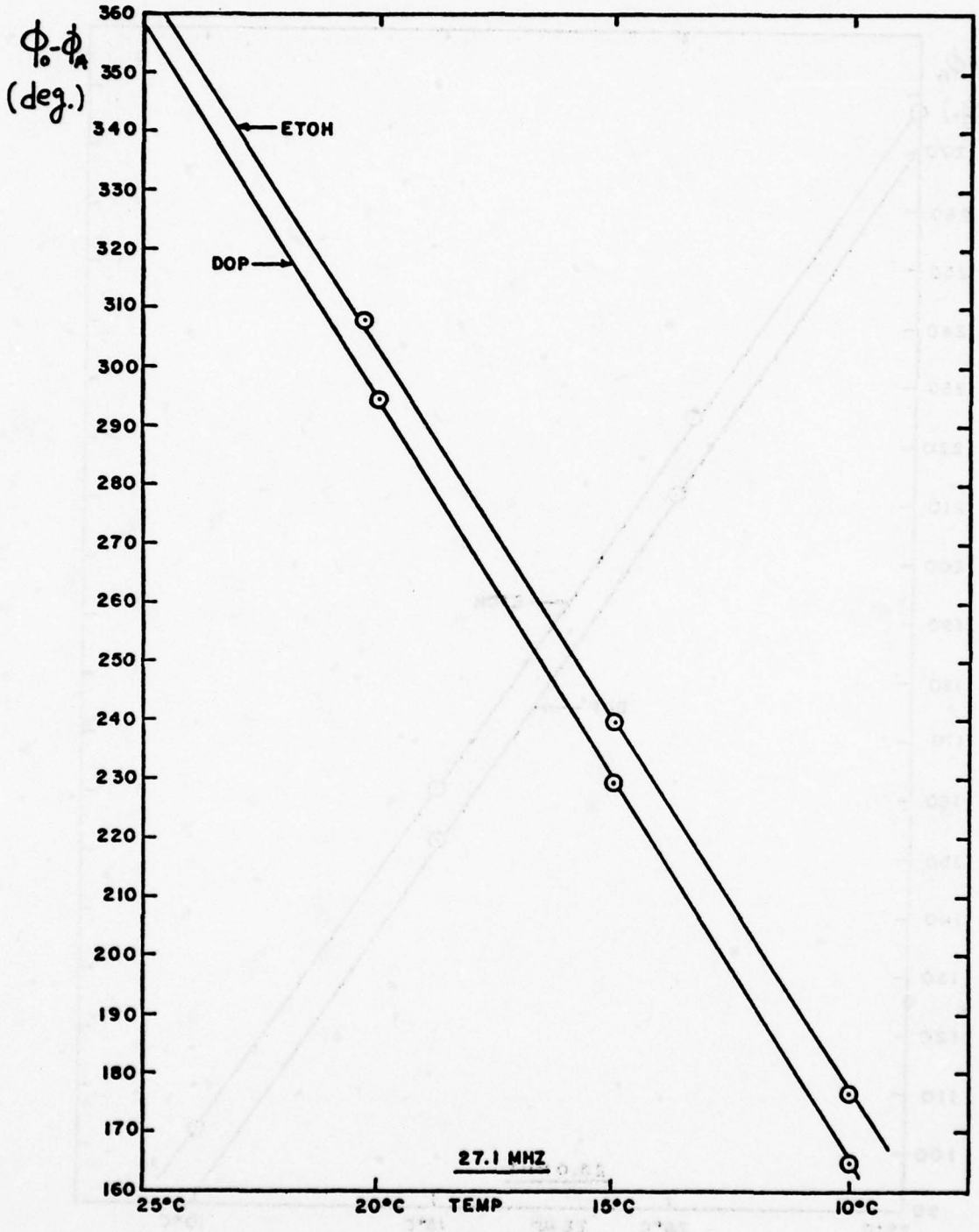

FIG. 16.8 PHASE vs TEMPERATURE

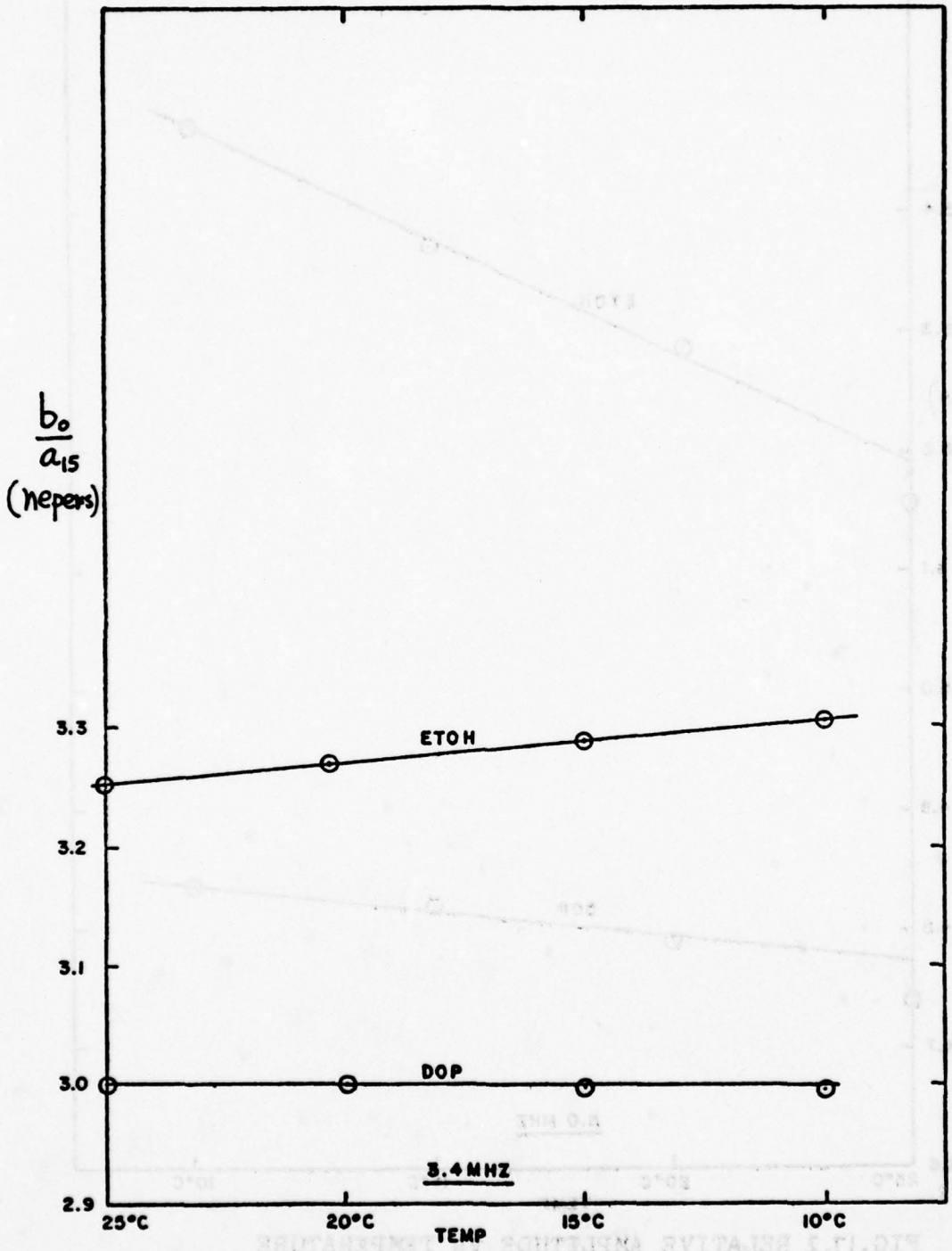

FIG.17.1 RELATIVE AMPLITUDE vs TEMPERATURE

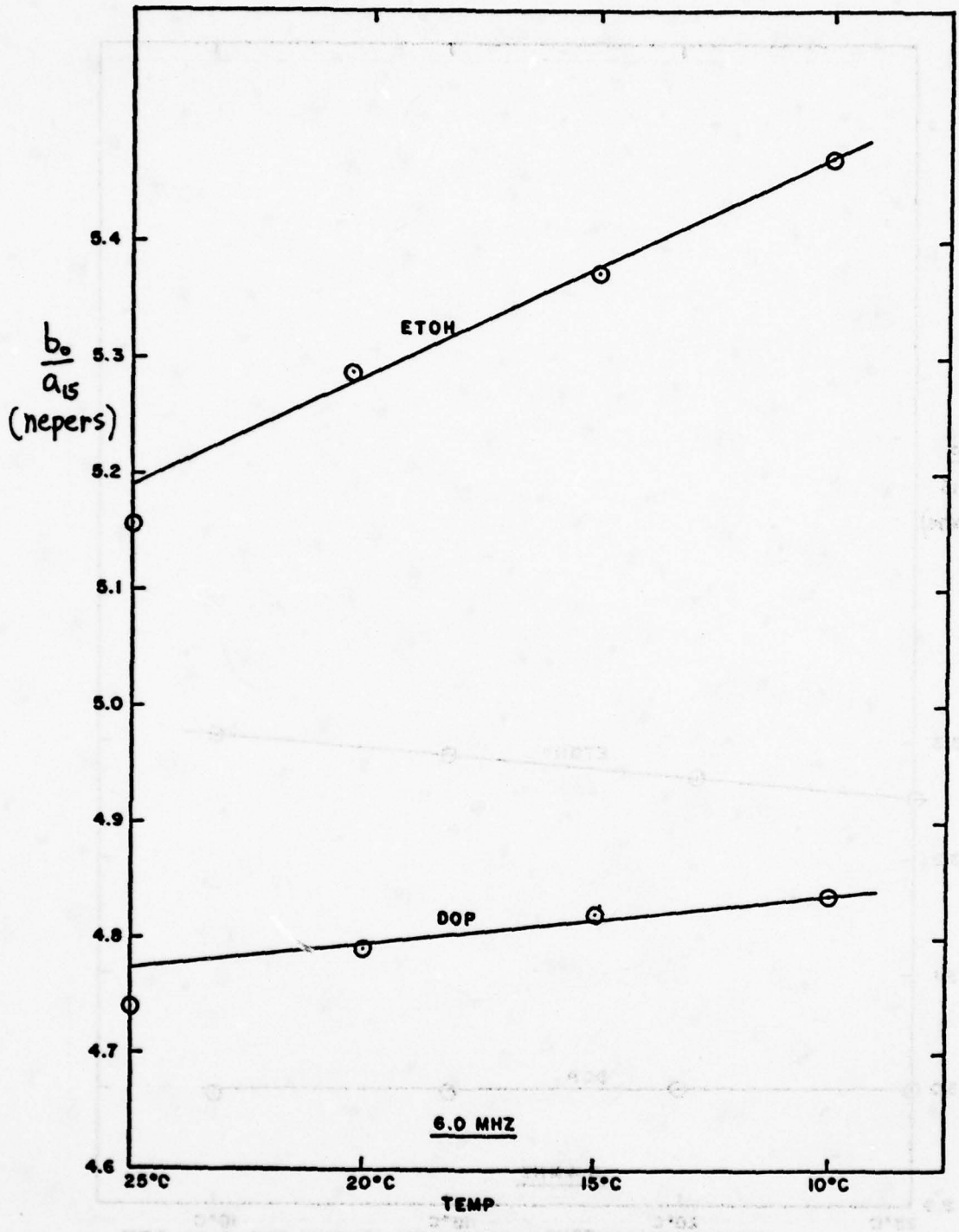

FIG.17.2 RELATIVE AMPLITUDE vs TEMPERATURE

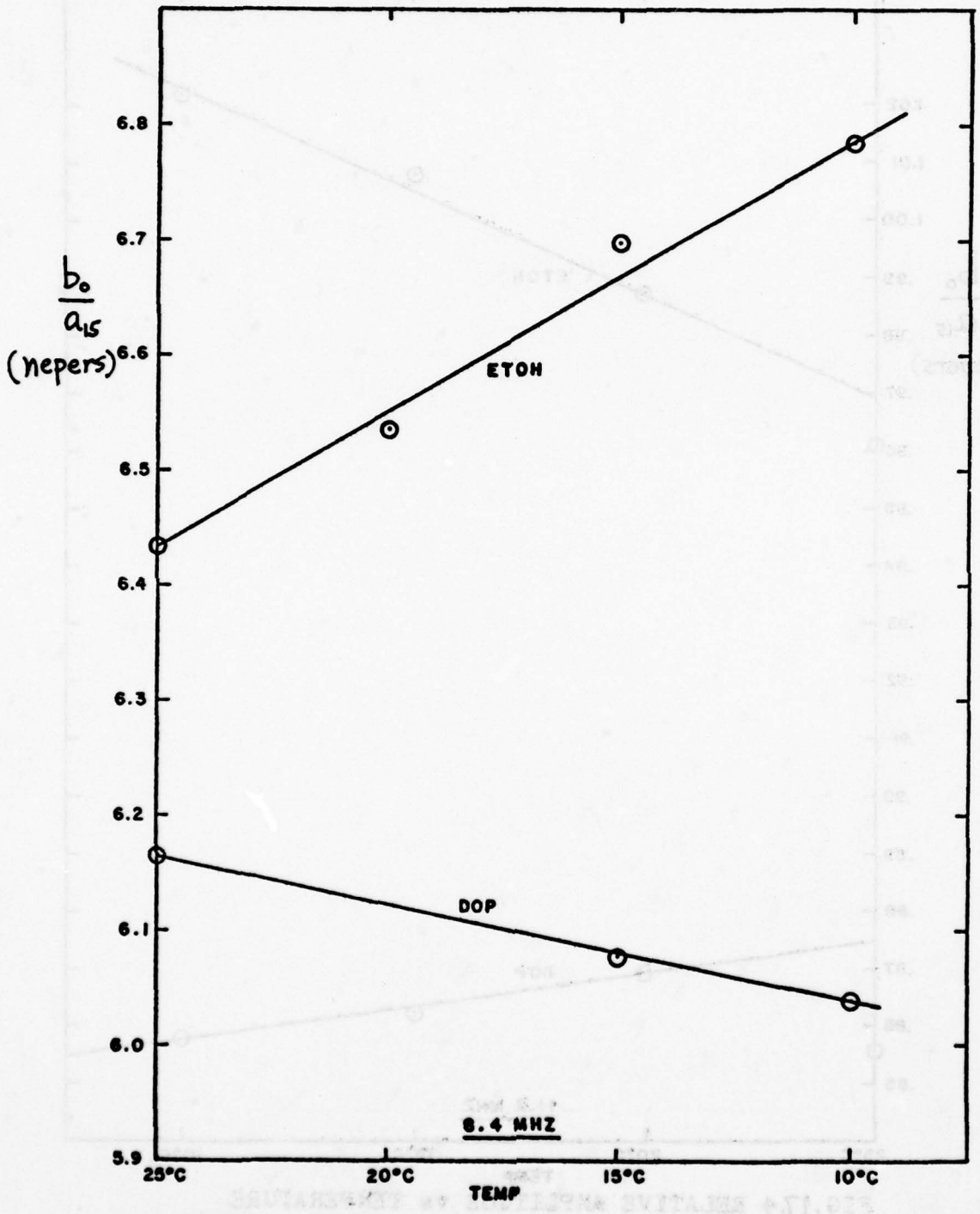

FIG.17.3 RELATIVE AMPLITUDE vs TEMPERATURE

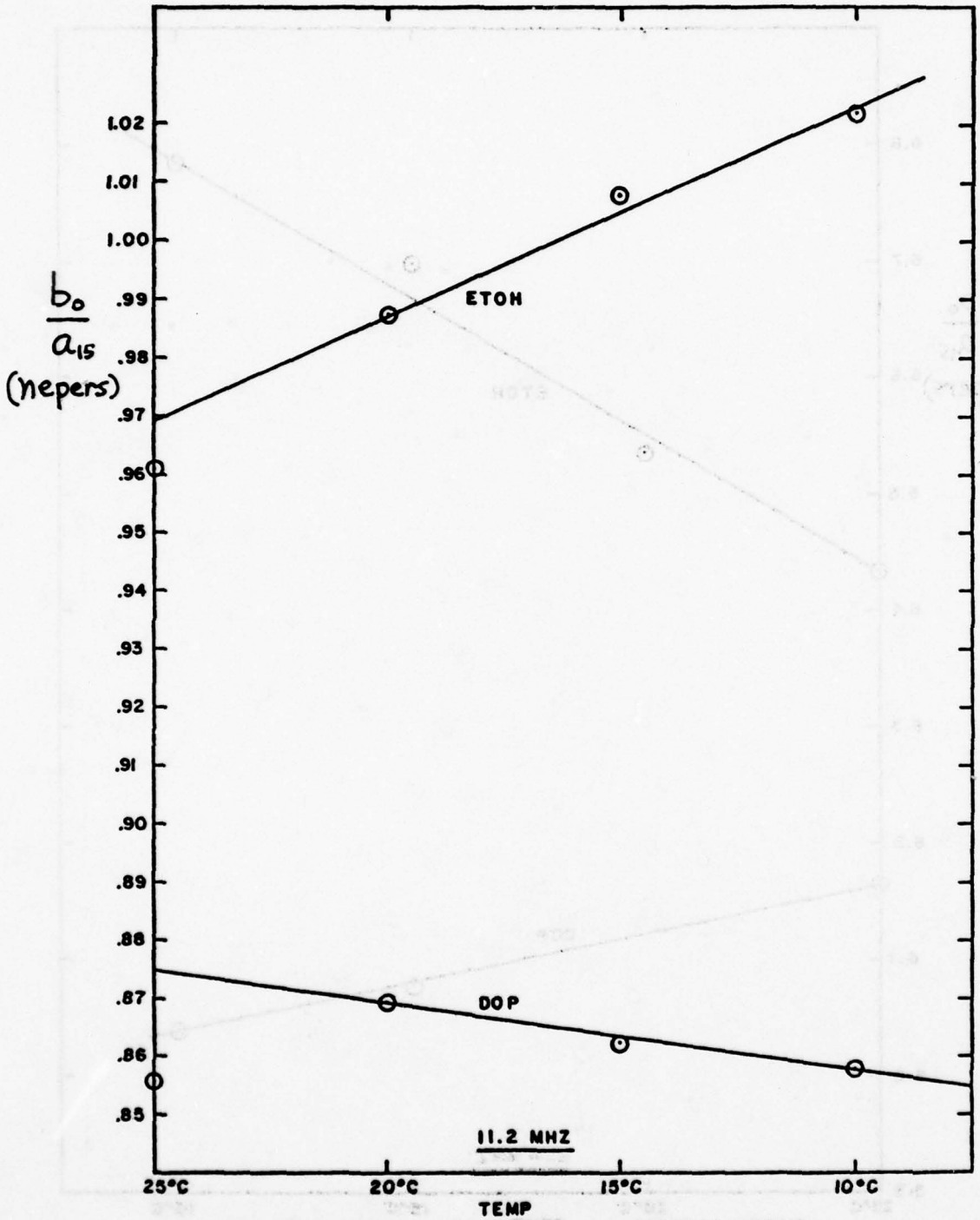

FIG. 17.4 RELATIVE AMPLITUDE vs TEMPERATURE

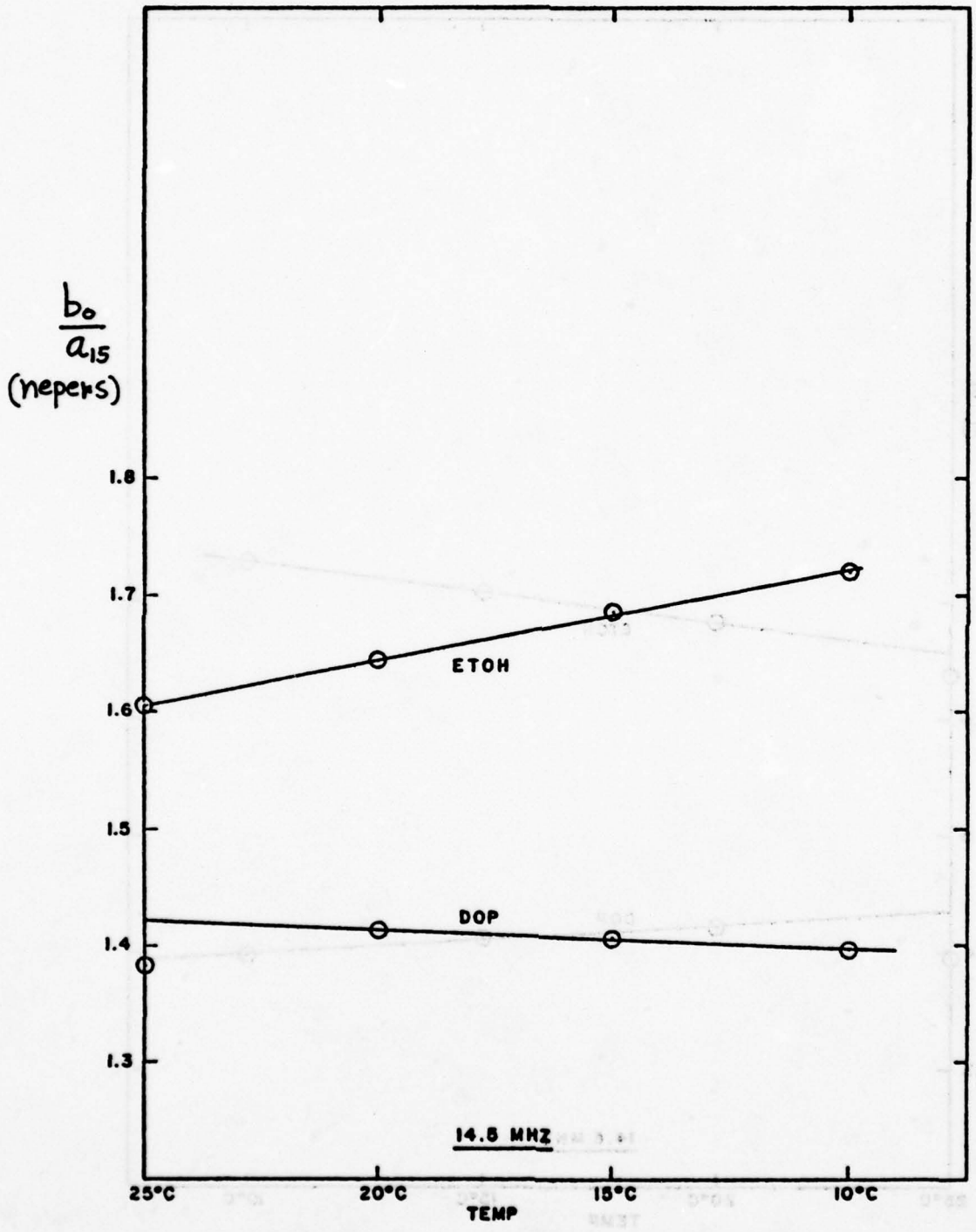

FIG. 17.5 RELATIVE AMPLITUDE vs TEMPERATURE

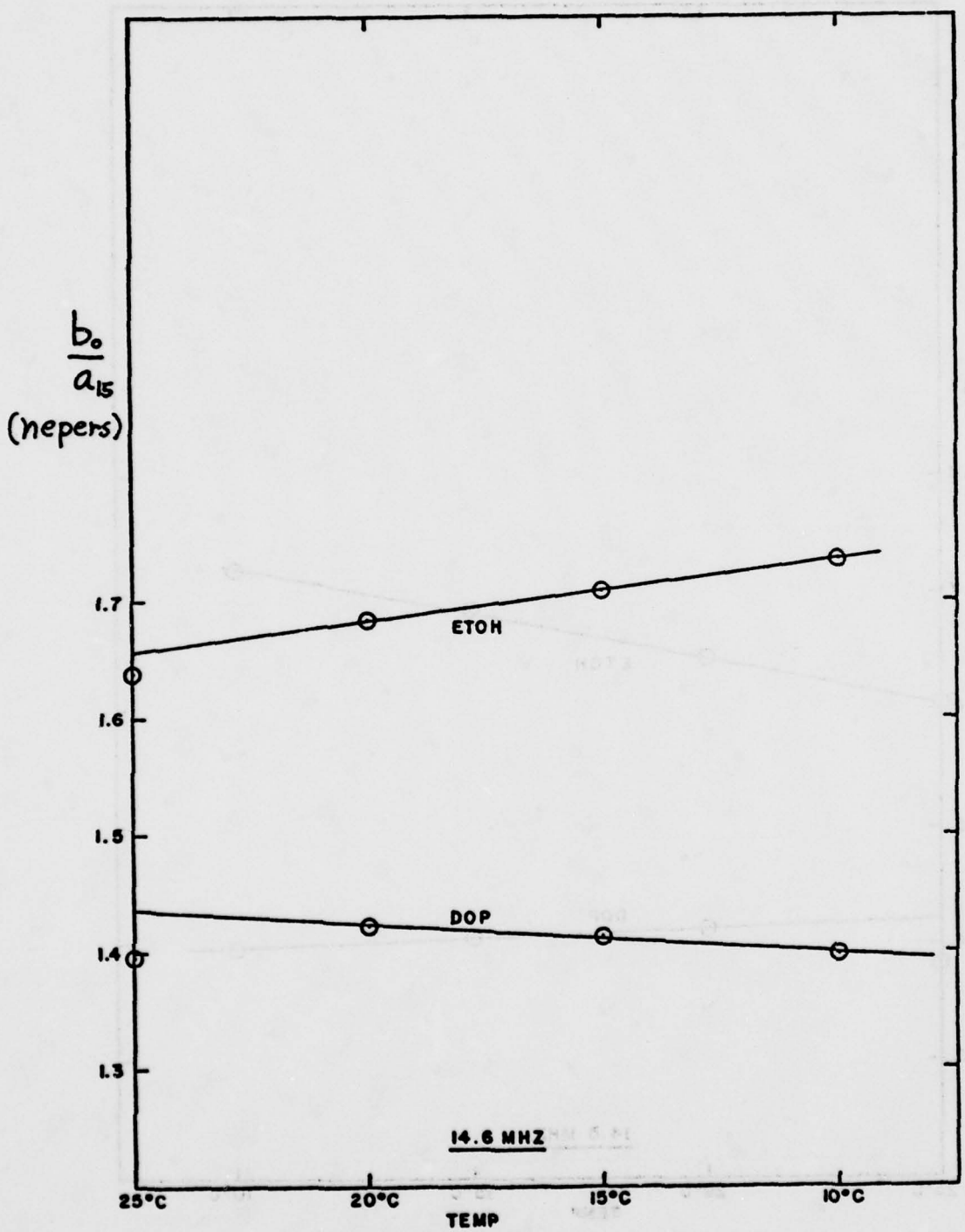

FIG.17.6 RELATIVE AMPLITUDE vs TEMPERATURE

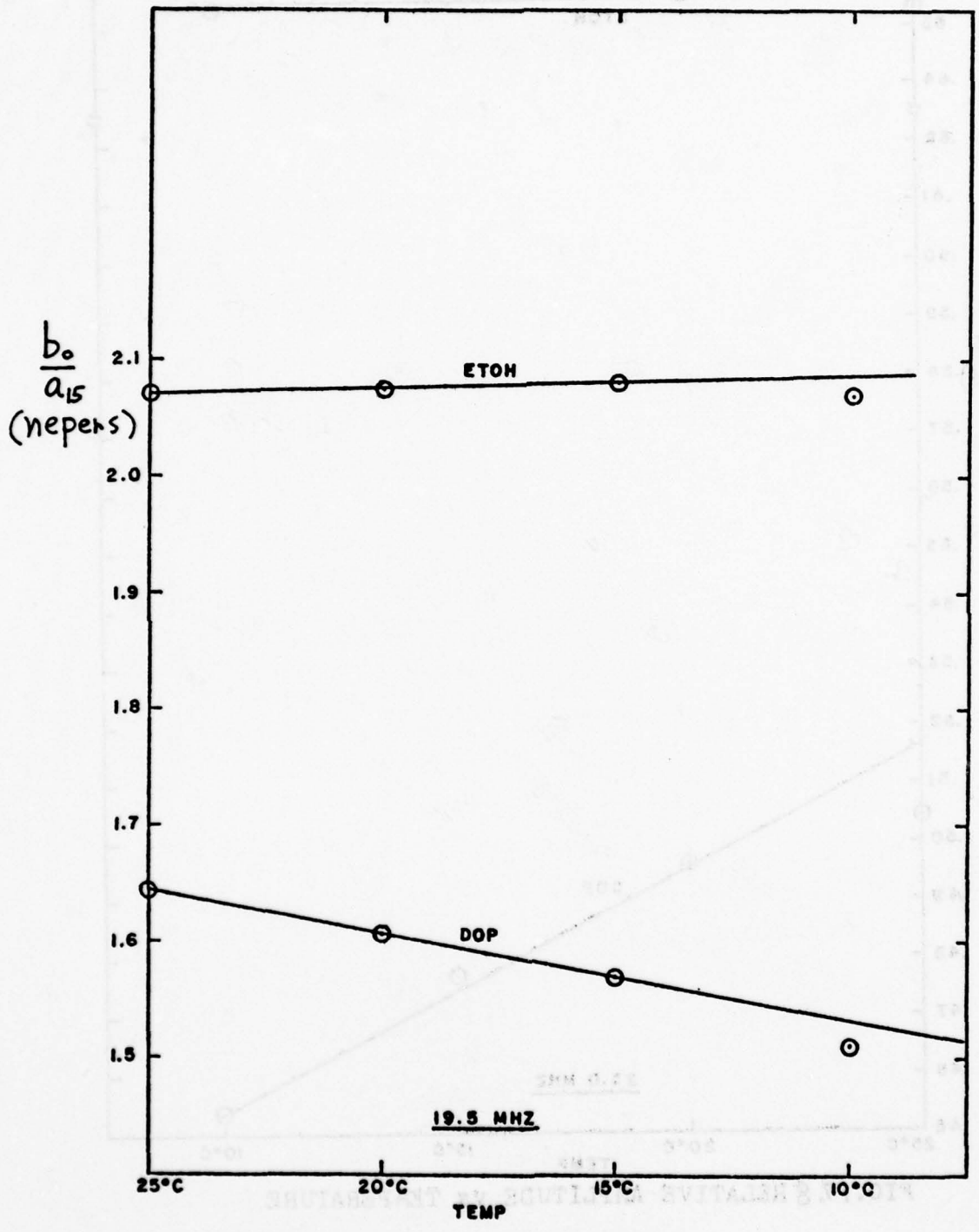

FIG. 17.7 RELATIVE AMPLITUDE vs TEMPERATURE

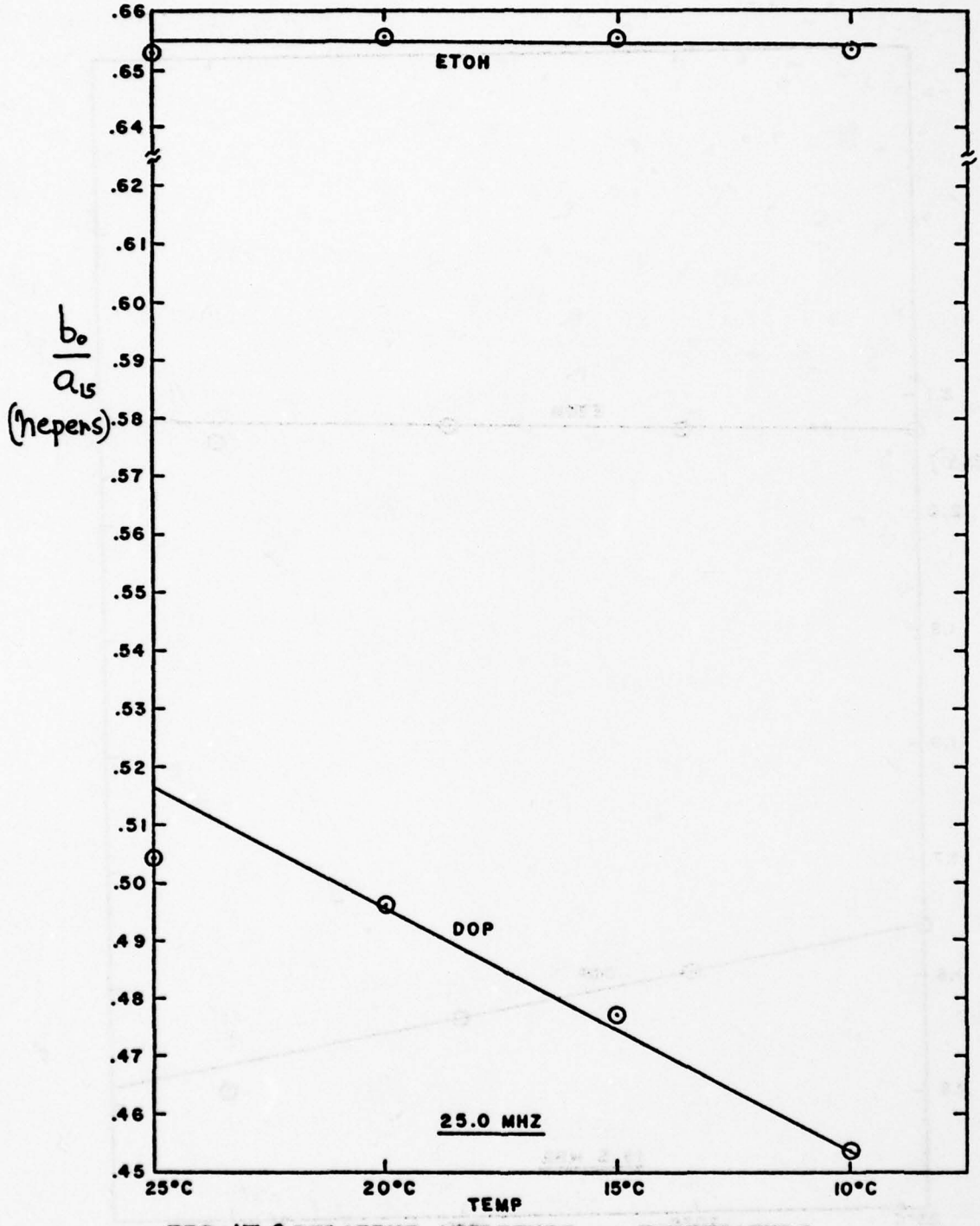

FIG. 17.8 RELATIVE AMPLITUDE vs TEMPERATURE

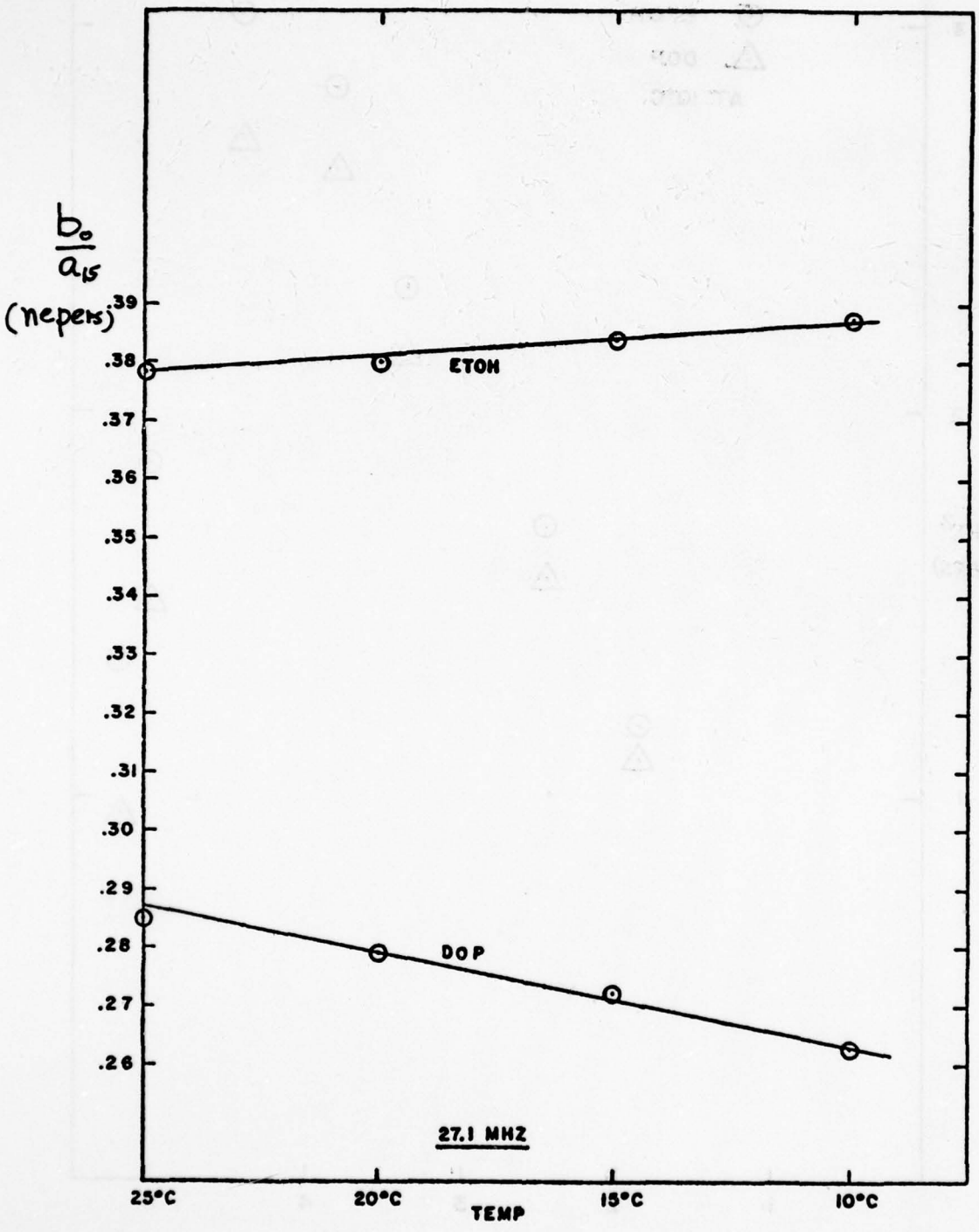

FIG. 17.9 RELATIVE AMPLITUDE vs TEMPERATURE

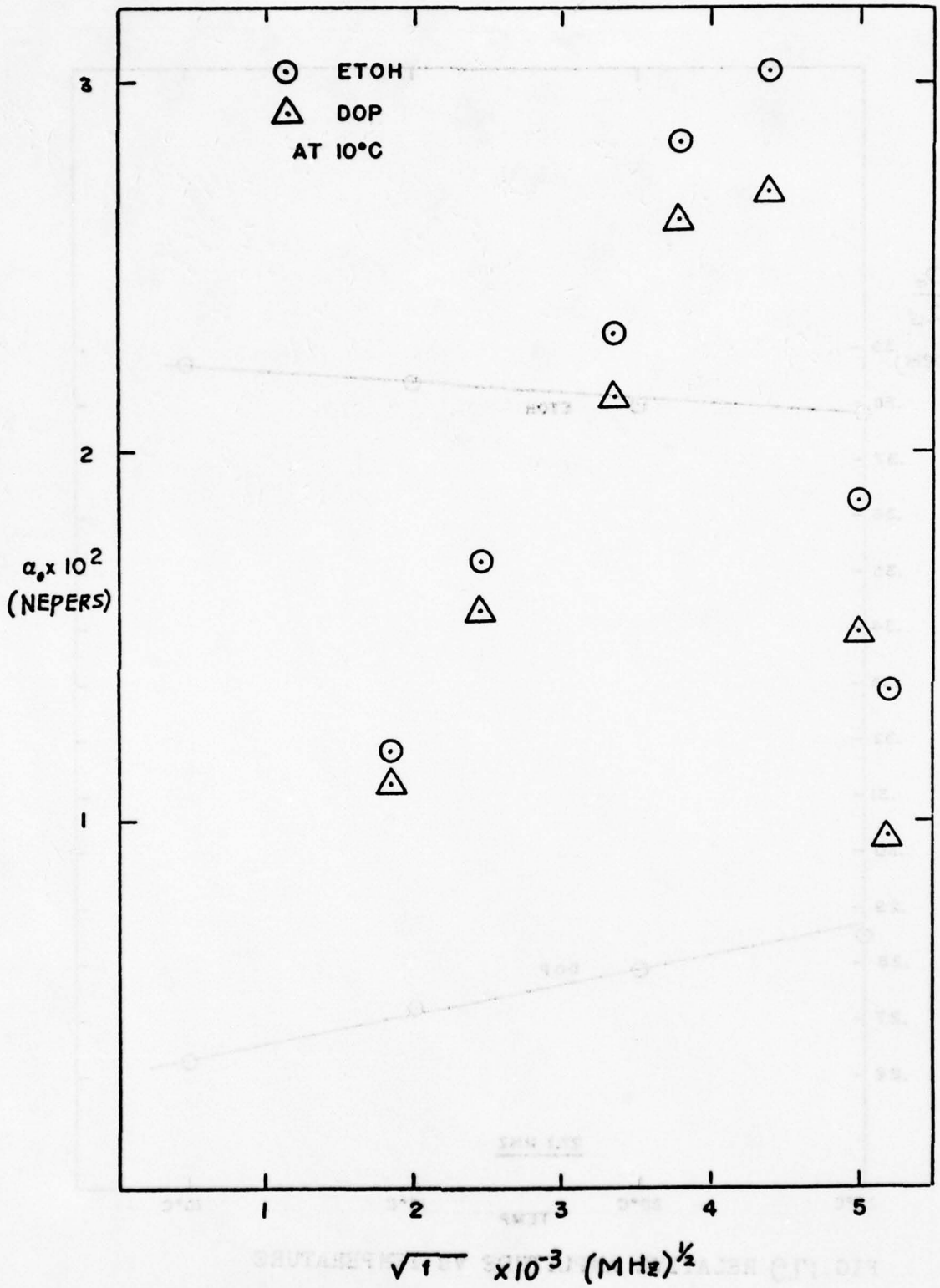

FIG. 18.1 ATTENUATION VS SQUARE ROOT OF FREQUENCY

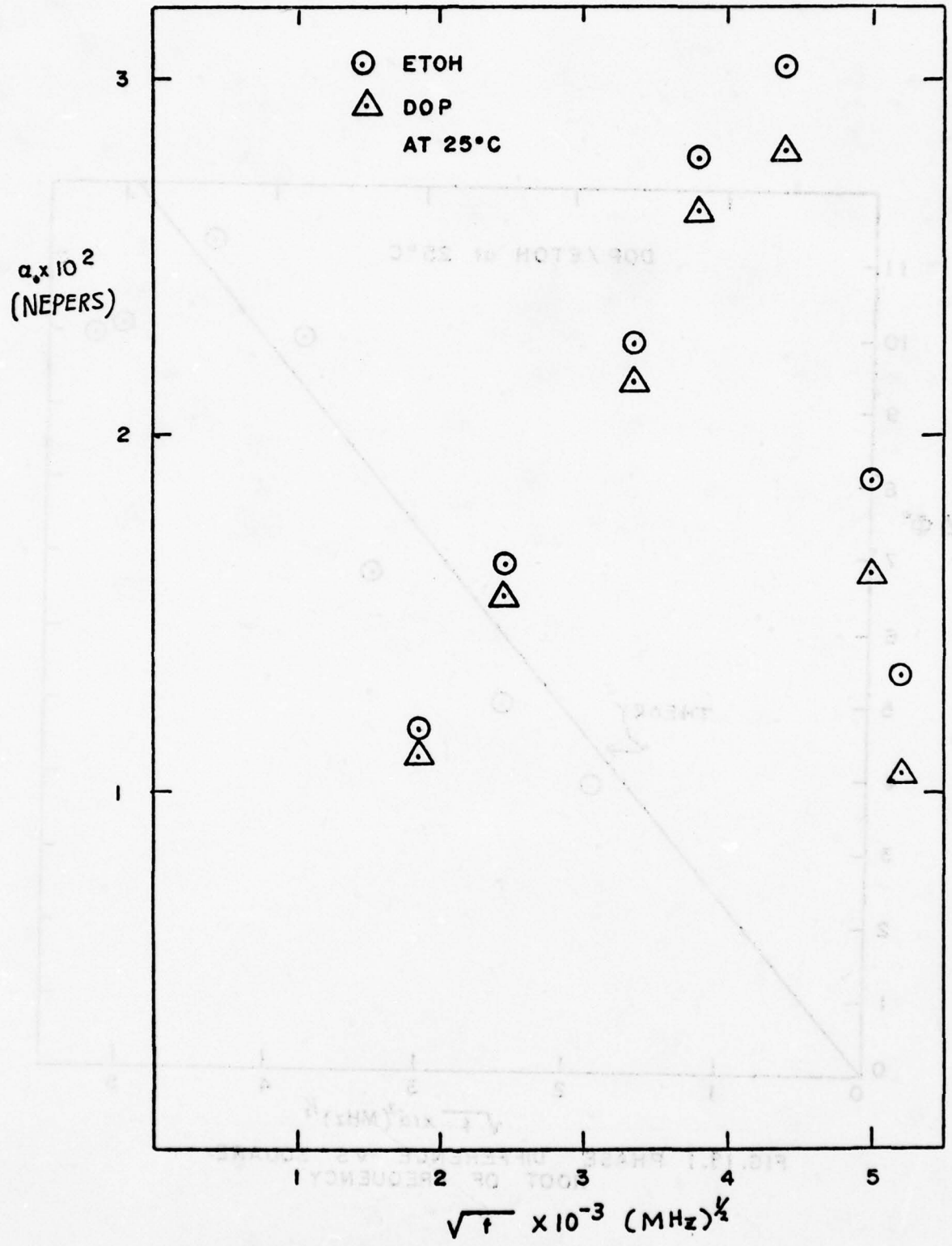

FIG. 18.2 ATTENUATION VS SQUARE ROOT OF FREQUENCY

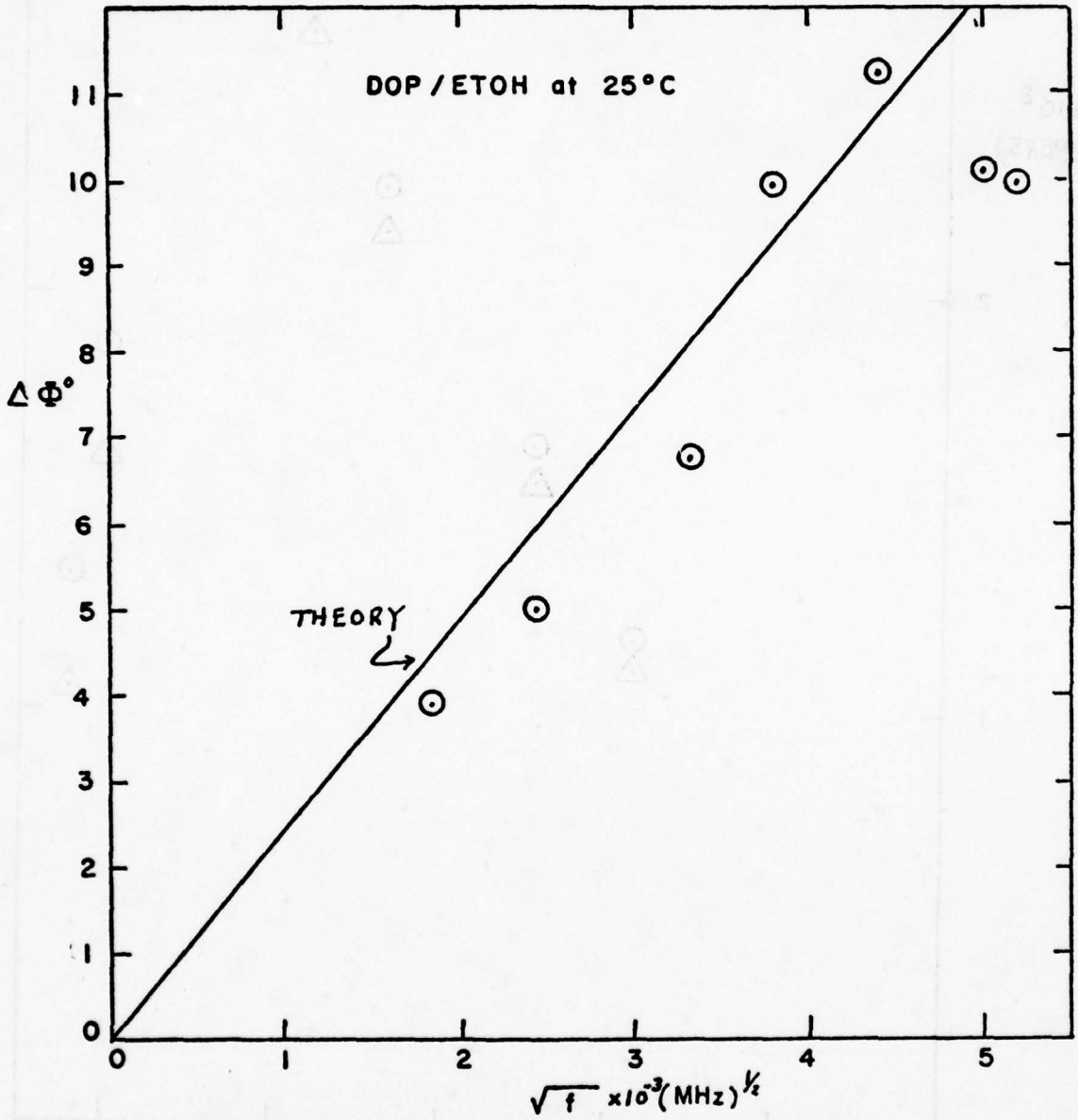

FIG. 19.1 PHASE DIFFERENCE VS SQUARE-ROOT OF FREQUENCY

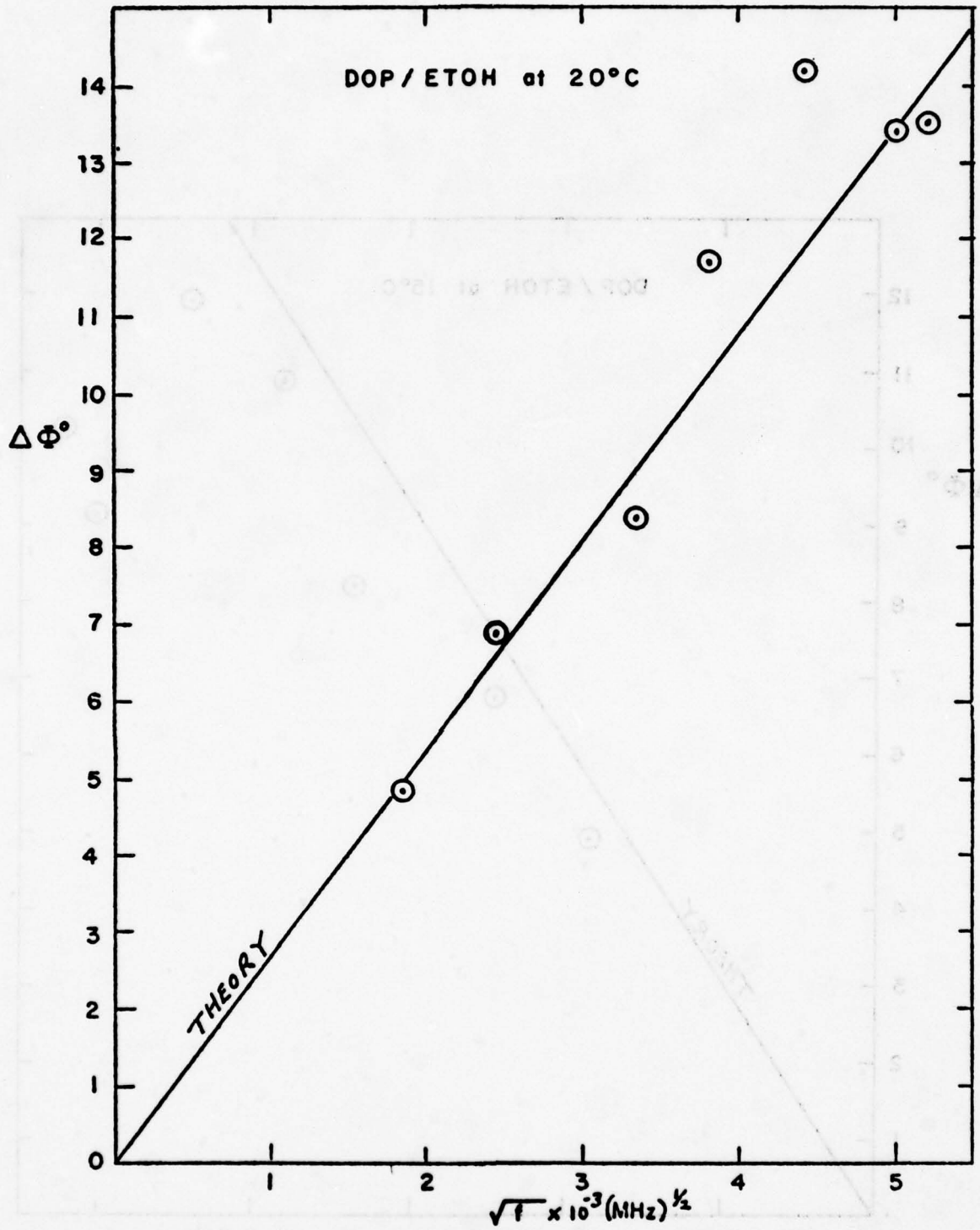

FIG. 19.2 PHASE DIFFERENCE VS SQUARE ROOT OF FREQUENCY

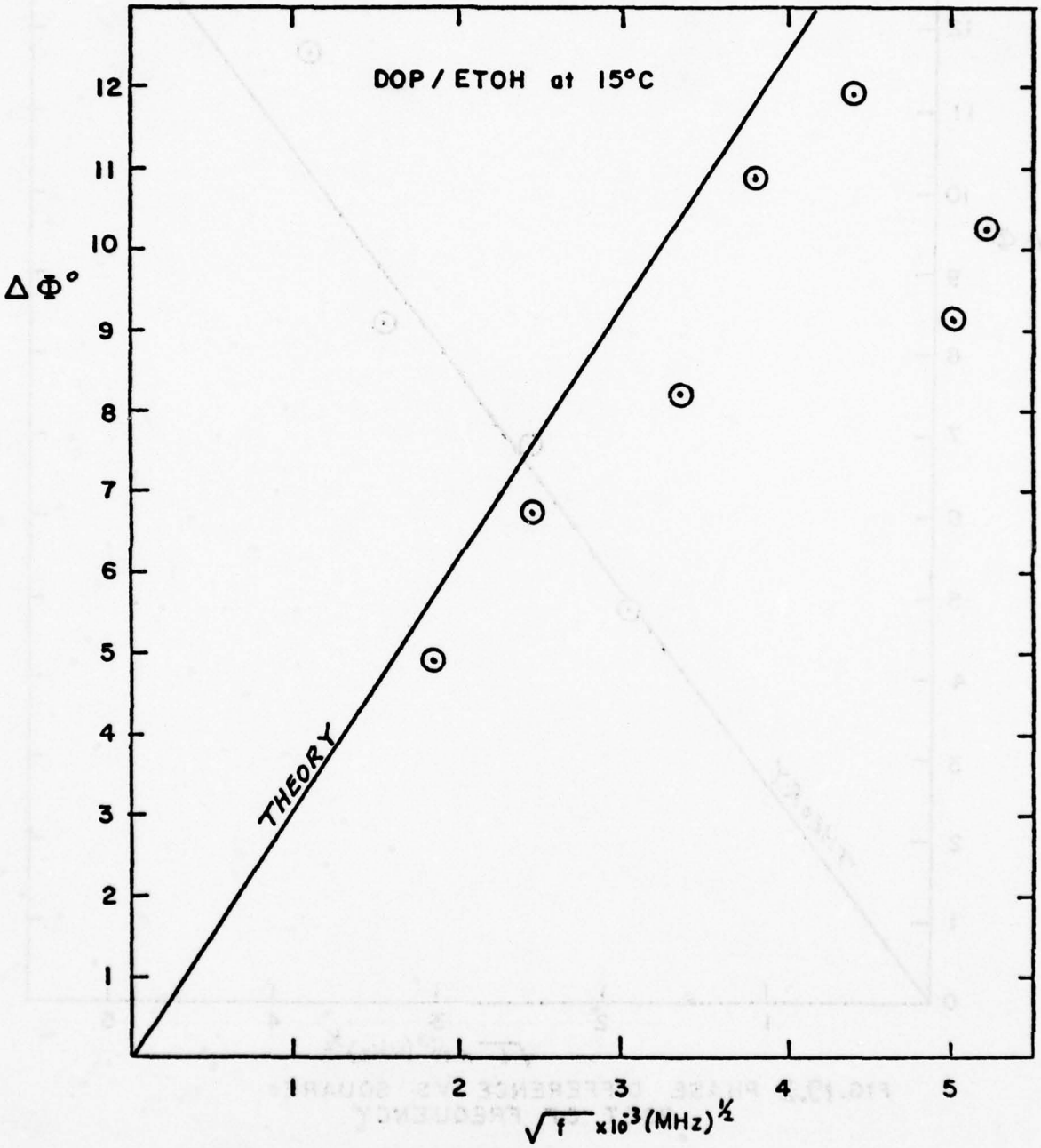

FIG. 19.3 PHASE DIFFERENCE VS SQUARE ROOT OF FREQUENCY

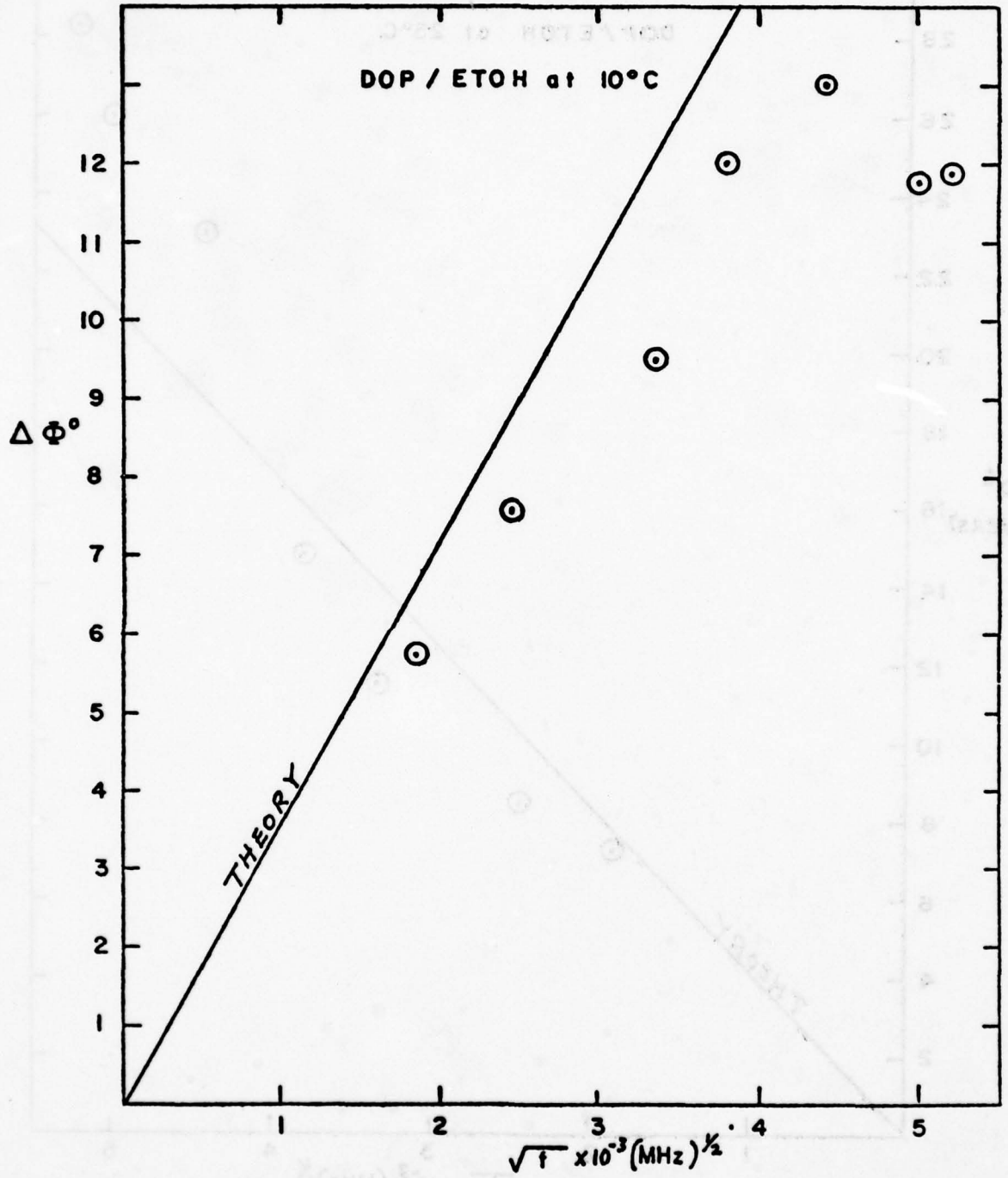

FIG. 19.4 PHASE DIFFERENCE VS SQUARE ROOT OF FREQUENCY

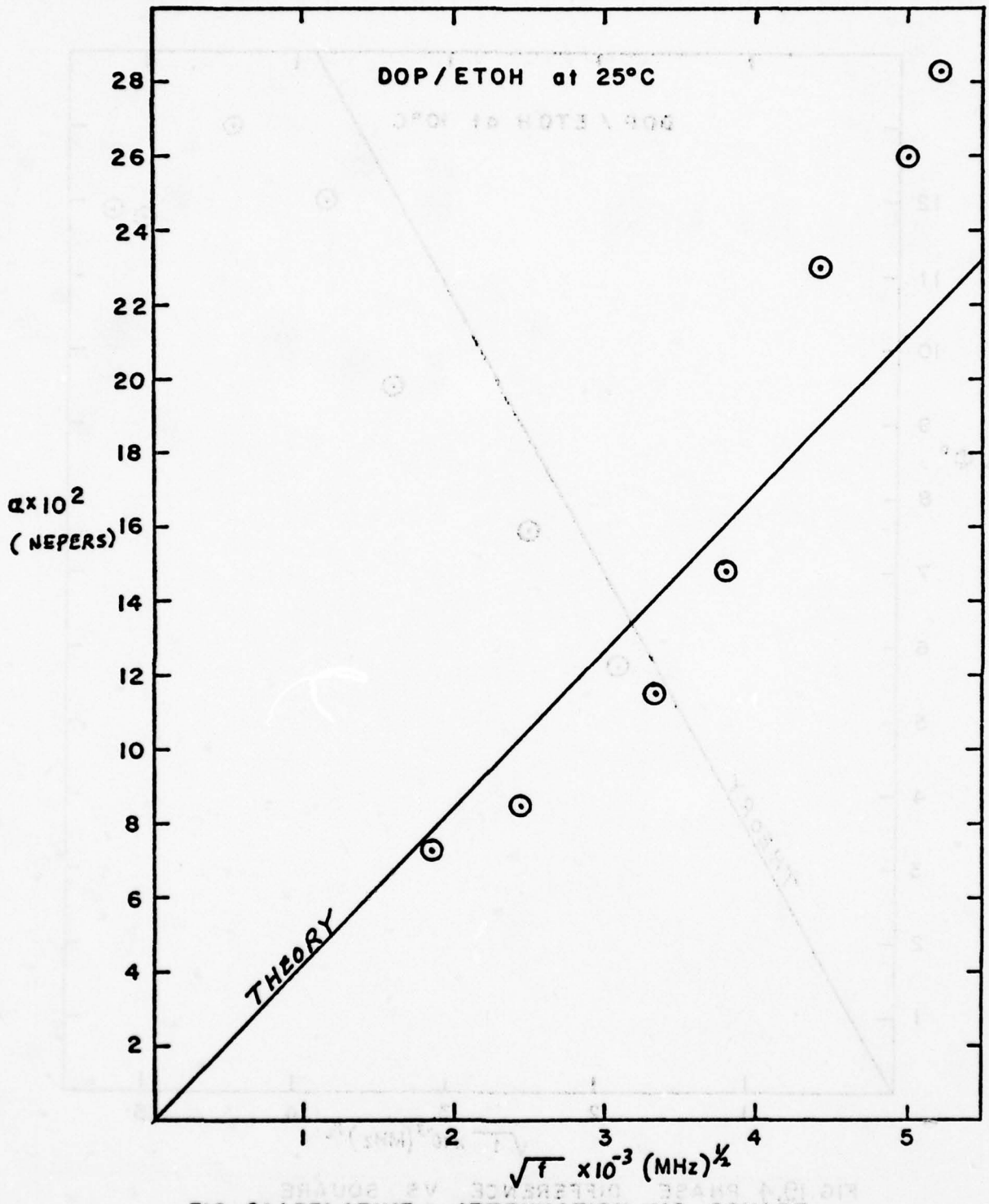

FIG. 20.1 RELATIVE ATTENUATION VS SQUARE ROOT OF FREQUENCY

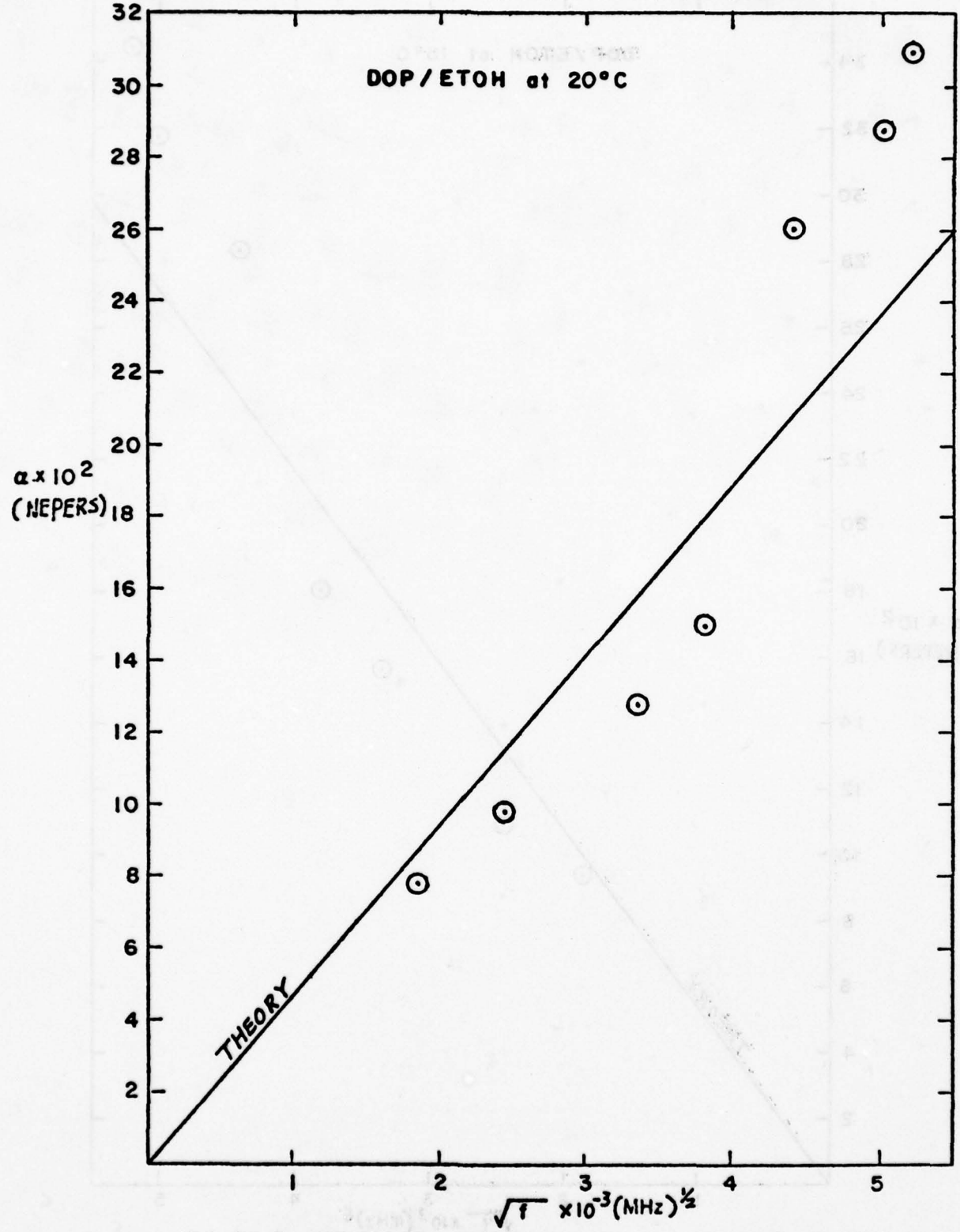

FIG. 20.2 RELATIVE ATTENUATION VS SQUARE ROOT OF FREQUENCY

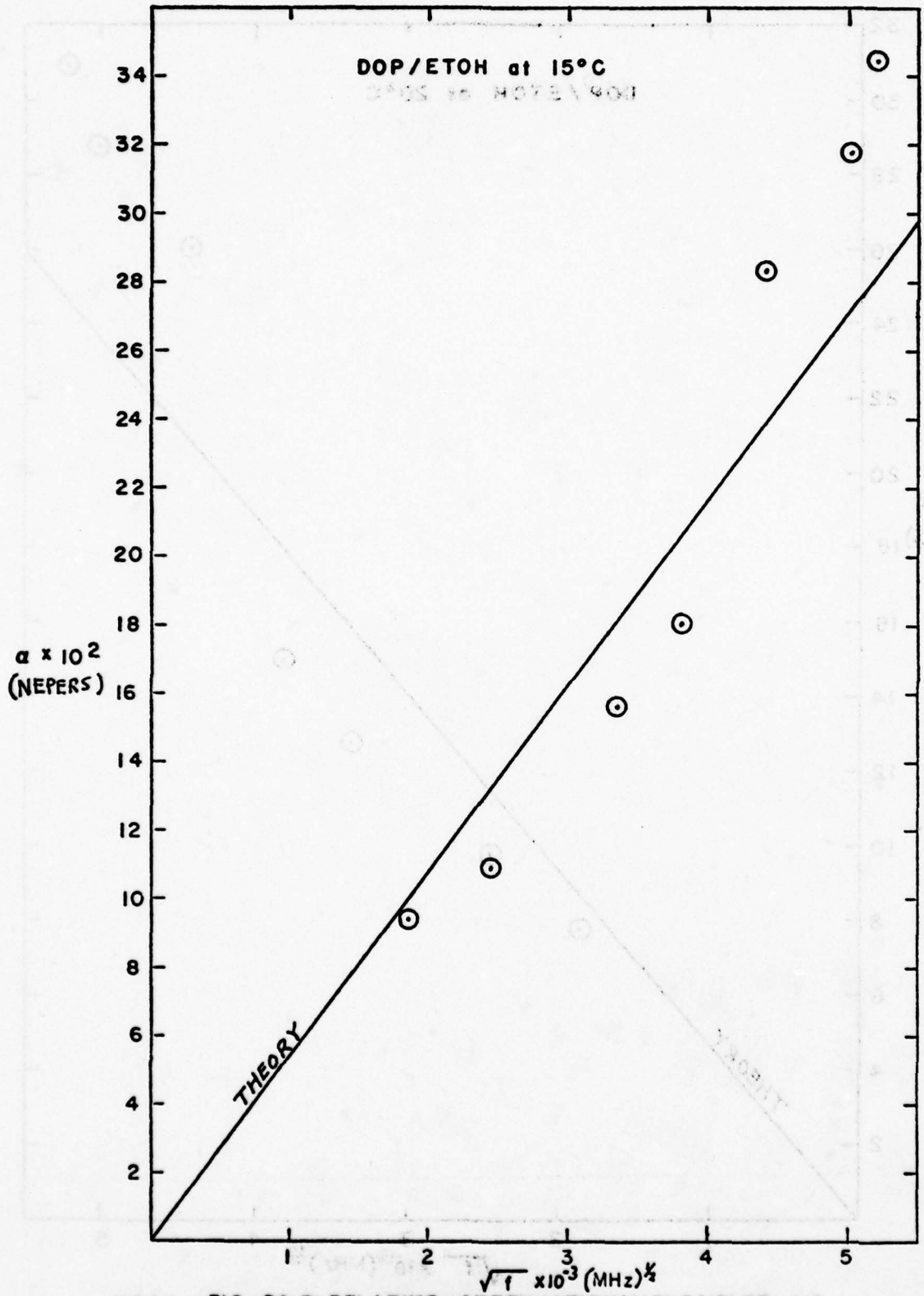

FIG. 20.3 RELATIVE ATTENUATION VS SQUARE ROOT OF FREQUENCY

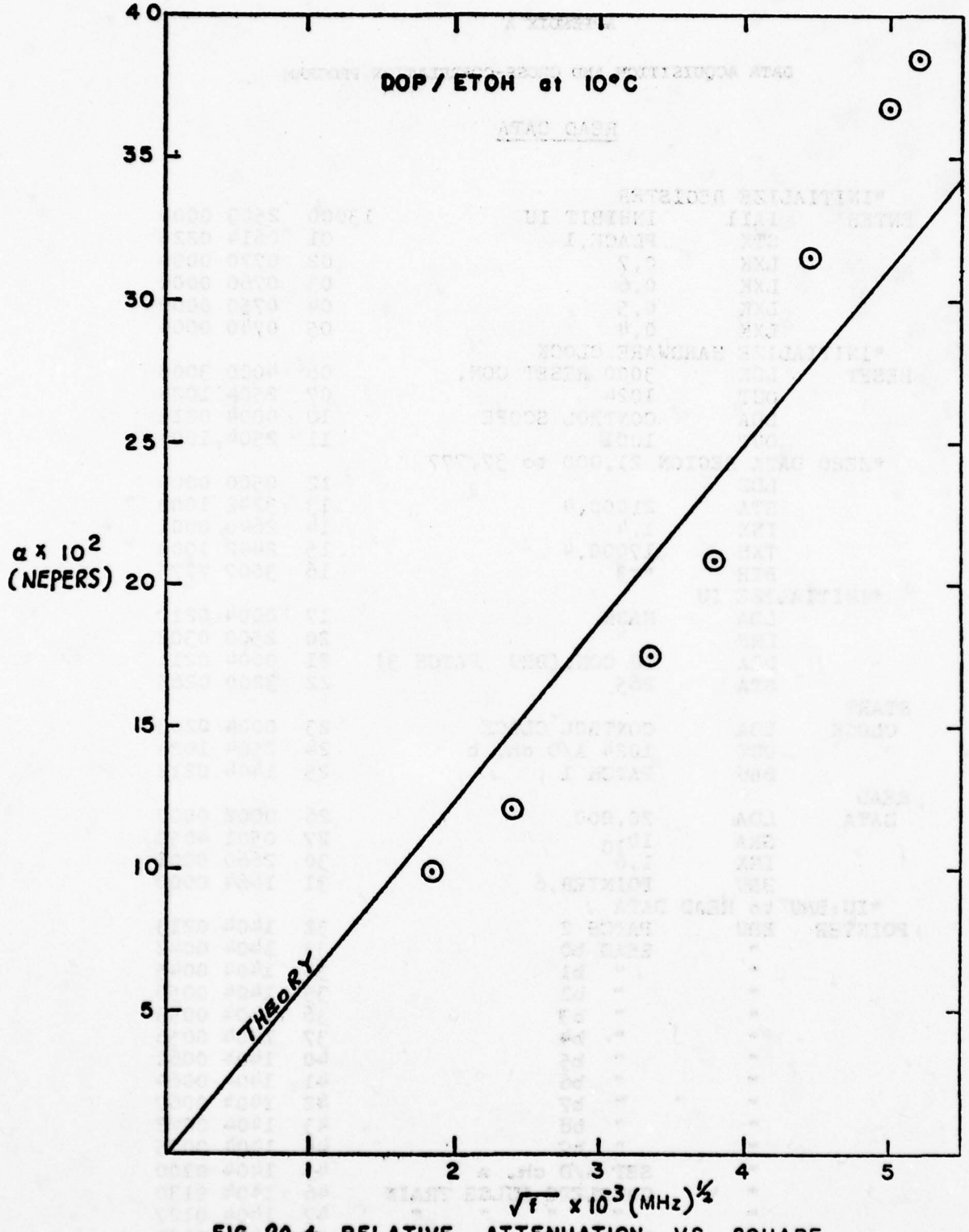

FIG. 20.4 RELATIVE ATTENUATION VS SQUARE ROOT OF FREQUENCY

APPENDIX A

DATA ACQUISITION AND CROSS-CORRELATION PROGRAM

READ DATA

```
  *INITIALIZE REGISTER
ENTER     IAI1     INHIBIT IU              13000  2503 0000
          STX      PLACE,1                    01  0614 0223
          LXK      0,7                        02  0770 0000
          LXK      0,6                        03  0760 0000
          LXK      0,5                        04  0750 0000
          LXK      0,4                        05  0740 0000
  *INITIALIZE HARDWARE CLOCK
RESET     LDK      3000 RESET CON.            06  4000 3000
          OUT      1024                       07  2504 1024
          LDA      CONTROL SCOPE              10  0004 0215
          OUT      1001                       11  2504 1001
  *ZERO DATA REGION 21,000 to 37,777
          LDZ                                 12  0500 0000
          STA      21000,4                    13  3242 1000
          INX      1,4                        14  2640 0001
          TXH      17000,4                    15  2442 1000
          BTR      *-3                        16  3007 7775
  *INITIALIZE IU
          LDA      MASK                       17  0004 0210
          LMR                                 20  2500 0302
          LDA      IU CON.(BRU  PATCH 3)      21  0004 0211
          STA      265                        22  3200 0265
START
 CLOCK    LDA      CONTROL CLOCK              23  0004 0203
          OUT      1024 A/D ch. b             24  2504 1024
          BRU      PATCH 1                    25  1404 0212
READ
 DATA     LDA      20,000                     26  0002 0000
          SRA      10₁₀                       27  0501 4052
          INX      1,6                        30  2660 0001
          BRU      POINTER,6                  31  1464 0000
  *IU:BRU to READ DATA
POINTER   BRU      PATCH 2                    32  1404 0213
           "       READ b0                    33  1404 0042
           "         "  b1                    34  1404 0045
           "         "  b2                    35  1404 0050
           "         "  b3                    36  1404 0053
           "         "  b4                    37  1404 0056
           "         "  b5                    40  1404 0061
           "         "  b6                    41  1404 0064
           "         "  b7                    42  1404 0067
           "         "  b8                    43  1404 0072
           "         "  b9                    44  1404 0075
           "       SET A/D ch. a              45  1404 0100
           "       COMPLETE PULSE TRAIN       46  1404 0130
           "         "   "    "   "          47  1404 0127
           "       READ a14                   50  1404 0101
           "       RESET A/D ch. b            51  1404 0104
```

```
                BRU     COMPLETE PULSE TRAIN 13052  1404 0124
                "       INX "7"                 53  1404 0106
                "       COMPLETE PULSE TRAIN    54  1404 0122
                "       TEST AVERAGE COMPLETE   55  1404 0111
                "       COMPLETE PULSE TRAIN    56  1404 0120
                "         "       "       "     57  1404 0117
                "         "       "       "     60  1404 0116
                "         "       "       "     61  1404 0115
                "         "       "       "     62  1404 0114
                "         "       "       "     63  1404 0113
                "         "       "       "     64  1404 0112
                "         "       "       "     65  1404 0111
                "         "       "       "     66  1404 0110
                "         "       "       "     67  1404 0107
                "         "       "       "     70  1404 0106
                "       40th POINTER ENTER      71  1404 0104
READ
NOTHING         NOP                             72  2620 0000
                NOP                             73  2620 0000
                NOP                             74  2620 0000
READ
 DATA bo        ADD     22200,7                 75  1172 2200
                STA     22200,7                 76  3272 2200
                NOP                             77  2620 0000
                BRU     * -1                   100  1407 7777
READ
 DATA b1        ADD     23400,7                101  1172 3400
                STA     23400,7                102  3272 3400
                NOP                            103  2620 0000
                BRU     * -1                   104  1407 7777
READ
 DATA b2        ADD     24600,7                105  1172 4600
                STA     24600,7                106  3272 4600
                NOP                            107  2620 0000
                BRU     * -1                   110  1407 7777
READ
 DATA b3        ADD     26000,7                111  1172 6000
                STA     26000,7                112  3272 6000
                NOP                            113  2620 0000
                BRU     * -1                   114  1407 7777
READ
 DATA b4        ADD     27200,7                115  1172 7200
                STA     27200,7                116  3272 7200
                NOP                            117  2620 0000
                BRU     * -1                   120  1407 7777
READ
 DATA b5        ADD     30400,7                121  1173 0400
                STA     30400,7                122  3273 0400
                NOP                            123  2620 0000
                BRU     * -1                   124  1407 7777
```

```
READ
 DATA b6   ADD     31600,7                  125  1173 1600
           STA     31600,7                  126  3273 1600
           NOP                              127  2620 0000
           BRU     * -1                     130  1407 7777
READ
 DATA b7   ADD     33000,7                  131  1173 3000
           STA     33000,7                  132  3273 3000
           NOP                              133  2620 0000
           BRU     * -1                     134  1407 7777
READ
 DATA b8   ADD     34200,7                  135  1173 4200
           STA     34200,7                  136  3273 4200
           NOP                              137  2620 0000
           BRU     * -1                     140  1407 7777
READ
 DATA b9   ADD     35400,7                  141  1173 5400
           STA     35400,7                  142  3273 5400
           NOP                              143  2620 0000
           BRU     * -1                     144  1407 7777
SET
A/D ch. a  LDA     CONTROL CLOCK            145  0004 0061
           OUT     A/D ch. a                146  2504 1004
           NOP                              147  2620 0000
           BRU     * -1                     150  1407 7777
READ
 DATA a14  ADD     36600,7                  151  1173 6600
           STA     36600,7                  152  3273 6600
           NOP                              153  2620 0000
           BRU     * -1                     154  1407 7777
RESET
A/D ch. b  LDA     CONTROL CLOCK            155  0004 0051
           OUT     A/D ch. b                156  2504 1024
           NOP                              157  2620 0000
           BRU     * -1                     160  1407 7777
INX "7"    INX     1,7                      161  2670 0001
           TXH     1161,7                   162  2473 6617
           BTR     * +5                     163  3004 0005
           LXK     0,7                      164  0770 0000
           INX     1,5                      165  2650 0001
TEST
AVERAGE
COMPLETE   TXH     456,5                    166  2453 7322
           BTS     FINI                     167  3404 0025
           NOP                              170  2620 0000
           BRU     * -1                     171  1407 7777
           NOP                              172  2620 0000
           TXH     40,6                     173  2463 7740
           BTR     * +2 WAIT LOOP           174  3004 0002
40th
POINTER
ENTER      LXK     0,6                      175  0760 0000
```

```
COMPLETE
PULSE
TRAIN       NOP                              13176  2620 0000
            BRU     * -1                       177  1407 7777
FINI        IAI1    INHIBIT IU                 214  2503 0000
            LDA     NOP                        215  0004 0014
            STA     265                        216  3200 0265
            LMO     1's                        217  0506 0000
            LMR                                220  2500 0302
            LDK     3000                       221  4000 3000
            OUT                                222  2504 1024
            LDP                                223  1504 0001
PATCH 1     LXK     0,3                        237  0730 0000
            LDZ     INITIALIZE PULSE           240  0500 0000
            OUT     1001                       241  2504 1001
            PAI                                242  2502 0000
            NOP                                243  2620 0000
            BRU     * -1                       244  1407 7777
PATCH 2     ADD     21000,7                    245  1172 1000
            STA     21000,7                    246  3272 1000
            NOP                                247  2620 0000
            BRU     * -1                       250  1407 7777
PATCH 3     INX     1,3                        251  2630 0001
            TXH     1,3                        252  2433 7767
            BTR     * +3                       253  3004 0003
            LDA     "BRU to READ DATA"         254  0001 3230
            STA     265                        255  3200 0265
            NOP                                256  2620 0000
            BRU     * -1                       257  1407 7777

  *TABLE
PLACE       BSS                                224  7777 7777
CONTROL SCOPE       DATA                       225  4000 0000
CONTROL CLOCK       DATA                       226  0014 2400
MASK                DATA                       227  7775 7777
IU CONSTANT         DATA BRU to READ DATA      230  1401 3026
                    CON    "NOP"               231  2620 0000
                    DATA "BRU to PATCH 3"      232  1401 3251
```

D/A DISPLAY

```
  *D/A DISPLAY MAIN
           STX1     PLACE                      17200  0614 0023
           LXK      0,7                          01   0770 0000
SAVE X7    STX      TABLE COUNTER(TEMP1),7       02   0674 0020
           LDA      DISPLAY SEQ,7                03   0071 7224
           STA      EXEC. #1                     04   3204 0014
           LDA      DISPLAY SEQ +1,7             05   0071 7225
           STA      EXEC. #2                     06   3204 0013
           SPB      REPACK TABLE                 07   3304 0033
           NOP                                   10   2620 0000
           NOP                                   11   2620 0000
           SPB      D/A DISPLAY                  12   3304 0054
NEXT
 DISPLAY   LDX      TEMP 1,7                     13   1674 0007
           INX      2,7                          14   2670 0002
           TXH      X7 ≥ 15                      15   2473 7763
           BTR      * -14(1)                     16   3007 7764
           LPR                                   17   3504 0004
           BSS      EXEC. #1                   17220  7777 7777
           BSS      EXEC. #2                     221  7777 7777
           BSS      TEMP 1, TABLE COUNTER        22   7777 7777
           BSS      PLACE                        23   7777 7777
  *DISPLAY SEQUENCE
DISPLAY
 SEQ.       TABLE 1  DATA al4                     24   0073 6600
                                                  25   2473 6617
            TABLE 2  DATA b0                      26   0072 2200
                                                  27   2473 6617
            TABLE 3  DATA b1                      30   0072 4600
                                                  31   2473 6617
            TABLE 4  DATA b2                      32   0072 4600
                                                  33   2473 6617
            TABLE 5  DATA b3                      34   0072 6000
                                                  35   2473 6617
            TABLE 6  DATA b4                      36   0072 7200
                                                  37   2473 6617
            TABLE 7  DATA Sin. F                  40   0073 5400
                                                  41   2473 6617
            EXEC. 1  LDA TABLE 7
            EXEC. 2  TXH N,7
```

```
  *REPACK TABLE AND APD ΔT
          STX1    PLACE                      17242  0614 0023
          LXK     0,7 Y COUNTER                243  0770 0000
          LXK     0,7 ΔT COUNTER               244  0760 0000
(1)       XEC     17220 to (LDA TABLE, 7)      245  0407 7753
          SLA     4 BITS                       246  4500 2044
          ANA     MASK                         247  2004 0030
          BRU     PATCH(17300)                 250  1401 7300
          STA     10000,7 DISPLAY TABLE,7      251  3271 0000
          INX     ΔT,6                         252  2660 0002
          INX     1,7                          253  2670 0001
          EXC     17221 to (TXH N,7)           254  0407 7745
          BTR     REPEAT (1)                   255  3007 7770
  *STORE Y=D IN THE REST OF TABLE
(2)       LDA     X6                           256  0000 0006
          STA     DISPLAY TABLE,7              257  3271 0000
          INX     ΔT,6                         260  2660 0003
          INX     1,7                          261  2670 0001
          TXH     1161,7                       262  2473 6617
          BTR     * (2)                        263  3007 7773
          LPR                                  264  3504 0001
          BSS     PLACE                        265  7777 7777
  *D/A DISPLAY PROTION
          LXK     0,7                          266  0770 0000
          LDA     DISPLAY,X7                   267  0070 0000
          OUT     D/A                          270  2504 1003
          INX     1,7                          271  2670 0001
          TXH     1161,7(# of display pts)     272  2473 6617
          BTR     * -4                         273  3007 7774
  *CHECK DEMAND IF NOT SET THEN REPEAT DISPLAY, IF NOT GO
   ON TO NEXT FCN
          JND                                  274  2504 0000
          LPR                                  275  3500 0001
          BRU     * -10                        276  1407 7770
          CON1    MASK                         277  7777 0000
PATCH     JND                                  300  2506 0000
          LDA                                  301  0004 0003
          ADD                                  302  1100 0006
          BRU                                  303  1401 7251
                  CON=3777 0000                304  7777 7777
```

STORE SIN θ PROGRAM

```
*INTO LOCATIONS 35400 to 36,561
        STX PLACE, 1                    13350  0614 0025
        FMS                                51  7401 4000
        LXK 0,7                            52  0770 0000
        LDZ                                53  0500 0000
        STA, Q                             54  3200 0010
        DST TEMP                           55  6304 0016
        SPB to SIN F                       56  3300 2340
        FIX                                57  7400 0010
        NOP                                60  2620 0000
        STA 35400,7                        61  3273 5400
        DLD CON 1 (floating pt.)           62  4104 0007
        FAD TEMP                           63  7004 0010
        DST TEMP                           64  6304 0007
        INX 1,7                            65  2670 0001
        TXH 1161,7                         66  2473 6617
        BTR                                67  3007 7767
        LPR                                70  3504 0005
        DATA CON 1                         71  1752 4467
        DATA CON 1                         72  3537 1300
        TEMP                               73  7777 7777
        TEMP                               74  7777 7777
        BSS PLACE                          75  7777 7777
```

MINI EXECUTIVE PROG.(SELECT DATA)

```
        STX1    PLACE                   13300   0614 0012
        LXK     0,4                       01    0740 0000
        STX     TEMP,4                    02    0644 0011
        SPB     CROSS-CORR AND PRINT      03    3301 3500
        LDX     TEMP,4                    04    1644 0007
        INX     4,4                       05    2640 0004
        TXH     24,4(also indicates
                the # of lines to be
                printed)                  06    2443 7754
        BTR     * -5                      07    3007 7773
        LPR                               10    3504 0002
        NOP                               11    2620 0000
        BSS     PLACE                     12    7777 7777
        BSS     TEMP                      13    7777 7777
*CROSS-CORRELATION AND PRINT
        STX1    PLACE                   13500   0614 0073
        LXK     0,7                       01    0770 0000
        LXK     0,6                       02    0760 0000
        LXK     234,5                     03    0750 0234
*CLEAR TABLE
        LDZ                               04    0500 0000
        STA     13563,6                   05    3264 0056
        INX     1,6                       06    2660 0001
        TXH     10,6                      07    2463 7770
        BTR     * -3                      10    3007 7775
*CALC SUMS
        LDZ                               11    0500 0000
        XEC,4 (LDQ A,7)                   12    0441 3400
        XEC,4 (MPY C,7)                   13    0441 3402
        DAD,4 (TEMP 1)                    14    5104 0047
        DST,4 (TEMP 1)                    15    6304 0046
        LDZ                               16    0500 0000
        XEC,4 (LDQ B,7)                   17    0441 3401
        XEC,4 (MPY C,7)                   20    0441 3402
        DAD,4 (TEMP 2)                    21    5104 0044
        DST,4 (TEMP 2)                    22    6304 0043
        LDZ                               23    0500 0000
        XEC,4 (LDQ A,7)                   24    0441 3400
        XEC,4 (MPY C π/2,5)               25    0441 3403
        DAD,4 (TEMP 3)                    26    5104 0041
        DST,4 (TEMP 3)                    27    6304 0040
        LDZ                               30    0500 0000
        XEC,4 (LDQ B,7)                   31    0441 3401
        XEC,4 (MPY C π/2,5)               32    0441 3403
        DAD,4 (TEMP 4)                    33    5104 0036
        DST,4 (TEMP 4)                    34    6304 0035
```

```
          INX       1,7                          13535  2670 0001
          INX       1,5                             36  2650 0001
          TXH       1161,5                          37  2453 6617
          BTS  to   RESET 5                         40  3404 0021
          TXH       1161,7                          41  2473 6617
          BTR  to   REPEAT(LOC. 13511
                           CALC. SUM)               42  3007 7747
*DONE, SUMS AND PRINT
          BRU  to   RECYCLE                         43  1401 3320
          BRU       *                               44  1404 0000
          LXK       0,3                             45  0730 0000
          DLD       TEMP 1,3                        46  4134 0015
          DRA                                       47  4500 4404
          SPB  to   (FIX PT. BINARY to
                     FIX PT. DECIMAL)               50  3300 1537
          LDK       K=1610                          51  4000 1610
          SPB  to   PRINT                           52  3300 1640
          INX       2,3                             53  2630 0002
          TXH       10,3(indicates how many
                    # of groups in a row)           54  2433 7770
          BTR       * -7(LOC. 13546)                55  3007 7771
          LDA       CON                             56  0004 0016
          SPB  to   PRINT                           57  3300 1640
          LPR                                       60  3504 0013
*RESET "5"
          LXK       0,5                             61  0750 0000
          BRU       * -21(LOC. 13541)               62  1407 7757
*DATA
          BSS       TEMP 1  A1C1                    63  7777 7777
                                                    64  7777 7777
          BSS       TEMP 2  B1C1                    65  7777 7777
                                                    66  7777 7777
          BSS       TEMP 3  A1C1π/2                 67  7777 7777
                                                    70  7777 7777
          BSS       TEMP 4  B1C1π/2                 71  7777 7777
                                                    72  7777 7777
          BSS       PLACE                           73  7777 7777
          DATA      CON=400 13576                   74  4001 3575
          DATA      LFLFCR=0240 5015                75  0240 6415
          DATA      CRLF 0=0320 5000                76  0320 5000
```

DATA SELECTION TABLE

```
A           LDQ       b0,7                          13400   4272 2200
B           LDQ       b1,7                            01    4272 3400
C           MPY       b9,7                            02    5573 5400
            MPY       b9,5                            03    5553 5400
A           LDQ       b2,7                            04    4272 4600
B           LDQ       b3,7   b9=C                     05    4272 6000
C           MPY       b9,7                            06    5573 5400
            MPY       b9,5                            07    5553 5400
A           LDQ       b4,7                            10    4272 7200
B           LDQ       b5,7                            11    4273 0400
C           MPY       b9,7                            12    5573 5400
            MPY       b9,5                            13    5553 5400
A           LDQ       b6,7                            14    4273 1600
B           LDQ       b7,7                            15    4273 3000
C           MPY       b9,7                            16    5573 5400
            MPY       b9,5                            17    5553 5400
A           LDQ       b8,7                            20    4273 4200
B           LDQ       a15,7                           21    4273 6600
C           MPY       b9,7                            22    5573 5400
            MPY       b9,5                            23    5553 5400


            NOP                                       13477   2620 0000

            BRU  to   RECYCLE      Locations          13543   1401 3320
  *RECYCLE  (¼(3<1557 + <167>)
            TXH       11,6                            13320   2463 7767
            BTS       BRU to WAS ONE                  13321   3404 0016
            INX       1,6                             13322   2660 0001
WAS NOT ONE
  *MULTIPLY TEMP REGION X3
            LXK       0,7                             13323   0770 0000
            DLD       TEMP 1,7                          24    4171 3563
            DAD       TEMP 1,7                          25    5171 3563
            DAD       TEMP 1,7                          26    5171 3563
            DST       TEMP 1,7                          27    6371 3563
            INX       2,7                               30    2670 0002
            TXH       10,7                              31    2473 7770
            BTR       * -6                              32    3007 7772
            LXK       0,7                               33    0770 0000
            NOP                                         34    2620 0000
            LXK       235,5                             35    0750 0235
            BRU to    CALC SUMS  LOC 13511              36    1401 3511
WAS ONE
            JNO                                         37    2506 0000
            BRU*                                        40    1404 0000
            BRU  to   13545(PRINT)                      41    1401 3545
```

APPENDIX B

Sample Printout Format of Cross-Correlated Values

After the cross-correlation has been carried out in CPU, the teletype prints out the terms in the following format:

012964 012964 067403 067402

012964 012965 067402 067403

012965 012964 067402 067402

012965 012964 067402 067401

012965 -019439 067402 -004932

and these terms are identified respectively as follows:

$b_o c\cos\phi_o$ $b_o c\cos\phi_o$ $b_o c\sin\phi_o$ $b_o c\sin\phi_o$

" " " "

" " " "

" " " "

" $a_{15} c\cos\phi_A$ " $a_{15} c\sin\phi_A$

From the above terms we obtain $(\phi_o - \phi_A)$ and b_0/a_{15} which are the phase difference between the zeroth echo and the input signal, and the amplitude ratio of the zeroth echo to input signal, respectively.

APPENDIX C

THEORY OF THE FABRY-PEROT INTERFEROMETER

INTRODUCTION

The Fabry-Perot interferometer is a multiple beam interferometer characterized by interference between many rays. The basic advantage over two beam interferometers such as the Michelson type is greatly increased resolution, roughly dependent on the number of interfering beams.

The construction of a Fabry-Perot consists of two plane partially reflecting surfaces oriented parallel to each other. These surfaces may be the opposite faces of a quartz plate or other similar low thermal expansion material. Such a fixed gap Fabry-Perot is known as an etalon. The other major design incorporates two opposed partially reflecting mirrors a distance d apart, where d may be varied. In both designs the gap between the surfaces is constant over the whole area to 1/50 to 1/200 of the wavelength of green light, depending on the specifications of the particular instrument. Our instrument, a Burleigh Instrument RC 10 is of the opposed mirrow type with the gap distance accurate to 1/200 wavelength.

THEORY

A treatment of the basic Fabry-Perot can be treated by considering the infinite number of partial reflections in the cavity. Referring to Fig.1, the path length difference between two successive reflections E_1 and E_2 is given by $\Delta = 2d \cos \theta$ where d is the distance between the plates and θ is the angle of incidence of the plane wave. This path difference introduces a correponding phase difference

$$\delta = k\Delta = \frac{4\pi d \cos \theta}{\lambda} \qquad (1)$$

where λ is the wavelength of light between the plates.

If the complex amplitude of the incident wave is taken as E_o, then the amplitudes of the transmitted waves are

$$E_1 = E_o t^2 \qquad E_2 = E_o t^2 r^2 e^{i\delta} \qquad E_3 = E_o t^2 r^4 e^{2i\delta} \text{ , etc.}$$

where r and t are the amplitude reflection and transmission coefficients. A constant phase factor corresponding to a single pass through the plates and common to all terms has been left out. If the transmitted waves are brought together, as by a focussing lens their amplitudes will add, yielding

$$E_t = E_o t^2 (1 + r^2 e^{i\delta} + r^4 e^{2i\delta} + \dots) \tag{2}$$

The term within the parentheses is a geometric series and can be evaluated, thus we get

$$E_t = \frac{E_o t^2}{1 - r^2 e^{i\delta}} = \frac{E_o T}{1 - R e^{i\delta}} \tag{3}$$

where $R = r^2$ and $T = t^2$ are the fraction of intensity reflected and transmitted at each interface. The quantity of interest is the fraction of intensity transmitted through the Fabry-Perot and is given by

$$\frac{I_t}{I_o} = \frac{\frac{1}{2} E_t E_t^*}{\frac{1}{2} E_o E_o^*} = \frac{T^2}{1 + R^2 - 2R \cos \delta} \tag{4}$$

With the substitutions $T = 1 - R$ (no mirror losses) and $\cos \delta = 1 - 2 \sin^2 \delta/2$ we finally arrive at the Fabry Perot transmission equation

$$\frac{I_t}{I_o} = \frac{1}{1 + \frac{4R \sin^2 (\delta/2)}{(1 - R)^2}} \tag{5}$$

This is the well-known Airy function. Its plot as a function of δ for various values of R is shown in Fig.2. Equation (5) is periodic in its argument δ and becomes a maximum for $\delta = 2n\pi$, $m = 0,1,2, \ldots$. Equating this expression with the definition of δ from Eq. (1), we get the maxima condition for Fabry-Perot transmission

$$2d \cos \theta = m\lambda \qquad m = 0,1,2, \ldots . \tag{6}$$

There are three quantities of interest referring to the Airy function. One quantity, the contract C, is the ratio of transmission maxima to transmission minima. Transmission maxima occurs for $\sin^2 \delta/2 = 0$, and transmission minima for $\sin^2 \delta/2 = 1$. Substituting into Eq. (5) we have

$$\left(\frac{I_t}{I_o}\right)_{max} = 1, \quad \left(\frac{I_t}{I_o}\right)_{min} = \frac{1}{1 + \frac{4R}{1-R}}$$

therefore

$$C = \frac{(I_t/I_o)_{max}}{(I_t/I_o)_{min}} = 1 + \frac{4R}{1-R} \tag{7}$$

A plot of contrast C versus reflectivity R is shown in Fig.3. Notice how rapidly contrast rises with R. In a real instrument, however, there are other factors more important than mirror reflectivity which limit the contrast, such as deviations in true surface flatness and variations in gap width over the aperture. The theoretical contrast of our instrument with R = 0.985 is 17,512. The actual contrast available is, however, closer to 1,000.

The second quantity of interest is the Free Spectral Range ($\Delta\lambda$FSR). Like the grating spectrometer the Fabry Perot suffers from overlapping of orders. The range of wavelengths which can be displayed in the same spectral

order without overlapping is called the Free Spectral Range. To derive this assume any λ and λ' are entering the Fabry-Perot such that the $(m+1)^{th}$ order of λ' exactly overlaps the nth order of λ. Clearly then, $\lambda'-\lambda$ provides an upper bound on the wavelength shift we can have without overlapping orders. Since the maximum condition ($\cos\theta \simeq 1$) is met for both λ and λ' at d (see Fig. 4) we have

$$2d = (m+1)\lambda' \tag{8a}$$

$$2d = m\lambda \tag{8b}$$

Solving for m in Eq. (8b) and substituting in (8a) we get

$$\Delta\lambda FSR = \lambda - \lambda' = \frac{\lambda\lambda'}{2d} \simeq \frac{\lambda^2}{2d} \tag{9}$$

The third quantity of interest is known as the Finesse. It is defined as the ratio of the Free Spectral Range (FSR) to the full width at half height (FWHH) of the transmission function of the Fabry Perot. In the ideal case the transmission function is the Airy function and the Finesse is a function of the mirror reflectivity alone. This is known as the Reflectiviry finesse.

The FWHH may be computed by setting $I_t/I_o = 1/2$ in the Airy formula [Eq.(5)]. We find that

$$\sin^2 \delta/2 = \frac{(1 - R)^2}{4R}$$

or

$$\sin \delta/2 = \pm \frac{1 - R}{2\sqrt{R}}$$

There are two values of δ, δ_1, and δ_2 which satisfy this condition, see Fig. 5. Since δ_1 and δ_2 are nearly equal to $2m\pi$ we can use the small angle approximation, yielding

$$\delta_1 = \frac{1 - R}{\sqrt{R}} + 2m\pi, \quad \delta_2 = \frac{R - 1}{\sqrt{R}} + 2m\pi.$$

Their difference $\delta_1 - \delta_2$ is given by

$$\delta_1 - \delta_2 = \frac{2(1 - R)}{\sqrt{R}} \tag{10}$$

From the definition of δ, Eq.(1) and referring to Fig. 5, we have

$$\delta_1 = \frac{4\pi d \cos \theta}{(\lambda + \Delta\lambda/2} \quad \text{and} \quad 2 = \frac{4\pi d \cos \theta}{(\lambda - \Delta\lambda/2)}$$

thus we have

$$\delta_1 - \delta_2 = \frac{1}{\lambda} (4\pi d \cos \theta) \left(1 - \frac{\Delta\lambda}{2\lambda}\right) - \frac{1}{\lambda} (4\pi d \cos \theta) \left(1 + \frac{\Delta\lambda}{2\lambda}\right)$$

Since $\frac{\Delta\lambda}{2} << \lambda$

$$\delta_1 - \delta_2 = \frac{\Delta\lambda}{\lambda 2} (4\pi d \cos \theta) \tag{11}$$

Equating this expression with Eq. (10) and solving for $\Delta\lambda$ we get as the FWHH

$$\Delta\lambda = \frac{1 - R}{\sqrt{R}} \frac{\lambda^2}{2\pi d \cos \theta} \tag{12}$$

The Finesse is simply the Free Spectral Range divided by this quantity

$$F_R = \frac{FSR}{\Delta\lambda} = \frac{\lambda^2 \sqrt{R} 2\pi d \cos \theta}{2d (1 - R)\lambda^2}$$

since $\cos \theta \approx 1$

$$F_R = \frac{\pi \sqrt{R}}{1 - R} \tag{13}$$

The actual instrument finesse is more than a function of mirror reflectivity. The other major factors limiting the net finesse are: (1) lack of parallelism and/or planeness of mirrors, (2) the size of the pinhole following the interferometer (determines the angular spread of the light entering the instrument) and (3) diffraction losses arising from the finite aperture of the interferometer. Each of these factors will broaden the instrument functions independently and the net instrument function will be a convolution of these

factors with the Airy function. If we approximate each of these profiles near a maximum as a Gaussian curve, we may obtain a simple expression for the net finesse. The convolution of two Gaussians is another Gaussian with a half intensity width which is the Pythagorian sum of the component half-widths. Since each Finesse is inversely Proportional to the halfwidth, we have

$$\frac{1}{F_I^2} = \sum_{i=1}^{N} \frac{1}{F_i^2}$$

where F_I is the net instrument finesse and the F_i are the component finesses. A brief description of the major component finesses follows.

Flatness finesse: $F_F = M/2$ for λ/M plate

where M is the fractional wave length deviation from planeness over the mirror aperture. Normally specified for λ = 5461 A.

Pinhole finesse: defined from $d - \frac{d}{\cos\theta} = \left(\frac{1}{F_p}\right)\lambda/2$ (15)

therefore $F_P = \frac{4\lambda f}{D^2 d}$, see Fig. 6. This will be treated in more detail in the next section.

Diffractive finesse: $F_D = \frac{2D^2}{\lambda d}$ (on axis) (16)

where D is the diameter of the limiting aperture. This factor is usually negligible except for very small apertures (less than 1 mm).

THE FABRY-PEROT AS A SPECTORMETER

There are two ways a Fabry-Perot may be used as a spectrometer. The first way which may be called the static or photographic method fixes the distance d and measures λ as a function of θ. The second method may be termed the photoelectric or scanning method. In this method θ is fixed usually to 0° and λ is measured as a function of d.

The photographic method uses the setup shown in Fig.7. The pattern in plane 1 produced by an extended monochromatic source is a series of concentric rings. The Airy function, Eq. (5), is a maximum for $2d \cos\theta = m\lambda$ Now is axially symmetric and the lens L_2 converts θ into r by $r = f_2\theta$. The condition for a maximum, $\cos\theta \frac{m\lambda}{2d}$ then becomes $\cos\frac{r}{f_2} = \frac{m\lambda}{2d}$. In the small angle approximation this becomes

$$1 - \frac{r}{2f_2} = \frac{m\lambda}{2d} \tag{17}$$

This is the basic equation for the photographic method. If we wish to plot the Airy function as a function of r (i.e., the location of the rings) we must have a starting point. Let's say there is a central maximum for the incident wavelenght λ_A of the order m_o so $2d = m_o\lambda_A$. We will subscript the pth ring from the center as r_{PA} and let $m = m_o + p$. In this way we can solve for the radius of the pth ring,

$$r_{PA}^2 = 2f_2^2[1 - \frac{(m_o - p)\lambda_A}{2d}]$$

since $m_o\lambda_A = 2d$, we get

$$r_{PA}^2 = \frac{f_2^2\, P\lambda_A}{d} \tag{18}$$

This plot is shown in Fig.8.

Unfortunately a central maximum in a photograph of the spectra is not always the case, more often the case is that the first maximum is a ring of a certain radius. This more general case is treated as follows. The Fabry-Perot maxima condition, Eq. (6), can be written

$$\frac{\cos\theta}{} = \frac{m}{2d} \tag{19}$$

For m and d held constant, the quantity cos θ/λ is a constant. Thus if two wavelenghts λ_A and λ_B are entering the Fabry-Perot they will have maxima of the same order $m = m_o$ at the angles θ_{AO} and θ_{BO} where

$$\frac{\cos\theta_{AO}}{\lambda_A} = \frac{\cos\theta_{BO}}{\lambda_B} \tag{20}$$

Here, the first subscript refers to the wavelength and the second refers to the relative order ($0 = m_o$, $1 = m_o + 1$, etc.). Since we are dealing with small angles we may use the approximations $\cos\theta = 1 - \frac{\theta^2}{2}$ and $\theta = r/f$. Condition (20) then becomes

$$\frac{1 - \frac{r_{AO}^2}{2f^2}}{\lambda_A} = \frac{1 - \frac{r_{BO}^2}{2f^2}}{\lambda_B}$$

or

$$\lambda_A\left(\frac{1 - \frac{r_{BO}^2}{2f^2}}{1 - \frac{r_{AO}^2}{2f^2}}\right) = \lambda_B$$

since $\frac{r_{AO}^2}{2f^2} \ll 1$

$$\lambda_A\left(1 - \frac{r_{BO}^2}{2f^2}\right)\left(1 + \frac{r_{AO}^2}{2f^2}\right) = \lambda_B$$

multiplying and ignoring higher order terms

$$\lambda_A\left(1 + \frac{r_{AO}^2}{2f^2} - \frac{r_{BO}^2}{2f^2}\right) = \lambda_B$$

Finally

$$\frac{\lambda_A}{2f^2}\left(r_{AO}^2 - r_{BO}^2\right) = \lambda_B - \lambda_A \tag{21}$$

This equation allows us to calculate λ_B if the other parameters are known. The effective focal length of the system f is difficult to measure, however, because the imaging system usually contains magnifying optics and a camera in addition to the primary lens (see Fig.7).

We wish to eliminate f from Eq. (21). The maxima condition (19) may be rewritten as $\frac{\cos\theta}{m} = \frac{\lambda}{2d}$. For fixed $\lambda = \lambda_A$ and fixed d, $\frac{\cos\theta}{m}$ is a constant for all θ and integers m. Thus

$$\frac{\cos\theta_{A1}}{m_o + 1} = \frac{\cos\theta_{AO}}{m_o} = \frac{\lambda_A}{2d}$$

Using the small angle approximation as before

$$\frac{1 - \frac{r_{A1}^2}{2f^2}}{m_o + 1} = \frac{1 - \frac{r_{AO}^2}{2f^2}}{m_o} = \frac{\lambda_A}{2d} \tag{22}$$

These are two equations in two unknowns m_o and f. Using the left side of (22) we have

$$m_o\left(1 - \frac{r_{A1}^2}{2f^2}\right) = (m_o + 1)\left(1 - \frac{r_{AO}^2}{2f^2}\right)$$

multiplication yeilds

$$m_o - \frac{m_o r_{A1}^2}{2f^2} = m_o - \frac{m_o r_{AO}^2}{2f^2} - \frac{r_{AO}^2}{2f^2} + 1$$

Simplifying, we now have an expression for m_o

$$m_o = \frac{2f^2}{r_{AO}^2 - r_{A1}^2} \tag{23}$$

Substituting this in the right side of Eq. (22) we have

$$\frac{1}{2f^2}\left(1 - \frac{r_{AO}^2}{2f^2}\right)\left(r_{AO}^2 - r_{AL}^2\right) = \frac{\lambda_A}{2d}$$

Ignoring $\frac{r_{AO}^2}{2f^2}$ because it is smaller than 1, we may solve for f

$$f^2 = \frac{d}{\lambda_A} (r_{AO}^2 - r_{A1}^2) \tag{24}$$

This is the quantity which we were looking for.

Substituting this result into Eq. (21) we get

$$\frac{\lambda_B \lambda_A}{2d} \left(\frac{r_{AO}^2 - r_{BO}^2}{r_{AO}^2 - r_{A1}^2} \right) = \lambda_B - \lambda_A$$

which, since $\lambda_B \quad \lambda_A$

$$\frac{\lambda_A^2}{2d} \left(\frac{r_{AO}^2 - r_{BO}^2}{r_{AO}^2 - r_{A1}^2} \right) = \lambda_B - \lambda_A$$

but $\frac{\lambda_A^2}{2d} = \Delta\lambda FSR$ so finally

$$\lambda_B - \lambda_A = (\Delta\lambda FSR) \left(\frac{r_{AO}^2 - r_{BO}^2}{r_{AO}^2 - r_{A1}^2} \right) \tag{25}$$

A graphical interpretation is given in Fig. 9.

Data that we have taken from Brillouin scattering measurements on several different liquids using the photographic method is located in the data section of this report.

The photoelectric or scanning method of Fabry-Perot spectroscopy obtains a spectra by varying the optical path length through the plates with θ held constant. The condition for maximum transmittance through the Fabry-Perot, Eq. (6), can be written

$$2nd \cos \theta = m\lambda.$$

The index of refraction n has not been included in previous discussions because it was considered constant and nearly equal to one. Thus we see

scanning may be done by either changing n or directly changing the distance d between the plates. The index of refraction may be changed by enclosing the Fabry-Perot in a pressure tight container and changing the pressure of the enclosed gas. Pressure scanning, as this method is called, relies on the fact that over a considerable range of pressures, the refractive index of a gas is directly proportional to the pressure.

The distance d can be directly changed by employing piezoelectric transducers. These transducers are placed symmetrically behind one mirror holder. Applying voltage to these transducers in parallel serves to translate that mirror, thus changing d. This method has numerous advantages over pressure scanning. The scanning rate can be much faster and the possibility exists of applying feedback voltages to the transducers to correct for drift thus maximizing the instrument finesse. Since our instrument employs piezoelectric scanning we will restrict our discussion to this method.

Unlike the photographic method, the scanning method fixes θ and measures λ as a function of d. An advantage of this method is that the spectra may be displayed on a scope or chart recorder, thus showing the line shape as well as the line position. This method has a additional advantage in that the results of each scan may be recorded in the memory of a computer. If the results of each scan are coherently added to the previous and accumulated over time the signal-to-noise ratio of the output spectra will improve by $\sqrt{N}$ where N is the number of scans. This procedure is known as signal averaging.

Assuming we are operating within the FSR in the output plane P of Fig. 10 different wavelengths will produce rings of different radii so by cutting an annular hole in a screen before the detector only a certain band of wavelengths will be detected such that the maximum condition

$$2d \cos \theta = m\lambda$$

is met, where θ is the angle of the annulus. A band of wave lengths will be transmitted because the annulus has a finite width which is equivalent to a spread in θ. From Eq. (6), then there will be a corresponding spread in λ. If a single wavelength is the imput this will manifest itself as a line broadening. According to Eq. (25) r^2 is directly proportional to λ. Figure 11 shows the intensity profile of the aperture and the Fabry-Perot, both plotted against r^2. The output from the Fabry-Perot has an underlying periodic structure dependent on λ. Thus we can define an annular screen finesse in a similar way to the reflectivity finesse--the ratio of the distance between peaks to the width of the aperture function.

$$F_A = \frac{B}{D} = \frac{r_{AO}^2 - r_{A1}^2}{a_o^2 - a_1^2} \tag{26}$$

but from Eq. (24)

$$r_{AO}^2 - r_{A1}^2 = \frac{f^2 \lambda_A}{d}$$

so

$$F_A = \frac{f^2 \lambda_A}{d\,(a_o^2 - a_1^2)} \tag{27}$$

In the limiting case when $a_1 = 0$ the annulus becomes a pinhole, thus we have a pinhole finesse

$$F_P = \frac{f^2 \lambda_A}{d a_o^2} = \frac{4 f^2 \lambda_A}{d D^2} \tag{28}$$

Where 0 is the pinhole diameter. Since the net finesse is given by

$$\frac{1}{F_{net}^2} = \frac{1}{F_R^2} + \frac{1}{F_F^2} + \frac{1}{F_P^2} \tag{29}$$

it is apparent that we want the pinhole finesse to be as large as practicable, so that it is not a major source of line broadening. Normally the pinhole finesse should be two to three times the desired operating finesse.

There is a tradeoff however between the size of the pinhole and the transmitted intensity. Referring to Fig. 12 we see that if the angular dispersion of the light is greater than the annular extent of the pinhole then some light is lost. But if the situation is like that shown in Fig. 12b the light is not lost and the resultant transmitted intensity is much greater. The conclusion here is that the angular spread of the input beam should be matched to the angular extent of the pinhole for the most efficient detection. This cannot always be accomplished due to finite size of object.

In our particulat case we will have an operating finesse of about 70 if possible, which dictates a pinhole finesse of 140 to 210. Referring to Eq. (28) we see that a pinhole finesse of 200 required a 250 μ pinhole. This is an angular (full diam) deviation of 9.8×10^{-4} r for a 25.4 cm fl lens. The pinholes we have and their associated pinhole finesses are as follows where f = 25.4 cm:

(cm)	D (μ)	F_P
.05	500	52
.02	200	323
.01	100	1292
.005	50	5168

Therefore the 200 μ pinhole is the most appropriate size. Since the size of our image is about 400 μ we can meet the angular matching condition be using a single lens of focal length f' = (2) (25.4) = 50.8 cm as shown in Fig. 13.

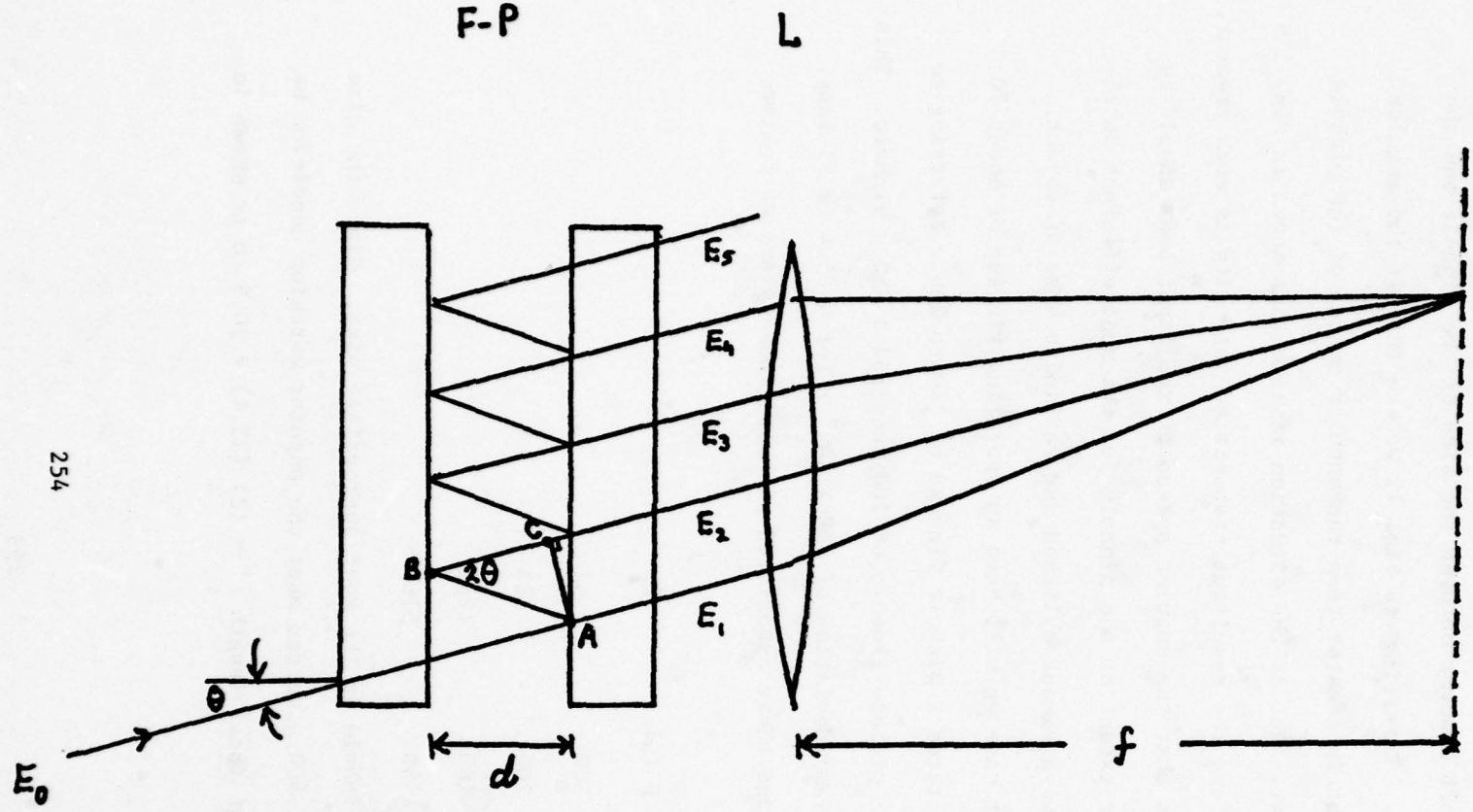

Fig.1. Fabry-Perot Geometry for Derivation of Transmission Equation

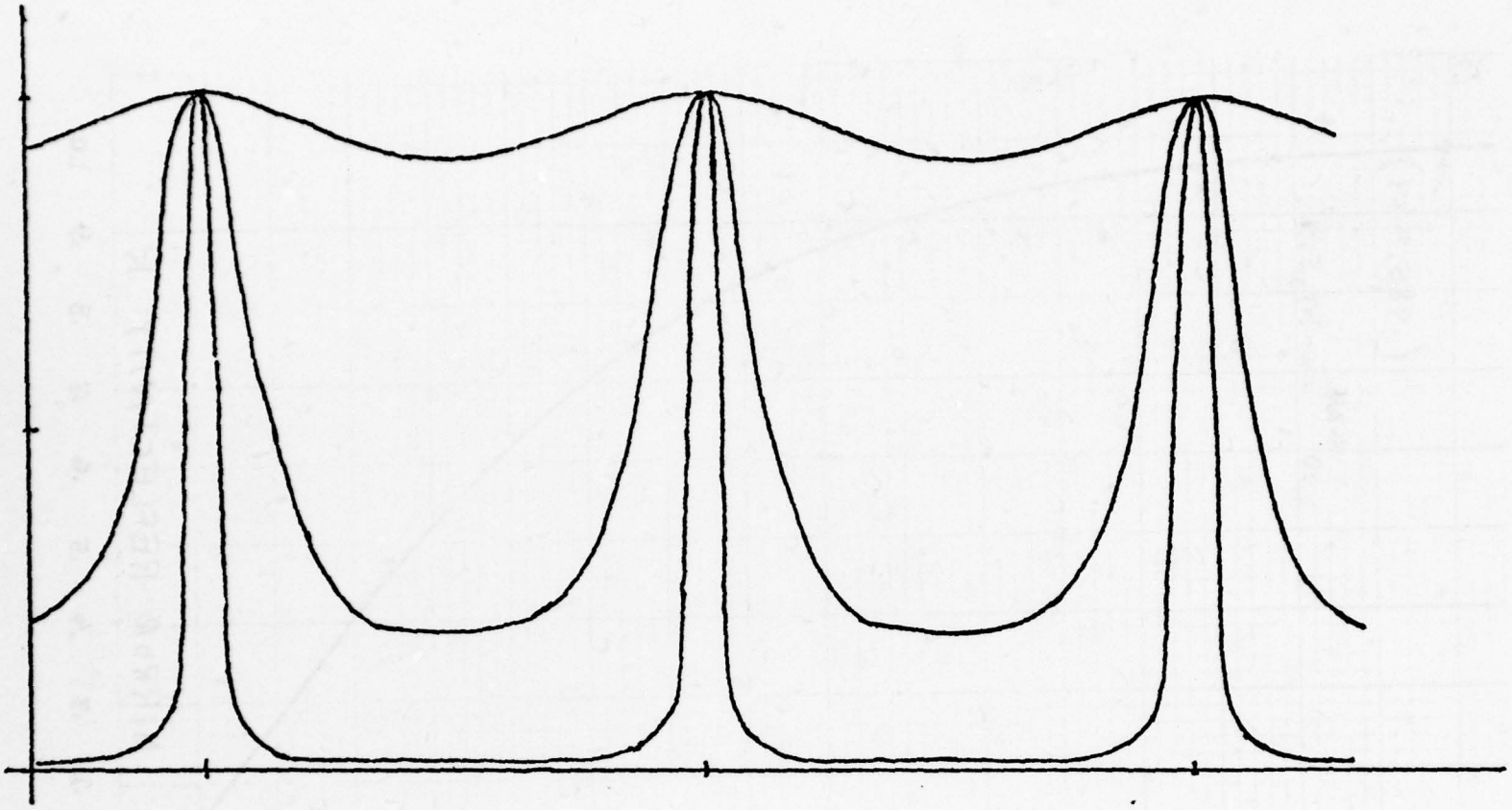

Fig.2. Airy Pattern for Various Values of Mirror Reflectivity R

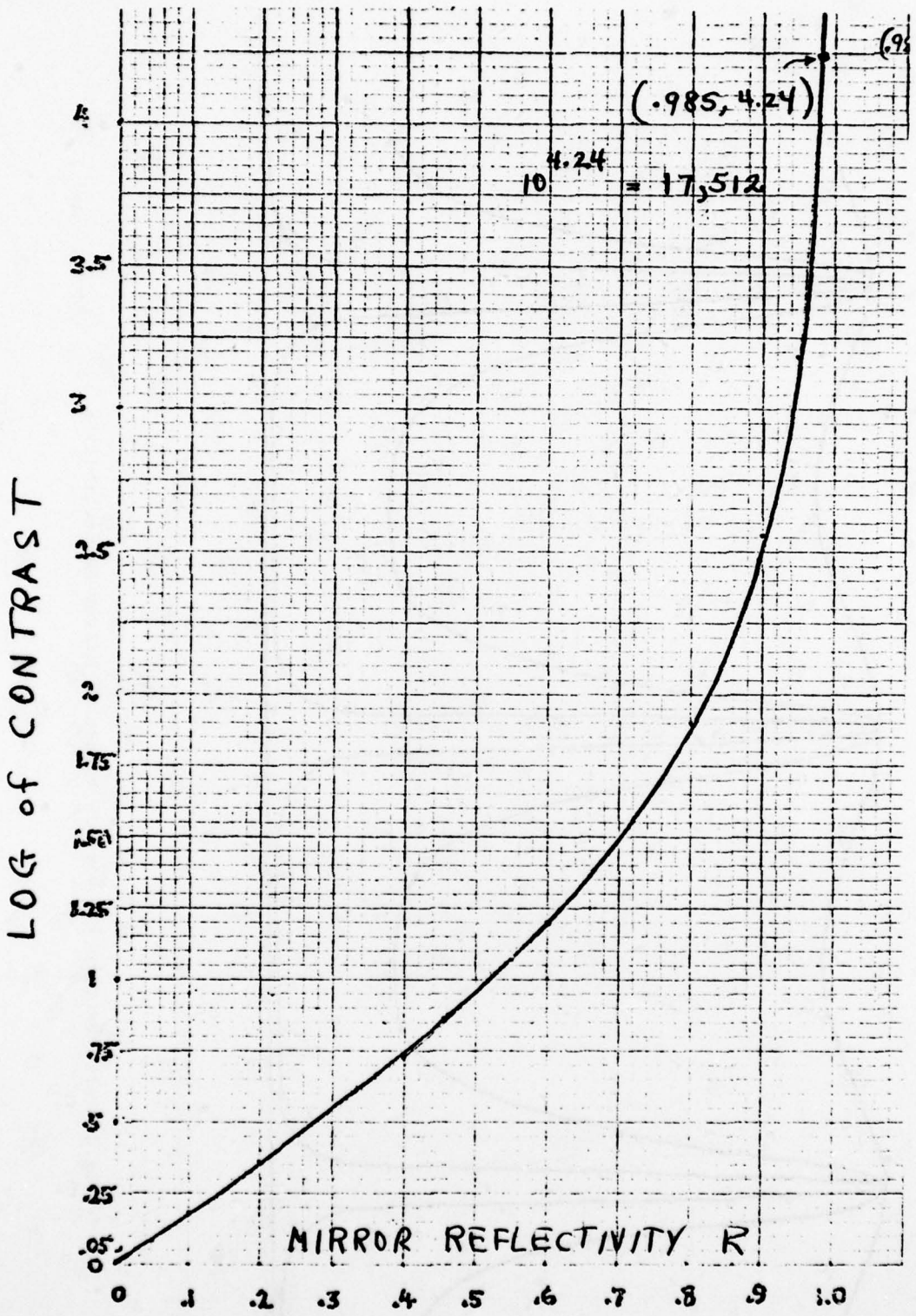

Fig.3. Fabry-Perot Contrast

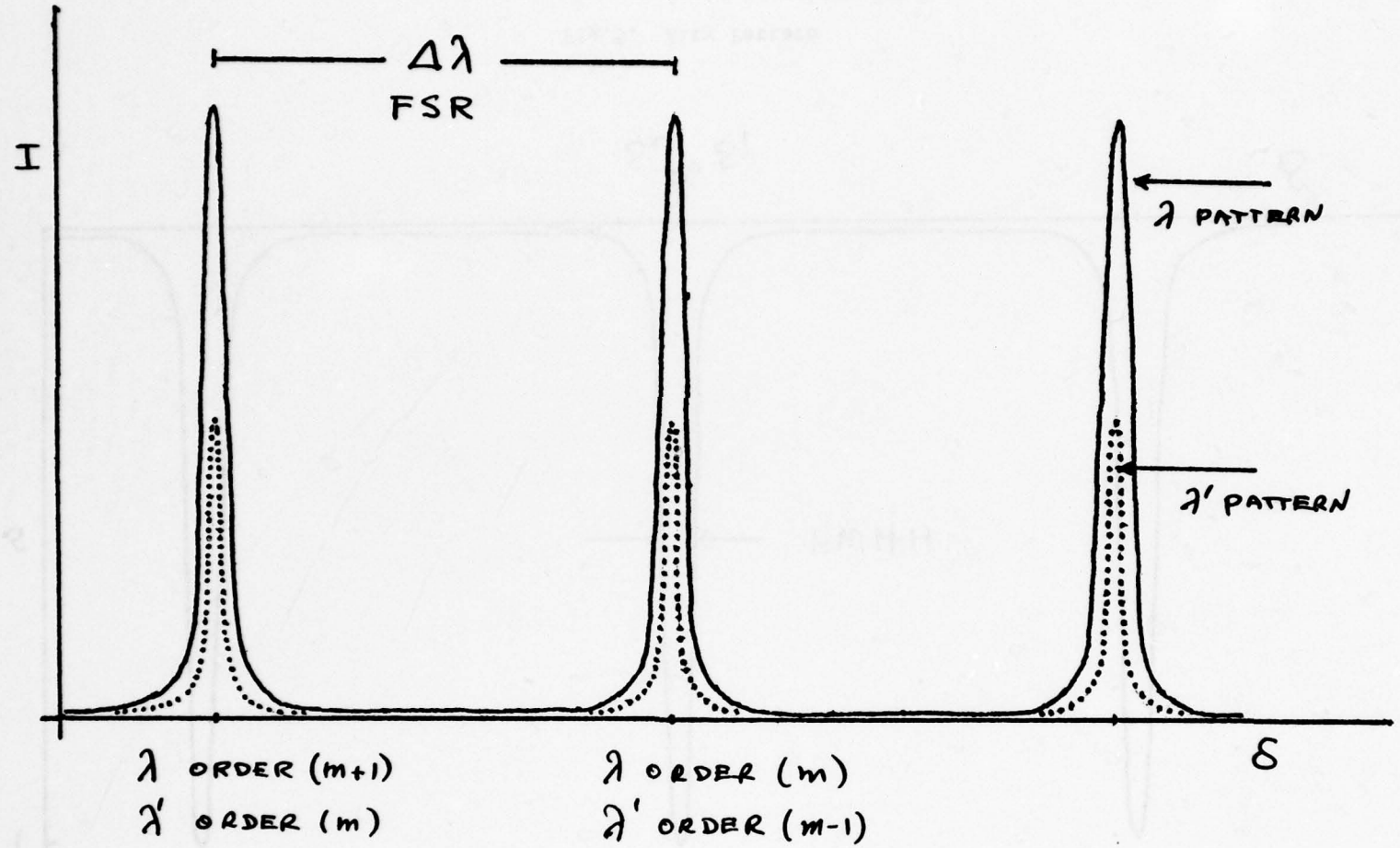

Fig.4. Intensity Contours for Two Wavelengths which Overlap

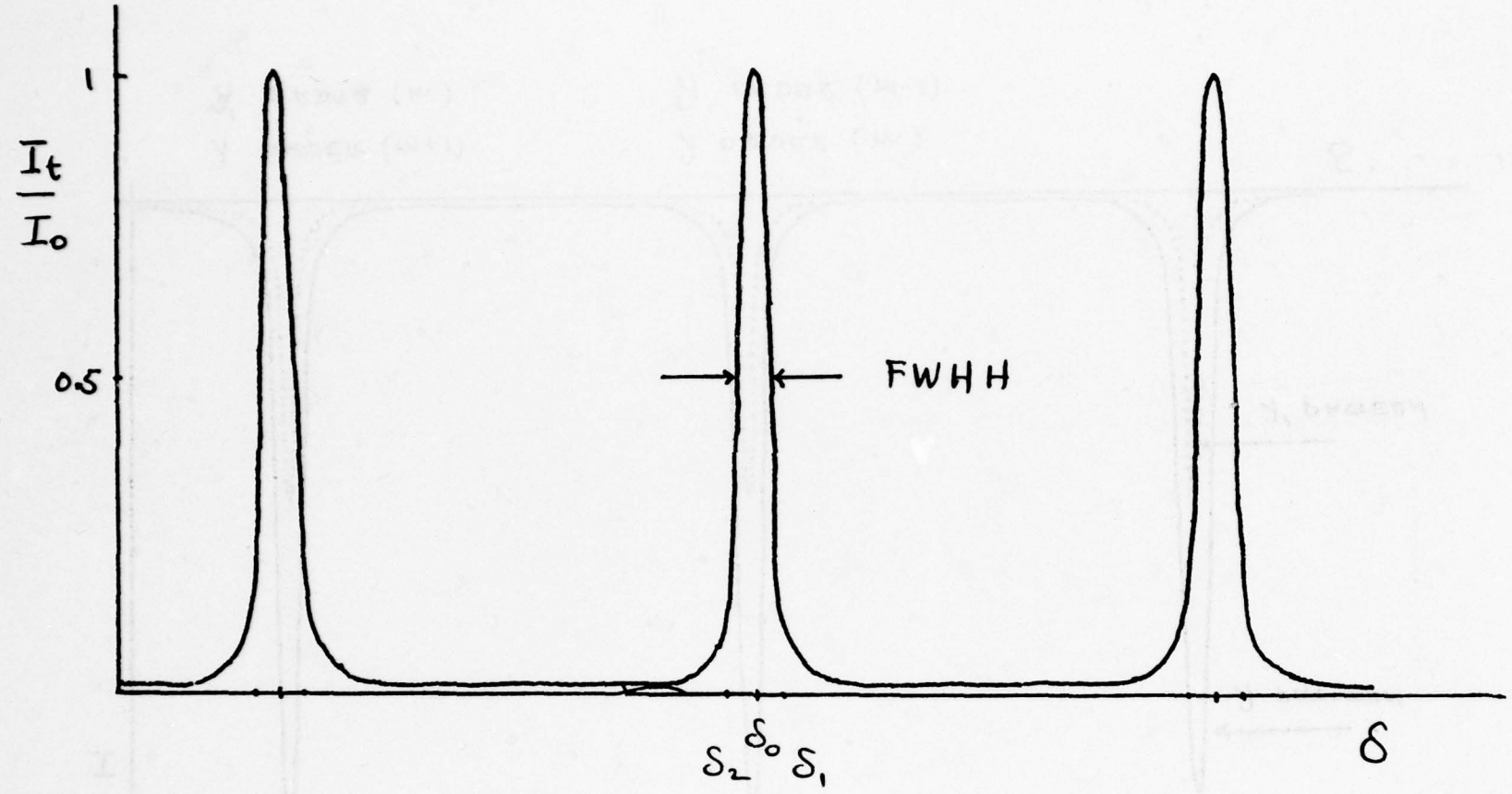

Fig.5. Airy Pattern

δ_0 is a maximum for λ

δ_1 is a maximum for $\lambda + \Delta\lambda/2$

δ_2 is a maximum for $\lambda - \Delta\lambda/2$

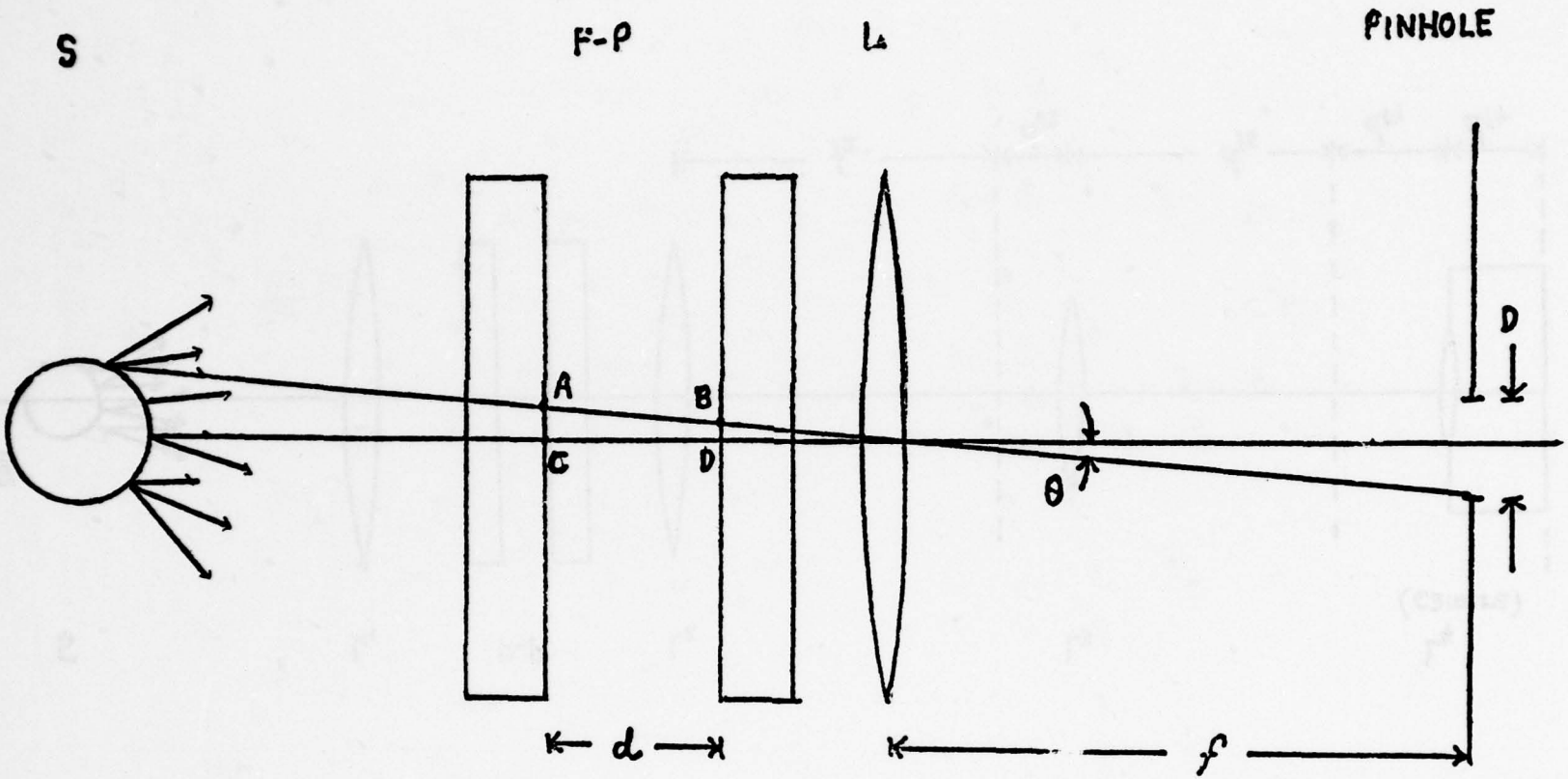

Fig.6. Geometry for Pinhole Finesse Calculations

Maximum path length difference permitted by pinhole $\Delta = AB - CD = \frac{d}{\cos \theta} - d$

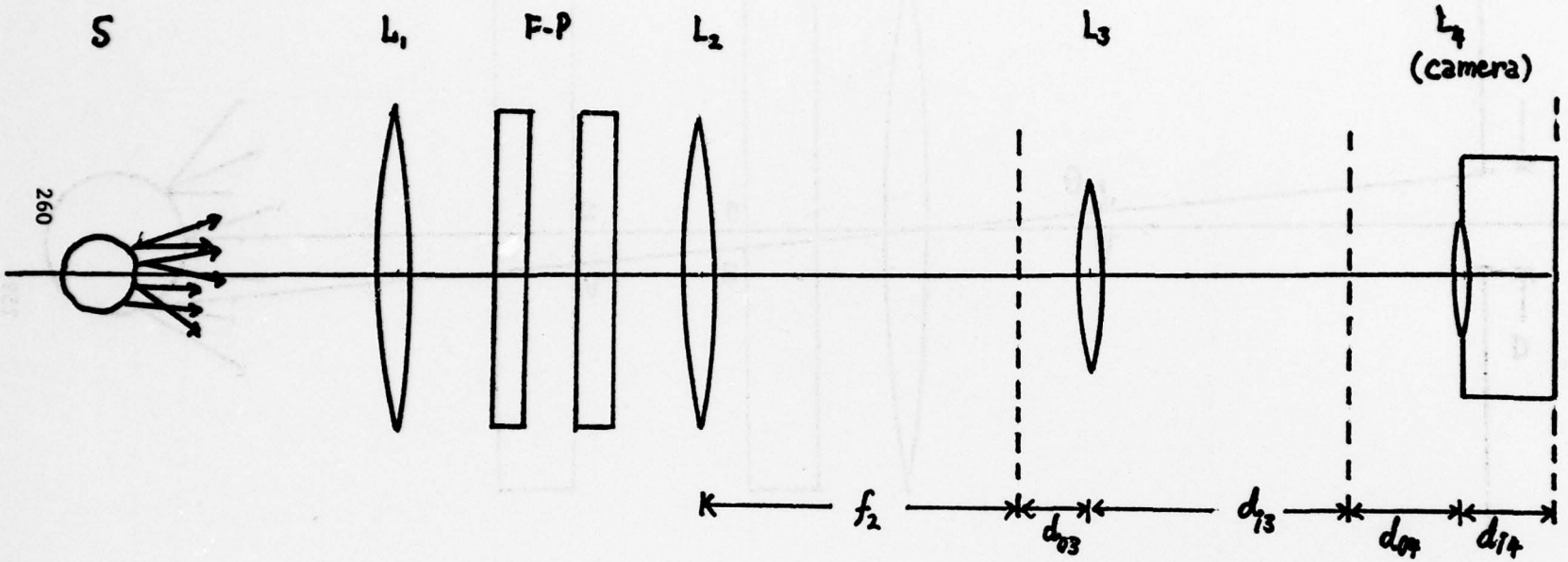

Fig.7. Typical Experimental Setup for Photographic Method

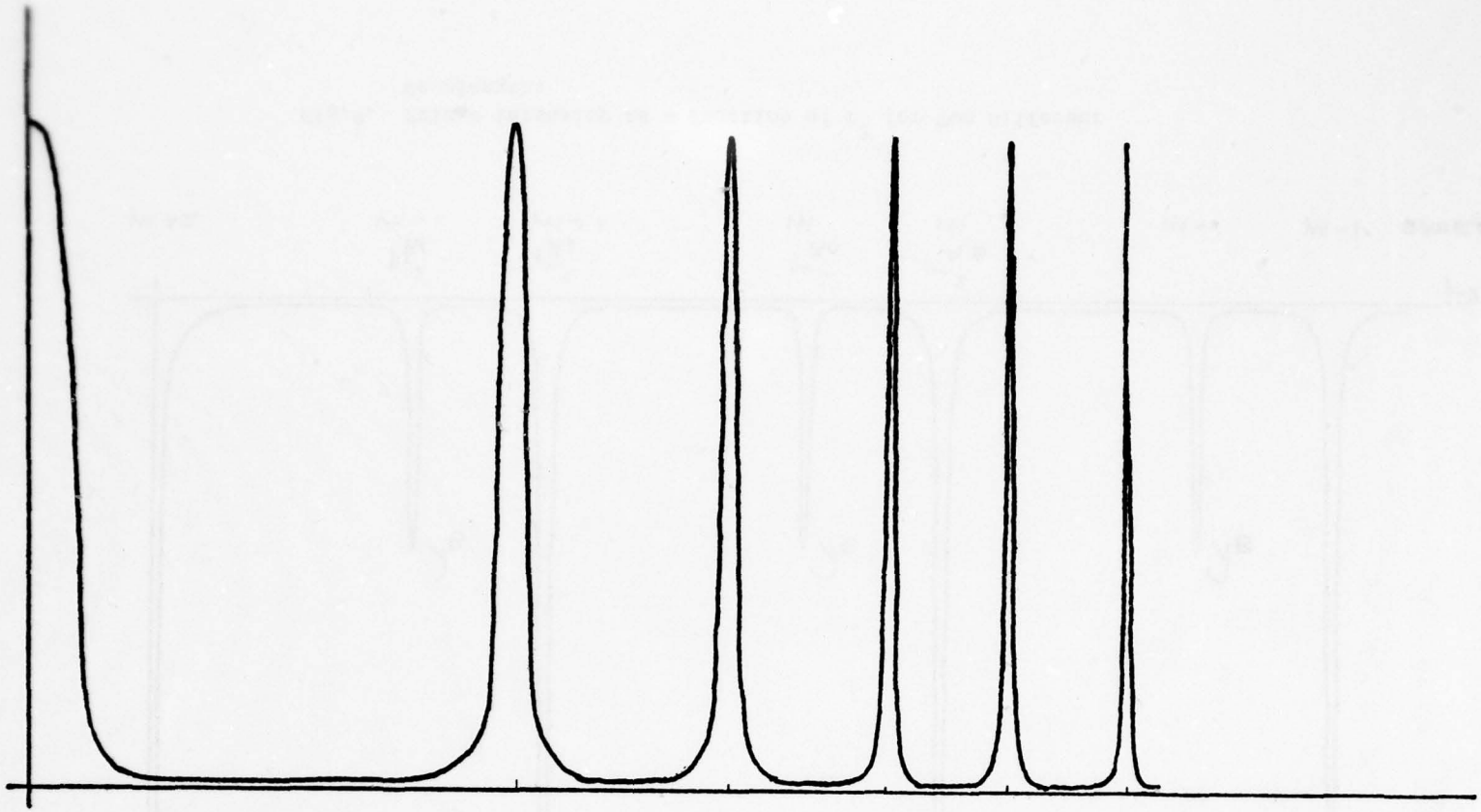

Fig.8. Airy Pattern as a Function of θ
Fringe Intensity as a Function of Fringe Radius r

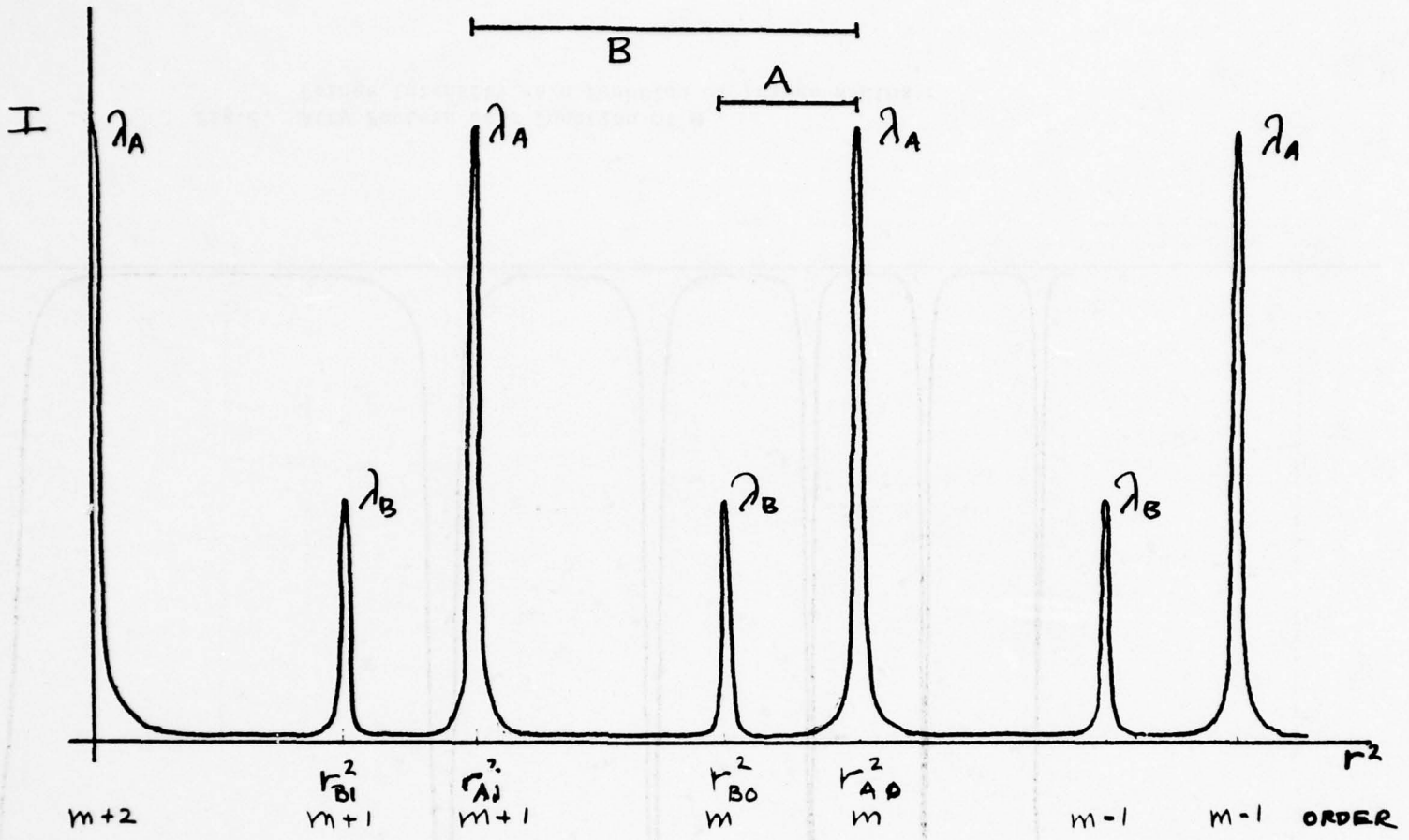

Fig.9. Fringe Intensity as a Function of r^2 for Two Different Wavelengths

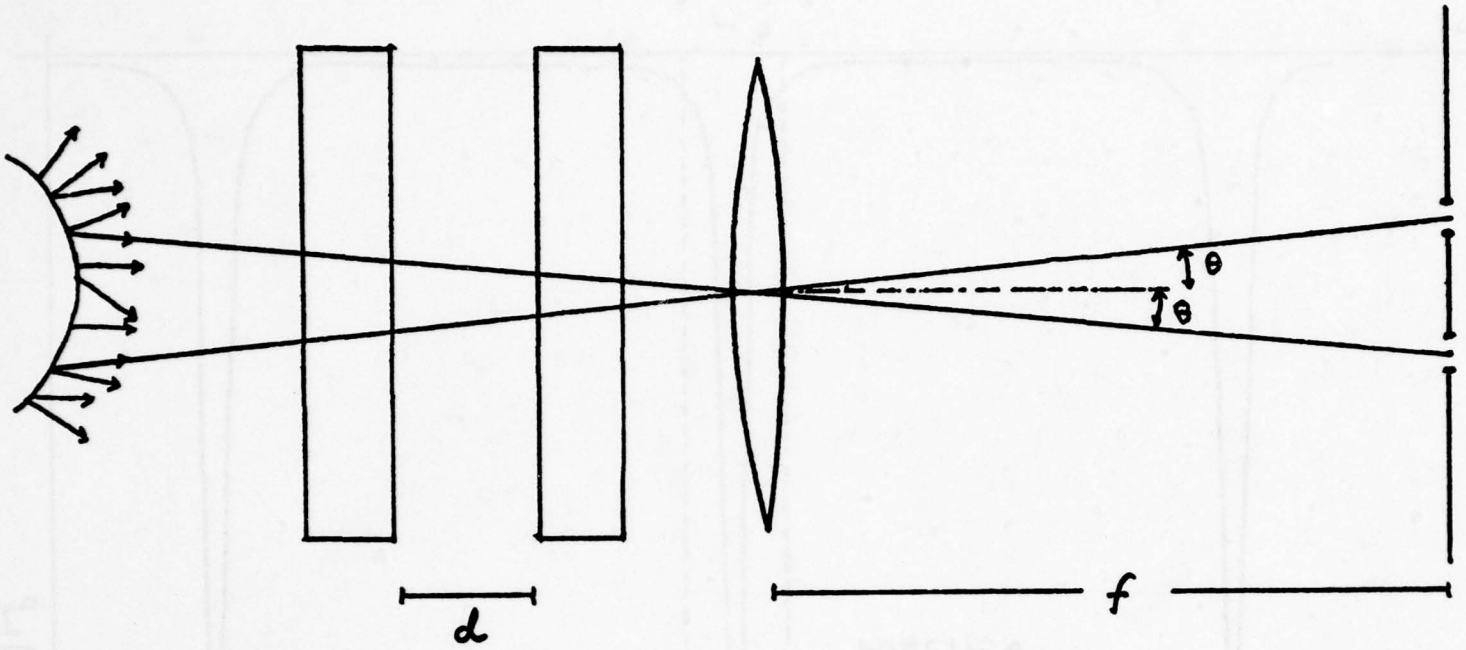

Fig.10. Geometry Showing Angle Selection by Use of an Annular Aperture

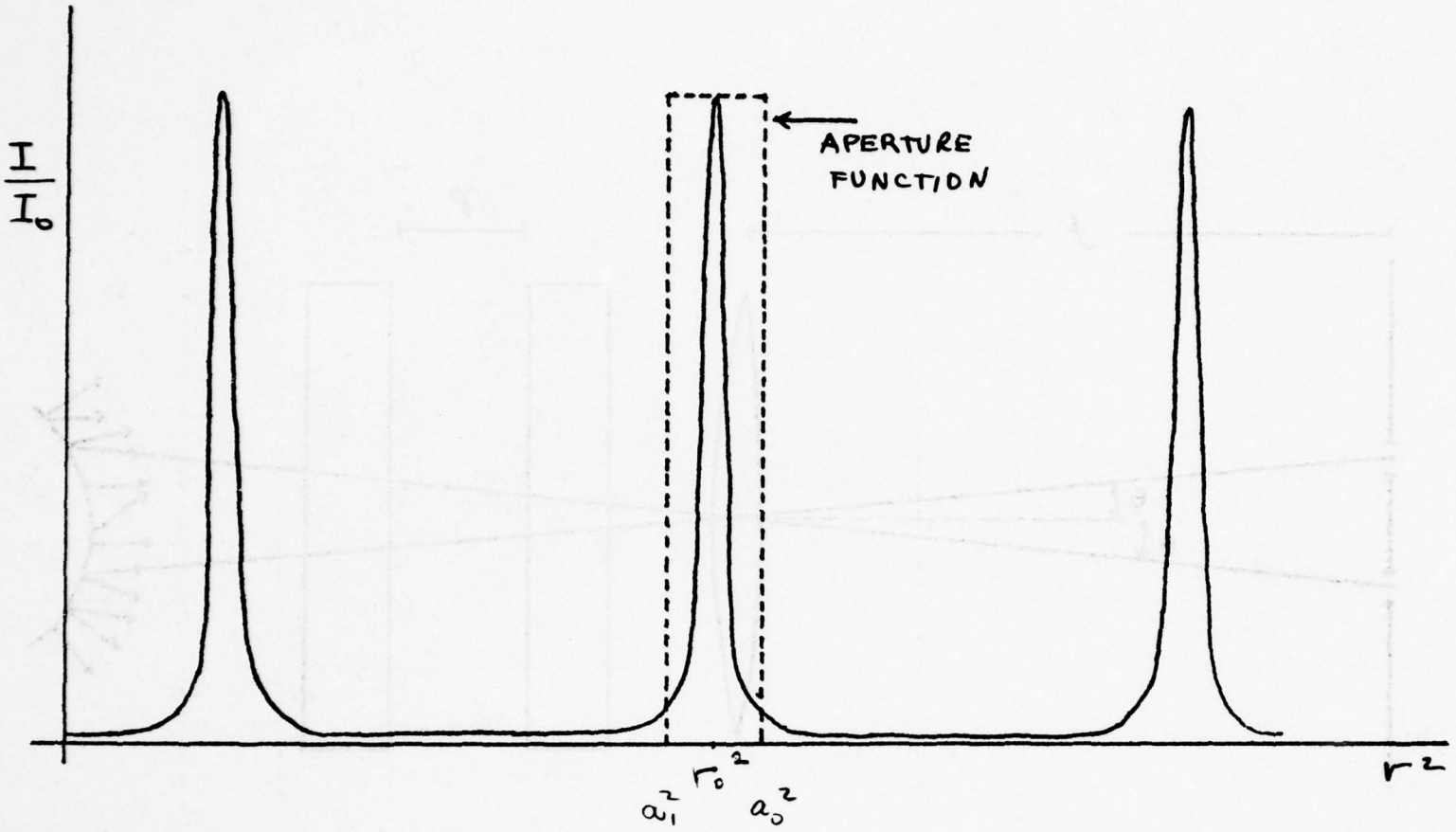

Fig.11. Fringe Intensity as a Function of r^2 Overlapped with Aperture Function of Annulus

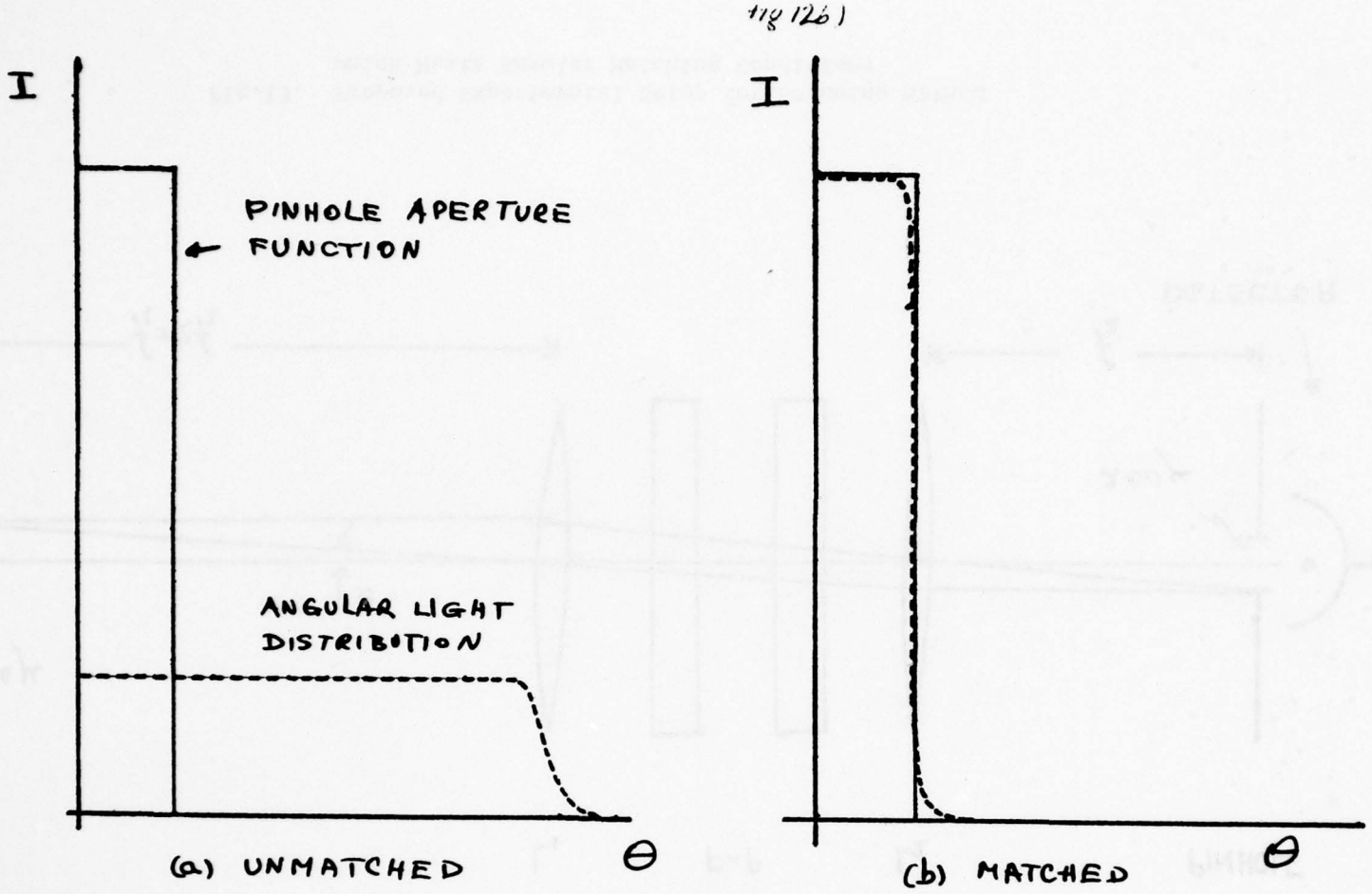

Fig.12. Pinhole Aperture and Light Intensity into Pinhole as a Function of θ ($\theta = \frac{r}{f}$)

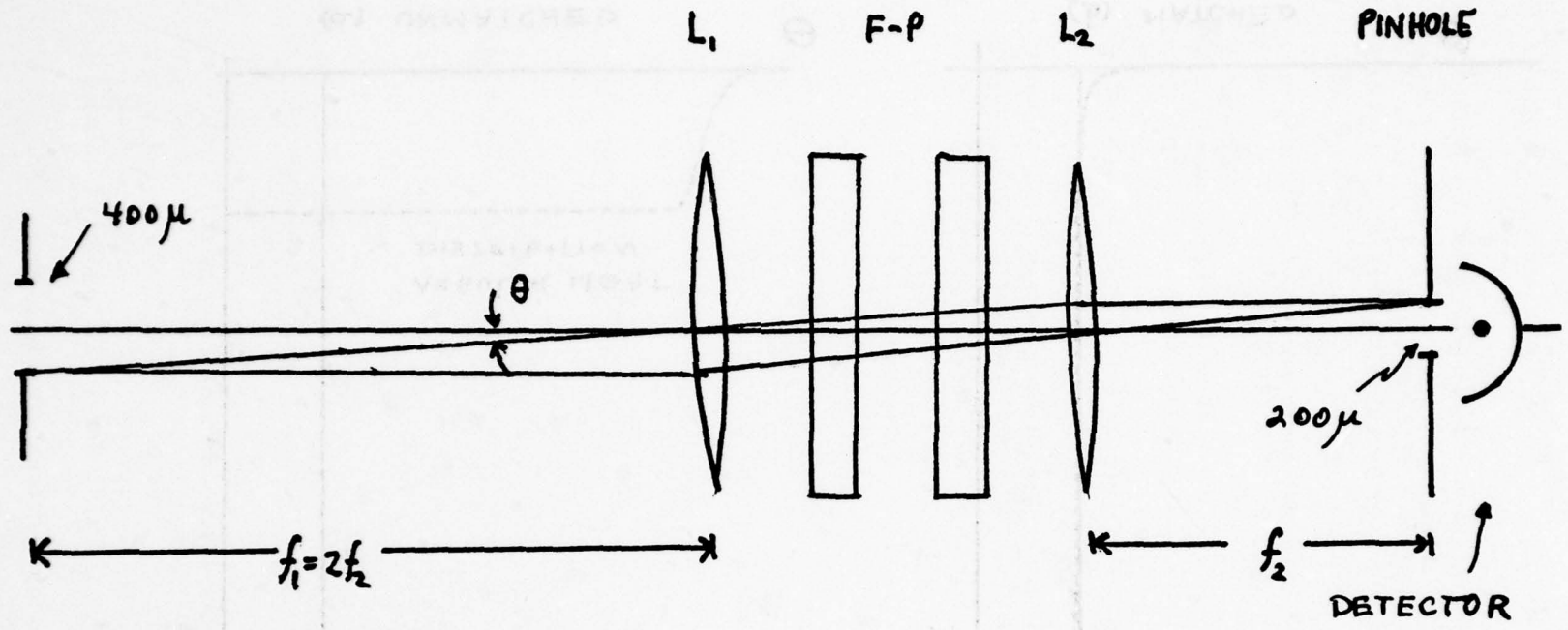

Fig.13. Proposed Experimental Setup for Scanning Method which Meets Angular Matching Conditions

REFERENCES

1. D. Dowson and G.R. Higginson, Elastohydrodynamic Lubrication, Pergamon Press, New York 1966.

2. T.E. Tallian, Elastodynamic Hertzian, Mechanical Engineering, p.14, November 1971.

3. H. Christensen, Elastohydrodynamic Theory of Spherical Bodies in Normal Approach, J. Lub. Tech., 92, 145 (1970).

4. E.G. Trachman, The Short-Time Viscosity Behavior of a Lubricant in a Hertzian Pressure Zone, J. Lub. Tech., Trans. ASME, 74 Lub-8.

5. J. Jakobsen and W.O. Winer, High-Shear Stress Behavior of Some Representative Lubricants, ASLE Preprint, 74 Lub-41.

6. W.R. Jones, Jr., R.L. Johnson, W.O. Winer and D.N. Sanborn, Pressure-Viscosity Measurements for Several Lubricants to 5.5×10^8 N/m^2 and 149°, NASA Technical Note NASA TN D-7736, 1974.

7. D.J. Plazek and J.H. Magill, Physical Properties of Aromatic Hydrocarbons IV. An Analysis of the Temperature Dependence of the Viscosity and the Compliance of 1, 3, 5 Tri-α-naphthylbenzene, J. Chem. Phys., 49, 3678 (1968).

8. A.K. Doolittle, Studies in Newtonian Flow. III. The Dependence of the Viscosity of Liquids on Molecular Weight and Free Space (in Homologous Series), J. Appl. Phys., 23, 236 (1952).

9. M. Cohen and D. Turnbull, Molecular Transport in Liquids and Glasses, J. Chem. Phys., 47, 2185 (1967).

10. J.H. Gibbs and E.A. DiMarzio, Nature of the Glass Transition and the Glassy State, J. Chem. Phys., 28, 373 (1958).

11. A.J. Barlow and E. Erginsav, Viscoelastic Relaxation in a Series of Short Chain Polydimethyl Siloxanes, J. Acoust. Soc. Am., 56, 83 (1974).

11a. G. Harrison and E.G. Trachman, The Role of Compressional Viscoelasticity in the Lubrication of Rolling Contacts, J. Lub. Tech., Trans. ASME, F94, 306 (1972).

12. R.S. Marvin and J.E. McKinney, Volume Relaxation in Amorphous Polymers, Physical Acoustics, Vol.IIB, p.165, Warren P. Mason, ed.. Academic Press, 1965.

13. J. Lamb, Thermal Relaxation in Liquids, Physical Acoustics, IIA, 203, Warren P. Mason, ed., Academic Press, 1965.

14. T.A. Litovitz and C.M. Davis, Structural and Shear Relaxation in Liquids, Physical Acoustics, IIA, 281, Warren P. Mason, ed., Academic Press, 1965.

15. J.D. Ferry, Viscoelastic Properties of Polymers, John Wiley & Sons, 1970.

16. H.Z. Cummins and R.W. Grammon, Rayleigh and Brillouin Scattering in Liquids: The Landau-Placzek Ratio, J. Chem. Phys., 44, 2785 (1966).

17. P.A. Fleury, Light Scattering as a Problem of Phonons and other Excitations, Physical Acoustics, Vol.VI, p.2, Warren P. Mason, ed., Academic Press, 1970.

18. J.D. Barnett, S. Block and G.T. Piermarini, An Optical Fluorescence System for Quantitative Pressure Measurement in the Diamond-Anvil Cell, Rev.Sci. Inst., 44, 1 (1973).

19. J.L. Lauer and M.E. Peterkin, Analysis of Infrared Spectra of Fluid Film in Simulated EHD Contacts, ASLE Preprint 74 LUB-34.

20. G.R. Paul and A. Cameron, An Absolute High Pressure Microviscometer Based on Refractive Index, Proc. Roy. Soc.A, London, 1 (1972).

21. H.Z. Cummins and E.R. Pike, Photon Correlation and Light Beating Spectroscopy, Plenum Press, New York 1974.

22. M.H. Birnboim and H. Weiss, A Novel Method for Viscosity Measurements at High Pressures, Presented in part, American Physical Society.

23. J.F. Dill, P.W. Drake and T.A. Litovitz, The Study of Viscoelastic Properties of Lubricants Using High Pressure Optical Techniques, ASLE Preprint 74 LC-5B-2.

24. H.J. McSkimin, Ultrasonic Methods for Measuring the Mechanical Properties of Liquids and Solids, Physical Acoustics, IA, 271, Warren P. Mason, ed., Academic Press.

25. Modern Very High Pressure Techniques, R.H. Wentorf, editor, Butterworths, 1962.

26. M.A. Lowenstein and M.H. Birnboim, A Method for Measuring Sedimentation and Diffusion of Macromolecules in Capillary Tubes by Total Intensity and Quasi-Elastic Light-Scattering Techniques, Biopolymers, 14, 419 (1975).

27. T.R. Meeker and A.M. Meitzler, in Physical Acoustics, Vol.IA, W.P. Mason, ed., Academic Press 1964.

28. D. Hunston, Ph.D. Thesis, "Determination of Viscoelastic Constants for Polymers."Chemistry Dept., Kent State University, December 1969.

29. Y. Kato and G.A. Zdasiuk, "Absolute Measurements of Brillouin Scattering Efficiencies of Molecular Liquids," J. Opt. Soc. Am., 65, 995 (1975).

30. S.E. Gustafsson, H.E. Gunilla Knape and L.M. Torell, "Brillouin Spectra of Ethyl Ether and Ethyl Alcohol," J.Phys. D: Appl. Phys., 7, 389 (1974).

31. G.C. Kennedy and W.T. Holser, Pressure-Volume-Temperature, p.373.

☆U.S.Government Printing Office: 1978 — 657-002/230